Mechanistic investigation of homo- and heteroaggregation of micro- and nanoparticles in aquatic systems

Oriekhova, Olena

UNIVERSITÉ DE GENÈVE **FACULTÉ DES SCIENCES**

Section des Sciences de la Terre et de l'Environnement
Département F.-A. Forel des Sciences
de l'Environnement et de l'Eau
Institut des Sciences de l'Environnement

Docteur Serge Stoll

Mechanistic Investigation of Homo- and Heteroaggregation of Micro- and Nanoparticles in Aquatic Systems

THÈSE

présentée à la Faculté des Sciences de l'Université de Genève
pour obtenir le grade de Docteur ès Sciences, mention sciences de l'environnement

par

Olena Oriekhova

de

Ukraine

Thèse N° 5240

GENÈVE
Atelier d'impression ReproMail
l'Université de Genève

2018

UNIVERSITÉ DE GENÈVE

FACULTÉ DES SCIENCES

DOCTORAT ÈS SCIENCES, MENTION SCIENCES DE L'ENVIRONNEMENT

Thèse de Madame Olena ORIEKHOVA

intitulée :

«Mechanistic Investigation of Homo- and Heteroaggregation of Micro- and Nano particles in Aquatic Systems»

La Faculté des sciences, sur le préavis de Monsieur S. STOLL, docteur et directeur de thèse (Département F.-A. Forel des sciences de l'environnement et de l'eau), Monsieur J. LABILLE, professeur (Centre européen de recherche et d'enseignement des géosciences de l'environnement, Université Aix-Marseille, Aix-en-Provence, France), Madame V. SLAVEYKOVA, professeure ordinaire (Département F.-A. Forel des sciences de l'environnement et de l'eau), Monsieur J. A. GALLEGO, docteur (Department of Marine Sciences, University of Gothenburg, Gothenburg, Sweden), autorise l'impression de la présente thèse, sans exprimer d'opinion sur les propositions qui y sont énoncées.

Genève, le 26 juillet 2018

Thèse - 5240 -

Le Décanat

N.B. - La thèse doit porter la déclaration précédente et remplir les conditions énumérées dans les "Informations relatives aux thèses de doctorat à l'Université de Genève".

Моим родителям посвящается

To my parents

"It doesn’t make any difference how beautiful your guess is, it doesn’t matter how smart you are, who made the guess, or what his name is…
If it disagrees with experiment, it’s wrong!"

Richard Feynman on the scientific method
Cornell University, 1964
youtu.be/OL6-x0modwY

Table of contents

Acknowledgements

I am very grateful to all people who contributed to the development of this project and supported me during this adventure. Particularly, I would like to thank

My supervisor and mentor Dr. Serge Stoll who recognised the potential in my CV, took me in his group, was not disappointed after my first literature review, introduced me to the scientific community through collaboration with local and international scientists and guided me through all the stages of this project. Thank you for your availability and always having a good mood!!!

Prof. Vera Slaveykova from the University of Geneva, Dr. Jérôme Labille from CEREGE at the University Aix – Marseille and Dr. Julián Alberto Gallego Urrea from the University of Gothenburg for having accepted to be part of a thesis committee, to dedicate their time to read my thesis and give valuable contributions to improve my work.

Members and former members of the Environmental physico-chemistry group. In particular, Arnaud, Chai, Fred, Fabrice, Fatehah, Lina and Marianne. All students with whom I have a chance to work! For your support during all these years in Versoix and in Geneva. For nice times spent together and good experiences and much advice you gave me!

All friends and co-workers of the Department Forel without whom scientific life would not have any pleasure. Many thanks to Alex, Katia and Philippe for their availability during all paper, software and lab issues. Special thanks to “les filles de Vera”: Séverine, Giulia, Nicole, Amandine, Teofana, Nadia, Perrine, Dorothea, Coralie, Rebecca etc. and a few guys Javier, Pierre and Sebastien. I would also like to mention: Andrea, Damien, Sonia, Tiago, Elena, Claire, Ena, Timon, Daphne, Irene, Jorrit, Alonso, Patrick, Naresh, Evi, Ziyu, Agathe, John, Dan, Jean-Luc and many, many others. The list is long.

My colleagues in Ukraine from the Institute of Colloid and Water Chemistry and from the Kyiv Polytechnic Institute who gave me the basis and desire to work in science and encouraged me to go further in different senses of the word.

My friends here and there and around the word who give me inspiration and support. Especially, Ira, Masha, Nadia and Inna.

My fiancé Stuart, for his love and support during this adventure. Thank you for your inexhaustible patience with all my ups and downs. And, of course, not to forget about many hours of proofreading and listening to my presentations!

My whole family, for their unconditional love and support. Especially, my mum and my brother Aliosha who allowed me to leave Ukraine and encouraged me to pursue my goal. Thanks to my parents for giving me the desire for and love of knowledge.

THANK YOU, MERCI, СПАСИБО, ДЯКУЮ!!!

Résumé

Les nanomatériaux manufacturés, produits en masse pour nos besoins quotidiens et leur larges applications dans le domaine industriel finissent irrémédiablement dans l'environnement. Le transport et le comportement des nanomatériaux manufacturés dans les systèmes aquatiques naturels sont influencés par la chimie de l'eau ainsi que par les propriétés intrinsèques des particules. L'objectif de ce travail est de développer une compréhension « mécanistique » des processus de transformation des nanomatériaux manufacturés dans divers systèmes aquatiques. Deux types de matériaux ont été utilisés : des nanoparticules métalliques en considérant du dioxyde de cérium (CeO_2) ainsi que des particules plastiques en considérant des billes de latex de polystyrène de taille micro et nano. La complexité des systèmes environnementaux a été ensuite reproduite à travers différents composés présents dans les systèmes aquatiques, tels que les substances humiques, les polysaccharides et les colloïdes inorganiques. Différentes conditions physico-chimiques concernant le changement de pH, le type d'électrolytes et la force ionique ont été reproduites. Le comportement des nanomatériaux manufacturés a été également testé dans les eaux naturelles du lac Léman et du Rhône.

Les nanoparticules (NPs) de CeO_2 sont les particules les plus utilisées dans les applications industrielles, donc potentiellement largement présentes dans l'environnement. La stabilité des NPs de CeO_2 lors de l'interaction avec les principaux composés de l'eau tels que la matière organique naturelle (MON) est étudiée. Comme modèle de MON, l'acide fulvique (AF) est considéré. Il est apparu que les complexes CeO_2/AF sont stables avec le temps et avec le changement de pH. La stabilité des complexes CeO_2/AF a été également testée dans des eaux synthétiques et naturelles. Pour une concentration d'AF représentative des milieux les NPs de CeO_2 sont stabilisées dans l'eau ultrapure et synthétique. Cependant, dans les eaux naturelles, les NPs et les complexes CeO_2/AF forment des agrégats. La stabilité des NPs a également été testée avec de l'alginate, un polysaccharide naturel. Le coating de surface est persistant en ce qui concerne le changement du pH de l'eau. La concentration en alginate, le pH de la solution et la présence de cations divalents sont des paramètres clés définissant la stabilité et l'effet de la stabilité du coating d'alginate autour des NPs de CeO_2, dans différentes conditions physico-chimiques de l'eau. L'effet d'un autre composé de l'eau – un colloïde inorganique (Fe_2O_3), important en matière d'hétéroagrégation du CeO_2 dans les systèmes

aquatiques, est également testé. Nous avons trouvé que l'hétéroagrégation n'est induite que dans des conditions électrostatiques favorables (concentration en sel et pH donnés).

Les conditions optimales de coagulation et la dose de coagulant ont été étudiées dans une optique d'élimination des particules microplastiques de l'eau. La neutralisation de charge est avancée comme le mécanisme principal de l'hétéroaggregation entre les particules nanoplastiques et les composés présents dans les eaux naturelles (alginate et Fe_2O_3).

Le comportement des NPs dans les eaux naturelles par rapport aux eaux synthétiques de composition similaire est différent, reflétant la complexité des systèmes aquatiques naturels par rapport aux conditions environnementales modélisées en laboratoire. Néanmoins, en simplifiant les systèmes naturels, les résultats obtenus nous permettent de mieux comprendre les mécanismes d'interaction.

Abstract

Engineered nanomaterials which are massively produced for our benefits and are present in many everyday products often end up in the environment due to the failures in collection, treatment and recycling. It is now well recognised that engineered nanomaterials constitute an important class of pollutants and that the fate and behaviour of engineered nanomaterials in aquatic systems are influenced by water chemistry as well as intrinsic particle properties. The aim of this work is to develop a mechanistic understanding of transformation processes of engineered nanomaterials in various aquatic systems. Two types of material such as metallic nanoparticles of cerium dioxide and plastic particles made of micro- and nanoplastic polystyrene latex beads were considered. The complexity of the environmental systems was reproduced by considering different water compounds, such as humic substances, polysaccharides and inorganic colloids and by using contrasting and changing water conditions including change of pH, type of electrolytes and ionic strength. The behaviour of engineered nanomaterials was also tested in natural waters from the Lake Geneva and the River Rhône.

CeO_2 nanoparticles (NPs) are widely used in industrial applications, hence potentially largely released to the environment. The stability of the CeO_2 NPs when interacting with main water compounds such as natural organic matter (NOM), inorganic colloids (ICs) and water ionic composition was investigated in this thesis. As a model of NOM fulvic acids (FAs) were considered. The CeO_2/FA complexes were found stable with time and regarding the pH change. We also investigated the behaviour of CeO_2/FA complexes in synthetic and natural waters. Environmentally relevant concentration of FAs was found to stabilise CeO_2 NPs in ultrapure and synthetic water. However, in natural waters CeO_2 NPs and CeO_2/FA complexes were found aggregated. The stability of another type of NOM coating was tested by using alginate as a surrogate of natural polysaccharides. The CeO_2/alginate coating was found persistent regarding the change of water pH. The alginate concentration, solution pH and the presence of divalent cations were found as key parameters defining the stability and effect of alginate coating around CeO_2 NPs in contrasting water conditions. When CeO_2 NPs are mixed with natural lake water heteroaggregation is observed, however, increase of alginate concentration reduces the heteroaggregation processes. To get an insight into heteroaggregation processes, the effect of another water compound – an inorganic colloid (Fe_2O_3 ICs), which

could induce the heteroaggregation of CeO_2 NPs in natural water, was also considered. It was found that the heteroaggregation is promoted only in electrostatic favourable conditions, i.e. in particular electrolyte concentrations and solution pH.

Then, the stability and behaviour of polystyrene nanoplastic particles were investigated in complex environmental matrices. The charge neutralisation mechanism was found responsible for the heteroaggregation between nanoplastic particles and natural water compounds such as alginate and Fe_2O_3 ICs. In addition, the optimal coagulation conditions and coagulant dosage were investigated in order to remove polystyrene microplastic particles from water.

The behaviour of engineered nanomaterials in natural waters compared to synthetic waters with similar composition was found significantly different reflecting the complexity of natural aquatic systems compared to artificial environmental conditions.

List of Tables

List of Figures

Abbreviations

CCC	Critical coagulation concentration
DLA	Diffusion limited aggregation
DLS	Dynamic light scattering
ENMs	Engineered nanomaterials
FAs	Fulvic acids
HAs	Humic acids
ICs	Inorganic colloids
IEP	Isoelectric point
JRC	Joint Research Centre
MNPs	Manufactured nanoparticles
NOM	Natural organic matter
NPs	Nanoparticles
NTA	Nanoparticle tracking analysis
PS	Polystyrene
PZC	Point of zero charge
RLA	Reaction limited aggregation
SEM	Scanning electron microscope
SI	Supporting information
TEM	Transmission electron microscope

Chapter I

Introduction

I.1 Introduction

Nowadays engineered nanomaterials (ENMs) are widely present in different areas of our life in cosmetics (sunscreen and toothpaste) in food (candy), paints, sport equipment, clothes etc. To understand what nanomaterials are, we use the definition released by The European Commission which states:

" 'Nanomaterial' means a natural, incidental or manufactured material containing particles, in an unbound state or as an aggregate or as an agglomerate and where, for 50 % or more of the particles in the number size distribution, one or more external dimensions is in the size range 1 nm - 100 nm." (EU, 2011).

In addition to the small size, the properties of nanomaterials are changing with decrease of particle size. For example, for cerium dioxide (CeO_2) nanomaterials catalytic and redox properties are dramatically changing compared to the bulk materials (Reed et al., 2014). This is the reason why ENMs are used in various industrial applications such as agricultures and soil remediation (Khot et al., 2012; Tungittiplakorn et al., 2004), paints and pigments (Al-Kattan et al., 2013), food and personal care products (Weir et al., 2012), packaging (Silvestre et al., 2011), automotive industry (Reed et al., 2014) and many others.

There are many different approaches to classify the nanomaterials, based on origin, for example, natural, anthropogenic and industrial. Nanomaterials could be free or bound to matrices. The ENMs could be categorised based on the materials they made of, such as organic, inorganic or mixed organic/inorganic (Stone et al., 2010). There are different types of ENMs such as elemental nanomaterials (for example, silver, gold nanoparticles, carbon nanotubes), metal oxides (such as titania, ceria, silica, zinc oxide) and nanoplastic materials (polystyrene nanobeads, polyethylene films, polyamide fibres etc.) (da Costa et al., 2016; Gottschalk et al., 2009).

Large application of ENMs in daily used customer products leads to their release into the environment. It was shown that huge amount (on the level of $300 \cdot 10^3$ metric tons/year estimate of 2010) of ENMs end up in soil, water and landfill (da Costa et al., 2016; Keller et al., 2013) which poses the threat to leaving organisms and human health.

To improve the risk assessment evaluation the understanding of nanomaterial fate and transformation, in particular, the aggregation processes in the environment and further possible ways of elimination are needed.

I.2 Factors affecting the fate of ENMs in aquatic systems

Aquatic systems are one of the environmental compartment where the estimated release of most used ENMs reaches the level of 30 000 metric tons/year in 2010 (Keller et al., 2013). The fate and behaviour of ENM will depend on various factors including water chemistry and intrinsic ENM properties. The effect of these factors on ENM fate are presented below in more details.

I.2.1 Water chemistry

ENMs can enter the aquatic system as either individual particle or aged materials or aggregates. Depending on water pH, ionic composition (ion valence), water hardness, ionic strength, presence of natural organic matter (NOM) and inorganic colloids (ICs), the behaviour of ENMs can drastically change and lead to various transformations (Fig. I.1).

NOM is one of the important water component that defines the stability of ENMs in aquatic system. NOM is a general name to denote all types of organic constituents in water, such as humic substances, polysaccharides, peptidoglycanes, hemicellulose, pectic compounds such as microbial cell walls and extracellular products, sugars etc (Buffle et al., 1998). For example, humic substances represent an assembly of organic macromolecules with heterogeneous functional groups such as hydroxyl (-OH), methyl (-CH_3), carboxyl (-COOH), and are present in the aquatic environment in the form of fulvic acids (FAs), humic acids (HAs) and humin. NOM plays also an important role in reducing the aggregation rates, stabilisation and dispersion of colloidal particles and engineered nanomaterials (Liu et al., 2012). For example, the adsorption of NOM on CeO_2 nanoparticles (NPs) was found to reduce the aggregation by increasing the electrostatic repulsions between particles (Quik et al., 2010). The coating of magnetic γFe_2O_3 NPs by HAs was found to stabilise these NPs due to the repulsive electrostatic and steric-electrostatic interactions (Ghosh et al., 2011). Even more, adsorption of HAs led to the disagglomeration of already formed TiO_2 nanoparticle agglomerates (Loosli et al., 2013).

Another major type of natural water compounds which has an effect on the stability of ENMs is inorganic colloids (ICs) (Buffle, 2006). The most common ICs are clays, aluminosilicates and iron oxihydroxides (Eyrolle and Charmasson, 2004, 2001; Filella, 2007). ICs are compact compounds with high size polydispersity, different mineralogy, and varied concentration in natural water from a few to hundreds mg/L (Eyrolle and Charmasson, 2004). In Rhône river water, ICs are mainly present as clay minerals, calcite,

quartz, muscovite and iron oxide and their concentration changed from 3 to 40 mg/L (sampling of Rhône water near Arles) (Slomberg et al., 2016). Another study indicates the proportions of Fe and Al observed in the colloidal phase in the Rhône river water reached 42% and 35%, respectively (Eyrolle and Charmasson, 2004). The size, including aggregation state, as well as surface chemistry of natural ICs define the availability of IC surface and possible interactions with ENMs (Slomberg et al., 2016).

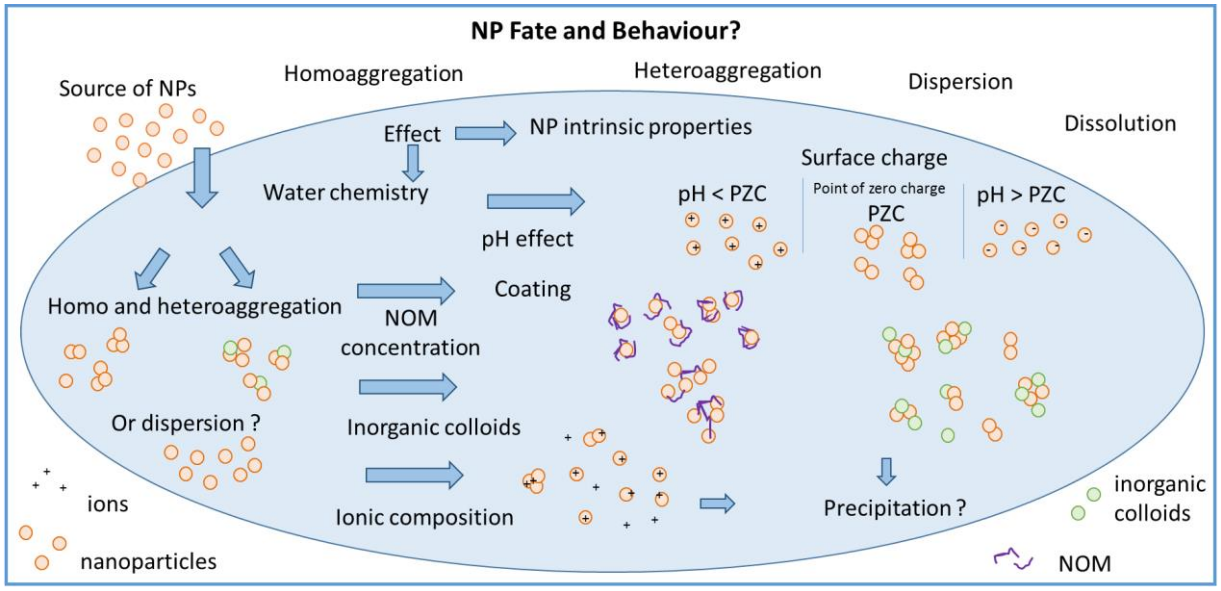

Fig. I.1. Schematic representation of physicochemical processes and parameters influencing ENM fate and behaviour in aquatic systems.

Ionic strength and electrolyte ion valency are other parameters that influence the stability of ENMs in aquatic system. Ionic strength takes into account the charge and the number of ions which are present in solution. Electrolytes modify the thickness of the double-layer and affect the electrostatic interactions, hence influencing ENM behaviour. The aggregation kinetics of CeO_2 NPs was investigated as a function of ionic strength at pH 5.7 (Zhang et al., 2012). Authors found that the critical coagulation concentration (CCC) in KCl was equal to 40 mM. Divalent ions, such as Ca^{2+} and Mg^{2+}, were found more effective for destabilisation and aggregation. The CCC for CeO_2 NPs (at pH 5.6) was approximately equal to 9.5 mM for $CaCl_2$ (Li et al., 2011). The fast aggregation was explained by an increase of the inverse of the Debye length which resulted in a decrease of repulsive electrostatic energy.

I.2.2 ENM intrinsic properties

Intrinsic properties of ENM such as size, aggregation state, shape and surface charge, are interconnected and play a key role in the environmental identity of ENMs.

The aggregation state of ENMs is directly related to the particle size as well as to the particle reactivity. The aggregation state also affects the behaviour of NPs in the environment and determines their toxicity (Rodea-Palomares et al., 2011; Röhder et al., 2014; Safi et al., 2010; von Moos and Slaveykova, 2013). It is known that smaller particles are more reactive due to the higher proportion of active centres on the surface compared to the bulk materials (Andreescu et al., 2014), and more toxic for the organisms (Cong et al., 2011; Fabrega et al., 2011; Moos et al., 2014). The aggregation state can be affected by the environmental conditions. Even if ENMs enter the aquatic environment in agglomerated state the presence of organic substances at natural concentration can lead to important surface changes and redispersion. TiO_2 NPs that where in contact at environmentally relevant concentration of HAs were disagglomerated and changed their surface charge towards further stabilisation (Loosli et al., 2014, 2013). Zinc oxide NPs were also partially disagglomerated due to the coating with Suwanee River HAs (Mohd Omar et al., 2014).

In aqueous solution particles acquire a surface charge, most commonly, due to the presence of surface chemical groups which can be ionised in the presence of water. Such acidic or basic surface groups can release or gain protons (H^+) depending on the pH of the solution (Gregory, 2005). As an example, the surface of metal oxide nanoparticle can be considered (Fig. I.2). At low pH value surface charge of oxide is positive and at high pH is negative, passing by the point of zero charge (PZC).

Surface deprotonation can be described by the following chemical equilibria (Oriekhova and Stoll, 2016a):

$$M\text{-}OH_2^+ + OH^- \rightarrow M\text{-}OH + H_2O \quad (I.1)$$

$$M\text{-}OH + OH^- \leftrightarrow M\text{-}O^- + H_2O \quad (I.2)$$

There are two situations when the surface charge on metal oxide NPs is equal to zero. First, in absence of both positive and negative charges referring to the PZC. The second situation, when there is an equal amount of positive and negative charges, is called the isoelectric point (IEP) (Jolivet et al., 2000). It is referring to the situation when positive

and negative charges compensate each other and very often is related to the specific adsorption of positive or negative species. These two concepts are crucial to control the stability of ENMs in aquatic systems as well as for the development of the ENM elimination processes and interpretation of aggregation results.

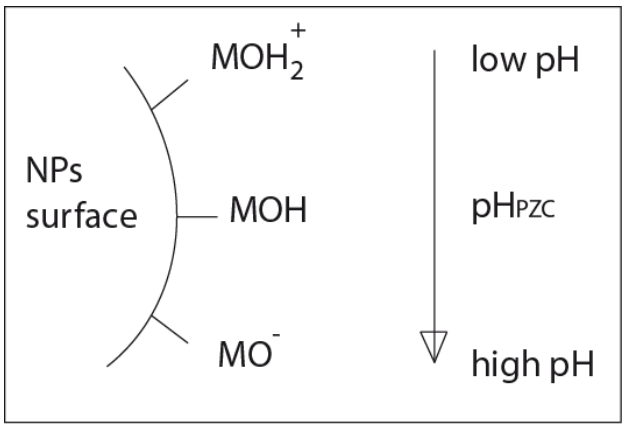

Fig. I.2. Schematic representation of ENM ionisation processes on the surface of metal oxide nanoparticles in aqueous solution (Adapted from (Oriekhova and Stoll, 2016b)).

I.3 CeO_2 nanoparticles

Cerium(IV) oxide (CeO_2) NPs belong to the ENMs and are produced at a large scale on the level of 1 000 tonnes/year (Piccinno et al., 2012). They have been included in the priority list of ENMs for risk evaluation by the Organization for Economic Cooperation and Development (OECD) (Liu et al., 2015). CeO_2 NPs are known for their exceptional catalytic properties due to the capacity to form a single oxygen-vacancy in the reduction of Ce^{4+} to Ce^{3+}(Calvache-Muñoz et al., 2017). The formation of the vacancy happened to the response to the changes of the physicochemical parameters such as temperature, partial oxygen pressure, doping with other ions, application of an electric field and surface stress (Sun et al., 2012). Due to this specific property CeO_2 NPs are used in several applications including catalytic converters, UV blocking and polishing agent, diesel fuel additive, electrochemical devices (such as solid oxide fuel cells, gas separation membranes, gas sensors) and even in everyday products (such as part of a component of the interior coating of self-cleaning ovens, compact fluorescent light etc.) (El-Toni et al., 2006; Sajith et al., 2010). Small size of NPs (below 15 nm) and higher proportion of the Ce^{3+} ions in the structure of CeO_2 NPs leads to higher red-ox activity as well as oxidative stress (Baalousha et al., 2016; Tella et al., 2014). The growing consumption of CeO_2 containing products leads to the release of these NPs to the environment via industrial discharges or surface

runoff from soils or wastewater treatment effluents (Gottschalk and Nowack, 2011; Keller et al., 2013).

I.4 Micro and nanoplastics

Another group of ENMs that recently became an emerging concern is nanoplastics. Production of plastic materials worldwide reaches the level of 322 million tonnes/year (Plastics – the Facts 2016). The estimated amount of plastic waste consists of 10% (by mass) of municipal waste (Barnes et al., 2009). Despite the plastic recycling, part of plastic litter still end up in the marine and fresh water environments (Faure et al., 2015; Thompson, 2006). It is not easy to detect nanoplastic particle in natural water samples because of the lack of the sampling and detection methods for such small particles. However, there is a first study confirming the presence of nanoplastic in water samples from the North Atlantic subtropical gyre (Ter Halle et al., 2017). The notion of nanoplastic is tightly related to the microplastic notion as the degradation of bigger fragments of plastic litter, including microplastics, lead to the formation of nanoplastics (Gigault et al., 2016; Lambert and Wagner, 2016). There is no yet an agreement about classification of plastics based on size. Most commonly, mesoplastic is defined as particles larger than 5 mm, microplastic particles are from 1 μm to 5 mm and nanoplastic below 1 μm (da Costa et al., 2016). Another way to group the plastics is dividing them into two categories based on material aging i.e. primary and secondary plastics (Syberg et al., 2015). Particles specifically produced as micro- or nanosized particles called primary plastics are mainly used in industry as abrasive agents or in cosmetics as facial cleaners. Whereas, secondary plastic is a result of a fragmentation and degradation processes from larger fragments of plastic litter to micro- or nanosized fragments (Gigault et al., 2016). There are different pathways of plastic pollution to the environment such as the direct rejection of the plastic litter, from the waste water treatment plant which include the washing liquid of synthetic clothes and cosmetics, urban runoffs, and the use of sewage sludge (which contains plastic pollution) as a fertilizer (Browne et al., 2011; Fendall and Sewell, 2009; Leslie et al., 2013). This is the reason why plastic pollution represent a significant environmental concern. Moreover, micro- and nanoplastics can release toxic chemical additives and adsorb, accumulate and transport pollutants in aquatic systems (Lee et al., 2014; Teuten et al., 2009); they are also more easily ingested by the organisms and accumulated throughout the food chain (Wagner et al., 2014; Wright et al., 2013).

I.5 Elimination of ENMs from aquatic systems

Water treatment plants (drinking and wastewater) use coagulation and flocculation processes to remove the suspended matter which can be both of natural and anthropogenic origin (Gregory, 1973; Neal et al., 2011; Westerhoff et al., 2011). During these processes suspended particles form large aggregates that can be easily removed by flocculation or filtration. The addition of coagulant allows to destabilize suspended colloidal particles and increase the collision efficiency between them (Gregory, 2005; Larue et al., 2003). Different type of coagulants and flocculants are used to enhance the coagulation. For example, inorganic and organic electrolytes and polyelectrolytes are used, such as the salts of iron(III), aluminum, polyaluminum chloride, acryloyloxyethyltrimethyl ammonium chloride and polyacrylamide polymers (Lin et al., 2013; Pinheiro et al., 2013). However, the optimal coagulation condition (dosage) is not easy to achieve as they are highly dependent on the particle concentration, charge and size but also on pH and solution composition which vary with time.

The removal of TiO_2 NPs from artificial ground and surface waters using three different types of coagulant was studied (Honda et al., 2014). Authors showed that using $FeSO_4$ and $Al_2(SO_4)_3$ it is possible to reach the removal level of 90%, whereas less than 60 % is obtained with $FeCl_3$ in surface water. Overall, the removal efficiency is highly dependent on operating conditions, NP concentration and coagulant dosage. Special attention should also be paid to the presence of NOM which alters the operating parameters, and hence affects the removal rate. The increase of coagulant dosage can lead to the decrease of the coagulation efficiency due to electrostatic stabilisation (Gao et al., 2007; Zou et al., 2011). The particle surface charge is playing a crucial role in stabilisation processes. Kobayashi et al., (2013) showed that the coagulation of sulphate latex beads in the presence of imogolite nanotubes is strongly charge dependent. When latex beads and nanotubes are oppositely charged, coagulation occurred only at the IEP and the efficiency of coagulation is dependent on electrokinetic potential and nanotube dosage. Hence, until now it is not clear how ENMs, including nanoparticles and micro- and nanoplastics, will be transformed through the treatment processes and which mechanisms are underlying these transformations.

I.6 Thesis objectives and outline

The main objective of this thesis is to develop a mechanistic understanding of transformation processes of engineered nanomaterials in various aquatic environments. For this purpose we used different types of ENMs such as cerium (IV) dioxide, micro-, and nanoplastic particles. Most of the current researches have concentrated on simplified systems and detailed mechanistic understanding is missing. In this thesis the complexity of environmental systems and variety of ENMs was addressed in the next ways: i) first, the complexity of natural colloids was taken into account by using a three component approach i.e. by considering humic substances, polysaccharides and inorganic colloids; ii) secondly, the complexity of water composition was also taken into account by testing contrasting water conditions including change of pH, electrolyte valency, water hardness and ionic strength; iii) finally, two different types of materials were tested i.e. metal oxide nanoparticles and plastic materials including aged materials. Moreover, the importance of coagulant dosage in order to eliminate microplastic particles in various conditions during coagulation processes was also investigated.

This introduction chapter which describes general trends in behaviour of ENMs in the environment is followed by Chapter II, where the theoretical and experimental approaches used to achieve thesis goals are presented. The "multidisciplinary" approach was used to combine methods from nanotechnology (nanoparticle tracking analysis, methods to disperse NPs in water systems), colloidal and physical chemistry (electrophoretic and dynamic light scattering measurements, microscopy methods), speciation calculations and environmental systems (fresh and synthetic waters, surrogates of NOM and IC) in order to reach the aims of this thesis. Chapter II is followed by five research chapters where main results of the research are present. The schematic representation of the experimental workflow is presented in Fig. I.3. In Chapters III – VI CeO_2 NPs are used to study their environmental behaviour. In Chapters III the effect of different environmental factors, such as the presence of NOM (fulvic acid), the effect of ionic strength, change of pH, dilution effect are investigated.

Chapter IV describes the behaviour of pristine and fulvic acid coated CeO_2 NPs in various environmental scenarios, i.e. natural and synthetic waters with varied concentration of NOM.

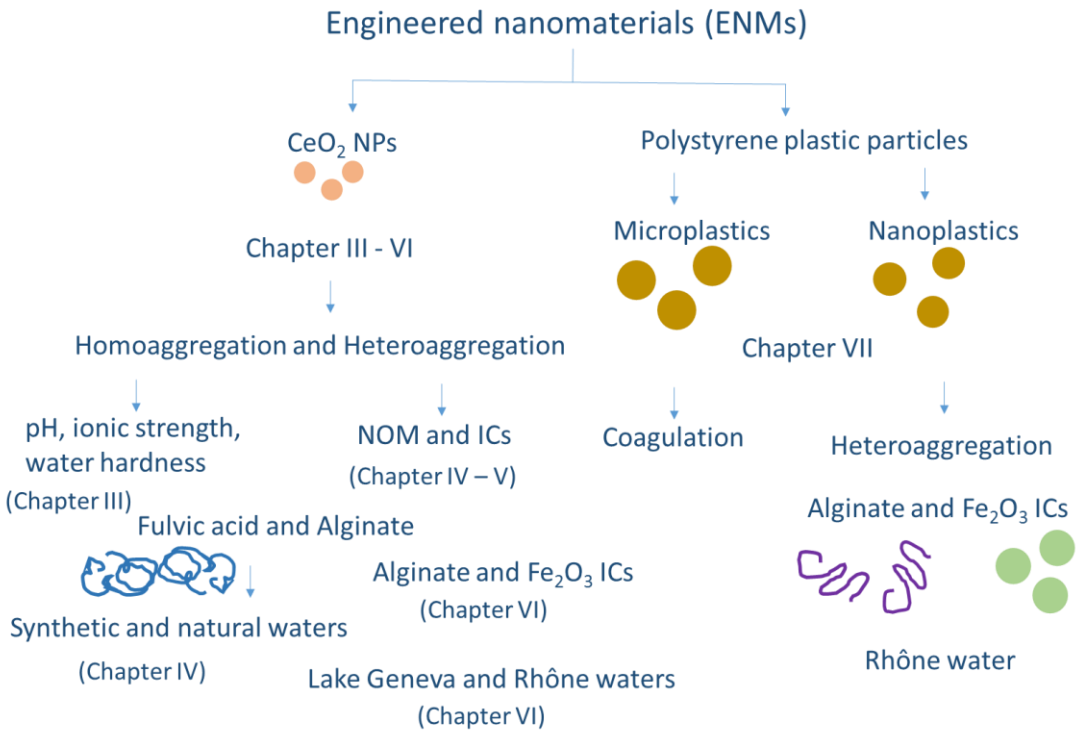

Fig. I.3. Schematic representation of the organisation of the research chapters presented in the thesis.

In Chapter V alginate is considered as a surrogate of NOM. CeO_2 NPs were coated with alginate and the effect of changing conditions, such as changing pH, ionic strength, alginate concentration, on the stability of coating formed was assessed.

In Chapter VI the heteroaggregation of CeO_2 NPs in the presence of both inorganic colloids and organic matter is investigated. As a surrogate of NOM we used alginate in this chapter. The binary system, pristine CeO_2 NPs and Fe_2O_3, was considered first and then the effect of water ionic composition was studied using synthetic and natural waters. The effect of component concentration was assessed. The kinetic of heteroaggregation was studied to obtain quantitative parameters to describe the processes and to deduce the mechanisms of heteroaggregation.

Chapter VII describes the heteroaggregation between polystyrene nanoplastics and inorganic colloids (Fe_2O_3.) The effect of alginate polysaccharide chains on the heteroaggregation is also investigated here. In order to get an insight into the heteroaggregation of nanoplastics and the effect of naturally present organic matter and inorganic colloids natural water from river Rhône is used.

To eliminate plastic particles from aquatic systems polystyrene microplastic particles are considered. The destabilisation processes are studied using iron (III)

chloride as a coagulant. The results obtained in this chapter allowed the discussion of the main destabilisation mechanisms.

The final Chapter VIII outlines the obtained results and gives the perspective for the future research.

I.7 List of papers

Papers included in this thesis.

Oriekhova, O., and Stoll, S., **2018,** Heteroaggregation of cerium dioxide nanoparticle in the presence of alginate and iron (III) oxide, Science of Total Environment (accepted in STOTEN), (Chapter **VI**).

Oriekhova, O., and Stoll, S., **2018**, Heteroaggregation of Nanoplastic Particles in the Presence of Inorganic Colloids and Natural Organic Matter, Environmental Science: Nano, February, https://doi.org/10.1039/C7EN01119A, (**Paper V**, Chapter **VII**).

Oriekhova, O., Le Coustumer, P., and Stoll, S., **2017**, Impact of biopolymer coating on the colloidal stability of manufactured CeO_2 nanoparticles in contrasting water conditions, Colloids and Surfaces A, v. 533, pp. 267–274, (**Paper III**, Chapter **V**).

Oriekhova, O., and Stoll, S., **2016**, Effects of pH and fulvic acids concentration on the stability of fulvic acids – cerium (IV) oxide nanoparticle complexes, Chemosphere, v. 144, pp. 131-137, (**Paper I**, Chapter **III**).

Oriekhova, O., and Stoll, S., **2016**, Stability of uncoated and fulvic acids coated manufactured CeO_2 nanoparticles in various conditions: From ultrapure to natural Lake Geneva waters, Science of the Total Environment, v. 562, pp. 327-334, (**Paper II**, Chapter **IV**).

Oriekhova, O., and Stoll, S., **2014**, Investigation of $FeCl_3$ induced coagulation processes using electrophoretic measurement, nanoparticle tracking analysis and dynamic light scattering: Importance of pH and colloid surface charge, Colloids and Surfaces. A, Physicochemical and Engineering Aspects, v. 461, pp. 212-219, (**Paper IV**, Chapter **VII**).

Collaborative papers that are not included in this thesis.

Le Coustumer, P., S. Stoll, **Oriekhova, O.**, Villanueva, J., Peyraube, N., Jeanton, H., Huneau, F., Grassl, B., Faucher, S., and Lespes G., Holistic Strategy to Study Nanoparticles and Metallic Trace Elements in Surface Waters, International Journal of Environmental Science, 2017, vol. 2, p. 238-247

Heinlaan, M., Muna, M., Juganson K., **Oriekhova, O.**, Stoll, S., Kahru A., and Slaveykova V. I., **2017**, Exposure to sublethal concentrations of Co_3O_4 and Mn_2O_3 nanoparticles induced elevated metal body burden in Daphnia magna, Aquatic Toxicology, v. 189, pp. 123–133.

Loosli, F., Omar, F.M., Carnal, F., **Oriekhova, O.**, Clavier, A., Chai, Z., and Stoll, S., **2014**, Manufactured Nanoparticle Behavior and Transformations in Aquatic Systems. Importance of Natural Organic Matter: Chimia, v. 68, no. 11, p. 783-787.

I.8 References

Al-Kattan, A., Wichser, A., Vonbank, R., Brunner, S., Ulrich, A., Zuin, S., Nowack, B., 2013. Release of TiO 2 from paints containing pigment-TiO 2 or nano-TiO 2 by weathering. Environ. Sci. Process. Impacts 15, 2186–2193. https://doi.org/10.1039/C3EM00331K

Andreescu, D., Bulbul, G., Özel, R.E., Hayat, A., Sardesai, N., Andreescu, S., 2014. Applications and implications of nanoceria reactivity: measurement tools and environmental impact. Environ. Sci. Nano 1, 445–458. https://doi.org/10.1039/C4EN00075G

Baalousha, M., Cornelis, G., J. Kuhlbusch, T.A., Lynch, I., Nickel, C., Peijnenburg, W., Brink, N.W. van den, 2016. Modeling nanomaterial fate and uptake in the environment: current knowledge and future trends. Environ. Sci. Nano 3, 323–345. https://doi.org/10.1039/C5EN00207A

Barnes, D.K.A., Galgani, F., Thompson, R.C., Barlaz, M., 2009. Accumulation and fragmentation of plastic debris in global environments. Philos. Trans. R. Soc. B Biol. Sci. 364, 1985–1998. https://doi.org/10.1098/rstb.2008.0205

Browne, M.A., Crump, P., Niven, S.J., Teuten, E., Tonkin, A., Galloway, T., Thompson, R., 2011. Accumulation of microplastic on shorelines woldwide: sources and sinks. Environ. Sci. Technol. 45, 9175–9179.

Buffle, J., 2006. The key role of environmental colloids/nanoparticles for the sustainability of life. Environ. Chem. 3, 155–158.

Buffle, J., Wilkinson, K.J., Stoll, S., Filella, M., Zhang, J., 1998. A Generalized Description of Aquatic Colloidal Interactions: The Three-colloidal Component Approach. Environ. Sci. Technol. 32, 2887–2899. https://doi.org/10.1021/es980217h

Calvache-Muñoz, J., Prado, F.A., Rodríguez-Páez, J.E., 2017. Cerium oxide nanoparticles: Synthesis, characterization and tentative mechanism of particle formation. Colloids Surf. Physicochem. Eng. Asp. 529, 146–159. https://doi.org/10.1016/j.colsurfa.2017.05.059

Cong, Y., Banta, G.T., Selck, H., Berhanu, D., Valsami-Jones, E., Forbes, V.E., 2011. Toxic effects and bioaccumulation of nano-, micron- and ionic-Ag in the polychaete, Nereis diversicolor. Aquat. Toxicol. 105, 403–411. https://doi.org/10.1016/j.aquatox.2011.07.014

da Costa, J.P., Santos, P.S.M., Duarte, A.C., Rocha-Santos, T., 2016. (Nano)plastics in the environment – Sources, fates and effects. Sci. Total Environ. 566, 15–26. https://doi.org/10.1016/j.scitotenv.2016.05.041

El-Toni, A.M., Yin, S., Hayasaka, Y., Sato, T., 2006. Synthesis and UV-shielding properties of silica-coated calcia-doped ceria nanoparticles via soft solution processes. J. Electroceramics 17, 9–14. https://doi.org/10.1007/s10832-006-9928-7

EU, 2011. Commission recommendation of 18 October 2011 on the definition of nanomaterial (2011/696/EU). Off. J. L 275, 38–40.

Eyrolle, F., Charmasson, S., 2004. Importance of colloids in the transport within the dissolved phase (< 450 nm) of artificial radionuclides from the Rhône river towards the Gulf of Lions (Mediterranean Sea). J. Environ. Radioact. 72, 273–286.

Eyrolle, F., Charmasson, S., 2001. Distribution of organic carbon, selected stable elements and artificial radionuclides among dissolved, colloidal and particulate phases in the Rhône River (France): Preliminary results. J. Environ. Radioact. 55, 145–155. https://doi.org/10.1016/S0265-931X(00)00188-0

Fabrega, J., Luoma, S.N., Tyler, C.R., Galloway, T.S., Lead, J.R., 2011. Silver nanoparticles: Behaviour and effects in the aquatic environment. Environ. Int. 37, 517–531. https://doi.org/10.1016/j.envint.2010.10.012

Faure, F., Demars, C., Wieser, O., Kunz, M., De Alencastro, L.F., 2015. Plastic pollution in Swiss surface waters: nature and concentrations, interaction with pollutants. Environ. Chem. 12, 582–591.

Fendall, L.S., Sewell, M.A., 2009. Contributing to marine pollution by washing your face: Microplastics in facial cleansers. Mar. Pollut. Bull. 58, 1225–1228. https://doi.org/10.1016/j.marpolbul.2009.04.025

Filella, M., 2007. Colloidal properties of submicron particles in natural waters. IUPAC Ser. Anal. Phys. Chem. Environ. Syst. 10, 17.

Gao, B.-Y., Yue, Q.-Y., Wang, Y., 2007. Coagulation performance of polyaluminum silicate chloride (PASiC) for water and wastewater treatment. Sep. Purif. Technol. 56, 225–230.

Ghosh, S., Jiang, W., McClements, J.D., Xing, B., 2011. Colloidal stability of magnetic iron oxide nanoparticles: Influence of natural organic matter and synthetic polyelectrolytes. Langmuir 27, 8036–8043. https://doi.org/10.1021/la200772e

Gigault, J., Pedrono, B., Maxit, B., Halle, A.T., 2016. Marine plastic litter: the unanalyzed nano-fraction. Environ. Sci. Nano 3, 346–350. https://doi.org/10.1039/C6EN00008H

Gottschalk, F., Nowack, B., 2011. The release of engineered nanomaterials to the environment. J. Environ. Monit. 13, 1145–1155.

Gottschalk, F., Sonderer, T., Scholz, R.W., Nowack, B., 2009. Modeled Environmental Concentrations of Engineered Nanomaterials (TiO2, ZnO, Ag, CNT, Fullerenes) for Different Regions. Environ. Sci. Technol. 43, 9216–9222. https://doi.org/10.1021/es9015553

Gregory, J., 2005. Particles in water: properties and processes. CRC Press.

Gregory, J., 1973. Rates of flocculation of latex particles by cationic polymers. J. Colloid Interface Sci. 42, 448–456. https://doi.org/10.1016/0021-9797(73)90311-1

Honda, R.J., Keene, V., Daniels, L., Walker, S.L., 2014. Removal of TiO2 Nanoparticles During Primary Water Treatment: Role of Coagulant Type, Dose, and Nanoparticle Concentration. Environ. Eng. Sci. 31, 127–134. https://doi.org/10.1089/ees.2013.0269

Jolivet, J.-P., Henry, M., Livage, J., 2000. Metal oxide chemistry and synthesis: from solution to solid state. Wiley-Blackwell.

Keller, A.A., McFerran, S., Lazareva, A., Suh, S., 2013. Global life cycle releases of engineered nanomaterials. J. Nanoparticle Res. 15, 1–17.

Khot, L.R., Sankaran, S., Maja, J.M., Ehsani, R., Schuster, E.W., 2012. Applications of nanomaterials in agricultural production and crop protection: a review. Crop Prot. 35, 64–70.

Kobayashi, M., Nitanai, M., Satta, N., Adachi, Y., 2013. Coagulation and charging of latex particles in the presence of imogolite. Colloids Surf. Physicochem. Eng. Asp. 435, 139–146. https://doi.org/10.1016/j.colsurfa.2012.12.057

Lambert, S., Wagner, M., 2016. Characterisation of nanoplastics during the degradation of polystyrene. Chemosphere 145, 265–268. https://doi.org/10.1016/j.chemosphere.2015.11.078

Larue, O., Vorobiev, E., Vu, C., Durand, B., 2003. Electrocoagulation and coagulation by iron of latex particles in aqueous suspensions. Sep. Purif. Technol. 31, 177–192.

Lee, H., Shim, W.J., Kwon, J.-H., 2014. Sorption capacity of plastic debris for hydrophobic organic chemicals. Sci. Total Environ. 470–471, 1545–1552. https://doi.org/10.1016/j.scitotenv.2013.08.023

Leslie, H.A., Van Velzen, M.J.M., Vethaak, A.D., 2013. Microplastic survey of the Dutch environment. Nov. Data Set Microplastics North Sea Sediments Treat. Wastewater Effl. Mar. Biota Amst. Inst. Environ. Stud. VU Univ. Amst.

Li, K., Zhang, W., Huang, Y., Chen, Y., 2011. Aggregation kinetics of CeO2 nanoparticles in KCl and CaCl2 solutions: measurements and modeling. J. Nanoparticle Res. 13, 6483–6491. https://doi.org/10.1007/s11051-011-0548-z

Lin, J.-L., Pan, J.R., Huang, C., 2013. Enhanced particle destabilization and aggregation by flash-mixing coagulation for drinking water treatment. Sep. Purif. Technol.

Liu, J., Legros, S., Ma, G., Veinot, J.G.C., von der Kammer, F., Hofmann, T., 2012. Influence of surface functionalization and particle size on the aggregation kinetics of engineered nanoparticles. Chemosphere 87, 918–924. https://doi.org/10.1016/j.chemosphere.2012.01.045

Liu, X., Ray, J.R., Neil, C.W., Li, Q., Jun, Y.-S., 2015. Enhanced Colloidal Stability of CeO2 Nanoparticles by Ferrous Ions: Adsorption, Redox Reaction, and Surface Precipitation. Environ. Sci. Technol. 49, 5476–5483. https://doi.org/10.1021/es506363x

Loosli, F., Coustumer, P.L., Stoll, S., 2013. TiO2 nanoparticles aggregation and disaggregation in presence of alginate and Suwannee River humic acids. pH and concentration effects on nanoparticle stability. Water Res. 47, 6052–6063.

Loosli, F., Le Coustumer, P., Stoll, S., 2014. Effect of natural organic matter on the disagglomeration of manufactured TiO2 nanoparticles. Environ. Sci. Nano 1, 154–160.

Mohd Omar, F., Abdul Aziz, H., Stoll, S., 2014. Aggregation and disaggregation of ZnO nanoparticles: Influence of pH and adsorption of Suwannee River humic acid. Sci. Total Environ. 468–469, 195–201. https://doi.org/10.1016/j.scitotenv.2013.08.044

Moos, N. von, Bowen, P., Slaveykova, V.I., 2014. Bioavailability of inorganic nanoparticles to planktonic bacteria and aquatic microalgae in freshwater. Environ. Sci. Nano 1, 214–232. https://doi.org/10.1039/C3EN00054K

Neal, C., Jarvie, H., Rowland, P., Lawler, A., Sleep, D., Scholefield, P., 2011. Titanium in UK rural, agricultural and urban/industrial rivers: Geogenic and anthropogenic colloidal/sub-colloidal sources and the significance of within-river retention. Sci. Total Environ. 409, 1843–1853.

Oriekhova, O., Stoll, S., 2016a. Effects of pH and fulvic acids concentration on the stability of fulvic acids – cerium (IV) oxide nanoparticle complexes. Chemosphere 144, 131–137. https://doi.org/10.1016/j.chemosphere.2015.08.057

Oriekhova, O., Stoll, S., 2016b. Stability of uncoated and fulvic acids coated manufactured CeO2 nanoparticles in various conditions: From ultrapure to natural Lake Geneva waters. Sci. Total Environ. 562, 327–334. https://doi.org/10.1016/j.scitotenv.2016.03.184

Piccinno, F., Gottschalk, F., Seeger, S., Nowack, B., 2012. Industrial production quantities and uses of ten engineered nanomaterials in Europe and the world. J. Nanoparticle Res. 14, 1–11. https://doi.org/10.1007/s11051-012-1109-9

Pinheiro, I., Ferreira, P.J., Garcia, F.A., Reis, M.S., Pereira, A.C., Wandrey, C., Ahmadloo, H., Amaral, J.L., Hunkeler, D., Rasteiro, M.G., 2013. An experimental design methodology to evaluate the importance of different parameters on flocculation by polyelectrolytes. Powder Technol., Special Issue: 5th International Granulation Workshop Granulation across the length scale 2011 238, 2–13. https://doi.org/10.1016/j.powtec.2012.08.004

Plastics-the Facts 2016. An analysis of European plastics production, demand and waste data, 2016. . Plastics Europe.

Quik, J.T.K., Lynch, I., Hoecke, K.V., Miermans, C.J.H., Schamphelaere, K.A.C.D., Janssen, C.R., Dawson, K.A., Stuart, M.A.C., Meent, D.V.D., 2010. Effect of natural organic matter on cerium dioxide nanoparticles settling in model fresh water. Chemosphere 81, 711–715. https://doi.org/10.1016/j.chemosphere.2010.07.062

Reed, K., Cormack, A., Kulkarni, A., Mayton, M., Sayle, D., Klaessig, F., Stadler, B., 2014. Exploring the properties and applications of nanoceria: is there still plenty of room at the bottom? Environ. Sci. Nano 1, 390–405. https://doi.org/10.1039/C4EN00079J

Rodea-Palomares, I., Boltes, K., Fernández-Piñas, F., Leganés, F., García-Calvo, E., Santiago, J., Rosal, R., 2011. Physicochemical characterization and ecotoxicological assessment of CeO2 nanoparticles using two aquatic microorganisms. Toxicol. Sci. 119, 135–145.

Röhder, L.A., Brandt, T., Sigg, L., Behra, R., 2014. Influence of agglomeration of cerium oxide nanoparticles and speciation of cerium(III) on short term effects to the green algae Chlamydomonas reinhardtii. Aquat. Toxicol. 152, 121–130. https://doi.org/10.1016/j.aquatox.2014.03.027

Safi, M., Sarrouj, H., Sandre, O., Mignet, N., Berret, J.-F., 2010. Interactions between sub-10 nm iron and cerium oxide nanoparticles and 3T3 fibroblasts : the role of the coating and aggregation state. Nanotechnology 21, 145103. https://doi.org/10.1088/0957-4484/21/14/145103

Sajith, V., Sobhan, C.B., Peterson, G.P., 2010. Experimental investigations on the effects of cerium oxide nanoparticle fuel additives on biodiesel. Adv. Mech. Eng. 2010, e581407. https://doi.org/10.1155/2010/581407

Silvestre, C., Duraccio, D., Cimmino, S., 2011. Food packaging based on polymer nanomaterials. Prog. Polym. Sci. 36, 1766–1782.

Slomberg, D.L., Ollivier, P., Radakovitch, O., Baran, N., Sani-Kast, N., Miche, H., Borschneck, D., Grauby, O., Bruchet, A., Scheringer, M., Labille, J., 2016. Characterisation of suspended particulate matter in the Rhone River: insights into analogue selection. Environ. Chem.

Stone, V., Nowack, B., Baun, A., van den Brink, N., von der Kammer, F., Dusinska, M., Handy, R., Hankin, S., Hassellöv, M., Joner, E., Fernandes, T.F., 2010. Nanomaterials for environmental studies: Classification, reference material issues, and strategies for physico-chemical characterisation. Sci. Total Environ. 408, 1745–1754. https://doi.org/10.1016/j.scitotenv.2009.10.035

Sun, C., Li, H., Chen, L., 2012. Nanostructured ceria-based materials: synthesis, properties, and applications. Energy Environ. Sci. 5, 8475–8505.

Syberg, K., Khan, F.R., Selck, H., Palmqvist, A., Banta, G.T., Daley, J., Sano, L., Duhaime, M.B., 2015. Microplastics: addressing ecological risk through lessons learned. Environ. Toxicol. Chem. 34, 945–953. https://doi.org/10.1002/etc.2914

Tella, M., Auffan, M., Brousset, L., Issartel, J., Kieffer, I., Paillès, C., Morel, E., Santaella, C., Angeletti, B., Artells, E., 2014. Transfer, Transformation, and Impacts of Ceria Nanomaterials in Aquatic Mesocosms Simulating a Pond Ecosystem. Environ. Sci. Technol. 48, 9004–9013.

Ter Halle, A., Jeanneau, L., Martignac, M., Jardé, E., Pedrono, B., Brach, L., Gigault, J., 2017. Nanoplastic in the North Atlantic Subtropical Gyre. Environ. Sci. Technol. 51, 13689–13697. https://doi.org/10.1021/acs.est.7b03667

Teuten, E.L., Saquing, J.M., Knappe, D.R., Barlaz, M.A., Jonsson, S., Björn, A., Rowland, S.J., Thompson, R.C., Galloway, T.S., Yamashita, R., 2009. Transport and release of chemicals from plastics to the environment and to wildlife. Philos. Trans. R. Soc. B Biol. Sci. 364, 2027–2045.

Thompson, R.C., 2006. Plastic debris in the marine environment: consequences and solutions. Mar. Nat. Conserv. Eur. 193, 107–115.

Tungittiplakorn, W., Lion, L.W., Cohen, C., Kim, J.-Y., 2004. Engineered Polymeric Nanoparticles for Soil Remediation. Environ. Sci. Technol. 38, 1605–1610. https://doi.org/10.1021/es0348997

von Moos, N., Slaveykova, V.I., 2013. Oxidative stress induced by inorganic nanoparticles in bacteria and aquatic microalgae – state of the art and knowledge gaps. Nanotoxicology 8, 605–630. https://doi.org/10.3109/17435390.2013.809810

Wagner, M., Scherer, C., Alvarez-Muñoz, D., Brennholt, N., Bourrain, X., Buchinger, S., Fries, E., Grosbois, C., Klasmeier, J., Marti, T., Rodriguez-Mozaz, S., Urbatzka, R., Vethaak, A.D., Winther-Nielsen, M., Reifferscheid, G., 2014. Microplastics in freshwater ecosystems: what we know and what we need to know. Environ. Sci. Eur. 26, 12. https://doi.org/10.1186/s12302-014-0012-7

Weir, A., Westerhoff, P., Fabricius, L., Hristovski, K., von Goetz, N., 2012. Titanium Dioxide Nanoparticles in Food and Personal Care Products. Environ. Sci. Technol. 46, 2242–2250. https://doi.org/10.1021/es204168d

Westerhoff, P., Song, G., Hristovski, K., Kiser, M.A., 2011. Occurrence and removal of titanium at full scale wastewater treatment plants: implications for TiO2 nanomaterials. J. Environ. Monit. 13, 1195–1203.

Wright, S.L., Thompson, R.C., Galloway, T.S., 2013. The physical impacts of microplastics on marine organisms: a review. Environ. Pollut. 178, 483–492.

Zhang, W., Crittenden, J., Li, K., Chen, Y., 2012. Attachment Efficiency of Nanoparticle Aggregation in Aqueous Dispersions: Modeling and Experimental Validation. Environ. Sci. Technol. 46, 7054–7062. https://doi.org/10.1021/es203623z

Zou, J., Zhu, H., Wang, F., Sui, H., Fan, J., 2011. Preparation of a new inorganic–organic composite flocculant used in solid–liquid separation for waste drilling fluid. Chem. Eng. J. 171, 350–356.

Chapter II

Theoretical and experimental approaches

II.1 Theoretical approach

Particles in water exhibit various interactions. Stability of particles is defined by the forces which underlay the interactions. If attractive forces dominate, particles are destabilised, they will attach to each other and aggregate. To the contrary, when the repulsive forces dominate particles are stable (Gregory, 2005). There are different types of interaction between two colloidal particles in suspension such as van der Waals, electrical double layer, hydration effects, hydrophobic, steric interaction of adsorbed layers, polymer bridging. Quantitative theory that describes stability of colloidal suspensions and takes into account the van der Waals and electrical double layer interactions is called DLVO theory and was developed by Derjaguin, Landau, Verwey and Overbeek (Derjaguin and Landau, 1941; Overbeek and Verwey, 1948). Other mentioned interactions were not taken into account in DLVO theory and are called non-DLVO interactions.

II.1.1 DLVO theory

The DLVO theory describes the total interaction energy between particles (V_T) as the sum of van der Waals attractions (V_{vdW}) and electrical double layer repulsions (V_{DL}) (equation II.1) (Elimelech et al., 1998):

$$V_T = V_{vdW} + V_{DL} \qquad \text{(II.1)}$$

The van der Waals forces depend on the electrical, magnetic and geometrical properties of the interacting particles and are composed of Keesom, Debye and London forces, in which properties of interacting particles in specific medium are described by the Hamaker constant. The electrostatic double layer repulsion forces are related to the properties of the electrical double layer around the particles and depend on the type of particles used (effect of surface charge and density), the pH and the ionic strength of the medium (Elimelech et al., 1998, Petosa et al., 2010).

II.1.1.1 Homo- and heteroaggregation

Homoaggregation refers to the interaction between identical particles (Fig. II.1). For example, homoaggregation between hematite or fullerene C_{60} nanoparticles in increasing electrolyte concentrations (Chen et al., 2006; Chen and Elimelech, 2007). Whereas, heteroaggregation refers to the interactions between different particles. For example,

titanium dioxide nanoparticle with silicon dioxide particles (Praetorius et al., 2014). There are various possible scenarios. Interactions between particles with the same or different size, with the same surface charge or oppositely charged or between charged and uncharged particles (Chen et al., 2016; Israelachvili, 2011). Heteroaggregation processes are time dependent and are characterised, first by formation of dimers, then trimers and finally larger aggregates (Fig. II.1).

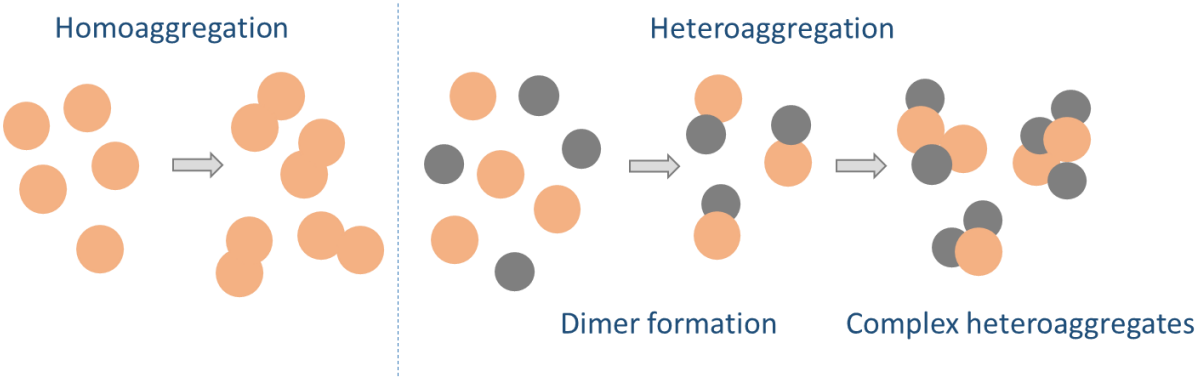

Fig. II.1. Schematic representation of the formation of homo- and heteroaggregates.

II.1.1.2 Smoluchowski approach

The aggregation process between two spherical particles was quantitatively described by von Smoluchowski (Smoluchowski, 1918). The rate of change of concentration of aggregates with size *m* formed by particles *i* and *j* (*m= i+ j*) is given by:

$$\frac{dn_m}{dt} = \frac{1}{2}\sum_{i=m-j=1}^{m-1} k_{ij} n_i n_j - n_m \sum_{m=1}^{\infty} k_{im} n_i \qquad \text{(II.2)}$$

were n_i is the number of aggregates of size *i*, n_j is the number of aggregates of size *j*, k_{ij} is the second-order kinetic rate constant.

Thus, the concentration of *m*-aggregate number is resulting from the formation and from the disappearance of aggregates with size *m*.

II.1.1.3 Kinetic aggregation rate

The kinetic rate constant is composed from two contributions (equation I.3) according to

$$k_{ij} = k_{ij}^{coll} \cdot \alpha_{ij} \qquad \text{(II.3)}$$

were k_{ij}^{coll} is the collision rate constant and α_{ij} is the attachment efficiency.

The collision rate constant depends on the physical factors such as temperature, particle size and density, hydrodynamic of flux. The attachment efficiency depends on chemical forces and defines the sticking probability, i.e. the probability that collision results in the formation of permanent bound.

The attachment efficiency can be defined as the inverse of the stability ratio (W) and depends on the balance between repulsive and attractive forces. To calculate the attachment efficiency the following equation can be used:

$$\alpha = \frac{1}{W} = \frac{k}{k_{\max}} \qquad \text{(II.4)}$$

were k is the aggregation rate of the studied system at any specific moment and k_{max} is the aggregation rate when all the collision between particles are efficient, i.e. results in the formation of permanent bonds.

When α = 0 the repulsive forces are dominant, no aggregation is observed. When α = 1 the attractive forces dominate and each collision is efficient and results in the formation of aggregates. This aggregation is also called diffusion limited aggregation (DLA) or fast aggregation and is controlled by the particle diffusion in medium. When α is between 0 and 1 we observe a reaction limited aggregation (RLA) which is controlled by the chemical reactivity of the particles. Such regime is also called slow regime since collision between particles are not efficient. The aggregation time when the transition between two regimes is observed allows us to determine the critical coagulation concentration (CCC), i.e. the electrolyte concentration required to reach the DLA regime.

The aggregation rate can be determined experimentally using the time resolved dynamic light scattering method (Metreveli et al., 2015; Zhang et al., 2012). The slope of the increase of the z-average hydrodynamic diameter versus time (dD_h/dt) can be fitted by a linear function in order to obtain the aggregation rate of a system in specific conditions. The attachment efficiency is then calculated by normalising the slopes obtained in different conditions (for example, at low ionic strength) by the slope obtained under DLA. The attachment efficiency calculated using the speed of the formation of the aggregates by measuring z-average hydrodynamic diameters is a global attachment efficiency, meaning representing the global behaviour of aggregating system.

II.1.2 Modelling of coagulant species

Iron(III) chloride ($FeCl_3$) was used as a coagulant in Paper IV Chapter VII to destabilise microplastic particles in suspension. For data interpretation, iron speciation determination consists an important issue. For that purpose, the MINTEQA2 software (developed by Allison Geoscience Consultants Inc. and HydroGeologic Inc.) was used to perform the modelling of iron(III) species. MINTEQA2 applies the thermodynamic and mass balance equations to solve geochemical equilibria and calculate the ion speciation/solubility. The calculation is divided in three stages: i) the computation of the activities of cationic and anionic species and neutral ion pairs, ii) the computation of the solubility of solids and minerals and iii) the calculation of the mass of solid that precipitates or dissolves by mass transfer submodel. (Ball et al., 1980; Felmy et al., 1984; Peterson et al., 1987).

To compute the activity coefficients the Davies equation is used (II.5) and the other parameters which are used during modelling are presented in Table II.1.

$$-\log f_{\pm} = 0.5 z_1 z_2 \left(\frac{\sqrt{I}}{1+\sqrt{I}} - 0.15 I \right), \qquad \text{(II.5)}$$

where $f_{\pm}$ is the mean modal activity coefficient of an electrolyte which dissociates into ions with charge z_1 and z_2 and I represents the ionic strength.

Table II.1. Parameters used for iron species modelling in MINTEQA2 software

Parameter	Value
Temperature, °K	298
Concentration of $FeCl_3$, mg/L	2
pH	1 – 12
Ionic strength, mol/L	$3.6 \cdot 10^{-5}$ – $6.2 \cdot 10^{-2}$ *

*pH dependent, calculated.

After salt dissolution hydrolysis occurred consequently. Many species, such as Fe^{3+}, $Fe(OH)^{2+}$, $Fe(OH)_2^{+}$, $Fe(OH)_3$ and $Fe(OH)_4^{-}$ can coexist in solution at the same time. The results of the modelling is presented in fig. II.2.

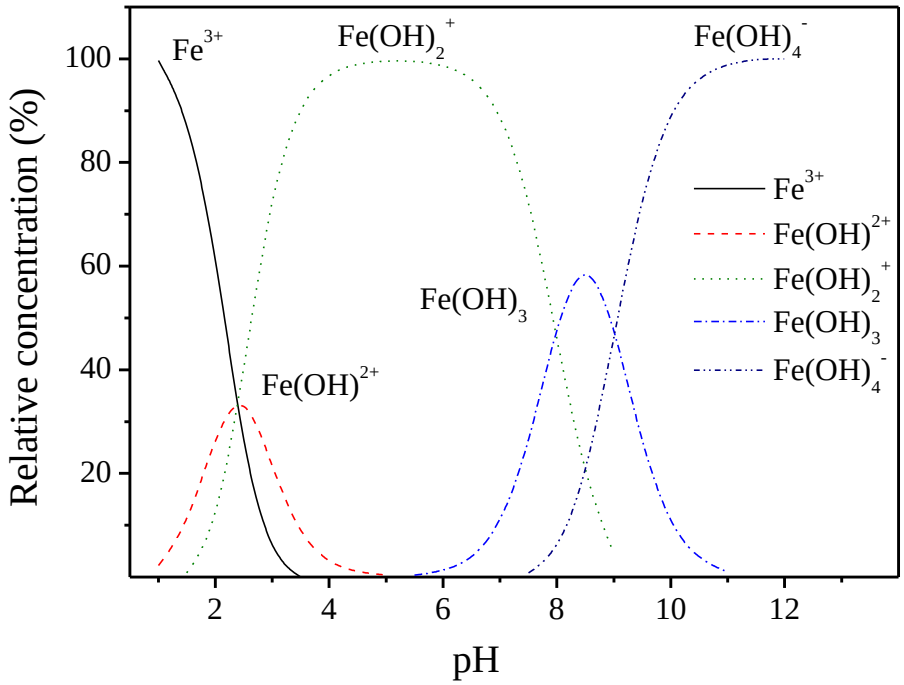

Fig. II.2. Speciation of iron(III) as a function of pH for a $FeCl_3$ solution at 2 mg/L. Fe^{3+} and $Fe(OH)^{2+}$ are mainly present in solution at pH less than 3. In the pH range from 4 to 6 the highest relative concentration is obtained for $Fe(OH)_2^{+}$ and at pH greater than 7 $Fe(OH)_4^{-}$ and insoluble $Fe(OH)_3$ are present.

The concentration of these species depends on pH and can be described by equations of hydrolysis equilibrium (equations (II.6) – (II.10)) (Barnum, 1983; Cornell and Schwertmann, 2003; Stefánsson, 2007):

$Fe^{3+} + H_2O = Fe(OH)^{2+} + H^+$	log K = – 2.19	(II.6)
$Fe^{3+} + 2H_2O = Fe(OH)_2^{+} + 2H^+$	log K = – 5.67	(II.7)
$Fe^{3+} + 3H_2O = Fe(OH)_3 + 3H^+$	log K = – 11.9	(II.8)
$Fe^{3+} + 4H_2O = Fe(OH)_4^{-} + 4H^+$	log K = – 21.6	(II.9)
$2Fe^{3+} + 2H_2O = Fe_2(OH)_2^{4+} + 2H^+$	log K = – 2.95	(II.10)

Therefore, Fe^{3+} and $Fe(OH)^{2+}$ are mainly present in solution at pH less than 3. In the pH range from 4 to 6 the highest relative concentration is obtained for $Fe(OH)_2^{+}$ and at pH greater than 7 $Fe(OH)_4^{-}$ and insoluble $Fe(OH)_3$ are present.

II.2 Experimental approach

II.2.1 Materials

II.2.1.1 CeO_2 NPs

CeO_2 NPs (code name NM-212) uncoated particles, as a powder were provided from JRC (Joint Research Centre) nanomaterial repository (Ispra, Italy). These NPs are representative test materials coming from a single batch in order to insure the reproducibility of results between different laboratories. The nominal particle diameter is equal to 28 ± 10 nm with a specific surface area of 27.2 ± 0.9 m^2/g (Singh et al., 2014). The suspension of NPs was prepared according to the dispersion protocol provided in Annex 1.2. Briefly, a 1 g/L stock suspension at pH 3.0 ± 0.1 was prepared and then sonicated with ultrasonic probe (Sonics Vibra cell, Blanc Labo S.A., Switzerland). The dilution of stock suspension by ultrapure water (Milli Q water, Millipore, Switzerland, with R > 18MOhm, TOC < 2ppb) was made to obtain the desirable particle concentration. pH was adjusted by adding appropriate amount of diluted HCl and NaOH (Merck, Germany).

The hydrodynamic diameters measured using two methods NTA and DLS are in good agreement and are equal to 177 ± 83 nm by NTA and 185 ± 75 nm by DLS (Fig. II.3).

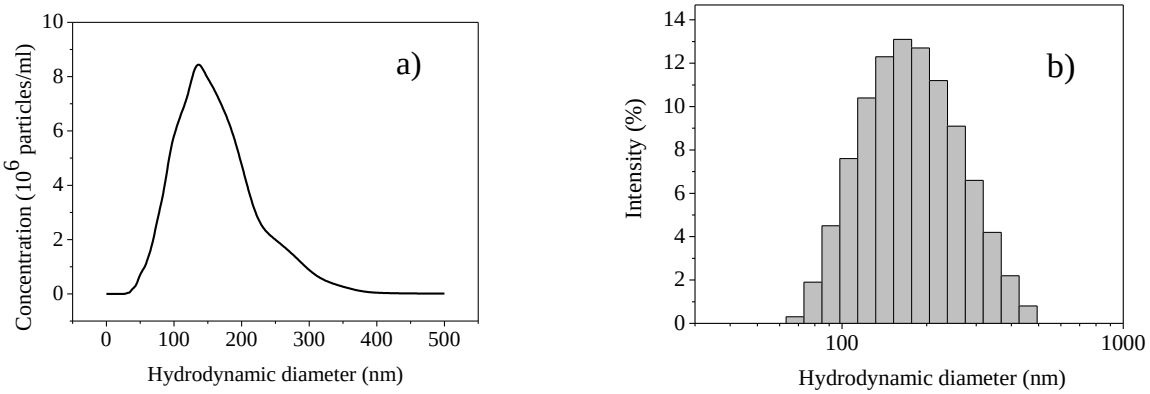

Fig. II.3. Size distribution of CeO_2 NPs using two methods NTA (a) and DLS (b). Z-average diameter and hydrodynamic diameter were equal to 177 ± 83 nm (NTA) and 185 ± 75 nm (DLS). A good agreement was found between these two methods indicating that individual CeO_2 NPs are forming aggregates. Experimental conditions: [CeO_2] = 10 mg/L (NTA), [CeO_2] = 50 mg/L (DLS), pH 3.0 ± 0.1.

Indicating that pristine CeO_2 NPs are forming homoaggregates when dispersed in ultrapure water. In SEM image (Fig. II.4) we can also distinguish individual particles from

homoaggregates and estimated size of pristine particles is in a good agreement with data provided by manufacturer.

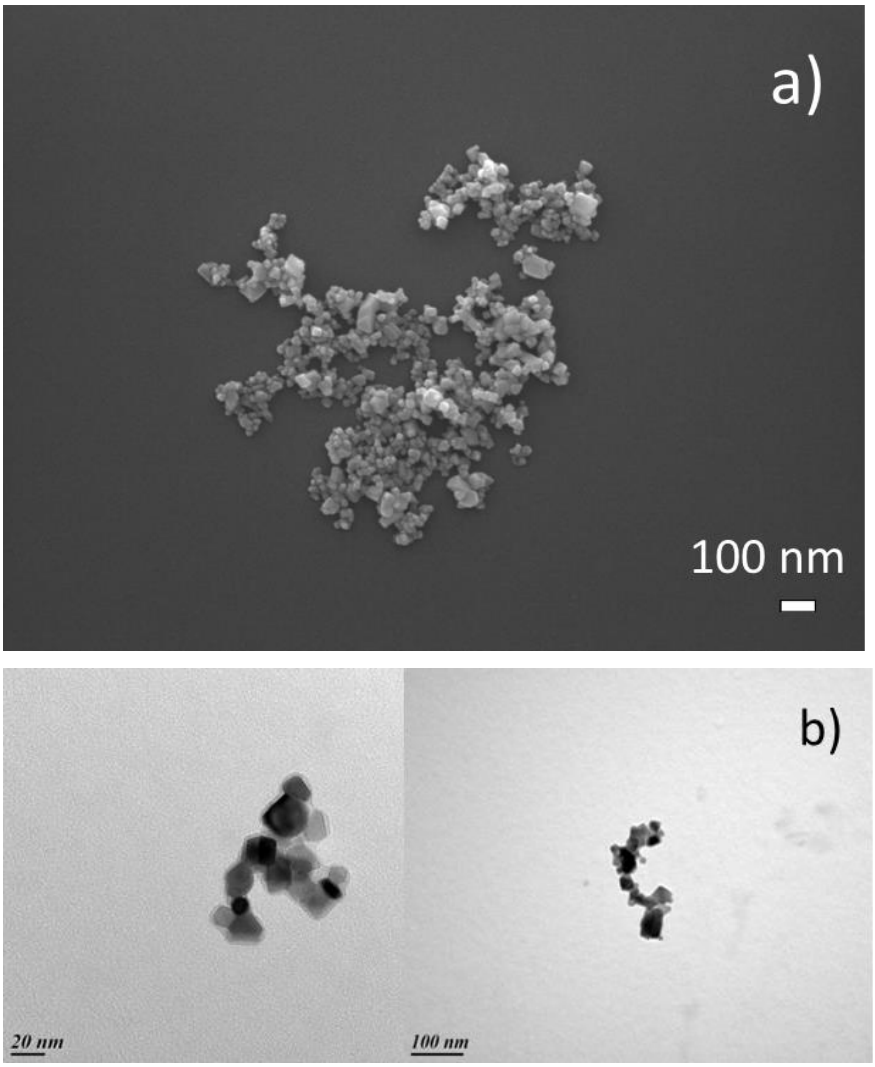

Fig. II.4. (a) SEM and (b) TEM image of pristine CeO_2 NPs in ultrapure water. [CeO_2] = 10 mg/L.

II.2.1.2 Nanoplastics and microplastics

As a plastic material we used polystyrene (PS) particles since this type of plastic is used in many applications for example in packaging, building and construction, electrical and electronics industries, and paints. The demand on polystyrene in Europe, including expanded polystyrene, reaches the level of $3.4 \cdot 10^6$ tonnes per year (Plastics-the Facts, 2016), thus, making this plastic materials extensively present in the environment. In addition, PS plastics are difficult to recycle and are highly resistant to biodegradation (Chaukura et al., 2016; Kaplan et al., 1979).

PS particles which we use in this study are available as dispersions and serve as model particles to assess the behaviour of PS nanoplastics in the environment. Latex polystyrene nanospheres were provided from Molecular Probes® (Life Technologies Corporation, USA) with a mean diameter equal to 20 ± 0.3 nm, density equal to 1.055 g/cm^3 (20°C) and specific surface area of 2.8·10^6 cm^2/g (provided by the manufacturer). Using SEM image analysis (Fig. II.5B) estimated size of the pristine nanoplastics was found between 25 and 63 nm.

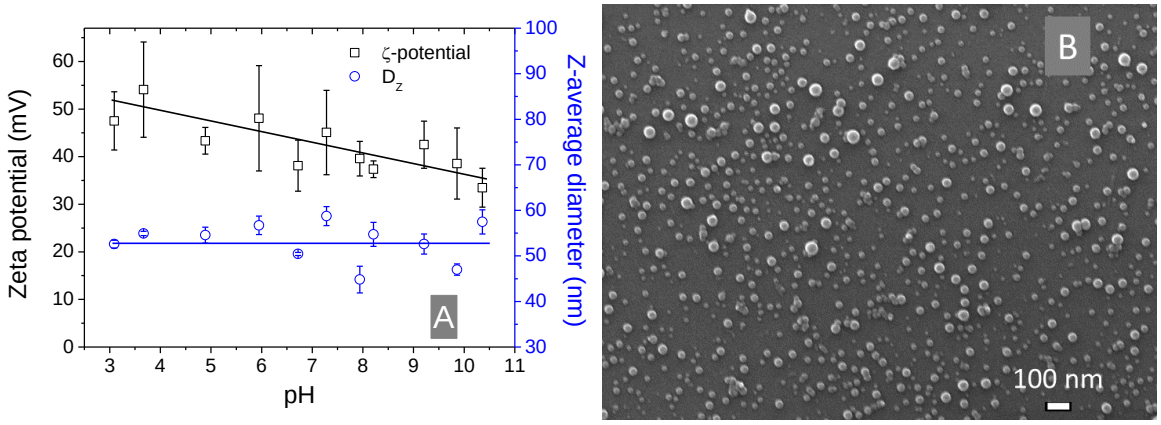

Fig. II.5. (A) Zeta potential and z-average hydrodynamic diameter of PS nanoplastic particles at different pH in ultrapure water. Zeta potential is decreasing with increase of pH. Z-average hydrodynamic diameter is found constant with a mean value equal to 53.1 ± 4.3 nm. Experimental conditions: [PS] = 50 mg/L, initial pH 3. (B) SEM image of pristine nanoplastics in ultrapure water: [PS] = 5 mg/L, the diameter of PS particles is found between 25 and 63 nm.

These PS nanoplastics are positively charged in a large pH domain (Fig. II.5A) with a surface charge density equal to 3.0 µC/cm^2, due to the presence of amidine groups. In aquatic systems, positive charges of nanoplastics favours the interaction with negatively charged natural colloids. A 400 mg/L stock suspension of nanoplastics at pH 3.0 was prepared by diluting original suspension with ultrapure water (R > 18 MΩ cm, Millipore, Switzerland) for which pH was previously adjusted to 3.

On the other hand, we used microplastic particles which are also made of polystyrene. In that case we used negatively charged microplastics. Their negative charge is due to the presence of sulphate functional groups on the surface. IDC Latex particles (Life Technologies Corporation, USA) have a diameter 0.99 ± 0.03 µm (TEM measurement, provided by manufacturer), initial concentration 78 g/L, density 1.055 g/cm^3 (20°C), specific surface area 5.7·10^4 cm/g and were free from surfactants. A stock suspension of

1 g/L microplastic was prepared and then diluted to the appropriate concentration with Milli Q water (R > 18 MΩ·cm). The suspension pH was adjusted by adding small amount of diluted HCl and NaOH (Merck, Germany). Negative values of zeta potential through full pH range (Fig. II.6) confirms presence of negatively charged functional groups. Microplastic hydrodynamic diameter was found in good agreement with data provided by manufacturer and was found equal to 1098 ± 224 nm (Fig. II.4 Inset).

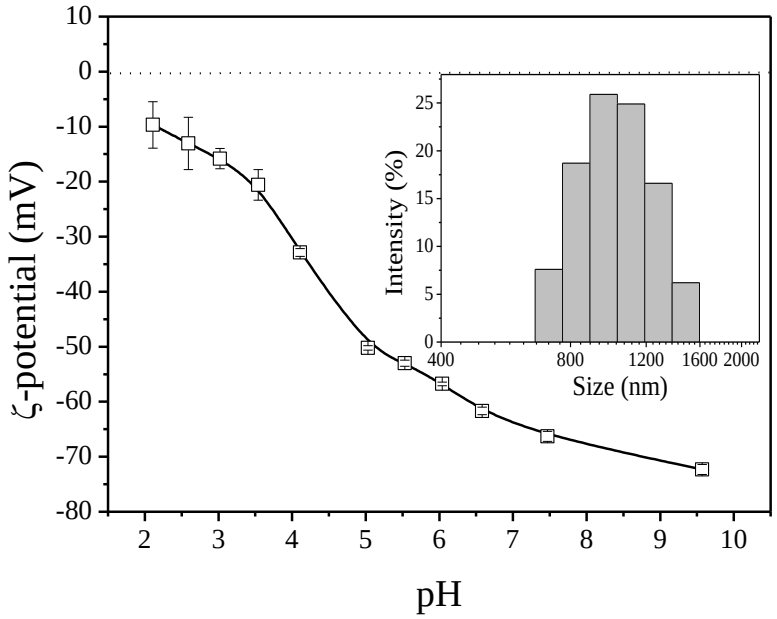

Fig. II.6. Zeta potential of sulphate polystyrene microplastic particles as a function of pH. Zeta potential is found negative in all pHs. Size distribution (inset) of particles using DLS method. Z-average hydrodynamic diameter is found equal to 1000 nm.

II.2.1.3 NOM

To evaluate the effect of NOM on the stability of ENMs released to natural water two types of materials have been considered, humic substances and polysaccharides.

As a surrogate of humic substance, the Suwannee River Fulvic acids (Standard II, 2S101F) were used and supplied by International Humic Substance Society (USA). FAs are mixtures of different types of organic acids and are more reactive compared to HAs due to the high concentration of hydroxyl (-OH) and carboxyl (-COOH) groups. Three structural models of FA molecules are presented in Fig. II.7 (Leenheer et al., 1995). FAs have low molecular weights and are soluble in a large pH range (Pettit, 2004). A 1 g/L suspension was first prepared from powder and then diluted to 100 mg/L by ultrapure

water. This suspension was our stock suspension from which we made our further dilutions.

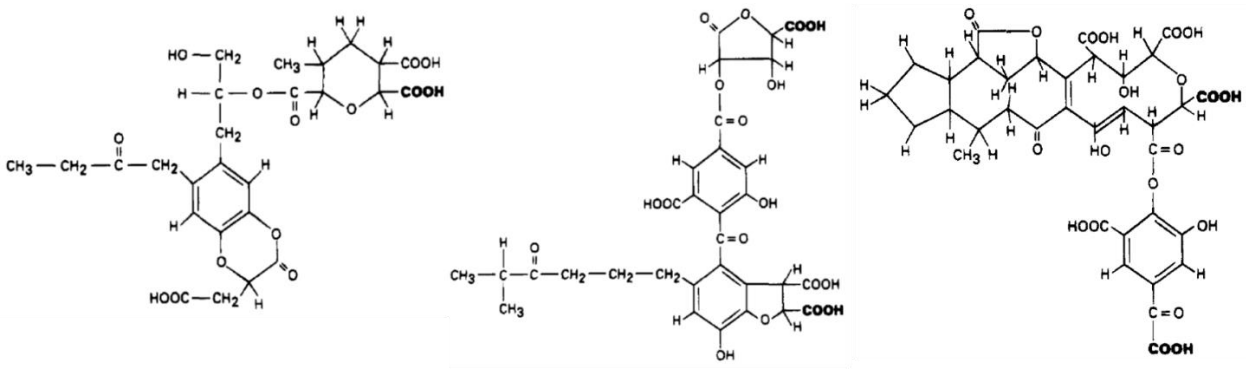

Fig. II.7. Structural models of Suwannee River fulvic acid molecules (Leenheer et al., 1995).

To characterize FAs a 50 mg/L suspension with addition of 0.001 M NaCl as background electrolyte was prepared at pH 3.0 ± 0.1. The titration was performed with diluted 0.01 M NaOH solution. FA surface charge was found negative through all pH range (Fig. II.8). All solutions were maintained in a dark place with temperature between 0 and 4 °C.

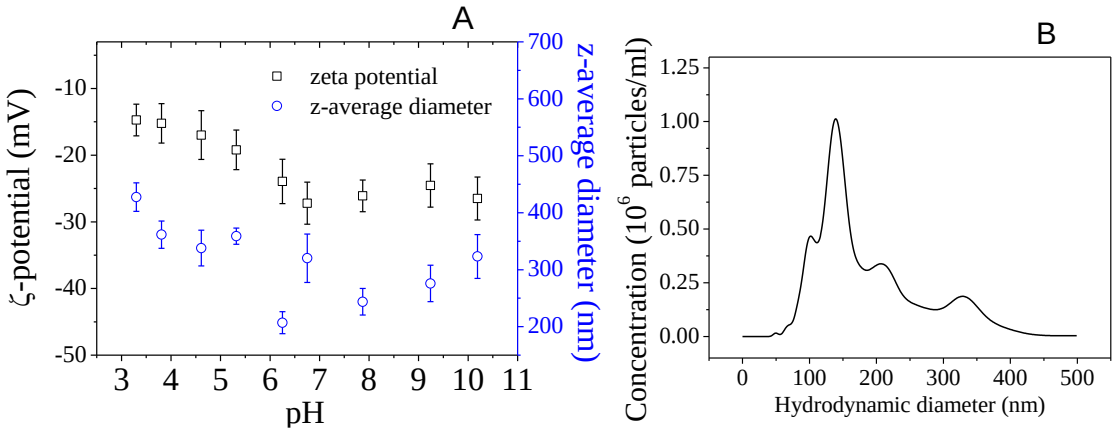

Fig. II.8. (A) FA zeta potential and z-average hydrodynamic diameter variation as a function of pH. Surface charges of FAs are negative at all pHs. Z-average hydrodynamic diameter varies from 200 to 400 nm. (B) FA size distribution is determined using NTA method. Average hydrodynamic diameter was found equal to 194 ± 89 nm. We observed the presence of polydisperse particles.

As a surrogate of natural polysaccharide we used alginate (A2158, Sigma Aldrich, Switzerland). The molecular weight of low viscosity alginate is equal to 50 kDa.(LeRoux et al., 1999). Alginate is a natural anionic polymer usually extracted from brown algae

such as *Laminaria hyperborea*, *Laminaria digitata*, *Laminaria japonica*, *Ascophyllum nodosum*, and *Macrocystis pyrifera*.

Alginate is a mixture of linear copolymers blocks of β-d-mannuronate (M) and α-l-guluronate (G) residues (Lee and Mooney, 2012). The carboxyl groups of mannuronic acid has a pK_a =3.38 and of guloronic acid pK_a =3.65 and can be protonated by inorganic acid. When the pH of solution is below the pK_a alginate tends to form a hydrogel (Rehm, 2009). The blocks of copolymers are composed of the individual or mixed residues (Fig. II.9A). We prepared a 100 mg/L stock solution in ultrapure water which was used for further dilution. To characterise alginate titration of 50 mg/L alginate solution was done. The variation of z-average diameters and zeta potential versus pH was recorded and presented in Fig. II.9B. To adjust the pH, diluted sodium hydroxide and hydrochloride acid 0.01 M (NaOH and HCl, Titrisol®113, Merck, Switzerland) were used. For suspension homogenisation, gentle agitation was applied during all the experiments with a magnet vortex and a rotational speed equal to 200 rpm.

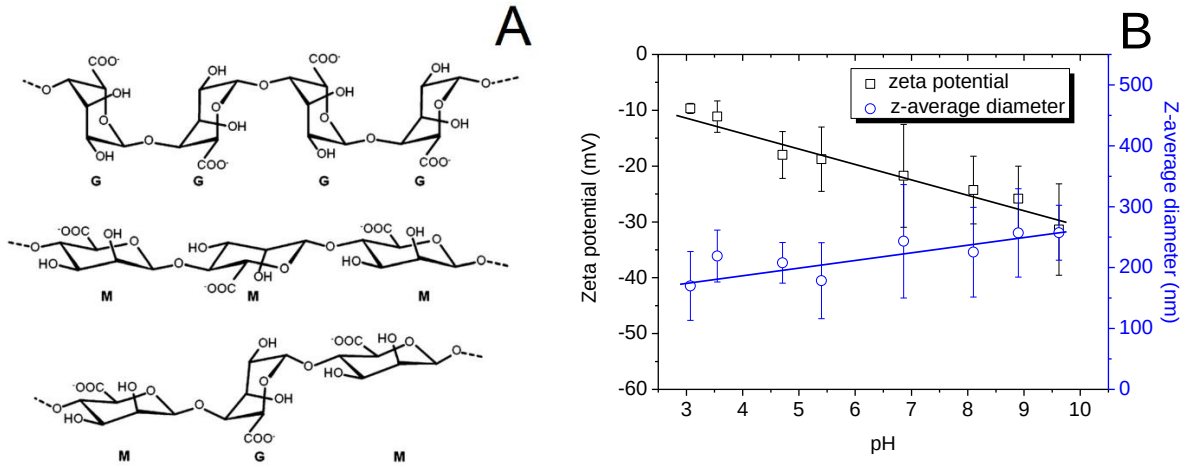

Fig. II.9. (A) Alginate structure composed from consecutive blocks of G, M and mixed MGM residues (Lee and Mooney, 2012). (B) Variation of alginate zeta potential and z-average hydrodynamic diameters as a function of pH. Zeta potential is negative in all pHs. Z-average diameters vary from 150 to 250 nm. Experimental conditions: [Alginate] = 50 mg/L.

II.2.1.4 ICs

As an analogue of inorganic colloids from river Rhône, iron (III) oxide (α-Fe_2O_3, 99%) (Nanoamor, Inc., USA) as a powder was used. The main characteristics of Fe_2O_3 are given in Table II.2. First, a 1 g/L suspension was prepared at pH 10. Such pH allows a better resuspension and higher stability of dispersed particles. Then, to obtain homogenised

suspension and well dispersed particles, sonication with an ultrasonic probe (CV18, Sonics Vibra cell, Blanc Labo S.A., Switzerland) during 15 min was performed. To prepare a 100 mg/L stock suspension, dilution with ultrapure water, for which pH was also previously adjusted to 10, was done. To characterise Fe_2O_3 particles we used SEM imaging (Fig. II.10A) and we measured z-average hydrodynamic diameter and zeta-potential as a function of pH (Fig. II.10B). Fe_2O_3 particles were found to have needle shapes. Zeta potential changed from negative to positive passing through a PZC at pH 5.8 ± 0.1. At environmentally relevant pH (pH 8.0 ± 0.2) Fe_2O_3 had a negative surface charge. Below the pH 5.0 and above the pH 8.0 nanoparticles are stable with z-average diameters less than 100 nm.

Table II.2. Characterisation analysis of Fe_2O_3 provided by manufacturer

Parameters	**Value**
Appearance	Red powder
pH value	6.7
Crystal	α
Original particle size, nm	30-50nm
Surface area, m^2/g	28
Purity, %	99.2

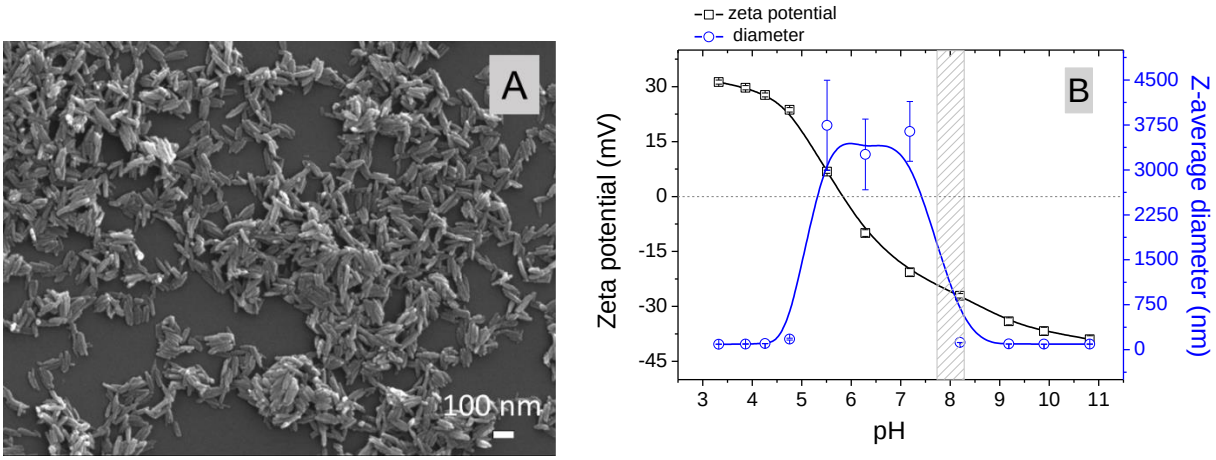

Fig. II.10. (A) SEM image of pristine Fe_2O_3 ICs in ultrapure water. (B) Fe_2O_3 IC zeta potential and z-average hydrodynamic diameter variation as a function of pH. Experimental conditions: [Fe_2O_3] = 10 mg/L. At environmental pH = 8.0 ± 0.2 Fe_2O_3 ICs are negatively charged.

II.2.2 Experimental technique

II.2.2.1 Dynamic light scattering (DLS) method and laser Doppler electrophoresis technique

Zeta potential ζ and z-average hydrodynamic diameter of particles were measured using a Malvern Zetasizer Nano ZS instrument (Malvern Instruments Ltd, UK). Schematic representation of the instrument is shown in Fig. II.11. A sample, containing particles of interest, is irradiated by the laser. The light scattered by particles is detected and then digital signal is processed in a correlator. Particles in a sample undergo Brownian motion, i.e. random movement due to the interaction with surrounded molecules. When particles are irradiated by the laser scattered light is changed. The fluctuation of the scattered light is fitted by one autocorrelation function to obtain the corresponding diffusion coefficient. Based on the diffusion coefficient and the properties of dispersion medium, we can define the hydrodynamic diameter using Stokes-Einstein equation (II.11) (Elimelech et al., 1998; Gregory, 2005).

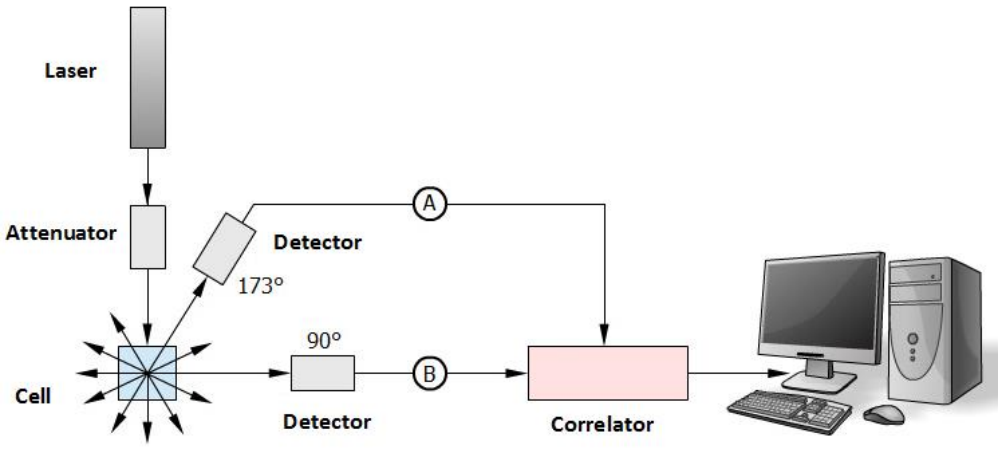

Fig. II.11. A schematic representation of DLS method using a Malvern Zetasizer Nano ZS instrument (Image from Malvern Instruments Ltd).

$$d_H = \frac{kT}{3\pi\eta D}, \qquad \text{(II.11)}$$

were d_H is hydrodynamic diameter of particles, D is the translational diffusion coefficient, k is the Boltzmann's constant, η is medium viscosity and T is the absolute temperature.

Charged particles suspended in a liquid will attract oppositely charged ions. Some of them are strongly bound, forming the so called Stern layer, others are loosely bound, forming a diffuse layer (Fig. II.12). When an electrical field is applied some of the ions will move together with particle and some of them not. The boundary defining the limit is called the slipping plane. The potential at the slipping plane is called the zeta potential. Malvern Zetasizer Nano ZS instrument uses laser Doppler electrophoresis technique to measure the particle velocity, when an electrical field is applied. A measuring cell has electrodes to which a potential is applied. Particles move towards the oppositely charged electrode, their velocity is measured and analysed to obtain electrophoretic mobility. Knowing the electrophoretic mobility and medium properties, the Henry equation (II.12) is used to calculate zeta potential.

$$U_E = \frac{2\varepsilon\xi}{3\eta} \cdot f(\mathrm{K}a), \qquad \text{(II.12)}$$

where ε corresponds to the relative permittivity ε_r (or dielectric constant) multiplied by the permittivity of free space, ε_0; η is the viscosity of the liquid; K is the Debye-Hükel parameter; a is the particle radius.

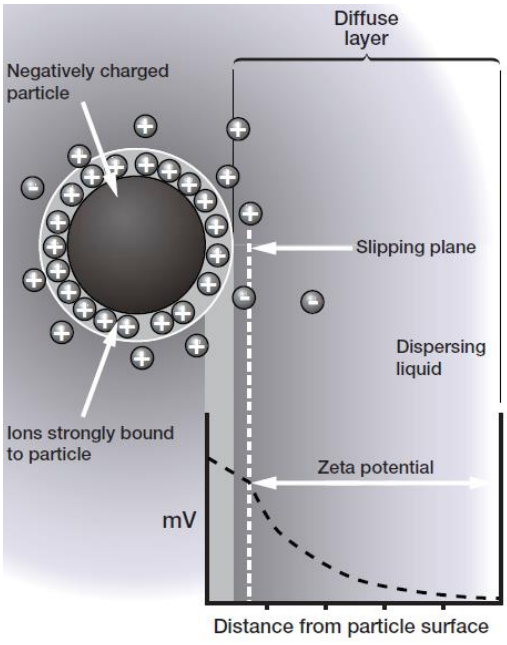

Fig. II.12. Schematic representation of double layer. The zeta potential is measured on the boundary of slipping plane (Image from Malvern Instruments Ltd).

To calculate *f(*K*a)* two approximations can be used depending on the particle size and sample ionic strength (Elimelech et al., 1998). The Smoluchowski approximation is used when the thickness of double layer is thin compared to particles size and the ionic strength is at least 10^{-3} M then *f(*K*a)* is equal to 3/2. Whereas, the Hückel approximation is used when the double layer is large compared to particle size and ionic strength is below 10^{-3} M then *f(*K*a)* is equal to 1. Using Smoluchowski approximation and inserting values for permittivity and viscosity of water at 298 °K, we obtain the relation between zeta potential and electrophoretic mobility (II.13):

$$\xi = 12.8 U_E , \qquad \text{(II.13)}$$

where ζ-potential is expressed in mV and electrophoretic mobility U_E in $\mu ms^{-1}/Vcm^{-1}$.

The advantages of DLS method are fast measurements (2-5 min per sample), easy sample handling, good reproducibility. Parameters (particle z-average hydrodynamic diameter and particle size distributions) are obtained in the same time and measurements are made in a broad range of sizes and concentrations of particle (1 – 1000 nm and 10^8 - 10^{12} particles/mL). However, the main drawback of the technique is an inaccurate determination of a particle size for a polydisperse sample. It happens because the results are biased toward bigger size particles due to the intensity of scattered light is proportional to the sixth power of particle radius ($I \sim d^6$) (Boyd et al., 2011; Hanus and Ploehn, 1999).

II.2.2.2 Nanoparticle tracking analysis method

Visualization and distribution of particles by size were investigated using nanoparticle tracking analysis (NTA) technique with a NanoSight LM14 instrument (NanoSight Ltd, UK).

The instrument uses a laser light source to illuminate nanoscale particles. The particles appear individually as point-scatterers moving under Brownian motion, the dispersed light is being captured by a high sensitivity camera, via the microscope (Fig. II.13). Particles are individually tracked and visualised on the screen of the control computer. NTA instrument captures a video of particles moving under Brownian motion and automatically locates and follows the centre of each particle. The device determines the average distance moved by each particle in *x* and *y* direction. The measurement is

done simultaneously for all particles. This value allows to obtain the diffusion coefficient and using the Stokes-Einstein equation (II.11) to calculate the sphere-equivalent, hydrodynamic diameter (Carr and Malloy, 2006; Hole et al., 2013).

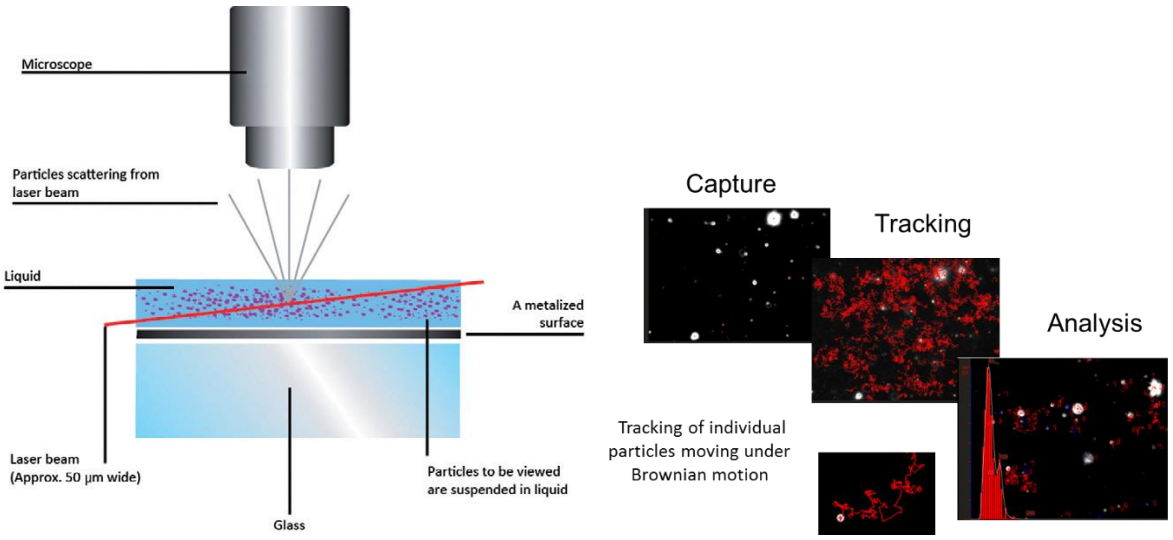

Fig. II.13. A schematic illustration of the nanoparticle visualisation using the NTA instrument. The main steps of particle tracking and analysis consist in capturing the video, tracking of individual particles moving under Brownian motion and analysis of the data (Image from NanoSight Ltd).

In order to visualize as many particles as possible and to reduce the noise to minimum level the camera settings should be appropriately adjusted during the video recording. The capture time is also to be adjusted according to the polydispersity of the sample. Higher sample polydispersity need longer capture times (from 90 to 160 sec).

There are many advantages of NTA technique such as an accurate measurement of the particle size for both monodisperse and polydisperse samples, a high peak resolution, the measurement of hydrodynamic diameter d_h directly and the size number distribution. The results obtained are based on particle by particle analysis and the possibility to visualize the sample. However, the results of measurements are highly dependent of the processing parameters and experimental protocol. The technique can be applied in a limited size and concentration range (size: 30 – 1000 nm and concentration: 10^7 – 10^9 particles/mL). The measurement and sample preparation are time consuming and labour intensive (Gallego-Urrea et al., 2010; Hole et al., 2013).

II.2.2.3 Electron microscopy methods

In order to obtain images of individual particles and aggregates and to visualise the morphology of particles, scanning electron microscopy (SEM) and transmission electron microscopy (TEM) were used. The schematic representation of the types of electrons detected by the techniques and schematic view of the both instrument are presented in Fig. II.14.

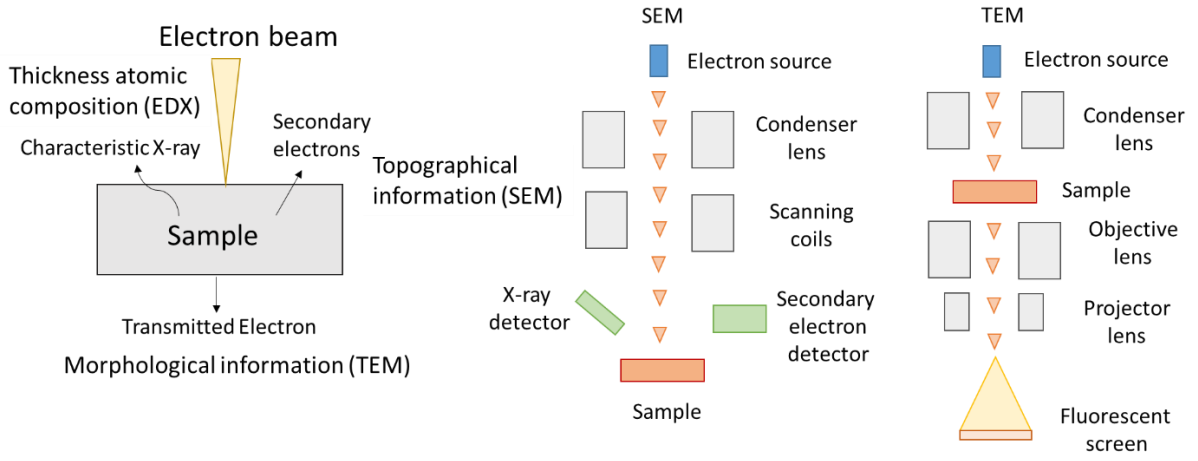

Fig. II.14. Schematic illustration of the working principle of electron microscopy methods (SEM and TEM).

SEM method provides the topographical information and chemical composition of the sample. A basic SEM consists of an electron gun that produces the electron beams with energy from 0.2 to 40 keV (Egerton, 2006). Electromagnetic optics is used to guide the beam and focus it. The detectors collect the electrons that come from the sample. When the electron beam interacts with the sample, different signals are emitted from different parts of the interaction volume. Typically, SEM detects secondary emitted electrons. The energy of the detected electron, its intensity and location of emission is used to put together the image. Other information that can be obtained using SEM is X-ray energy which depends on the elemental composition of the sample (Egerton, 2006). In our work we used a JEOL JSM-7001FA SEM operated with a following parameters: voltage 15 kV, probe current 1 nA.

In TEM, an electron beam penetrates a thin specimen and transmitted electrons are used to obtain the morphological information about the sample. The TEM is able to display the magnified images and to produce the electron-diffraction patterns in order to obtain crystallographic information.

TEM consists of the three main parts: the illumination system with the source of the electrons and lenses; the specimen stage, which contains the sample; and the imaging system with lenses. Electron beam can generate energy from 100 to 400 keV (Williams et al., 1998). The imaging lenses of a TEM produce a magnified image or an electron-diffraction pattern of the specimen on a viewing screen or camera system. The spatial resolution of the image is largely dependent on the quality and design of these lenses. Hitachi A7650 TEM was used in our work with a large aperture (100μm apparent diameter) operating under a 80 keV accelerating voltage.

The advantages of microscopic techniques are the possibility of a direct measurement of particle morphology and size, imaging of surface coating and modification. There are some drawbacks of the technique such as it is a time consuming analysis (image acquisition and analysis). During sample preparation the formation of artefacts is possible because of the drying process (aggregation). The equipment is expensive and the analysis is a subject of personal bias because the operator might overlook some particles. The operator should perform a particle-by-particle analysis in order to determine the particle edge in a consistent and reproducible manner.

II.3 References

Ball, J.W., Jenne, E.A., Nordstrom, D.K., 1980. Additional and revised thermochemical data and computer code for WATEQ2: A computerized chemical model for trace and major element speciation and mineral equilibria of natural waters. Water Resources Division, US Geological Survey.

Barnum, D.W., 1983. Hydrolysis of cations. Formation constants and standard free energies of formation of hydroxy complexes. Inorg. Chem. 22, 2297–2305. https://doi.org/10.1021/ic00158a016

Boyd, R.D., Pichaimuthu, S.K., Cuenat, A., 2011. New approach to inter-technique comparisons for nanoparticle size measurements; using atomic force microscopy, nanoparticle tracking analysis and dynamic light scattering. Colloids Surf. Physicochem. Eng. Asp. 387, 35–42.

Carr, B., Malloy, A., 2006. NanoParticle Tracking Analysis–The NANOSIGHT system.

Chaukura, N., Gwenzi, W., Bunhu, T., Ruziwa, D.T., Pumure, I., 2016. Potential uses and value-added products derived from waste polystyrene in developing countries: A review. Resour. Conserv. Recycl. 107, 157–165. https://doi.org/10.1016/j.resconrec.2015.10.031

Chen, K.L., Elimelech, M., 2007. Influence of humic acid on the aggregation kinetics of fullerene (C60) nanoparticles in monovalent and divalent electrolyte solutions. J. Colloid Interface Sci., Matijevic Festschrift 309, 126–134. https://doi.org/10.1016/j.jcis.2007.01.074

Chen, K.L., Mylon, S.E., Elimelech, M., 2006. Aggregation kinetics of alginate-coated hematite nanoparticles in monovalent and divalent electrolytes. Environ. Sci. Technol. 40, 1516–1523.

Chen, Q., Xu, S., Liu, Q., Masliyah, J., Xu, Z., 2016. QCM-D study of nanoparticle interactions. Adv. Colloid Interface Sci., Clayton Radke Festschrift 233, 94–114. https://doi.org/10.1016/j.cis.2015.10.004

Cornell, R.M., Schwertmann, U., 2003. The iron oxides: structure, properties, reactions, occurrences and uses. John Wiley & Sons.

Derjaguin, B., Landau, L., 1941. The theory of stability of highly charged lyophobic sols and coalescence of highly charged particles in electrolyte solutions. Acta Physicochim URSS 14, 58.

Egerton, R., 2006. Physical principles of electron microscopy: an introduction to TEM, SEM, and AEM. Springer Science & Business Media.

Elimelech, M., Jia, X., Gregory, J., Williams, R., 1998. Particle deposition & aggregation: measurement, modelling and simulation. Butterworth-Heinemann.

Felmy, A.R., Girvin, D.C., Jenne, E.A., 1984. MINTEQ--a Computer Program for Calculating Aqueous Geochemical Equilibria: February 1984. National Technical Information Service.

Gallego-Urrea, J.A., Tuoriniemi, J., Pallander, T., Hassellöv, M., 2010. Measurements of nanoparticle number concentrations and size distributions in contrasting aquatic environments using nanoparticle tracking analysis. Environ. Chem. 7, 67–81.

Gregory, J., 2005. Particles in water: properties and processes. CRC Press.

Hanus, L.H., Ploehn, H.J., 1999. Conversion of intensity-averaged photon correlation spectroscopy measurements to number-averaged particle size distributions. 1. Theoretical development. Langmuir 15, 3091–3100.

Hole, P., Sillence, K., Hannell, C., Maguire, C.M., Roesslein, M., Suarez, G., Capracotta, S., Magdolenova, Z., Horev-Azaria, L., Dybowska, A., Cooke, L., Haase, A., Contal, S., Manø, S., Vennemann, A., Sauvain, J.-J., Staunton, K.C., Anguissola, S., Luch, A., Dusinska, M., Korenstein, R., Gutleb, A.C., Wiemann, M., Prina-Mello, A., Riediker, M., Wick, P., 2013. Interlaboratory comparison of size measurements on nanoparticles using nanoparticle tracking analysis (NTA). J. Nanoparticle Res. 15, 1–12. https://doi.org/10.1007/s11051-013-2101-8

Israelachvili, J.N., 2011. Intermolecular and surface forces. Academic press.

Kaplan, D.L., Hartenstein, R., Sutter, J., 1979. Biodegradation of polystyrene, poly (metnyl methacrylate), and phenol formaldehyde. Appl. Environ. Microbiol. 38, 551–553.

Lee, K.Y., Mooney, D.J., 2012. Alginate: properties and biomedical applications. Prog. Polym. Sci. 37, 106–126.

Leenheer, J.A., Wershaw, R.L., Reddy, M.M., 1995. Strong-acid, carboxyl-group structures in fulvic acid from the Suwannee River, Georgia. 2. Major structures. Environ. Sci. Technol. 29, 399–405.

LeRoux, M.A., Guilak, F., Setton, L.A., 1999. Compressive and shear properties of alginate gel: effects of sodium ions and alginate concentration. J. Biomed. Mater. Res. 47, 46–53.

Metreveli, G., Philippe, A., Schaumann, G.E., 2015. Disaggregation of silver nanoparticle homoaggregates in a river water matrix. Sci. Total Environ., Special Issue: Engineered nanoparticles in soils and waters 535, 35–44. https://doi.org/10.1016/j.scitotenv.2014.11.058

Overbeek, J.T.G., Verwey, E.J.W., 1948. Theory of the Stability of Lyophobic Colloids: The interaction of Sol Particles Having an Electric Double Layer.

Peterson, S.R., Hostetler, C.J., Deutsch, W.J., Cowan, C.E., 1987. Minteq User's Manual (No. NUREG/CR-4808; PNL-6106). Pacific Northwest Lab., Richland, WA (USA); Nuclear Regulatory Commission, Washington, DC (USA). Div. of Waste Management.

Pettit, R.E., 2004. Organic matter, humus, humate, humic acid, fulvic acid and humin: Their importance in soil fertility and plant health. CTI Res.

Plastics-the Facts 2016. An analysis of European plastics production, demand and waste data, 2016. . Plastics Europe.

Praetorius, A., Labille, J., Scheringer, M., Thill, A., Hungerbühler, K., Bottero, J.-Y., 2014. Heteroaggregation of Titanium Dioxide Nanoparticles with Model Natural Colloids under Environmentally Relevant Conditions. Environ. Sci. Technol. 48, 10690–10698. https://doi.org/10.1021/es501655v

Rehm, B.H., 2009. Alginates: biology and applications. Springer.

Singh, C., Friedrichs, S., Ceccone, G., Gibson, N., Jensen, K.A., Levin, M., Infante, H.G., Carlander, D., Rasmussen, K., 2014. Cerium Dioxide, NM-211, NM-212, NM-213. Characterisation and test item preparation. European Commission, Joint Research Centre, European Union. https://doi.org/10.2788/80203

Smoluchowski, M. v, 1918. Versuch einer mathematischen Theorie der Koagulationskinetik kolloider Lösungen. Z. Für Phys. Chem. 92, 129–168.

Stefánsson, A., 2007. Iron (III) hydrolysis and solubility at 25 C. Environ. Sci. Technol. 41, 6117–6123.

Williams, D.B., Carter, C.B., Veyssiere, P., 1998. Transmission electron microscopy: a textbook for materials science. Springer.

Zhang, W., Crittenden, J., Li, K., Chen, Y., 2012. Attachment Efficiency of Nanoparticle Aggregation in Aqueous Dispersions: Modeling and Experimental Validation. Environ. Sci. Technol. 46, 7054–7062. https://doi.org/10.1021/es203623z

Chapter III

Behaviour of CeO_2 nanoparticles in presence of electrolytes (mono, di and trivalent ions), pH changing condition and effect of dilution

Published as

Oriekhova, O., and Stoll, S., 2016, Effects of pH and fulvic acids concentration on the stability of fulvic acids – cerium (IV) oxide nanoparticle complexes, Chemosphere, v. 144, pp. 131-137 (Paper I).

III.1 Introduction

Cerium dioxide (CeO_2) NPs have found variety of industrial applications such as UV blocking and polishing agent, diesel fuel additive, component of catalytic converters etc. (El-Toni et al., 2006; Sajith et al., 2010). There are many pathways NPs enter into the environment via industrial discharges, surface runoff from soils, and wastewater treatment effluents (Gottschalk et al., 2009; Mitrano et al., 2014). The stability and reactivity of NPs is dependent on many factors such as particle characteristics but also the properties of water such as pH, ionic strength, presence of natural colloids and organic compounds (Grillo et al., 2015; Petosa et al., 2010). Natural organic matter (NOM) is one of the major water component controlling the fate of NPs released to aquatic systems. Depending on nature and NOM concentration, NPs can be stabilised, aggregated or even dispersed (Liu et al., 2012; Loosli et al., 2013). Therefore, in natural environmental condition, NPs will exist as NPs-NOM complexes. However, aging of such complexes in changing conditions is still a matter of debates, in particular, regarding the NOM corona stability including adsorption processes.

Another factor that influence the stability of NPs in aquatic system is the solution ionic strength. The type and valence of electrolyte play a key role in the modification of surface charge, hence influencing NP behaviour. There are different mechanisms responsible for particle aggregation. In the presence of monovalent ions, such as Na^+ or K^+, charge screening is mainly responsible for NPs aggregation. Whereas, in the presence of divalent ions, such as Ca^{2+} and Mg^{2+}, specific adsorption and charge neutralisation is main mechanisms leading to aggregation (Loosli et al., 2015; Zhang et al., 2012). On the other hand, there is a lack of information about the effect of trivalent electrolyte on NP stability. Therefore, we investigated the effect of mono, di and trivalent electrolyte on the aggregation of NPs-NOM complexes.

In this chapter, we investigated the effect of changing of some environmental factors such as changing pH, presence of electrolytes, fulvic acid concentration on the stability of pristine CeO_2 NPs and coated with fulvic acid. The stability of coated particles upon the dilution and with time was also evaluated. In particular, the effect of FA concentration was investigated in three pH domains which correspond to three electrostatic scenarios: at pH = 3.0 ± 0.1 < pH_{PZC}, at pH = 7.0 ± 0.1 close to pH_{PZC} and at pH = 10.0 ± 0.1 > pH_{PZC}.

III.2 Main results

First, the characterisation of pristine CeO_2 NPs and FAs was done using DLS and NTA methods to obtain particle size distribution and hydrodynamic diameters. Then electrophoretic measurements were performed to follow the particle surface charge. The suspension of CeO_2 NPs was prepared in ultrapure water at pH 3.0 ± 0.1 the measurement of zeta potential was performed as a function of pH up to pH 10. We found that below pH 4.5 NPs are highly positively charged and stable with hydrodynamic diameters equal to 185 ± 75 nm (by DLS) and 177 ± 83 nm (by NTA). With increase of pH we observed charge inversion and above pH 8 NPs exhibited negative charges. The point of zero charge (PZC) was found at pH equal to 6.8 ± 0.1. FAs were negative in full pH range with zeta potential varying from −10 to −25 mV. Average hydrodynamic diameter measured by NTA method was equal to 194 ± 89 nm. According to the results, three pH domains and different interaction scenarios between CeO_2 NPs and FA were defined:

- below pH < pH_{PZC} where CeO_2 NPs are strongly positively charged and FAs are negatively charged;
- pH around pH_{PZC} where CeO_2 surface charge is around 0 and FAs are negatively charged;
- and above the pH_{PZC} where both NPs and NOM are negatively charged.

III.2.1 Effect of FAs and electrolyte concentration on CeO_2 NP stability

The pH < pH_{PZC} represents favorable conditions for the interaction between positively charged CeO_2 NPs and negatively charged FA molecules, thus forming strong CeO_2/FA complexes. To achieve the IEP, where the highest level of agglomeration occurs and agglomerate reach the size up to 2700 nm, 0.25 mg/L FAs is needed (Fig. III.1). Further increase of FAs concentration leads to the charge inversion and zeta potential stabilisation. Agglomerates of CeO_2 NPs are partially disagglomerated with z-average hydrodynamic diameter down to 1700 nm.

We also studied the interaction between CeO_2 NPs and FAs at pH 7.0 ± 0.1 and pH 10.0 ± 0.1. In the first case, we observed partial disagglomeration in the presence of high concentration of FAs. Z-average particle diameter was found to decrease to 1500 nm. The surface charge of particle became negative with zeta potential values equal to −35 mV, hence indicating adsorption of FAs. In the second case, partial adsorption of FA molecules was found to induce a limited decrease of z-average diameter from 720 ± 28 to 600 ± 45 nm.

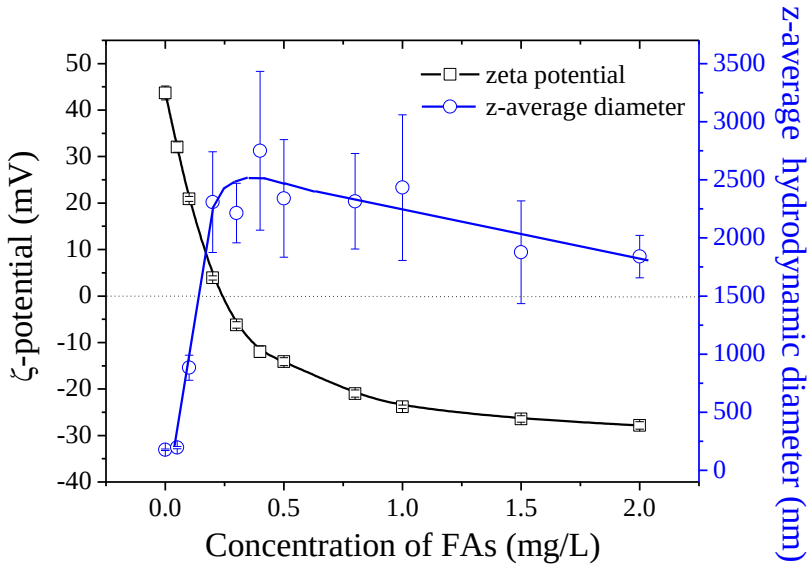

Fig. III.1. Zeta potential and z-average hydrodynamic diameter of CeO_2 NPs in the presence of different concentrations of FAs at pH < pH_{PZC}. A good agreement is found between zeta potential variation and the aggregation-stabilisation of the CeO_2 suspension. [CeO_2] = 50 mg/L.

The influence of monovalent electrolyte (NaCl) on the stability of CeO_2 NPs was investigated at pH < pH_{PZC}. In this pH condition NPs are stable with positive surface charges. In the presence of NaCl (Fig. A1.1 in Annex) zeta potential decreases rapidly at low electrolyte concentrations, less than 0.1 M, and reaches plateau at higher electrolyte concentrations (> 0.1 M). Increase of NaCl concentrations leads to the decrease of zeta potential from +55 to +25 mV, due to the decrease of the thickness of diffuse layer. Particles can come closer to each other then, van der Waals attraction is sufficient to outweigh the double layer repulsion, hence leading to particle destabilisation. Consequently, z-average hydrodynamic diameters are increasing with increase of salt concentration from base line value less than 200 nm to 2500 nm (Fig. III.2).

The attachment efficiencies between uncoated CeO_2 NPs in increasing NaCl concentrations was then calculated. Two aggregation regimes: diffusion limited and reaction limited were found. When the aggregation is diffusion limited attachment efficiency approaches to the value 1. The CCC was determined and equal to 0.11 ± 0.02 M (Fig. III.3). Hence, this value gives the minimal concentration of NaCl that is necessary to destabilise 50 mg/L uncoated CeO_2 NPs.

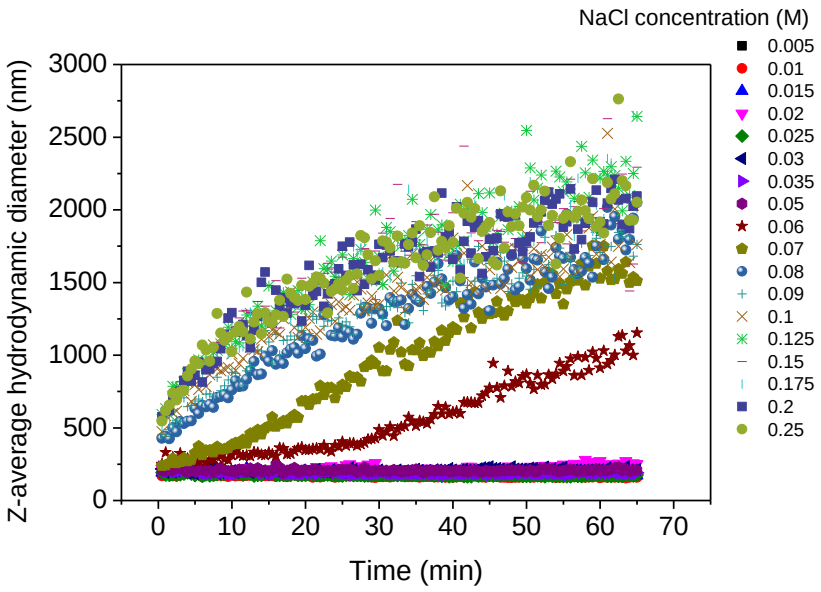

Fig. III.2. Z-average hydrodynamic diameter variation of uncoated CeO_2 NPs as a function of salt concentration. Kinetics of aggregation is enhanced by increasing the ionic strength of the CeO_2 dispersion. Experimental condition: $[CeO_2]$ = 50 mg/L, pH < pH_{PZC}. Z-average hydrodynamic diameters increase with time and with increase of NaCl concentrations.

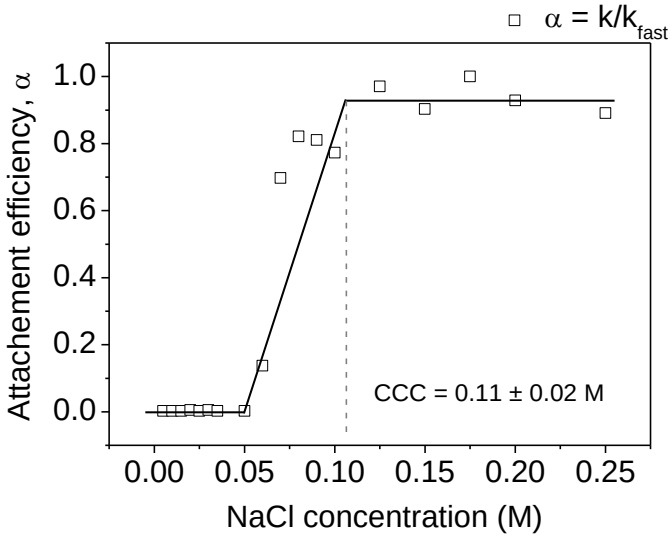

Fig. III.3. Attachment efficiency of CeO_2 NPs as a function of NaCl concentration. Critical coagulation concentration (CCC) is found equal to 0.11 ± 0.01 M. Experimental condition: $[CeO_2]$ = 50 mg/L, pH < pH_{PZC}.

III.2.2 Stability of FAs-CeO_2 NPs complexes

To evaluate the effect of natural water environment on the stability of CeO_2/FA complexes different environmental factors such as time, pH, dilution effect and the presence of mono- , di- and trivalent electrolytes were considered.

pH effect

We have chosen the most favourable condition to form electrostatic complexes i.e. pH 3.0 ± 0.1 and excess of FAs by considering solution concentrations equal to 50 mg/L CeO_2 and 2 mg/L FAs. The formed complexes have been stable during 7 weeks with z-average hydrodynamic diameters equal to 220 ± 40 nm and zeta potential to –25 ± 7 mV. The stability of CeO_2/FA complexes was also studied in changing pH condition (Fig. III.4).

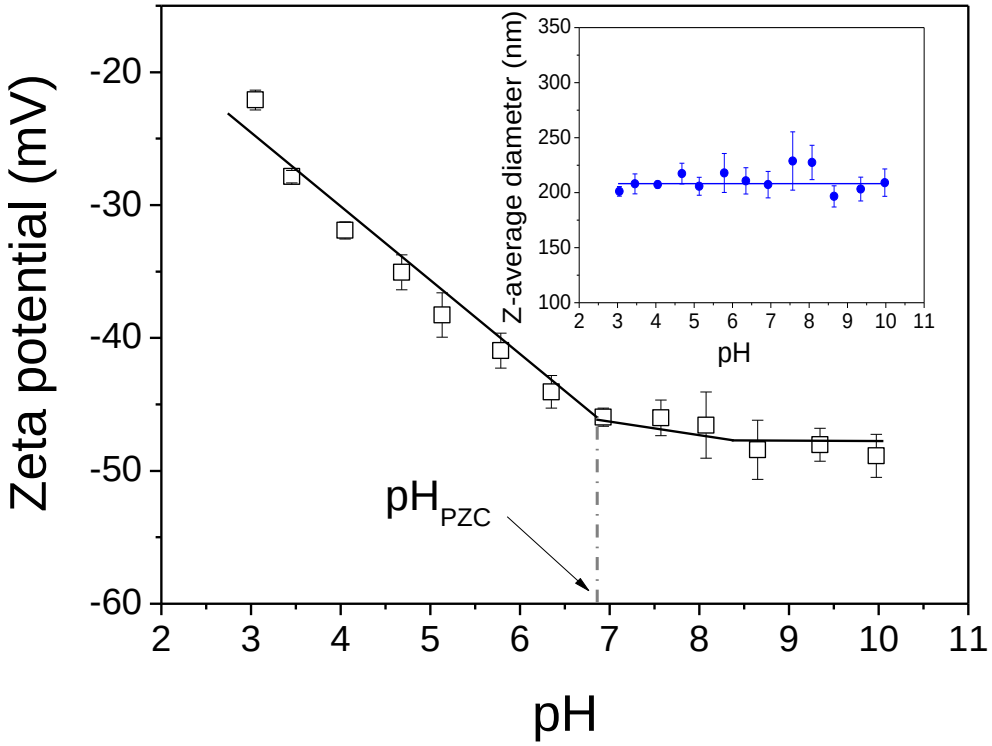

Fig. III.4. Variation of zeta potential and z-average hydrodynamic diameter (insert) of CeO_2 NPs coated with FAs as a function of pH. Zeta potential decrease with increase of pH. Stability of z-average hydrodynamic diameter is observed in the full pH range.

The zeta potential was found negative in full pH range, to decrease and then reach a plateau, whereas z-average diameter was stable and equal to 220 ± 40 nm. Such variations are related to the modification of the acid-base properties of CeO_2 NPs in presence of FAs. The adsorption of FAs induces the CeO_2 charge inversion, so that zeta potential is negative. Increase of pH leads to the neutralisation of the charges on the CeO_2 surface by hydroxyl ions, decrease and stabilisation of zeta potential.

Effect of mono and divalent electrolytes

To evaluate the effect of ionic strength on the stability of CeO_2/FA complexes two electrolytes (sodium chloride and calcium chloride) were used. First, the suspension of CeO_2/FAs was prepared and pH was set to an environmentally relevant value (8.0 ± 0.1). Then we sequentially increased the salt concentration from 0.5 to 0.75 M for NaCl and from 0.25 to 50 mM for $CaCl_2$ (Fig. A.1.2). The attachment efficiencies of coated CeO_2 calculated from the growth of the z-average hydrodynamic diameters as a function of electrolyte concentrations are presented in Fig. III.5. The CCC values for two salts have been determined and correspond to 0.39 ± 0.02 M for NaCl and 2.9 ± 0.3 mM for $CaCl_2$. The difference of CCC values, more than 100 times, can be explained by the Schulze-Hardy rule, indicating that the CCC is proportional to the ion charge (CCC ~ $1/z^6$, where z is ion valency) (Gregory, 2005). Divalent ions have a stronger screening effect and a higher affinity to the highly negative surface of CeO_2/FA complexes compared to monovalent ions. Thus, less concentrated $CaCl_2$ solution than NaCl is needed to destabilise coated particles, due to the higher positive charge and specific adsorption of Ca^{2+} ions on the NPs surface. The zeta potential values of coated CeO_2 NPs before addition of electrolyte are around –51.1 ± 0.6 mV (Annex 1, Fig. A1.3a). The addition of small amount of divalent salt leads to a high response and a change of zeta potential of about 30 units to the value –21 ± 0.7 mV comparing to NaCl when the addition of higher concentration changes zeta potential only on the 14 units (ζ = –37.3 ± 1.0 mV) (Fig. A1.3).

The increase of concentrations of both electrolytes leads to the gradual increase of zeta potential values (zeta potential becomes less negative) from –37.3 ± 1.0 to –16.8 ± 6.0 mV for NaCl and from – 21.9 ± 0.7 to –15.4 ± 0.8 mV for $CaCl_2$.The enhancement of aggregation by Ca^{2+} ions is explained by bridging effect through formation of intermolecular complexes between coated NPs and divalent ions (Li and Chen, 2012). The CCC ratio of NaCl of uncoated and coated CeO_2 NPs was also assessed and found equal to 3.5. More concentrated solution of NaCl was necessary in order to aggregate NPs as FAs create a stabilising coating around particles. Such conclusion is also confirmed by the values of zeta potential. For coated particles zeta potential is more negative and is equal to –51.1 ± 0.6 mV compared to uncoated particle (ζ = –21.1 ± 0.8 mV).

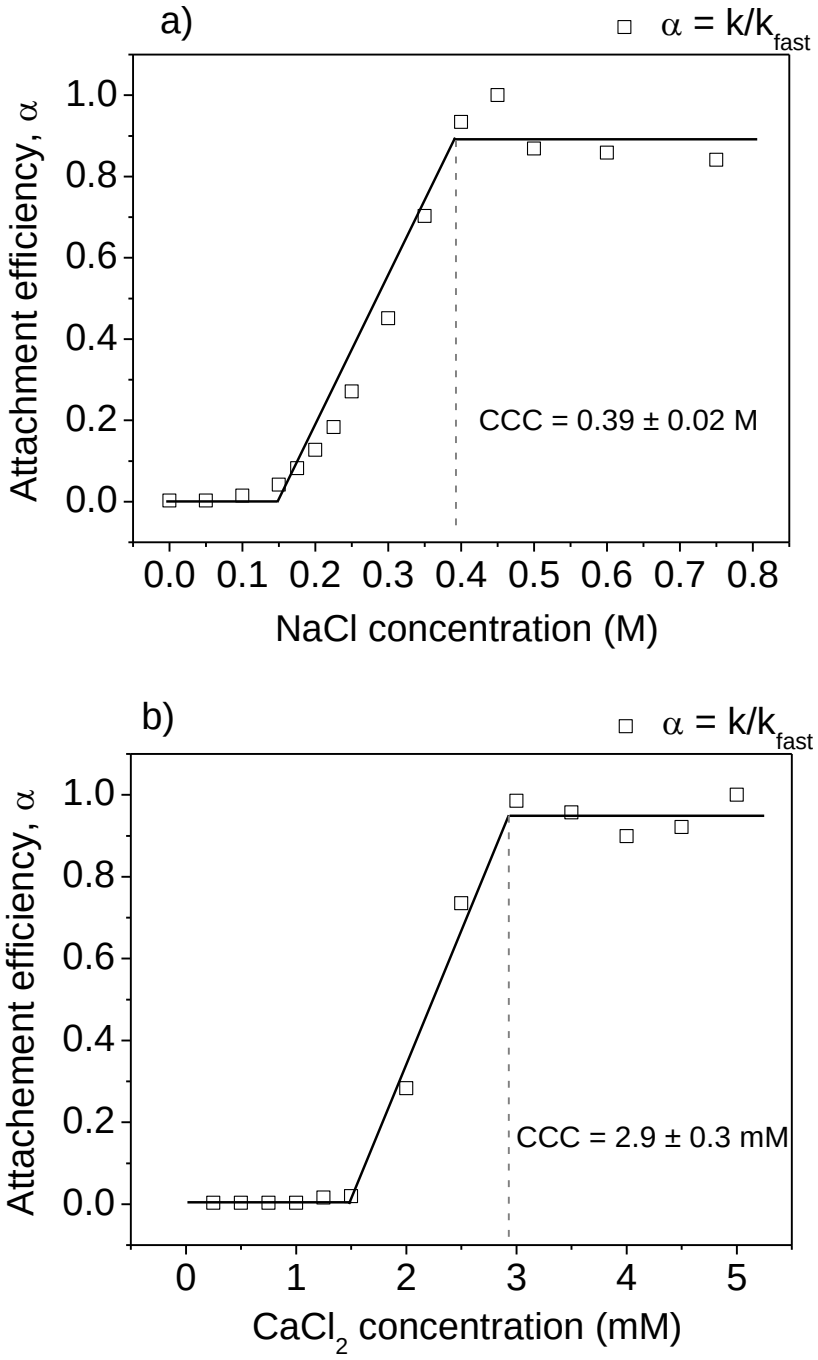

Fig. III.5. Attachment efficiency between coated CeO_2 NPs as a function of electrolyte concentration: a) NaCl, CCC (NaCl) = 0.39 M; b) $CaCl_2$, CCC ($CaCl_2$) = 2.9 mM. Experimental condition: [CeO_2] = 50 mg/L, [FAs] = 2 mg/L, pH = 8.0 ± 0.1.

Effect of trivalent electrolytes

The results of aggregation kinetic experiments of CeO_2/FA complexes in the presence of iron and aluminium chloride are presented in Annex 1, Fig. A1.4 and Fig. A1.5. Significant aggregation occurred for concentrations above $1 \cdot 10^{-4}$ M for $FeCl_3$ and $3 \cdot 10^{-5}$ M for $AlCl_3$. Our results indicate that trivalent electrolytes are more efficient to destabilised CeO_2/FA

complexes compared to mono- and divalent due to their higher charge and better ability to specifically adsorb on the NP surface.

Dilution effect

CeO_2/FA complexes in environmental aquatic condition will undergo significant transformation including dilution. To test the effect of dilution on the stability of already formed complexes series of suspensions with dilution factor equal to 20 were prepared. The compound concentrations are provided in Table III.1. Two pHs were tested: 3.0 ± 0.1 and 8.0 ± 0.1. Zeta potentials and z-average hydrodynamic diameters are presented in Fig. III.6.

Table III.1. Compound concentrations for dilution experiments

Compound	**Concentration, mg/L**				
Dilution factor	1	2	4	10	20
CeO_2 MNMs	100	50	25	10	5
FAs	4	2	1	0.4	0.2

At pH 3.0 as well as at pH 8.0 no significant difference in sizes and surface charge properties are observed up to a dilution factor equal to 20. Zeta potential is stable and is equal to –29.7 ± 1.7 mV at pH 3.0 and –44.6 ± 1.6 mV at pH 8.0. The higher value of zeta potential at higher pH corresponds to the more negative charge of FAs at pH 8.0 compared to pH 3.0. Values of z-average diameter do not exceed 325 nm at pH 3.0 and 300 nm at pH 8.0. Our results indicate that dilution has no effect on the coating stability at low and neutral pH.

We demonstrated that due to the adsorption of negatively charged FAs on the positively charged CeO_2 NPs strong electrostatic complexes are formed at $pH < pH_{PZC}$. Once formed such CeO_2/FA complexes are stable with time and in changing environmental conditions (upon pH change and dilution).

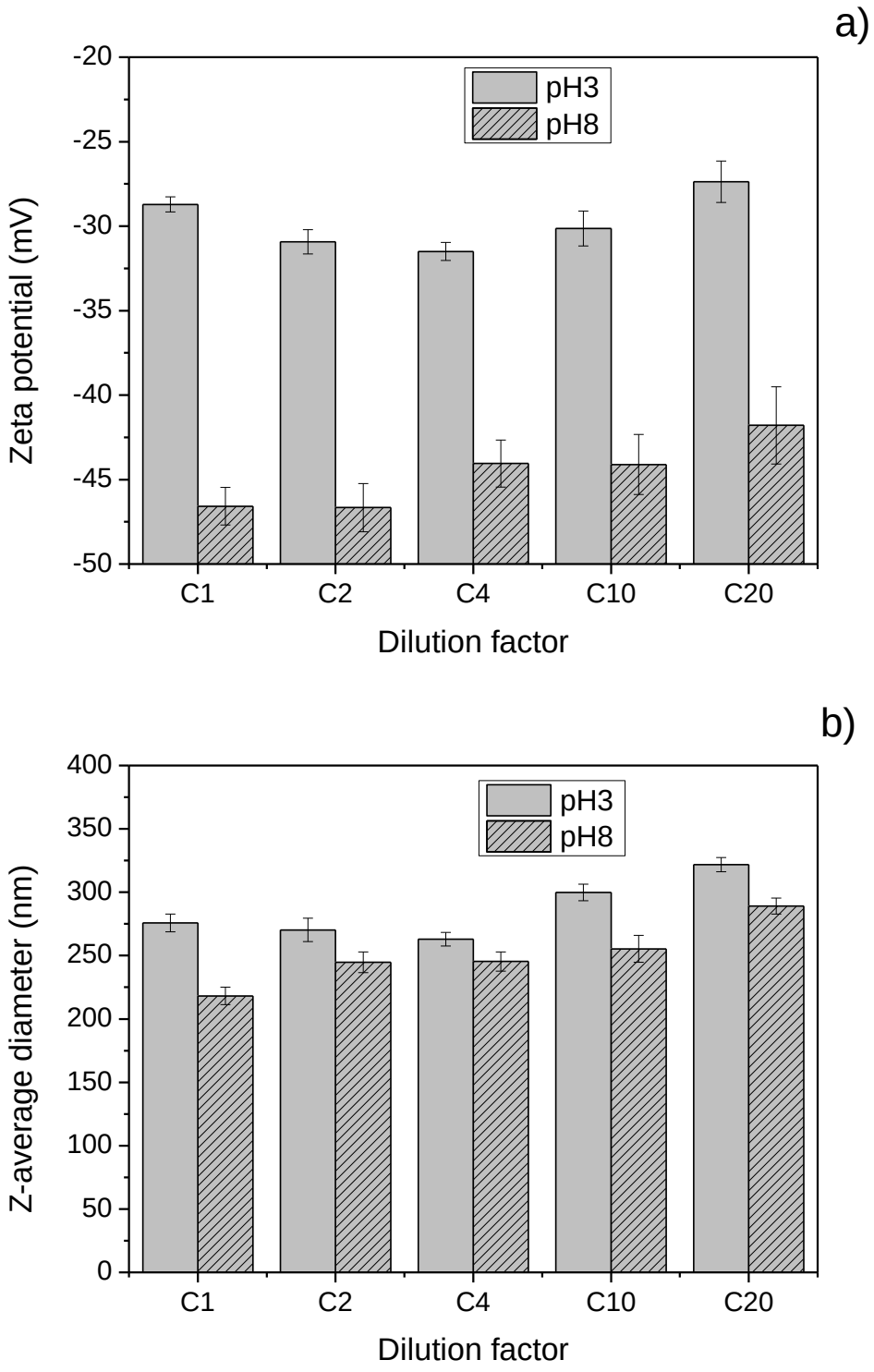

Fig. III.6. (a) Zeta potential and (b) z-average hydrodynamic diameter of CeO_2/FA complexes in pH and concentration changing conditions. Dilution factor corresponds to the following concentration values: C1 – CeO_2 MNMs concentration is equal 100 mg/L, FAs concentration is 4 mg/L; C2 – [CeO_2] = 50 mg/L, [FAs] = 2 mg/L; C4 – [CeO_2] = 25 mg/L, [FAs] = 1 mg/L; C10 – [CeO_2] = 10 mg/L, [FAs] = 0.4 mg/L; C20 – [CeO_2] = 5 mg/L, [FAs] = 0.2 mg/L.

III.3 References

Buettner, K.M., Rinciog, C.I., Mylon, S.E., 2010. Aggregation kinetics of cerium oxide nanoparticles in monovalent and divalent electrolytes. Colloids Surf. Physicochem. Eng. Asp. 366, 74–79. doi:10.1016/j.colsurfa.2010.05.024

El-Toni, A.M., Yin, S., Hayasaka, Y., Sato, T., 2006. Synthesis and UV-shielding properties of silica-coated calcia-doped ceria nanoparticles via soft solution processes. J. Electroceramics 17, 9–14. doi:10.1007/s10832-006-9928-7

Gottschalk, F., Sonderer, T., Scholz, R.W., Nowack, B., 2009. Modeled Environmental Concentrations of Engineered Nanomaterials (TiO2, ZnO, Ag, CNT, Fullerenes) for Different Regions. Environ. Sci. Technol. 43, 9216–9222. doi:10.1021/es9015553

Gregory, J., 2005. Particles in water: properties and processes. CRC Press.

Grillo, R., Rosa, A.H., Fraceto, L.F., 2015. Engineered nanoparticles and organic matter: A review of the state-of-the-art. Chemosphere 119, 608–619. doi:10.1016/j.chemosphere.2014.07.049

Li, K., Chen, Y., 2012. Effect of natural organic matter on the aggregation kinetics of CeO2 nanoparticles in KCl and CaCl2 solutions: Measurements and modeling. J. Hazard. Mater. 209–210, 264–270. doi:10.1016/j.jhazmat.2012.01.013

Li, K., Zhang, W., Huang, Y., Chen, Y., 2011. Aggregation kinetics of CeO2 nanoparticles in KCl and CaCl2 solutions: measurements and modeling. J. Nanoparticle Res. 13, 6483–6491. doi:10.1007/s11051-011-0548-z

Liu, J., Legros, S., Ma, G., Veinot, J.G.C., von der Kammer, F., Hofmann, T., 2012. Influence of surface functionalization and particle size on the aggregation kinetics of engineered nanoparticles. Chemosphere 87, 918–924. doi:10.1016/j.chemosphere.2012.01.045

Loosli, F., Coustumer, P.L., Stoll, S., 2013. TiO2 nanoparticles aggregation and disaggregation in presence of alginate and Suwannee River humic acids. pH and concentration effects on nanoparticle stability. Water Res. 47, 6052–6063.

Loosli, F., Le Coustumer, P., Stoll, S., 2015. Effect of electrolyte valency, alginate concentration and pH on engineered TiO2 nanoparticle stability in aqueous solution. Sci. Total Environ., Special Issue: Engineered nanoparticles in soils and waters 535, 28–34. doi:10.1016/j.scitotenv.2015.02.037

Mitrano, D.M., Rimmele, E., Wichser, A., Erni, R., Height, M., Nowack, B., 2014. Presence of nanoparticles in wash water from conventional silver and nano-silver textiles. ACS Nano 8, 7208–7219. doi:10.1021/nn502228w

Petosa, A.R., Jaisi, D.P., Quevedo, I.R., Elimelech, M., Tufenkji, N., 2010. Aggregation and Deposition of Engineered Nanomaterials in Aquatic Environments: Role of Physicochemical Interactions. Environ. Sci. Technol. 44, 6532–6549. doi:10.1021/es100598h

Sajith, V., Sobhan, C.B., Peterson, G.P., 2010. Experimental investigations on the effects of cerium oxide nanoparticle fuel additives on biodiesel. Adv. Mech. Eng. 2010, e581407. doi:10.1155/2010/581407

Zhang, W., Crittenden, J., Li, K., Chen, Y., 2012. Attachment Efficiency of Nanoparticle Aggregation in Aqueous Dispersions: Modeling and Experimental Validation. Environ. Sci. Technol. 46, 7054–7062. doi:10.1021/es203623z

Paper I

Oriekhova, O., and Stoll, S., 2016, Effects of pH and fulvic acids concentration on the stability of fulvic acids – cerium (IV) oxide nanoparticle complexes, Chemosphere, v. 144, pp. 131-137.

Chemosphere 144 (2016) 131–137

Contents lists available at ScienceDirect

Chemosphere

journal homepage: www.elsevier.com/locate/chemosphere

Effects of pH and fulvic acids concentration on the stability of fulvic acids – cerium (IV) oxide nanoparticle complexes

Olena Oriekhova, Serge Stoll*

University of Geneva, Earth and Environmental Science Section, F.-A. Forel Institute, Group of Environmental Physical Chemistry, 10 Route de Suisse, CH-1290 Versoix, Switzerland

HIGHLIGHTS

- Environmental amounts of FAs are sufficient to stabilize CeO_2 NPs suspensions.
- When pH < pH_{PZC} strong electrostatic complexes are formed between FAs and CeO_2 NPs.
- Stable complexes are obtained with time and in pH changing conditions.
- Fulvic acids adsorption is changing the CeO_2 acid-base properties.
- Irreversible aggregates are formed with successive addition of FAs passing the IEP.

GRAPHICAL ABSTRACT

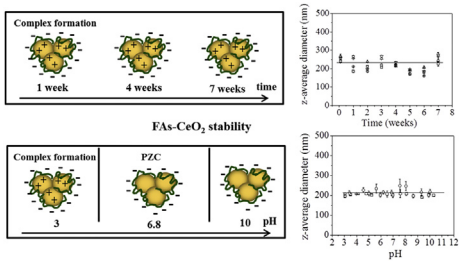

ARTICLE INFO

Article history:
Received 13 February 2015
Received in revised form
11 August 2015
Accepted 15 August 2015
Available online xxx

Keywords:
CeO_2 nanoparticles
Fulvic acids
Nanoparticle coating
Nanoparticle stability
Nanoparticle surface charge and pH
Hydrophobic effect

ABSTRACT

The behavior of cerium (IV) oxide nanoparticles has been first investigated at different pH conditions. The point of zero charge was determined as well as the stability domains using dynamic light scattering, nanoparticle tracking analysis and scanning electron microscopy. A baseline hydrodynamic diameter of 180 nm was obtained indicating that individual CeO_2 nanoparticles are forming small aggregates. Then we analyzed the particle behavior at variable concentrations of fulvic acids for three different pH-electrostatic scenarios corresponding to positive, neutral and negative CeO_2 surface charges. The presence of fulvic acids was found to play a key role on the CeO_2 stability via the formation of electrostatic complexes. It was shown that a small amount of fulvic acids (2 mg L^{-1}), representative of environmental fresh water concentrations, is sufficient to stabilize CeO_2 nanoparticles (50 mg L^{-1}). When electrostatic complexes are formed between negatively charged FAs and positively charged CeO_2 NPs the stability of such complexes is obtained with time (up to 7 weeks) as well as in pH changing conditions. Based on zeta potential variations we also found that the fulvic acids are changing the CeO_2 acid-base surface properties. Obtained results presented here constitute an important outcome in the domain of risk assessment, transformation and removal of engineered nanomaterials released into the environment.

1. Introduction

Due to their specific physicochemical properties, in comparison to bulk materials, engineered nanoparticles are widely incorporated into a large number of consumer products (Kessler, 2011). In particular, cerium(IV) oxide (CeO_2) nanoparticles (NPs) are currently

* Corresponding author.
E-mail addresses: Olena.Oriekhova@unige.ch (O. Oriekhova), Serge.Stoll@unige.ch (S. Stoll).

http://dx.doi.org/10.1016/j.chemosphere.2015.08.057
0045-6535/

used in several applications: as a component of catalytic converters, as UV blocking or polishing agent or as diesel fuel additive (El-Toni et al., 2006; Sajith et al., 2010). The growing consumption of products containing CeO_2 NPs will constantly increase their presence in the environment via industrial discharges or surface runoff from soils or wastewater treatment effluents (Gottschalk and Nowack, 2011; Labille et al., 2010; Mitrano et al., 2014). When NPs enter in aquatic systems they interact with natural colloids and microorganisms and undergo different transformations. Nanoparticle stability, reactivity, bioavailability is strongly influenced by the physicochemical characteristic of aquatic media such as pH, ionic strength, presence of natural colloids and organic compounds (Clavier et al., 2015; Grillo et al., 2015; Motellier et al., 2013; Petosa et al., 2013).

One of the important components that define the fate of engineered NPs in the environment is natural organic matter (NOM). Generally, NOM consists of a mixture of humic substances, polysaccharides, algal and bacterial residues, viruses, polyacrylic, alginic acids, DNA etc. (Wilkinson et al., 1999). From 20 to 50% NOM is represented by humic substances (Frimmel and Abbt-Braun, 1999) that are an assembly of organic macromolecules with heterogeneous functional groups such as hydroxyl (−OH), methyl ($-CH_3$), carboxyl (−COOH), and is present in the aquatic environment in the form of fulvic acids (FAs), humic acids (HAs) and humin. Humic substances are very reactive, especially with water pollutants such as metals, forming strong complexes with Fe(III), Al(III), Cu(II), Mn(II) and other metals that leads to the transformation of original materials (Neubauer et al., 2013; Rosa et al., 2007; Von Wandruszka, 2000). NOM plays also an important role in reducing the aggregation rates, stabilization and dispersion of colloidal particles and engineered nanomaterials (Liu et al., 2012). For example, CeO_2 nanoparticle aggregation was found to be reduced by the increase of the electrostatic repulsions in presence of adsorbed NOM (Quik et al., 2010). Particle zeta potential decreased from −15 to −55 mV and up to 88% of initially added CeO_2 NPs remained suspended in deionized water. In another example, magnetic γFe_2O_3 NPs were coated with HAs ensuring the colloidal stability due to the repulsive electrostatic and steric–electrostatic interactions (Ghosh et al., 2011). Li and Chen (2012) also showed that even relatively low concentration of HAs (1 ppm) had a stabilizing effect on CeO_2 NPs even in presence of high concentration of monovalent electrolyte. The same authors showed that behavior of CeO_2 NPs in presence of divalent electrolyte was related to the concentration of both humic substances and salt. They determined the critical coagulation concentration (CCC) of KCl and $CaCl_2$ in the presence and absence of HAs. CCC was found to increase at high HAs concentration, hence confirming the stabilizing effect of HAs. Keller et al. (2010) showed that organic substances present in natural freshwater adsorb onto the surface of NPs resulting in a barrier to aggregation. The same authors demonstrated that in mesocosm freshwater, ceria, titanium and zinc oxide NPs remained stable with size around 300 nm over time (500 min). They also found that when metal oxide surface is coated with NOM, the particle charge is defined by the charge of NOM. Such NOM-metal oxide complexes were found negatively charged and the attachment efficiency between them was so small that even an increase in particle concentration had no effect on the aggregation rate.

One of the important factors that affects the behavior of NPs in the environment and determines its toxicity is the aggregation state (Rodea-Palomares et al., 2011; Röhder et al., 2014; Safi et al., 2010; von Moos and Slaveykova, 2013). It is known that particle size plays a key role in their reactivity and that smaller particles are more toxic for organisms (Cong et al., 2011; Fabrega et al., 2011; Moos et al., 2014). It should be noted that even if NPs enter the environment in agglomerated state the presence of organic substances at natural concentration can lead to important surface changes and redispersion. Loosli et al. (2014, 2013) showed that environmentally relevant concentration of HAs can lead to the disagglomeration of TiO_2 NPs and change of surface charge towards its further stabilization. Mohd Omar et al. (2014) also demonstrated that Suwanee River HAs were able to promote partial disaggregation of zinc oxide NPs due to NOM coating.

Research on CeO_2 NPs fate in an aquatic environment has mainly focus on toxicological studies (Molina et al., 2014; Rodea-Palomares et al., 2011; Röhder et al., 2014) and interaction with organic matters at short time scale (Grillo et al., 2015; Quik et al., 2010). Little attention has been given to the stability of CeO_2-NOM complexes with time (weeks and months) and upon modification of the physicochemical conditions of the dispersion media. Owing to the CeO_2 NPs unique properties investigation of their stability, surface transformation and ageing in more and more realistic synthetic or naturals waters has therefore to be developed to increase our understanding of the nanoparticle fate when released in natural aquatic systems.

In this context, the aim of our study is to investigate the stability and ageing of CeO_2 NPs in the presence of NOM, particularly fulvic acids, in a systematic way as a function of time and upon pH fluctuations. First, CeO_2 NPs are characterized; size distribution, zeta-potential and the point of zero charge (PZC) of the nanoparticles are defined. Then, environmentally relevant ranges of FAs concentration are chosen in order to investigate the effect of NOM on particle behavior. We focused on three different scenarios 1) interaction between positively charged NPs and negatively charged FAs, 2) uncharged CeO_2 NPs interacting with negatively charged FAs and 3) interaction between negatively charged NPs and negatively charged FAs. Then, the stability of FAs–CeO_2 nanoparticle complexes is investigated over time and versus pH changes by considering size and surface charge variations.

2. Materials and methods

2.1. Materials

Uncoated CeO_2 NPs as a powder were kindly provided from the JRC Nanomaterials repository NanoMILE project (code name of particles NM-212). The primary particle size is equal to 28.4 ± 10.4 nm and specific surface area 27.8 ± 1.5 $m^2\ g^{-1}$ (XRD and BET methods from Singh et al., 2014). The suspension of nanoparticles was prepared according to the dispersion protocol provided in the supporting information (SI, S1). First, a 1 g L^{-1} stock suspension at pH 3.0 ± 0.1 was prepared. The sonication of this suspension was done once after first preparation with sonication probe. For the successive experiments dilution was made and a suspension of 50 mg L^{-1} was prepared with ultrapure water (Milli Q water, Millipore, Switzerland, with R > 18MOhm, TOC < 2 ppb). Such concentration was used to optimize the signal during the dynamic light scattering and electrophoretic measurements. Sodium chloride was used as background electrolyte with concentration 0.001 M to obtain stable signal during electrophoretic measurements. pH was adjusted by adding appropriate amount of diluted HCl and NaOH (Merck, Germany).

The Suwannee River Fulvic acids (Standard II, 2S101F) were purchased from International Humic Substance Society, USA. First, a 1 g L^{-1} solution was prepared and then diluted to 100 mg L^{-1}. This solution was our stock solution from which we made our further dilutions. FAs surface charge was negative in all range of pH (SI, S2). All solutions were maintained in a dark place with temperature between 0 and 4 °C.

2.2. Particle characterization

Uncoated and FAs coated CeO_2 NPs were imaged with a JEOL JSM-7001FA scanning electron microscope (SEM). For each samples 10 μL of NPs suspension was placed on one aluminum stub covered with 5 × 5 mm silica wafer Agar Scientific (G3390) and wrapped with 3–5 nm of gold coating.

Zeta potential and z-average hydrodynamic diameter were measured using laser Doppler technique and dynamic light scattering method accordingly using a Malvern Zetasizer Nano ZS (Malvern Instruments Ltd, UK). The autocorrelation function accumulated ten runs for each samples for five parallel measurements with time delay of 5 s. First, electrophoretic mobility was measured and then Smoluchowsky approximation (Gregory, 2005) was used to calculate zeta potential. Particle size distribution was investigated using the nanoparticle tracking analysis (NTA) technique with a NanoSight LM14 instrument (NanoSight Ltd, UK). The NTA LM14 consists of a nanoparticle viewing unit with an integrated blue laser illumination (wave length of 405 nm), CMOS high sensitivity camera and integrated temperature control unit. All measurements were performed in triplicates.

2.3. Experimental procedures

For the experiments dealing with NPs and FAs complexes two different suspensions of CeO_2 NPs and FAs were prepared. First, 50 mg L^{-1} CeO_2 suspensions at pH 3.0, 7.0 and 10.0 ± 0.1 were prepared. Then a 100 mg L^{-1} stock solution of FAs was successively added to achieve appropriate final concentrations. The time interval between each FAs addition was 15 min. The agitation was done during all experiment with magnet vortex with rotational speed equal to 200 rpm.

The stability of FAs–CeO_2 complexes was investigated over a long period of time, up to 7 weeks. Final concentrations corresponded to 50 mg L^{-1} for CeO_2 NPs and 2 mg L^{-1} for FAs and final suspension pH was equal to 3.0 ± 0.1. The control of suspension pH was made during all experiments and measurements were made every week.

For experiments of stability versus pH a 50 mg L^{-1} suspension of CeO_2 NPs with 2 mg L^{-1} FAs was prepared at pH 3.0 ± 0.1. After 2 h of equilibration we sequentially increased the suspension pH from 3.0 to 10.0. The equilibration time between each measurement was 15 min.

3. Results and discussion

3.1. Characterization of cerium oxide nanoparticles

We combined different techniques to characterize CeO_2 NPs and to provide full information on particles size distribution, morphology and surface charge.

First, size distribution and z-average diameter of CeO_2 NPs at pH 3.0 ± 0.1 using two methods NTA and DLS (SI, S3) were measured. We chose this pH as it corresponds to a stable domain regarding aggregation and where NPs exhibit highly positive surface charges (zeta potential was equal to +51.3 ± 1.3 mV). Z-average diameter and hydrodynamic diameter were found equal to 185 ± 75 nm (DLS) and 177 ± 83 nm (NTA). The results were found in good agreement between them and with literature data (Singh et al., 2014). Such baseline hydrodynamic diameters suggest that individual nanoparticles are forming aggregates when diluted in ultrapure water. In addition, the same suspension at pH 3.0 ± 0.1 was investigated using SEM. Images presented in Fig. 1b illustrate the formation of dimers, trimers and larger aggregates in ultrapure water. Particle size varies from 30 nm for individual particles to 200–300 nm for aggregates. Our data correlates with TEM images obtained by Singh et al. (2014) of CeO_2 NPs which were found aggregated and showed irregular shapes and non-homogeneous primary particle size variation.

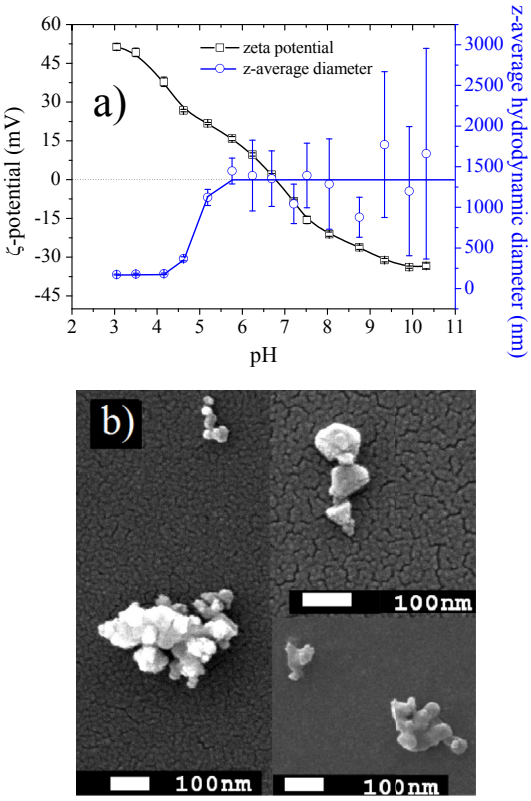

Fig. 1. (a) Zeta potential and z-average hydrodynamic diameter variation as a function of pH increase. In acid environment CeO_2 NPs are positively charged whereas in basic environment they are negatively charged. The pH_{PZC} is found equal to 6.8 ± 0.1. Below pH 4.5 ± 0.1 nanoparticles are stable with z-average diameters less than 200 nm [CeO_2] = 50 mg L^{-1}, [NaCl] = 0.001 M. (b) SEM images of CeO_2 NPs in ultrapure water at pH 3.0 ± 0.1. We observe individual particles with diameters of 30 nm and aggregates with sizes from 200 to 300 nm on SEM images. The size of individual particles corresponds to the value provided by the manufacturer (NM-212 JRC repository).

One important parameter that characterizes the stability domain of nanoparticles is the PZC. To define the pH_{PZC} we performed electrophoretic mobility and size distribution measurements in a range of pH from 3 to 10. The titration procedure was made in presence of 0.001 M NaCl as background electrolyte. Titration was performed from acid to basic environment by addition of 0.01 M NaOH. The equilibration time between each modification of pH was 15 min. The agitation was done during all experiment with magnet vortex with rotational speed equal to 200 rpm. As shown in Fig. 1a, when pH < 4.5 ± 0.1 the surface of CeO_2 NPs is found strongly positively charged. NPs are stable in this domain which is also confirmed by the size distribution with z-average hydrodynamic diameters less than 200 nm. Further increasing the pH leads to the decrease of surface charge until the PZC is reached and then to charge inversion. The surface of CeO_2 NPs is found strongly negatively charged at pH > 8.0 ± 0.1. In the PZC region nanoparticle aggregation occurred and z-average hydrodynamic diameters are found in the range between 800 and 1500 nm. As illustrated in Fig. 1a further pH increase does not result in a significant decrease of the z-average diameters (disaggregation). We found the value of pH_{PZC} equal to 6.8 ± 0.1. This result is close to the theoretical value of pH_{PZC} = 7 (Jolivet et al., 2000) and to the experimental result obtained by Buettner et al. (2010), in

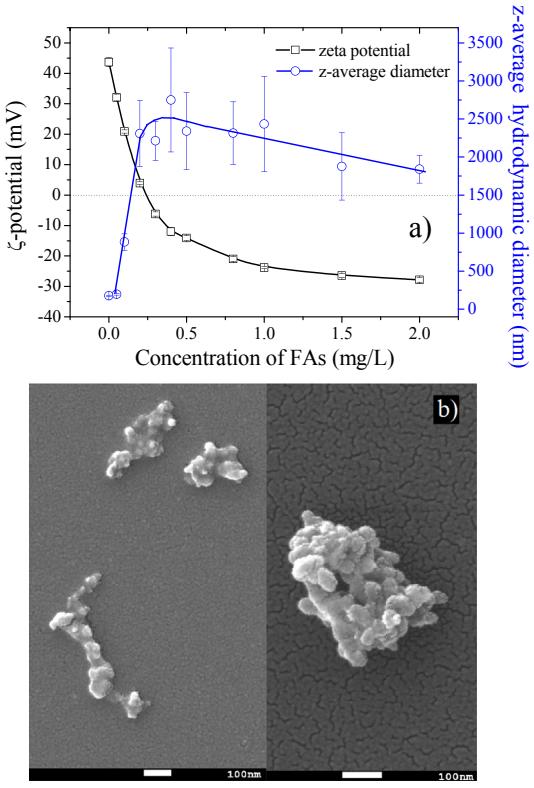

Fig. 2. (a) Zeta potential and z-average hydrodynamic diameter of CeO_2 NPs in the presence of different concentrations of FAs at pH < pH_{PZC}. 0.25 mg L^{-1} FAs is needed to change the nanoparticle charge from positive to negative and to stabilize the suspension. A good agreement is found between zeta potential variation and the aggregation-stabilization of the CeO_2 suspension [CeO_2] = 50 mg L^{-1} (b) SEM images of CeO_2 NPs with FAs 2 mg L^{-1} at pH 3.0 ± 0.1. A significant coating is observed when comparison is made with images obtained in ultrapure water.

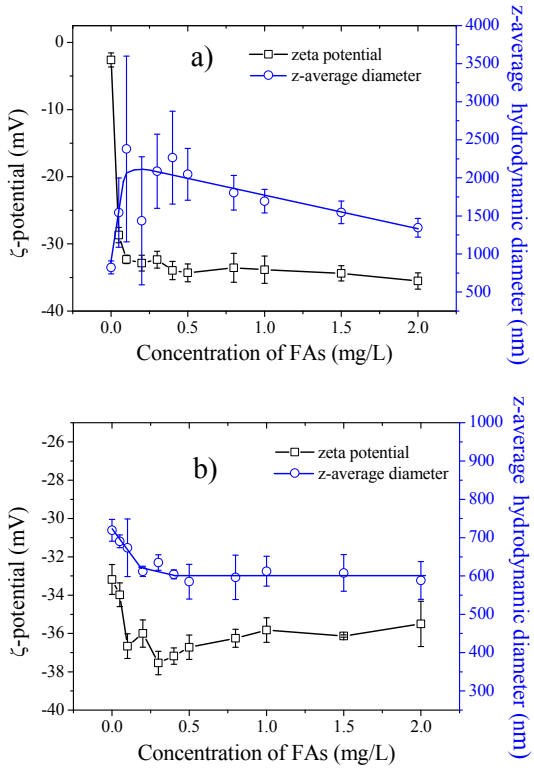

Fig. 3. Zeta potential and z-average hydrodynamic diameter of CeO_2 NPs in the presence of different concentration of FAs. (a) pH = 7.0 ± 0.1 close to pH_{PZC}, (b) pH = 10.0 ± 0.1 > pH_{PZC}. In presence of FAs, CeO_2 zeta potentials are found significantly negative. At the pH_{PZC}, 0.25 mg L^{-1} of FAs is found sufficient to stabilize the CeO_2 aggregates.

pure water with pH_{PZC} = 6.5. In this study it was shown that the PZC was a function of particle synthesis conditions and varied from 5.8 to 7.6 depending on the concentration of methanol that was used for the synthesis. In the literature there is no consistency according to the PZC of cerium oxide NPs. Quik et al. (2010) reported the PZC of CeO_2 NPs in deionized water was equal to 8.0 and a similar value was found by Limbach et al. (2008). Differences can be explained by the presence of various components/groups on the surface of nanoparticles and in the composition variation of cerium oxides (redox state) as particles are usually obtained from different sources (Baalousha et al., 2010; Zhang et al., 2004).

3.2. Effect of FAs on CeO_2 NPs stability

We investigated the influence of different concentrations of FAs on nanoparticle surface charge and size in three different pH domains corresponding to three electrostatic scenario: at pH = 3.0 ± 0.1 < pH_{PZC}, at pH = 7.0 ± 0.1 close to pH_{PZC} and at pH = 10.0 ± 0.1 > pH_{PZC}.

pH < pH_{PZC}. In this pH domain CeO_2 NPs are initially strongly positively charged. With increase of FAs concentration, surface charge of particles changed from positive to negative values (Fig. 2a). This pH domain represents favorable conditions for adsorption of FAs molecules as they are negatively charged in all range of pH (SI, S2). FAs and positively charged CeO_2 are thus forming electrostatic complexes. FAs concentration of 0.25 mg L^{-1} is needed to reach an isoelectric point (IEP). Then by further increasing the FAs concentration charge inversion is obtained. When FAs concentration is equal to 2 mg L^{-1} the value of zeta potential is equal to −28.6 ± 0.7 mV. Below IEP, CeO_2 NPs are stable and their z-average hydrodynamic diameter is equal to the baseline value found in part 3.1. At the IEP the surface charges of particles are neutralized and results in aggregation with an increase of z-average hydrodynamic diameters up to 2700 nm. Further increase of FAs concentration leads to stabilization (and partial disaggregation) with z-average particle diameter around 1700 nm. To get insight into the aggregate structure using SEM we investigated mixtures of CeO_2 NPs and FAs with final concentrations equal to 50 and 2 mg L^{-1} accordingly (Fig. 2b). Aggregates were found embedded into a matrix made of NOM. An organic coating around NPs was observed if comparison is made with SEM pictures of the nanoparticles in ultrapure water (Fig. 1b).

pH ≈ pH_{PZC}. We performed experiments at pH 7.0 ± 0.1. At this pH the surface charge of CeO_2 NPs is close to zero (Fig. 3a) and results in particle aggregation with a z-average diameter equal to 824 ± 86 nm. Successive addition of FAs leads to the fast decrease of zeta potential due to the adsorption of negatively charged FAs molecules. The value of zeta potential is rapidly stabilized around −35 mV after the first addition of FAs. Z-average particle diameter is first growing up (at low FAs concentration) and then decreases to 1500 nm hence indicating that the adsorption of FAs leads to the stabilization (and partial disaggregation) of already formed aggregates. Electrostatic and steric repulsion forces are not here strong enough to disagglomerate aggregates to their initial baseline size or towards the dispersion of individual NPs.

pH > pH_{PZC}. We performed the experiments at pH 10.0 ± 0.1. At this pH both NPs and FAs exhibit a negative surface charge. CeO_2 initial zeta potential is equal to −33.2 ± 0.8 mV (Fig. 3b). The presence of FAs is not changing significantly the values of CeO_2 zeta potential that are around −36 mV in all range of FAs concentrations

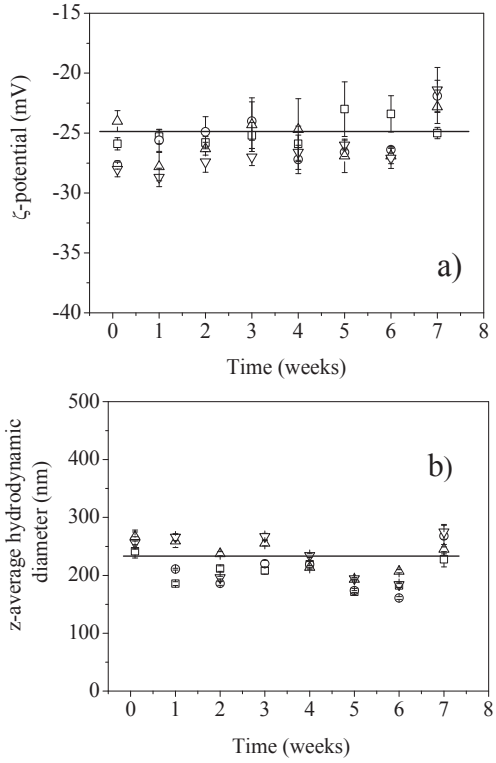

Fig. 4. Stability of CeO_2 NPs coated with FAs at 2 mg L^{-1} with time. Zeta potential (a) was stable over time with a value equal to −25 ± 7 mV as well as z-average diameter (b) which was stable and equal to 220 ± 40 nm. Different symbols correspond to four independent experiments in the same experimental conditions.

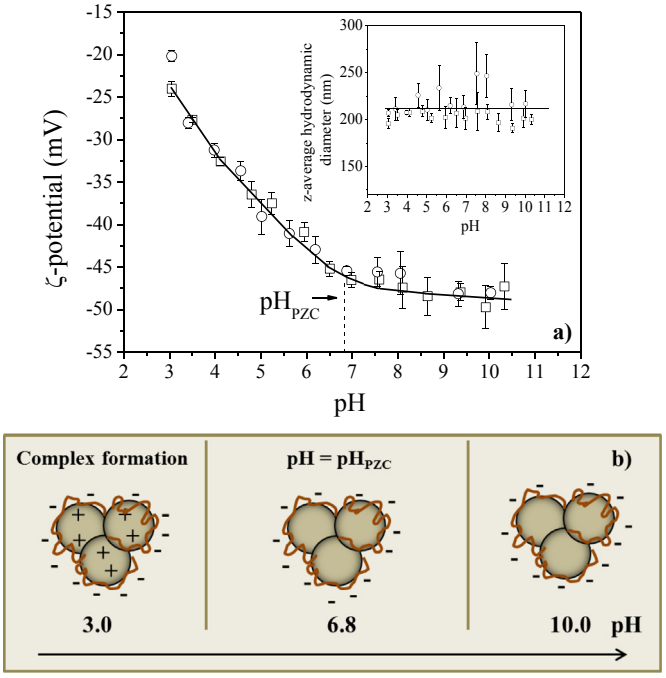

Fig. 5. (a) Variation of zeta potential and z-average hydrodynamic diameter (insert) of CeO_2 NPs coated with FAs as a function of pH. Zeta potential is found to decrease rapidly until the pH_{PZC} due to the deprotonation process of the CeO_2 NPs. Then a plateau value is obtained indicating that the presence of negatively charged FAs limits the presence of negative charges at the nanoparticle surface. Stability of z-average hydrodynamic diameter is observed in the full pH range. (b) Schematic representation of CeO_2 surface charge variation as a function of pH. At pH 3.0 ± 0.1 FAs–CeO_2 NPs complexes are negatively charged. With pH inverse the CeO_2 surface charge is deprotonated until pH_{PZC}. By increasing pH, the emergence of negative surface charge at CeO_2 surface is limited by the presence of negatively charged FAs.

up to 2 mg L^{-1}. We found a small decrease of z-average particle diameter in presence of FAs from 720 ± 28 to 600 ± 45 nm. Such changes can be related to the limited adsorption of NOM on the particle surface, due to the presence of hydrophobic interactions (Palomino et al., 2013).

3.3. Stability of FAs–CeO_2 NPs complexes

Considering the results obtained in part 3.2 we decided to check the stability of FAs – CeO_2 NPs complexes over time and by changing the pH. Electrostatic complexes were formed by considering a 50 mg L^{-1} CeO_2 suspension with a final FAs concentration equal to 2 mg L^{-1} at pH 3.0 ± 0.1. In such condition negatively charged complexes are formed with a z-average hydrodynamic diameter equal to 220 ± 40 nm and zeta potential −25 ± 7 mV. If we compare this value with average hydrodynamic diameter in Fig. 1a, we can conclude that the way how the aggregates were formed plays a crucial role in final particle size. When the particles pass through IEP the formation of aggregates is irreversible process due to the importance of particle–particle van der Waals and particle-FAs-particle hydrophobic interactions which are increasing the aggregate cohesive energy. Addition of supplementary amount of FAs does not lead to the disaggregation, regarding the change of surface charge. Nevertheless, direct addition of the same amount of FAs is enough to create a coating around nanoparticles due to the electrostatic interaction between oppositely charged NPs and FAs that leads to their stabilization.

3.3.1. Stability with time

Stability data are shown in Fig. 4. We measured zeta potentials and z-average hydrodynamic diameters during 7 weeks of four independently prepared suspensions. We showed that FAs adsorption, surface charge inversion and stabilization of NPs are fast processes. Both z-average particle diameters and zeta potential values are found stable with time. The values of nanoparticle zeta potential were found equal to −25 ± 7 mV. Z-average hydrodynamic diameter was also stable up to 7 weeks and was in the range 220 ± 40 nm i.e. slightly higher than the baseline value obtained in the absence of FAs. Our results then suggest, and as a first approximation, that the adsorbed FAs layer thickness is close to 35 nm i.e. small in comparison with the aggregate sizes.

3.3.2. Stability with pH change

As shown in section 3.1, pH variation is expected to change the nanoparticle surface properties from positive charges at low pH to negative charges at high pH. Zeta potential and z-average diameter variations of coated CeO_2 NPs as a function of pH are presented in Fig. 5a. First, it should be noted that the zeta potential is negative in all pH range and is decreasing from −24.0 ± 0.9 to −49.7 ± 2.5 mV. Two different domains are obtained. In the first domain, the values of zeta potential rapidly decrease with increase of pH from −24.0 ± 0.9 to −45.2 ± 0.9 mV until the pH corresponding to the PZC. Then, above the pH_{PZC} the increase of pH does not significantly influence zeta potential that is now in the range from −45.2 ± 0.9 to −49.7 ± 2.5 mV. Meanwhile, we observed a constant z-average hydrodynamic diameter that was equal to 220 ± 40 nm in all pH range. Such variations can be explained by the electrostatic properties of the FAs–CeO_2 complexes and in particularly by the modification of the acid-base properties of CeO_2 NPs in presence of FAs. At pH 3 nanoparticles are positively charged.

Consequently, addition of negatively charged FAs leads to the rapid adsorption of FAs on the nanoparticle surface (Fig. 5b). A 2 mg L^{-1} FAs concentration induces a rapid and significant charge inversion of CeO_2 NPs. After formation of FAs–CeO_2 complexes zeta potential is negative and the particle hydrodynamic diameter increased from baseline value 185 nm to 220 nm. Then increase of pH leads to the decrease of the value of zeta potential due to the neutralization of the positively charged surface sites of CeO_2 NPs by hydroxyl ions (Jolivet et al., 2000) according to the equation (1):

$$M - OH_2^+ + OH^- \rightarrow M - OH + H_2O \quad (1)$$

The neutralization of CeO_2 surface charge occurs at a pH value which is close to the pH_{PZC} as shown in Fig. 5a. Then by increasing further the pH, since zeta potential is stable, the second deprotonation step (2):

$$M - OH + OH^- \leftrightarrow M - O^- + H_2O \quad (2)$$

is found more difficult to achieve. Further surface deprotonation above pH_{PZC} is not significant enough because of the increase of repulsive electrostatic interactions due to the presence of negatively charged FAs at the nanoparticle surface. The particle size did not change during the pH modification and equal to 220 nm owing to the high cohesive energy between FAs and NPs. To destabilize formed complexes the desorption of FAs molecules should be done, but this process is not energetically favorable. This is an important point indicating that FAs adsorption at the nanoparticle surface can significantly change their surface acid-base properties.

4. Conclusion

The behavior of CeO_2 NPs in presence of FAs was investigated using three complementary techniques (DLS, NTA and SEM), two main parameters (average diameter and zeta potential) were analyzed and we focused on influence of pH and FAs concentration. The first important outcome here is to show that the way how the FAs–CeO_2 NPs complexes were formed influence the size and further behavior of particles. When the FAs concentration is gradually increased we demonstrated the formation of large aggregates, contrarily direct addition of low FAs concentrations, representative of environmental freshwater conditions, is found sufficient to stabilize relatively highly concentrated CeO_2 NPs suspensions against aggregation. In addition, when pH < pH_{PZC} strong electrostatic complexes are formed between FAs and CeO_2 NPs and charge inversion is observed.

The second important outcome indicates that the FAs–CeO_2 complexes, once formed, are stable with time up to 7 weeks but also regarding important pH variations. We believe this constitutes an important result since, from environmental risk assessment point of view, stabilization of CeO_2 NPs with time and in changing pH conditions could significantly enhance their mobility and residence time throughout aquatic systems and water treatment processes.

Acknowledgments

The authors are grateful for the financial support received from the Swiss National Foundation (project 200021_135240). The work leading to the results also received funding from the European Union Seventh Framework Programme (FP/2007–2013) under agreement NMP4-LA-2013-310451. We also acknowledge to Agathe Martignier for the help with SEM experiments and Fabrice Carnal for helpful discussions.

Appendix A. Supplementary data

Supplementary data related to this article can be found at http://dx.doi.org/10.1016/j.chemosphere.2015.08.057.

References

Baalousha, M., Le Coustumer, P., Jones, I., Lead, J.R., 2010. Characterisation of structural and surface speciation of representative commercially available cerium oxide nanoparticles. Environ. Chem. 7, 377–385.
Buettner, K.M., Rinciog, C.I., Mylon, S.E., 2010. Aggregation kinetics of cerium oxide nanoparticles in monovalent and divalent electrolytes. Colloids Surf. Physicochem. Eng. Asp. 366, 74–79. http://dx.doi.org/10.1016/j.colsurfa.2010.05.024.
Clavier, A., Seijo, M., Carnal, F., Stoll, S., 2015. Surface charging behavior of nanoparticles by considering site distribution and density, dielectric constant and pH changes. A Monte Carlo approach. Phys. Chem. Chem. Phys. 17, 4346–4353. http://dx.doi.org/10.1039/C4CP04733H.
Cong, Y., Banta, G.T., Selck, H., Berhanu, D., Valsami-Jones, E., Forbes, V.E., 2011. Toxic effects and bioaccumulation of nano-, micron- and ionic-Ag in the polychaete, Nereis diversicolor. Aquat. Toxicol. 105, 403–411. http://dx.doi.org/10.1016/j.aquatox.2011.07.014.
El-Toni, A.M., Yin, S., Hayasaka, Y., Sato, T., 2006. Synthesis and UV-shielding properties of silica-coated calcia-doped ceria nanoparticles via soft solution processes. J. Electroceram. 17, 9–14. http://dx.doi.org/10.1007/s10832-006-9928-7.
Fabrega, J., Luoma, S.N., Tyler, C.R., Galloway, T.S., Lead, J.R., 2011. Silver nanoparticles: behaviour and effects in the aquatic environment. Environ. Int. 37, 517–531. http://dx.doi.org/10.1016/j.envint.2010.10.012.
Frimmel, F.H., Abbt-Braun, G., 1999. Basic characterization of reference NOM from Central Europe — Similarities and differences. Environ. Int. 25, 191–207. http://dx.doi.org/10.1016/S0160-4120(98)00116-0. Nom-typing.
Ghosh, S., Jiang, W., McClements, J.D., Xing, B., 2011. Colloidal stability of magnetic iron oxide nanoparticles: influence of natural organic matter and synthetic polyelectrolytes. Langmuir 27, 8036–8043. http://dx.doi.org/10.1021/la200772e.
Gottschalk, F., Nowack, B., 2011. The release of engineered nanomaterials to the environment. J. Environ. Monit. 13, 1145–1155.
Gregory, J., 2005. Particles in Water: Properties and Processes. CRC Press.
Grillo, R., Rosa, A.H., Fraceto, L.F., 2015. Engineered nanoparticles and organic matter: a review of the state-of-the-art. Chemosphere 119, 608–619. http://dx.doi.org/10.1016/j.chemosphere.2014.07.049.
Jolivet, J.-P., Henry, M., Livage, J., 2000. Metal Oxide Chemistry and Synthesis: from Solution to Solid State. Wiley-Blackwell.
Keller, A.A., Wang, H., Zhou, D., Lenihan, H.S., Cherr, G., Cardinale, B.J., Miller, R., Ji, Z., 2010. Stability and aggregation of metal oxide nanoparticles in natural aqueous matrices. Environ. Sci. Technol. 44, 1962–1967.
Kessler, R., 2011. Engineered nanoparticles in consumer products: understanding a new ingredient. Environ. Health Perspect. 119, A120–A125.
Labille, J., Feng, J., Botta, C., Borschneck, D., Sammut, M., Cabie, M., Auffan, M., Rose, J., Bottero, J.-Y., 2010. Aging of TiO_2 nanocomposites used in sunscreen. Dispersion and fate of the degradation products in aqueous environment. Environ. Pollut. 158, 3482–3489.
Li, K., Chen, Y., 2012. Effect of natural organic matter on the aggregation kinetics of CeO_2 nanoparticles in KCl and $CaCl_2$ solutions: measurements and modeling. J. Hazard. Mater. 209–210, 264–270. http://dx.doi.org/10.1016/j.jhazmat.2012.01.013.
Limbach, L.K., Bereiter, R., Müller, E., Krebs, R., Gälli, R., Stark, W.J., 2008. Removal of oxide nanoparticles in a model wastewater treatment plant: influence of agglomeration and surfactants on clearing efficiency. Environ. Sci. Technol. 42, 5828–5833. http://dx.doi.org/10.1021/es800091f.
Liu, J., Legros, S., Ma, G., Veinot, J.G.C., von der Kammer, F., Hofmann, T., 2012. Influence of surface functionalization and particle size on the aggregation kinetics of engineered nanoparticles. Chemosphere 87, 918–924. http://dx.doi.org/10.1016/j.chemosphere.2012.01.045.
Loosli, F., Coustumer, P.L., Stoll, S., 2013. TiO_2 nanoparticles aggregation and disaggregation in presence of alginate and Suwannee River humic acids. pH and concentration effects on nanoparticle stability. Water Res. 47, 6052–6063.
Loosli, F., Le Coustumer, P., Stoll, S., 2014. Effect of natural organic matter on the disagglomeration of manufactured TiO_2 nanoparticles. Environ. Sci. Nano 1, 154–160.
Mitrano, D.M., Rimmele, E., Wichser, A., Erni, R., Height, M., Nowack, B., 2014. Presence of nanoparticles in wash water from conventional silver and nanosilver textiles. ACS Nano 8, 7208–7219. http://dx.doi.org/10.1021/nn502228w.
Mohd Omar, F., Abdul Aziz, H., Stoll, S., 2014. Aggregation and disaggregation of ZnO nanoparticles: influence of pH and adsorption of Suwannee River humic acid. Sci. Total Environ. 468–469, 195–201. http://dx.doi.org/10.1016/j.scitotenv.2013.08.044.
Molina, R.M., Konduru, N.V., Jimenez, R.J., Pyrgiotakis, G., Demokritou, P., Wohlleben, W., Brain, J.D., 2014. Bioavailability, distribution and clearance of tracheally instilled, gavaged or injected cerium dioxide nanoparticles and ionic cerium. Environ. Sci. Nano 1, 561–573. http://dx.doi.org/10.1039/C4EN00034J.
Moos, N., von, Bowen, P., Slaveykova, V.I., 2014. Bioavailability of inorganic nanoparticles to planktonic bacteria and aquatic microalgae in freshwater. Environ. Sci. Nano 1, 214–232. http://dx.doi.org/10.1039/C3EN00054K.

Motellier, S., Derrough, S., Locatelli, D., Amdaoud, M., Lhaute, K., 2013. Direct quantification of TiO_2 nanoparticles in suspension by grazing-incidence X-ray fluorescence spectrometry: influence of substrate pre-treatment in the deposition process. Spectrochim. Acta Part B At. Spectrosc. 88, 1–9. http://dx.doi.org/10.1016/j.sab.2013.07.003.

Neubauer, E., Schenkeveld, W.D.C., Plathe, K.L., Rentenberger, C., von der Kammer, F., Kraemer, S.M., Hofmann, T., 2013. The influence of pH on iron speciation in podzol extracts: iron complexes with natural organic matter, and iron mineral nanoparticles. Sci. Total Environ. 461–462, 108–116. http://dx.doi.org/10.1016/j.scitotenv.2013.04.076.

Palomino, D., Yamunake, C., Coustumer, P.L., Stoll, S., 2013. Stability of TiO_2 nanoparticles in presence of fulvic acids. Importance of pH. J. Colloid Sci. Biotechnol. 2, 62–69. http://dx.doi.org/10.1166/jcsb.2013.1033.

Petosa, A.R., Öhl, C., Rajput, F., Tufenkji, N., 2013. Mobility of nanosized cerium dioxide and polymeric capsules in quartz and loamy sands saturated with model and natural groundwaters. Water Res. 47, 5889–5900. http://dx.doi.org/10.1016/j.watres.2013.07.006.

Quik, J.T.K., Lynch, I., Hoecke, K.V., Miermans, C.J.H., Schamphelaere, K.A.C.D., Janssen, C.R., Dawson, K.A., Stuart, M.A.C., Meent, D.V.D., 2010. Effect of natural organic matter on cerium dioxide nanoparticles settling in model fresh water. Chemosphere 81, 711–715. http://dx.doi.org/10.1016/j.chemosphere.2010.07.062.

Rodea-Palomares, I., Boltes, K., Fernández-Piñas, F., Leganés, F., García-Calvo, E., Santiago, J., Rosal, R., 2011. Physicochemical characterization and ecotoxicological assessment of CeO_2 nanoparticles using two aquatic microorganisms. Toxicol. Sci. 119, 135–145.

Röhder, L.A., Brandt, T., Sigg, L., Behra, R., 2014. Influence of agglomeration of cerium oxide nanoparticles and speciation of cerium(III) on short term effects to the green algae *Chlamydomonas reinhardtii*. Aquat. Toxicol. 152, 121–130. http://dx.doi.org/10.1016/j.aquatox.2014.03.027.

Rosa, A.H., Goveia, D., Bellin, I.C., Tonello, P.S., Antunes, M.L.P., Filho, D., Luiz, N., Filho, R., Pereira, U., 2007. Lability study of Cu(II), Cd(II), Mn(II) and Ni(II) complexed by aquatic humic substances using organomodified cellulose membranes. Quím. Nova 30, 59–65. http://dx.doi.org/10.1590/S0100-40422007000100014.

Safi, M., Sarrouj, H., Sandre, O., Mignet, N., Berret, J.-F., 2010. Interactions between sub-10 nm iron and cerium oxide nanoparticles and 3T3 fibroblasts : the role of the coating and aggregation state. Nanotechnology 21, 145103. http://dx.doi.org/10.1088/0957-4484/21/14/145103.

Sajith, V., Sobhan, C.B., Peterson, G.P., 2010. Experimental investigations on the effects of cerium oxide nanoparticle fuel additives on biodiesel. Adv. Mech. Eng. e581407. http://dx.doi.org/10.1155/2010/581407.

Singh, C., Friedrichs, S., Ceccone, G., Gibson, N., Jensen, K.A., Levin, M., Infante, H.G., Carlander, D., Rasmussen, K., 2014. Cerium Dioxide, NM-211, NM-212, NM-213. Characterisation and Test Item Preparation. European Commission, Joint Research Centre, European Union. http://dx.doi.org/10.2788/80203.

von Moos, N., Slaveykova, V.I., 2013. Oxidative stress induced by inorganic nanoparticles in bacteria and aquatic microalgae – state of the art and knowledge gaps. Nanotoxicology 8, 605–630. http://dx.doi.org/10.3109/17435390.2013.809810.

Von Wandruszka, R., 2000. Humic acids: their detergent qualities and potential uses in pollution remediation. Geochem. Trans. 1, 10–15.

Wilkinson, K.J., Balnois, E., Leppard, G.G., Buffle, J., 1999. Characteristic features of the major components of freshwater colloidal organic matter revealed by transmission electron and atomic force microscopy. Colloids Surf. Physicochem. Eng. Asp. 155, 287–310. http://dx.doi.org/10.1016/S0927-7757(98)00874-7.

Zhang, F., Wang, P., Koberstein, J., Khalid, S., Chan, S.-W., 2004. Cerium oxidation state in ceria nanoparticles studied with X-ray photoelectron spectroscopy and absorption near edge spectroscopy. Surf. Sci. 563, 74–82. http://dx.doi.org/10.1016/j.susc.2004.05.138.

Chapter IV

Aggregation of CeO_2 NPs and FA coated CeO_2 NPs in changing environmental conditions

Published as

Oriekhova, O., and Stoll, S., 2016, Stability of uncoated and fulvic acids coated manufactured CeO_2 nanoparticles in various conditions: From ultrapure to natural Lake Geneva waters, Science of the Total Environment, v. 562, pp. 327-334 (Paper II).

IV.1 Introduction

To understand the fate of CeO_2 NPs in natural environment the systematic study of the NP behaviour in relevant natural water conditions should be performed. When NPs are released to natural aquatic system many processes occur such as aggregation, coating, sedimentation, dispersion and dissolution which are dependent on the particle as well as water properties. The concentration of divalent ions, water pH and concentration of dissolved organic carbon are defined (Ottofuelling et al., 2011) as main parameters which influence TiO_2 NPs aggregation in synthetic and natural waters. NOM from naturally water reach in organic matter is more effective in stabilising NPs compared to NOM surrogate such as Suwannee River. Keller et al. (2010) studied the behaviour of TiO_2, ZnO and CeO_2 NPs in eight different types of water from seawater to river and groundwater. They showed that the electrophoretic mobility in various water is independent of pH but strongly influenced by NOM and ionic strength. The adsorption of NOM onto the NP surface reduced their aggregation, stabilising them under many environmental conditions. The presence of inorganic colloids is another factor that can influence the stability of NPs in natural water (Labille et al., 2015; Praetorius et al., 2014). It was shown by Labille et al. (2015) that the aggregation of TiO_2 NPs in the presence of smectite clays is mainly driven by heteroaggregation whereas the homoaggregation between NPs is negligible.

In this chapter, we investigate the stability of pristine CeO_2 NPs and FA coated CeO_2 NPs at different FA concentrations in ultrapure water considering several scenarios. The effect of pH variation on CeO_2/FA complexes is studied. The behaviour of pristine and FAs-coated CeO_2 NPs when added in solutions at environmental pH is also investigated. Then the stability of CeO_2 NPs in synthetic waters without and in the presence of variable FA concentrations has been studied. Finally, the comparison of results is made with Lake Geneva water. The mechanisms responsible for the CeO_2 aggregation are discussed.

IV.2 Main results

To investigate the role of FAs on CeO_2 NP stability we studied uncoated and coated NPs in changing pH conditions. First, we prepared three suspensions, pristine CeO_2 and coated CeO_2 with 0.5 and 2 mg/L FAs, at pH 3. Then we increase the pH. Even at low pH in the presence of FAs a charge reversal is obtained, zeta potential is equal to –6.2 ± 0.6 and –22.0 ± 0.7 mV for 0.5 and 2 mg/L, respectively. With increase of pH, zeta potential of

pristine particles decreases and then charge inversion is observed, whereas for coated particles zeta potential became even more negative. Coated with 2 mg/L FAs CeO_2 is stable in full pH range with constant diameters which are equal to 210.8 ± 9.6 nm. In the absence and at low FA concentration the aggregation is observed due to the dominance of the attractive van der Waals forces over the electrostatic repulsive forces.

A synthetic water, which reproduces the chemical composition of Lake Geneva water, was considered to mimic the ionic composition. CeO_2 NPs were introduced to this synthetic water as well as in filtered Lake Geneva water to investigate the stability of NPs in environmental conditions. Zeta potential and z-average hydrodynamic diameter measured in the different water samples are presented in Fig. IV.1. S1 corresponds to CeO_2 in synthetic water, S2 and S3 to CeO_2 in synthetic water in the presence of FAs (0.5 and 2 mg/L), respectively, and S4 corresponds to CeO_2 in filtered Lake Geneva water. In all water samples zeta potential was negative and varied in the range from –13.3 ± 0.6 mV to –23.4 ± 0.8 mV (Fig. IV.1a). The presence of 2 mg/L FAs is found to stabilise CeO_2 NPs despite the effect of ionic strength, z-average diameter is equal to 224 ± 8 nm. In the presence of 0.5 mg/L FAs, suspension is found less stable with the size of aggregate up to 2000 nm. CeO_2 is mostly aggregated in pure synthetic water (S1) with z-average diameter up to 4000 nm due to the effect of mono and divalent electrolytes.

In Lake Geneva water (S4) CeO_2 NPs are also found aggregated in contrast to the sample S3 which is expected to fully represent the chemical composition of natural Lake Geneva water. Such results indicate that the presence of inorganic colloids as well as the heterogeneity of dissolved organic matter in natural water have different properties, reactivity and more important effects on the stability of CeO_2 NPs compared to solutions containing Suwanee River FAs. Our results are also supported by SEM images (Fig. IV.2) of CeO_2 NPs in filtered Lake Geneva water indicating the formation of large heteroaggregates in which CeO_2 are embedded in a complex matrix made of dissolved organic matter, natural salts and inorganic colloids.

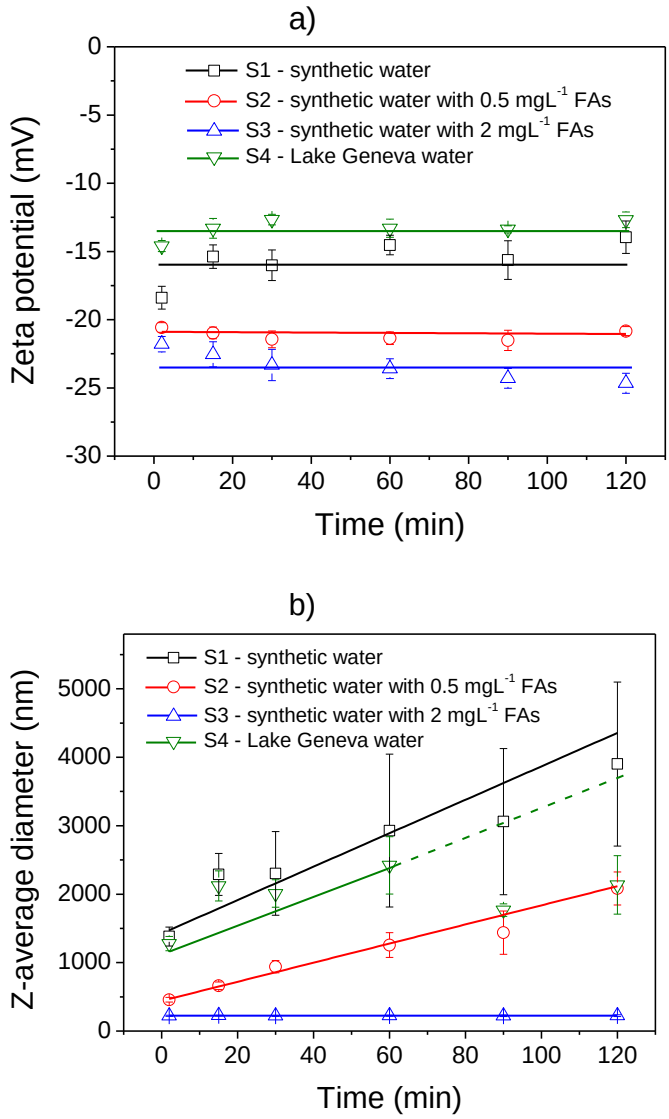

Fig. IV.1. (a) Zeta potential and (b) z-average hydrodynamic diameter of CeO_2 NPs as a function of time in different water samples: S1 – synthetic water; S2 – synthetic water with 0.5 mg L^{-1} FAs; S3 – synthetic water with 2 mg L^{-1} FAs; S4 – Lake Geneva water. A good agreement is obtained between zeta potential values and hydrodynamic diameters.

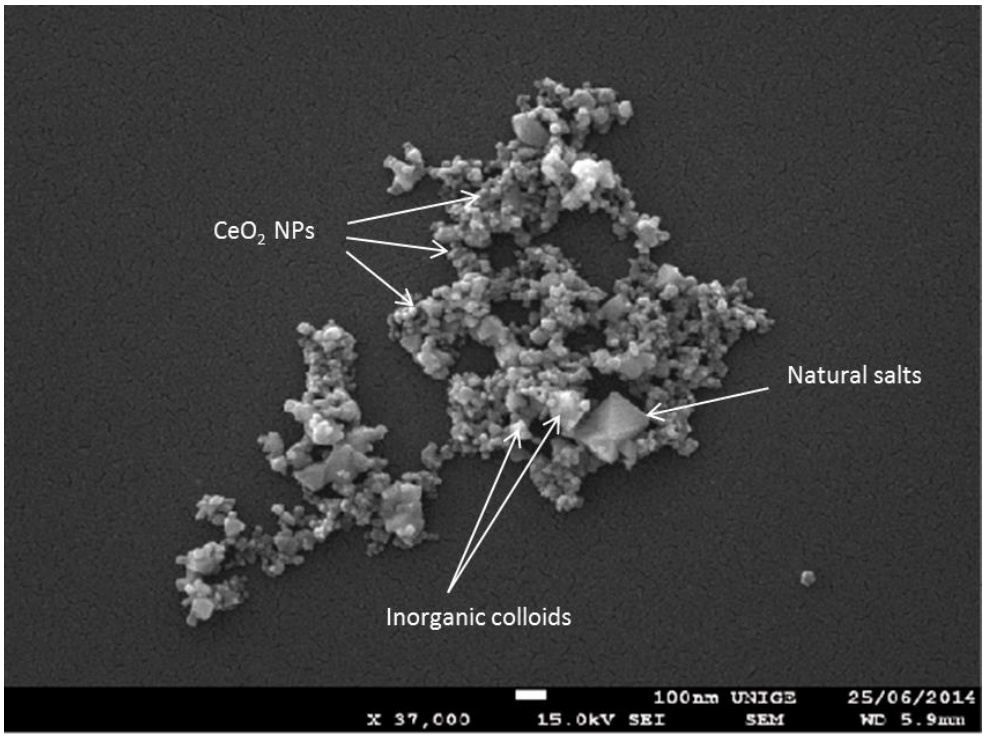

Fig. IV.2. SEM images of CeO_2 NPs in natural Lake Geneva water. NPs are found aggregated and embedded in a complex matrix made of dissolved organic matter, natural salts and inorganic colloids.

IV.3 References

Gallego-Urrea, J.A., Tuoriniemi, J., Pallander, T., Hassellöv, M., 2010. Measurements of nanoparticle number concentrations and size distributions in contrasting aquatic environments using nanoparticle tracking analysis. Environ. Chem. 7, 67–81.

Keller, A.A., Wang, H., Zhou, D., Lenihan, H.S., Cherr, G., Cardinale, B.J., Miller, R., Ji, Z., 2010. Stability and aggregation of metal oxide nanoparticles in natural aqueous matrices. Environ. Sci. Technol. 44, 1962–1967.

Labille, J., Harns, C., Bottero, J.-Y., Brant, J., 2015. Heteroaggregation of Titanium Dioxide Nanoparticles with Natural Clay Colloids. Environ. Sci. Technol. 49, 6608–6616. doi:10.1021/acs.est.5b00357

Ottofuelling, S., Von Der Kammer, F., Hofmann, T., 2011. Commercial titanium dioxide nanoparticles in both natural and synthetic water: comprehensive multidimensional testing and prediction of aggregation behavior. Environ. Sci. Technol. 45, 10045–10052.

Praetorius, A., Labille, J., Scheringer, M., Thill, A., Hungerbühler, K., Bottero, J.-Y., 2014. Heteroaggregation of Titanium Dioxide Nanoparticles with Model Natural Colloids under Environmentally Relevant Conditions. Environ. Sci. Technol. 48, 10690–10698. doi:10.1021/es501655v

Paper II

Oriekhova, O., and Stoll, S., 2016, Stability of uncoated and fulvic acids coated manufactured CeO_2 nanoparticles in various conditions: From ultrapure to natural Lake Geneva waters, Science of the Total Environment, v. 562, pp. 327-334.

Science of the Total Environment 562 (2016) 327–334

Contents lists available at ScienceDirect

Science of the Total Environment

journal homepage: www.elsevier.com/locate/scitotenv

Stability of uncoated and fulvic acids coated manufactured CeO_2 nanoparticles in various conditions: From ultrapure to natural Lake Geneva waters

Olena Oriekhova, Serge Stoll *

Institute F.-A. Forel, University of Geneva, Faculty of Science, Uni Carl Vogt, Group of Environmental Physical Chemistry, 66, Boulevard Carl-Vogt, CH 1211 Geneva, 4, Switzerland

HIGHLIGHTS

- Fulvic acids coating is stable in pH changing conditions.
- Stability of CeO_2 in synthetic and ultrapure waters is improved by fulvic acids.
- In Lake Geneva water CeO_2 aggregation is observed.
- Competitive processes are controlling CeO_2 surface properties and stability.

GRAPHICAL ABSTRACT

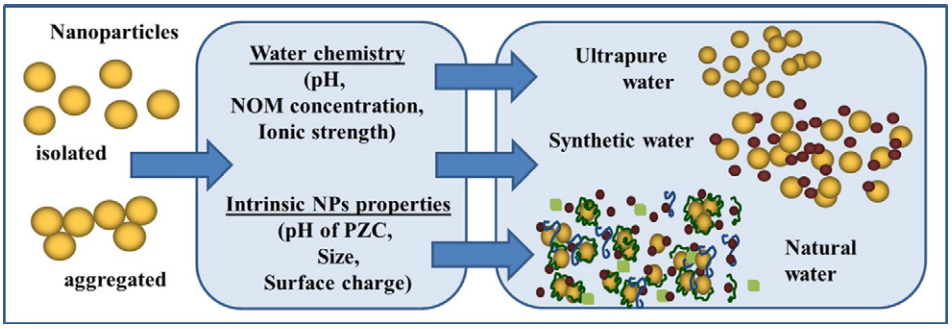

ARTICLE INFO

Article history:
Received 19 January 2016
Received in revised form 9 March 2016
Accepted 25 March 2016
Available online 19 April 2016

Editor: D. Barcelo

Keywords:
CeO_2 nanoparticle stability
Fulvic acids coating
Aggregation
Complexation
Surface charge modification

ABSTRACT

Understanding the behavior of engineered nanoparticles in natural water and impact of water composition in changing conditions is of high importance to predict their fate once released into the environment. In this study we investigated the stability of uncoated and Suwannee River fulvic acids coated CeO_2 manufactured nanoparticles in various environmental conditions. The effect of pH changes on the nanoparticle and coating stability was first studied in ultrapure water as well as the variation of zeta potentials and sizes with time in presence of fulvic acids at environmental pH. Then the stability of CeO_2 in synthetic and natural Lake Geneva waters was investigated as a function of fulvic acids concentration. Our results indicate that the adsorption of environmentally relevant concentrations of Suwannee River fulvic acids promotes CeO_2 stabilization in ultrapure water as well as synthetic water and that the coating stability is high upon pH variations. On the other hand in natural Lake Geneva water CeO_2 NPs are found in all cases aggregated due to the effect of heterogeneous organic and inorganic compounds.

1. Introduction

Cerium dioxide (CeO_2) nanoparticles are widely used in different applications such as additives to diesel fuels, components of interior coating of self-cleaning ovens and in many electrochemical devices (Garcia et al., 2005; Reed et al., 2014). The presence of such nanoparticles in a large number of commercial products is expected to result in their

* Corresponding author.
E-mail addresses: Olena.Oriekhova@unige.ch (O. Oriekhova), Serge.Stoll@unige.ch (S. Stoll).

http://dx.doi.org/10.1016/j.scitotenv.2016.03.184
0048-9697/

release into the environment through effluents from waste water treatment plants, aerosol deposition, industrial spillage and possible local pollution events (Gottschalk and Nowack, 2011; Neal et al., 2011). The fate and behavior of manufactured nanoparticles (NPs) in the environment depend on many physical and chemical processes such as aggregation (homo-aggregation and hetero-aggregation), coating, sedimentation, dispersion and dissolution, but also on the intrinsic nanoparticle properties (size, shape and surface charge) and the chemistry of surrounding medium (pH, ionic strength) (Ghosh et al., 2014; Labille et al., 2014; Sani-Kast et al., 2015). In addition, when NPs enter in aquatic systems they interact with different components, such as natural organic matter (NOM), dissolved ions, and inorganic particles. NOM, in particular humic substances, are expected to adsorb and form a coating on the NPs surface (Schaumann et al., 2015; Yang et al., 2009). Such a coating can result in NPs stabilization or disaggregation as shown by Baalousha (2009) and Loosli et al. (2014). On the other hand, the presence of mono- and divalent electrolytes preferentially results to fast aggregation via cation bridging and surface charge screening processes (Loosli et al., 2015). Humic substances represent a major part of NOM in natural water and are present in the form of fulvic acids (FAs), humic acids (HAs) and humin (Frimmel, 1998; Frimmel and Abbt-Braun, 1999). FAs are mixtures of different types of organic acids and are more reactive compared to HAs due to the high concentration of hydroxyl (–OH) and carboxyl (–COOH) groups. FAs have low molecular weights and are soluble in a large pH range (Pettit, 2004). FAs have different effects than HAs on colloid surfaces (Harbour et al., 2007) and nanoparticles (Domingos et al., 2009; Oriekhova and Stoll, 2016).

The stability of NPs regarding aggregation and importance of natural organic matter in natural and synthetic waters has been investigated in the literature by considering many different situations. Ottofuelling et al., (2011) investigated colloidal stability of commercial TiO_2 NPs in different types of synthetic and natural waters. The authors identified the key parameters having the strongest influence on the NPs aggregation behavior. These parameters are the concentration of divalent ions, the water pH and the concentration of dissolved organic carbon. In addition, they found that NOM surrogate (Suwannee River natural organic matter) was less effective in stabilizing NPs in comparison with natural water which is rich in organic matter. To explain the stabilization effect of NOM on the NPs behavior it is important to consider the different possible mechanisms of NPs aggregation. Keller et al. (2010) studied the behavior of three different metal oxide nanoparticles (TiO_2, ZnO and CeO_2) in eight different aqueous media from seawater to river and groundwater. They showed that NOM and ionic strength are dominant factors in particle electrophoretic mobilities and that the adsorption of NOM onto the NPs surface significantly reduced their aggregation, stabilizing them under many environmental conditions. Metreveli et al. (2015) studied the disaggregation processes of citrate coated Ag NPs in a Rhine River water matrix. It was shown that the presence of Suwannee River humic acid induces electrosteric stabilization of particles at low Ca^{2+} concentrations and cation-bridging flocculation at high Ca^{2+} concentrations. The environmental fate of silver nanoparticles in seawater mesocosms was also studied by Cleveland et al. (2012). It was shown that silver NPs were rapidly removed from water column by adsorption to the sediment and biomass, dissolution and formation of chloro-complexes. Quik et al. (2010) also considered the adsorption of NOM on the NPs surface as the main mechanism to decrease the sedimentation of CeO_2 NPs in algae medium. However, the authors didn't mention the type of humic substances they used and they performed the experiments at fixed pH and only in algae medium. In later research (Quik et al., 2014) they focused more on the estimation of hetero-aggregation rates in order to use these data for parametrization during modeling. They demonstrated that in natural river water (from river Rhine) natural colloids play a dominant role in hetero-aggregation of CeO_2 NPs. Studying the aggregation processes of TiO_2 NPs with natural colloids, by considering smectite clays, Labille et al. (2015) demonstrated that the fate of released NPs in natural water is mainly driven by hetero-aggregation with natural colloids whereas the homo-aggregation of NPs is negligible.

Despite of the existing studies on NPs behavior in different types of natural waters (river, ground and seawater) the stability and properties of the complexes they can form with NOM is still not well understood. Therefore, a better knowledge of NPs stability (including agglomeration, disagglomeration, surface coating, and pH change effects) both in synthetic and natural waters is still necessary in order to predict the fate of NPs in the environment. In the present work, we investigate and compare the behavior of CeO_2 NPs by considering several complementary scenarios. The first one is related to the influence of pH variation on the stability of uncoated and FAs-coated CeO_2 NPs, coating stability, and behavior of CeO_2 NPs when added in solutions at environmental pH and containing FAs. This study was performed in ultrapure water so as to better isolate key parameters and for comparison with synthetic waters. Then the stability of CeO_2 NPs has been investigated in various synthetic waters at variable FAs concentration. Finally comparison was made by considering Lake Geneva water as a dispersion medium for the CeO_2 NPs.

2. Materials and methods

2.1. CeO_2 NPs

CeO_2 NPs were provided as a powder from JRC nanomaterial repository (Ispra, Italy) and as a part of NanoMILE project with the code name NM-212, corresponding to uncoated particles with primary particle diameter equal to 28 ± 10 nm and a specific surface area equal to 27.2 ± 0.9 $m^2\ g^{-1}$ (Singh et al., 2014). Concerning the dispersion protocol, the powder was weighed and dispersed in ultrapure water, previously adjusted pH to 3.0, to obtain a 1 g L^{-1} CeO_2 stable stock suspension. Sonication during 15 min was done using an ultrasonic probe (Sonics Vibra cell, probe model CV18, Blanc Labo S.A., Switzerland). We applied the following parameters: ultrasonic processors – 130 W; resonance frequency of probe – 20 kHz; amplitude – 75%. Aliquots of the stock suspension were used to prepare diluted suspensions for further experiments. A 50 mg L^{-1} CeO_2 suspension was used in all experiments unless indicated. Such a concentration was used to optimize the signal during the dynamic light scattering and electrophoretic measurements. A detailed protocol how to prepare the suspension from powder is provided in Oriekhova and Stoll (2016).

To adjust the suspension pHs, diluted sodium hydroxide and hydrochloride acid 0.01 M solutions (NaOH and HCl, Titrisol®113, Merck, Switzerland) were used. All stock solutions were stored in a dark place at 4 °C.

2.2. Fulvic acids (FAs)

Suwannee River Fulvic acid Standard II, 2S101F (International Humic Substance Society, USA) was used as a surrogate of NOM. The corresponding powder was diluted in ultrapure water to obtain stock solutions of 1 g L^{-1}, and, a 100 mg L^{-1} solution was prepared for further dilution. To induce the NOM coating around CeO_2 NPs, 0.5 and 2 mg L^{-1} FAs solutions were used. A 0.5 mg L^{-1} FAs solution was used owing to the fact that this concentration is close to the isoelectric point conditions (Oriekhova and Stoll, 2016). A 2 mg L^{-1} FAs concentration was used as it corresponds to i) an excess of NOM and ii) the reported concentration of dissolved organic carbon in Lake Geneva water (Table 1).

2.3. Synthetic water

To mimic the composition of Lake Geneva water (Table 1) we developed a method to prepare the synthetic fresh water solutions based on the work of Hammes et al. (2013) and Smith et al. (2002). The following electrolytes were used; $CaCl_2 \cdot 6H_2O$, $MgCl_2 \cdot 6H_2O$, $Mg(NO_3)_2 \cdot 6H_2O$,

Table 1
Concentration of major elements in Lake Geneva water (Rapin and Klein, 2011; Strawczynski, 2011).

Name of element	Unit	Value
Dissolved organic carbon	mg C L^{-1}	0.95
Nitrate, NO_3^{2-}	mg N L^{-1}	0.61
Sodium Na^+	mg L^{-1}	6.42
Potassium K^+	mg L^{-1}	1.57
Calcium Ca^{2+}	mg L^{-1}	45.3
Magnesium Mg^{2+}	mg L^{-1}	6.16
Chloride Cl^-	mg L^{-1}	9.13
Sulfate SO_4^{2-}	mg L^{-1}	47.71
Alkalinity	mg L^{-1} of $CaCO_3$	92
Suspended particulate matter	mg L^{-1}	1

$CaSO_4 \cdot 2H_2O$, $CaCO_3$, $NaHCO_3$, $KHCO_3$. All chemicals were reagent grade or better (Fluka, Acros Organics and Sigma-Aldrich, Switzerland). The protocol and the corresponding concentrations of electrolytes are provided in supporting information (SI1). The presence of organic carbon was imitated by addition of FAs.

2.4. Lake Geneva water

Lake Geneva water was sampled in Versoix (GE, Switzerland). Before performing the experiments, water was filtered with a pore size equal to 0.45 μm, analyzed and stored in a dark place at constant temperature (4 °C) no longer than three weeks. The major ion composition and physicochemical parameters were measured and are provided in supporting information (SI2).

2.5. SEM imaging and X-ray energy dispersive spectrometry

A JEOL JSM-7001FA scanning electron microscope (SEM) was used to obtain images of CeO_2 NPs in synthetic and natural waters. For each sample, 10 μL of the NPs dispersion were placed on one aluminum stub covered with a 5 × 5 mm silica wafer Agar Scientific (G3390) and wrapped with 3–5 nm of gold or platinum coating. Energy dispersive spectrometry (EDS) was performed on samples of natural Lake Geneva water with CeO_2 NPs. The spectra were relatively qualitative due to the high scanning volume in comparison to the size of natural colloids, CeO_2 NPs concentration and presence of the silica wafer which gave the higher responses. The instrument was set with following parameters: voltage 15 kV, probe current 1 nA.

2.6. Dynamic light scattering methods (DLS)

Particle size distribution and z-average hydrodynamic diameters of uncoated and FAs coated NPs, as well as NPs in synthetic and natural waters, were measured with a Malvern Zetasizer Nano ZS (Malvern Instruments Ltd, UK). The autocorrelation function accumulated at least ten runs for each samples for five parallel measurements with time delay of 5 s. The Stokes-Einstein equation (1) was applied to calculate the hydrodynamic diameter d_H from the translational diffusion coefficient D according to,

$$d_H = \frac{kT}{3\pi\eta D}. \quad (1)$$

The polydispersity index for stabilized particles (coated and uncoated) was not found greater than 0.3 and for aggregated particles was found less than 0.6. To obtain the zeta potential, the electrophoretic mobility was measured using the Doppler technique with the Malvern Zetasizer Nano ZS and then the Smoluchowski equation (Gregory, 2005) was used:

$$U_E = \frac{\varepsilon\xi}{\eta}. \quad (2)$$

To characterize the uncoated CeO_2 NPs, 100 mL of the 50 mgL^{-1} suspension were prepared at pH 3.0 ± 0.1 with 0.001 M NaCl as a background electrolyte. The pH was increased from pH 3.0 to 10.0 using 0.01 M NaOH. Z-average hydrodynamic diameter and zeta potential were systematically measured 15 min after pH adjustment. The control of pH was done during all experiments with a Hach Lange HQ40d portable meter and a pH probe PHC101 (Hach Lange, Switzerland). Suspension homogenization was achieved in all experiments by using a magnet vortex with rotational speed equal to 200 rpm. The same procedure was used for coated CeO_2 NPs. 50 mg L^{-1} CeO_2 NPs suspensions with 0.5 and 2 mg L^{-1} FAs were prepared at pH 3.0 so as to obtain NOM-coated NPs. DLS measurements were performed after each increase of pH.

To follow the NPs stability with time and at varied FAs concentration three independent CeO_2 suspensions were prepared in ultrapure water with 0.5 and 2 mg L^{-1} FAs. Z-average hydrodynamic diameters and zeta potentials were measured immediately after preparation and every 30 min during 2 h and after each 6 h during 24 h. The same procedure was used in the case of synthetic and filtered Lake Geneva waters.

3. Results and discussion

To get an insight into the role of NOM on CeO_2 NPs stability as well as NOM coating stability we studied first a simplified system by considering uncoated and coated NPs in changing pH conditions. Then the role of organic coating was investigated in synthetic waters and comparison was made with Lake Geneva water.

3.1. Influence of pH variation on uncoated and coated CeO_2 NPs

Zeta potential variation as a function of pH for uncoated and coated CeO_2 NPs is first investigated (Fig. 1a). Coated CeO_2 are prepared at low pH by mixing positively charged CeO_2 NPs with negatively charged FAs. In the absence of FAs (uncoated) CeO_2 dispersed in ultrapure water with a background electrolyte 0.001 M NaCl at pH 3.0 ± 0.1 have a positive surface charge with a zeta potential value equal to +51.3 ± 1.3 mV and z-average hydrodynamic diameter equal to 173.4 ± 5.6 nm. On the other hand, CeO_2 NPs coated with FAs at 0.5 and 2 mg L^{-1} in the same pH conditions exhibit negative surface charges, with a zeta potential equal to −6.2 ± 0.6 and −22.0 ± 0.7 mV, respectively. Here, in the presence of FAs, charge reversal is obtained at low pH denoting the strong affinity between positively charged CeO_2 and negatively charged FAs thus resulting in the formation of strong FAs-CeO_2 complexes. Increase of pH for uncoated particles leads to charge inversion with a point of zero charge (PZC) equal to 6.8 ± 0.1 as shown in Fig. 1a. On the other hand coated NPs zeta potential values remain negative in the full pH range and a continuous decrease of the zeta potential is observed until the PZC of the CeO_2 NPs.

As indicated in Fig. 1b, z-average hydrodynamic diameters for uncoated NPs increase up to 2000 nm with change of pH from acid to basic conditions. When pH reaches the PZC region NPs are aggregated irreversibly since no significant decrease of the z-average hydrodynamic diameter is observed with charge reversal. For coated NPs with 2 mg L^{-1} FAs, the diameters are found constant and equal to 210.8 ± 9.6 nm in the full pH range (Fig. 1b). This denotes the strong stabilizing effect of FAs coating (both steric and electrostatic) regardless pH changing conditions. However, when the concentration of FAs is not high enough to saturate NPs surface (FAs concentration equal to 0.5 mg L^{-1}) suspension behavior is more complex. At pH 3.0 zeta potential is equal to −6.2 ± 0.6 mV. This value generally corresponds to unstable conditions if reference to DLVO theory (Elimelech et al., 1998) or

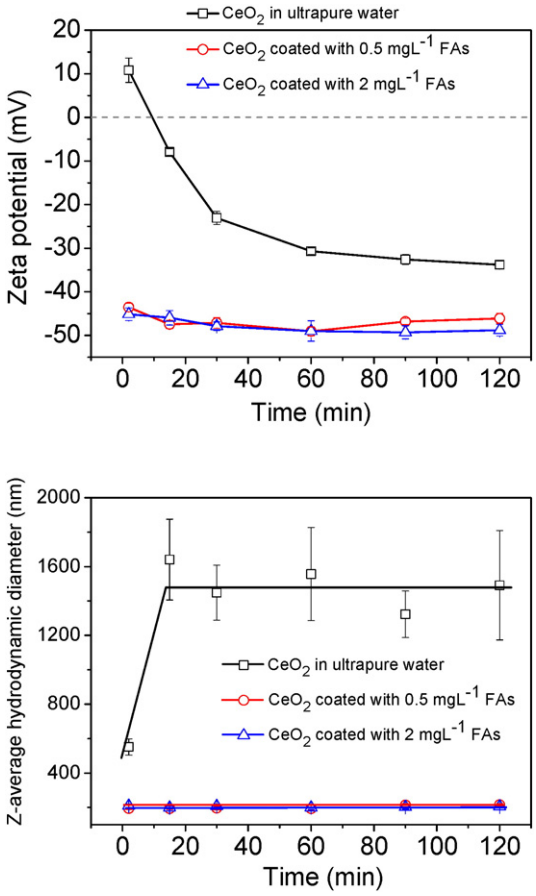

Fig. 1. (a) Zeta potential and (b) z-average hydrodynamic diameters as a function of pH of CeO_2 NPs uncoated and coated with FAs. Experimental condition: $[CeO_2] = 50$ mg L^{-1}, [NaCl] = 0.001 M, starting pH = 3.0 ± 0.1, [FAs] = 0.5 mg L^{-1} and [FAs] = 2 mg L^{-1}. For uncoated CeO_2 NPs charge inversion is observed with an increase of pH. For CeO_2 NPs coated with FAs zeta potential is negative and is decreasing with increasing pH.

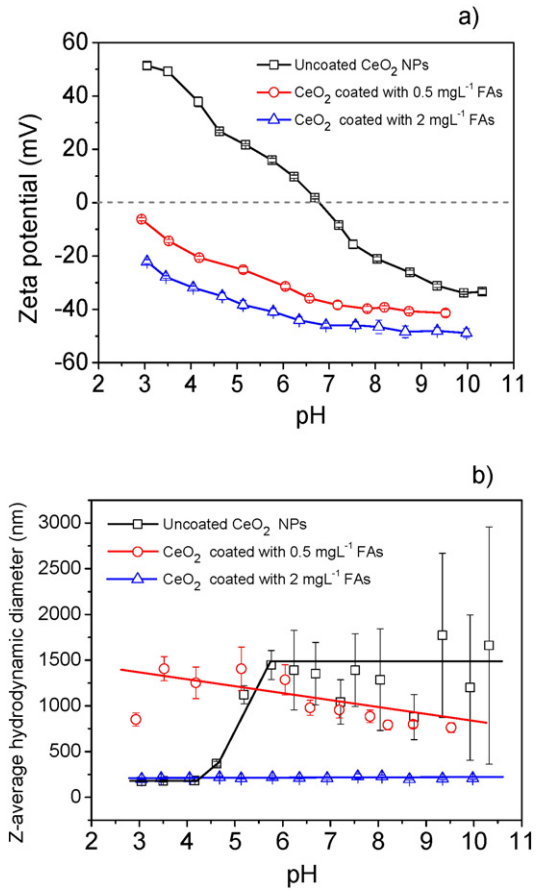

Fig. 2. (a) Zeta potential and (b) z-average hydrodynamic diameter of uncoated and coated with 0.5 and 2 mg L^{-1} FAs CeO_2 NPs as a function of time. Experimental condition: $[CeO_2] = 50$ mg L^{-1}, pH = 8.1 ± 0.2, [FAs] = 0.5 mg L^{-1} and [FAs] = 2 mg L^{-1}. In the presence of FAs NPs are stabilized in contrast with NPs in in the absence of FAs.

experimental results (Li and Sun, 2011; Palomino et al., 2013) is made. NPs aggregation can occur due to the predominance of van der Waals (vdW) forces over the electrostatic repulsive forces. The aggregate mean hydrodynamic diameters are then equal to 1405 ± 240 nm and they decrease to 763 ± 53 nm with the increase of pH. This disaggregation process is expected to be related to the increase of the electrostatic forces within the aggregates due to the increase of electrostatic charge of the FAs.

These results indicate the strong size stabilizing effect of NOM when surface coating is completely achieved even in pH changing conditions.

3.2. Time stability of CeO_2 NPs in presence of NOM at environmental pH

To understand the effect of FAs concentration on NPs stability at environmental pH we investigated the variation of zeta potentials and z-average hydrodynamic diameters with time in three different conditions (Fig. 2).

First, positively charged NPs from the stock suspension were dispersed in ultrapure water at pH 8.0. In Fig. 2a we observe a continuous decrease of particle surface charge with time followed by charge inversion. At low pH NPs surface is here positively charged due to the presence of $[M–OH_2]^+$ groups (Jolivet et al., 2000). Then the increase of pH leads to deprotonation and formation of negatively charged $[M–O]^-$ groups on the NPs surface (Fig. 3a). It should be noted that the stabilization of surface charge does not occurred immediately but 60 min after the mixing. Then the zeta potential became stable and equal to −32.4 ± 0.9 mV (Fig. 2a, squares). Meanwhile large aggregates are rapidly formed with z-average diameters equal to 1457 ± 241 nm due to the fact that the NPs surface charge rapidly decreases through the point of zero charge resulting in a decrease of the electro repulsive forces. It should be noted that pH was maintained stable at pH 8.1 ± 0.2 by addition of appropriate amounts of diluted NaOH and that no significant pH variation was observed after pH stabilization.

Then in a second time, positively charged CeO_2 NPs were added to a suspension containing 0.5 and 2 mg L^{-1} FAs at pH 8.0. In contrast with previous result NPs surface charge was found to change almost immediately and became stable during full time of experiment. The mean values of zeta potential during 60 min were found equal to −46.7 ± 1.0 and −47.7 ± 1.5 mV for 0.5 and 2 mg L^{-1}, respectively. As shown in Fig. 3b at pH 3.0 $[M–OH_2]^+$ groups are prevailing on the NPs surface resulting in a positive surface charge. When positive NPs are introduced to ultrapure water that contains highly negatively charged FAs, the adsorption of the organic molecules occurs immediately due to the electrostatic attractive interactions, hence changing the surface charge properties of NPs from positive to negative (Fig. 3b). Moreover, FAs coating is found to prevent NPs from aggregation, since z-average diameters are equal to 200.5 ± 7.7 nm and 204.2 ± 11.0 nm when FAs concentration is equal to 0.5 and 2 mg L^{-1}, respectively (Fig. 2b, circles and up triangles).

Results of section 3.1 and 3.2 clearly indicate that when two routes of NOM-CeO_2 NPs complexes formation are considered (forming first the FAs-CeO_2 complexes at low pH then adjusting pH to 8, versus mixing FAs and CeO_2 at fixed pH = 8) final NOM-CeO_2 NPs properties can be very different in particular regarding the aggregate formation.

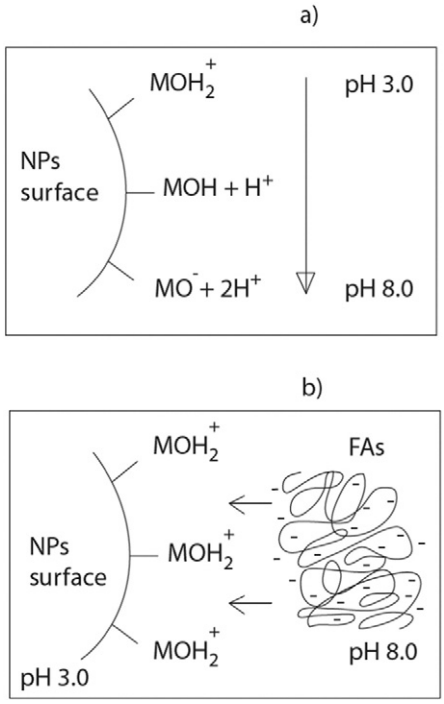

Fig. 3. Schematic representation of the NPs surface modifications: (a) in pH variable conditions and (b) in presence of FAs at pH 8. In presence of FAs at pH 8 surface charge modification is induced by the fast adsorption of FAs.

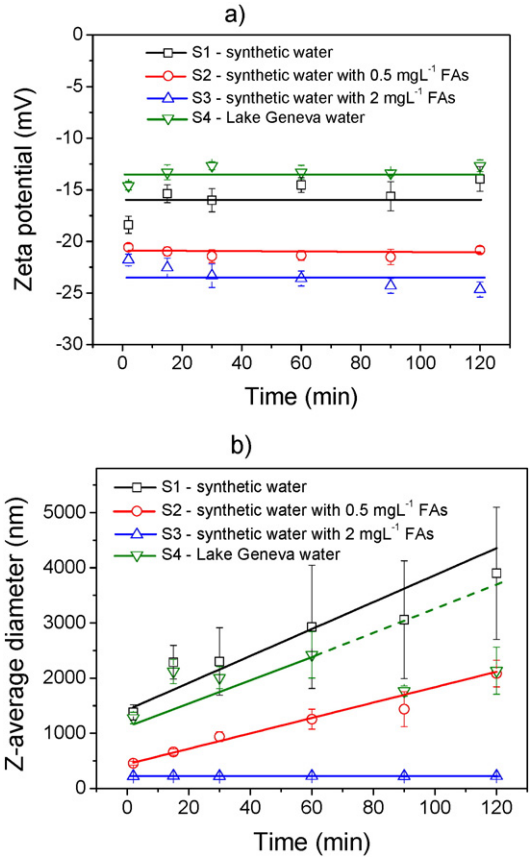

Fig. 4. (a) Zeta potential and (b) z-average hydrodynamic diameter of CeO_2 NPs as a function of time in different water samples: S1 – synthetic water; S2 – synthetic water with 0.5 mg L^{-1} FAs; S3 – synthetic water with 2 mg L^{-1} FAs; S4 – Lake Geneva water. A good agreement is obtained between zeta potential values and aggregation rates.

3.3. Behavior of CeO_2 NPs in synthetic and natural waters

To get an insight into the behavior of CeO_2 NPs in conditions more representative of environmental systems two types of samples are now considered: synthetic water which is expected to reproduce the chemical composition of Lake Geneva water and filtered water from Lake Geneva. Positively charged NPs from the stock suspension were added to these samples to obtain a final concentration equal to 50 mg L^{-1}. Zeta potential and z-average hydrodynamic diameter variations as a function of time in the different water samples are presented in Fig. 4. S1 corresponds to CeO_2 in synthetic water, S2 and S3 to CeO_2 in synthetic water with two different FAs concentrations equal to 0.5 and 2 mg L^{-1} respectively. S4 corresponds to CeO_2 in filtered Lake Geneva water. In all cases the NPs surface charge is found to rapidly change from positive $+51.3 \pm 1.3$ mV to negative values in a range from -13.3 ± 0.6 mV to -23.4 ± 0.8 mV (Fig. 4a). However significant differences exist as a function of water composition. In particular the presence and concentration of FAs play a key role in surface charge properties. CeO_2 NPs added to the synthetic water with 2 mg L^{-1} FAs exhibit the most negative surface charge (-23.4 ± 0.8 mV). By decreasing FAs concentration to 0.5 mg L^{-1}, zeta potential is found less negative (-21.1 ± 0.5 mV). In synthetic as well as Lake Geneva water surface charge is also found negative but less negative than in the previous cases. For synthetic water this can be explained mainly by the absence of the negatively charged FAs but also by the adsorption of divalent cations on the NPs negative surface as shown in Fig. 5a. It should be noted here that charge reversal is found less important i) in Lake Geneva water if comparison is made with synthetic water at 2 mg L^{-1} FAs and ii) in synthetic water with FAs than in ultrapure water with FAs due to the complexation of cations with FAs (Fig. 5b).

Concerning size variations, at 2 mg L^{-1}, FAs z-average hydrodynamic diameters are stable during 2 h and equal to 223.7 ± 8.4 nm. This value also corresponds to the diameter value of FAs-CeO_2 complexes formed in ultrapure water at pH 8 (Fig. 2b). The reason of such stability is the steric stabilization and the presence of repulsive forces between particles due to the FAs coating (Fig. 5b). With less concentrated FAs (0.5 mg L^{-1}), NPs suspension is found less stable regarding the negative particle surface charge (-21.1 ± 0.5 mV). As a result we can observe an increase of aggregate size during 120 min with maximum around 2000 nm (Fig. 4b, circles). Aggregation is more pronounced when CeO_2 NPs are added in synthetic water S1. Particle zeta potential is negative and equal to -15.6 ± 1.0 mV and NPs are forming large aggregates with an increase of size up to 4000 nm (Fig. 4b, squares) after 120 min. In almost all cases, a good agreement is found between the zeta potential measurements and the z-average diameters i.e. the increase of the aggregation rate with the decrease of the absolute value of the zeta potential.

In Lake Geneva water NPs are also found aggregated (Fig. 4b, down triangles) in contrast to the sample S3 with synthetic water and 2 mg L^{-1} FAs (Fig.4b, up triangles) which is expected here to be the more representative synthetic suspension regarding natural Lake Geneva water. CeO_2 NPs in Lake Geneva water sample exhibit negative surface charges with a zeta potential equal to -13.3 ± 0.6 mV (Fig. 4a) which is close to the zeta potential mean value -16.2 ± 0.3 mV which was found by Graham et al. (2014) for natural colloids from the Vidy Bay, Lake Geneva. Such data indicate that the impact of dissolved organic matter is probably not so important than in synthetic water for several reasons. First, because of the presence and competitive effects with heterogeneous colloidal-sized fractions with sizes here less than 0.45 μm (Fig. 5c) which are composed of inorganic colloids such as aluminum oxides, aluminosilicates, iron oxy-hydroxide and manganese oxy-hydroxides (Baalousha et al., 2006; Graham et al., 2014). Indeed, the importance of hetero-aggregation of TiO_2 NPs in the presence of clays such as montmorillonite has already been reported in the

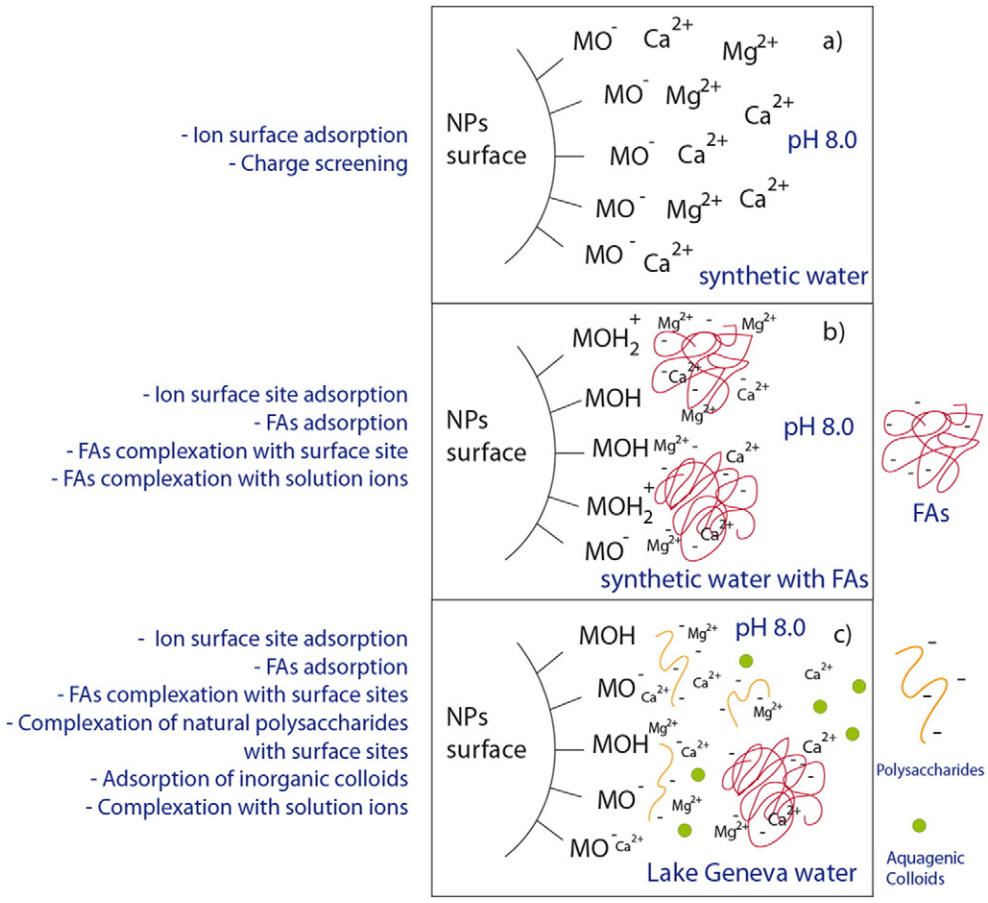

Fig. 5. Schematic representation of the possible competition mechanisms when NPs are released in various water samples: (a) synthetic water; (b) synthetic water with FAs; (c) natural Lake Geneva water.

literature (Labille et al., 2015; Zhou et al., 2012). Second, because of the heterogeneity of dissolved organic matter in natural water which is a mixture of humic substances, fibrillar polysaccharides and peptidoglycans (Wilkinson et al., 1999) having different physicochemical properties and reactivities.

These results are supported by SEM images of CeO_2 NPs in synthetic water without and in presence of FAs (Fig. 6a and b). It is shown that coated with FAs (Fig. 6b) NPs are forming only small aggregates with sizes around 200–250 nm in contrast to the large aggregates obtained in absence of FAs (Fig. 6a). These results indicate that FAs will prevent aggregation of CeO_2 NPs in synthetic water when a concentration ratio of FAs/CeO_2 NPs equal to 1/25 is considered (2 mg L^{-1} FAs and 50 mg L^{-1} CeO_2). We believe also that the same effect will be reproduced considering environmental concentrations of NPs which are expected to be on the level of ng L^{-1} and μg L^{-1} (Gottschalk et al., 2013). In such case FAs will be in excess regarding NPs concentrations hence resulting to stable dispersions and possible aggregate redispersion (Loosli et al., 2013). The SEM image of CeO_2 NPs in filtered Lake Geneva water (Fig. 7) also confirmed the formation of large hetero-aggregates in which NPs are embedded in a complex matrix made of natural salts (crystals with regular rhombic shape) and inorganic colloids (white particles with larger sizes). The EDS analysis of SEM sample (Fig.7b) and the results of element analysis (SI, Table S5) are indicating the presence of Na^+, Ca^{2+}, and Mg^{2+} electrolytes. However, regarding the low concentration of natural colloids (1 mg L^{-1}, Table 1) compared to other components (including 50 times difference with the concentration of CeO_2 NPs), no indication of elements such as Al, Fe or Mn was found. Such results can be explained also by filtration of the sample with 0.45 μm filter to avoid the presence of large colloids and low EDS resolution compared to SEM imaging which analyses the volume of sample including surrounding area (such as platinum coating, silica wafer, and CeO_2 NPs).

4. Conclusions

The stability and aggregation of uncoated and coated CeO_2 NPs in different environmental conditions were studied. Size distribution and electrophoretic measurements were used to obtain z-average hydrodynamic diameter and particle surface charge. A good agreement was found between the aggregation rate and zeta potential measurements made on the different suspensions. We also investigated the influence of environmental pH and FAs coating on CeO_2 stability and conclude that when the NPs are coated with FAs, strong complexes are formed regarding important pH variations. We demonstrated that at pH 8 in ultrapure water even small amounts of FAs are enough to prevent NPs aggregation. In synthetic water environmentally relevant concentration of FAs were found to stabilize CeO_2 NPs and the stabilizing effect was found to increase with the FAs concentration. In contrast, in natural water, CeO_2 NPs were found aggregated. This was attributed to the presence of heterogeneous aquagenic compounds, such as inorganic particles and NOM having different properties, hence promoting heteroaggregation rather than stabilization. Our result indicates that not only the concentration of electrolyte, but also the type and valency of ions, via specific adsorption processes and complexation with FAs, plays important role in nanoparticle destabilization and aggregation. We demonstrated here that the behavior of CeO_2 NPs can be significantly different if comparison is made between synthetic waters and natural waters even if the ionic composition and total organic carbon concentration are identical. As a result the complexity of such systems, CeO_2

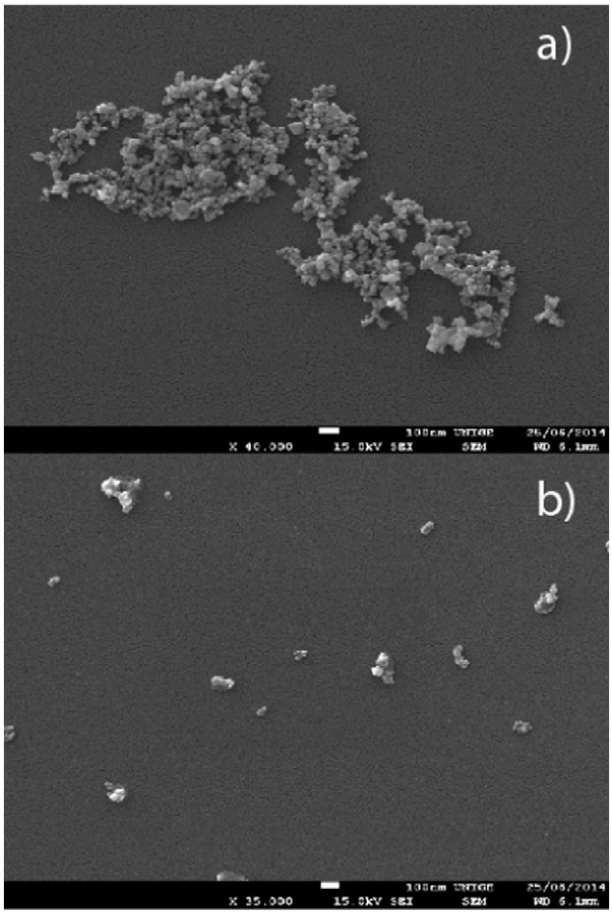

Fig. 6. SEM images of CeO_2 NPs in different water samples: a) synthetic water; b) synthetic water with 2 mg L^{-1} FAs. In synthetic water without FAs NPs are found aggregated and embedded in a matrix made from salts. In the presence of FAs NPs are stabilized and dispersed and the size of aggregate is equal to 200–250 nm.

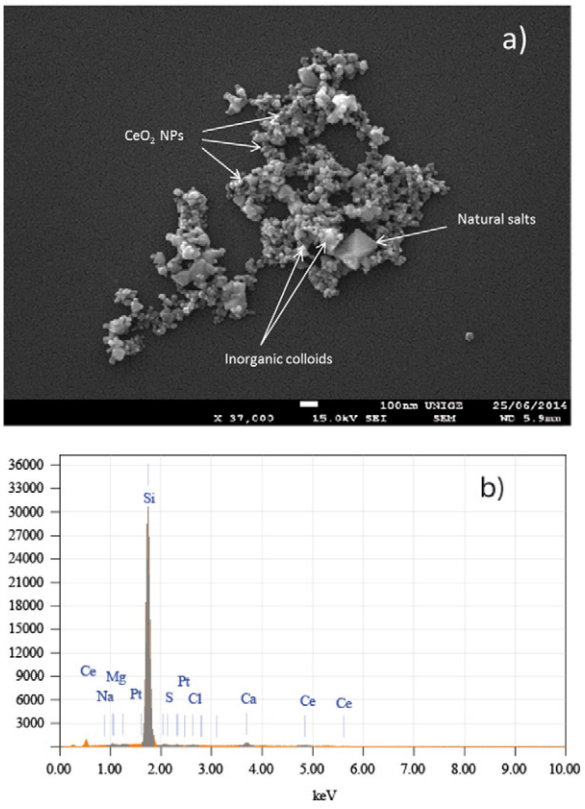

Fig. 7. SEM images of CeO_2 NPs in natural Lake Geneva water. NPs are found aggregated and embedded in a complex matrix made of dissolved organic matter, natural salts and inorganic colloids. b) EDS spectrum of the elemental analysis of CeO_2 NPs in natural Lake Geneva water (counting rate is 12,008 cps) showing the presence of Si, Pt, Ce, Ca, Mg, Na, S, Cl and indicating the presence of silica wafer, platinum coating, CeO_2 NPs, and various electrolytes.

NPs in synthetic water with NOM, is far away from reflecting the complexity of natural aquatic systems.

Acknowledgements

The authors are grateful for the financial support received from the Swiss National Foundation (project 200021_135240) and the European Commission's 7th Framework Programme project "NanoMILE" (contract no. NMP4-LA-2013-310451). We also acknowledge Agathe Martignier for her help and suggestions during the SEM measurements and EDS analysis.

Appendix A. Supplementary data

Supplementary data to this article can be found online at http://dx.doi.org/10.1016/j.scitotenv.2016.03.184.

References

Baalousha, M., 2009. Aggregation and disaggregation of iron oxide nanoparticles: influence of particle concentration, pH and natural organic matter. Sci. Total Environ. 407, 2093–2101. http://dx.doi.org/10.1016/j.scitotenv.2008.11.022.

Baalousha, M., V. D. Kammer, F., Motelica-Heino, M., Baborowski, M., Hofmeister, C., Le Coustumer, P., 2006. Size-based speciation of natural colloidal particles by flow field flow fractionation, inductively coupled plasma-mass spectroscopy, and transmission electron microscopy/X-ray energy dispersive spectroscopy: colloids–trace element interaction. Environ. Sci. Technol. 40, 2156–2162. http://dx.doi.org/10.1021/es051498d.

Cleveland, D., Long, S.E., Pennington, P.L., Cooper, E., Fulton, M.H., Scott, G.I., Brewer, T., Davis, J., Petersen, E.J., Wood, L., 2012. Pilot estuarine mesocosm study on the environmental fate of silver nanomaterials leached from consumer products. Sci. Total Environ. 421–422, 267–272. http://dx.doi.org/10.1016/j.scitotenv.2012.01.025 (Special Section: Reviews of Trace Metal Pollution in China).

Domingos, R.F., Tufenkji, N., Wilkinson, K.J., 2009. Aggregation of titanium dioxide nanoparticles: role of a fulvic acid. Environ. Sci. Technol. 43, 1282–1286. http://dx.doi.org/10.1021/es8023594.

Elimelech, M., Jia, X., Gregory, J., Williams, R., 1998. Particle Deposition & Aggregation: Measurement, Modelling and Simulation. Butterworth-Heinemann.

Frimmel, F.H., 1998. Characterization of natural organic matter as major constituents in aquatic systems. J. Contam. Hydrol. 35, 201–216. http://dx.doi.org/10.1016/S0169-7722(98)00133-8.

Frimmel, F.H., Abbt-Braun, G., 1999. Basic characterization of reference NOM from Central Europe — similarities and differences. Environ. Int. 25, 191–207. http://dx.doi.org/10.1016/S0160-4120(98)00116-0 Nom-typing.

Garcia, T., Solsona, B., Taylor, S.H., 2005. Nano-crystalline ceria catalysts for the abatement of polycyclic aromatic hydrocarbons. Catal. Lett. 105, 183–189. http://dx.doi.org/10.1007/s10562-005-8689-2.

Ghosh, S., Pradhan, N.R., Mashayekhi, H., Dickert, S., Thantirige, R., Tuominen, M.T., Tao, S., Xing, B., 2014. Binary short-range colloidal assembly of magnetic iron oxides nanoparticles and fullerene (nC60) in environmental media. Environ. Sci. Technol. 48, 12285–12291.

Gottschalk, F., Nowack, B., 2011. The release of engineered nanomaterials to the environment. J. Environ. Monit. 13, 1145–1155.

Gottschalk, F., Sun, T., Nowack, B., 2013. Environmental concentrations of engineered nanomaterials: Review of modeling and analytical studies. Environ. Pollut. 181, 287–300. http://dx.doi.org/10.1016/j.envpol.2013.06.003.

Graham, N.D., Stoll, S., Loizeau, J.-L., 2014. Colloid characterization at the sediment-water interface of Vidy Bay Lake Geneva Fundam. Appl. Limnol. Für Hydrobiol. 184, 87–100.

Gregory, J., 2005. Particles in Water: Properties and Processes. CRC Press.

Hammes, J., Gallego-Urrea, J.A., Hassellöv, M., 2013. Geographically distributed classification of surface water chemical parameters influencing fate and behavior of nanoparticles and colloid facilitated contaminant transport. Water Res.

Harbour, P.J., Dixon, D.R., Scales, P.J., 2007. The role of natural organic matter in suspension stability: 1. Electrokinetic–rheology relationships. Colloids Surf. A Physicochem. Eng. Asp. 295, 38–48. http://dx.doi.org/10.1016/j.colsurfa.2006.08.028.

Jolivet, J.-P., Henry, M., Livage, J., 2000. Metal Oxide Chemistry and Synthesis: From Solution to Solid State Wiley-Blackwell.

Keller, A.A., Wang, H., Zhou, D., Lenihan, H.S., Cherr, G., Cardinale, B.J., Miller, R., Ji, Z., 2010. Stability and aggregation of metal oxide nanoparticles in natural aqueous matrices. Environ. Sci. Technol. 44, 1962–1967.

Labille, J., Slomberg, D., Sani-Kaast, N., Praetorius, A., Ollivier, P., Radakovitch, O., Brant, J., Scheringer, M., Bottero, J.-Y., 2014. Assessing the heteroaggregation of manufactured nanoparticles with geogenic colloids in surface water. EGU General Assembly Conference Abstracts, p. 5400.

Labille, J., Harns, C., Bottero, J.-Y., Brant, J., 2015. Heteroaggregation of titanium dioxide nanoparticles with natural clay colloids. Environ. Sci. Technol. 49, 6608–6616. http://dx.doi.org/10.1021/acs.est.5b00357.

Li, S., Sun, W., 2011. A comparative study on aggregation/sedimentation of TiO2 nanoparticles in mono-and binary systems of fulvic acids and Fe (III). J. Hazard. Mater. 197, 70–79.

Loosli, F., Coustumer, P.L., Stoll, S., 2013. TiO2 nanoparticles aggregation and disaggregation in presence of alginate and Suwannee River humic acids. pH and concentration effects on nanoparticle stability. Water Res. 47, 6052–6063.

Loosli, F., Le Coustumer, P., Stoll, S., 2014. Effect of natural organic matter on the disagglomeration of manufactured TiO2 nanoparticles. Environ. Sci. Nano 1, 154–160.

Loosli, F., Le Coustumer, P., Stoll, S., 2015. Effect of electrolyte valency, alginate concentration and pH on engineered TiO2 nanoparticle stability in aqueous solution. Sci. Total Environ. 535, 28–34.

Metreveli, G., Philippe, A., Schaumann, G.E., 2015. Disaggregation of silver nanoparticle homoaggregates in a river water matrix. Sci. Total Environ. 535, 35–44.

Neal, C., Jarvie, H., Rowland, P., Lawler, A., Sleep, D., Scholefield, P., 2011. Titanium in UK rural, agricultural and urban/industrial rivers: geogenic and anthropogenic colloidal/sub-colloidal sources and the significance of within-river retention. Sci. Total Environ. 409, 1843–1853.

Oriekhova, O., Stoll, S., 2016. Effects of pH and fulvic acids concentration on the stability of fulvic acids – cerium (IV) oxide nanoparticle complexes. Chemosphere 144, 131–137. http://dx.doi.org/10.1016/j.chemosphere.2015.08.057.

Ottofuelling, S., Von Der Kammer, F., Hofmann, T., 2011. Commercial titanium dioxide nanoparticles in both natural and synthetic water: comprehensive multidimensional testing and prediction of aggregation behavior. Environ. Sci. Technol. 45, 10045–10052.

Palomino, D., Yamunake, C., Coustumer, P.L., Stoll, S., 2013. Stability of TiO2 nanoparticles in presence of fulvic acids. Importance of pH. J. Colloid Sci. Biotechnol. 2, 62–69. http://dx.doi.org/10.1166/jcsb.2013.1033.

Pettit, R.E., 2004. Organic matter, humus, humate, humic acid, fulvic acid and humin: their importance in soil fertility and plant health CTI Res.

Quik, J.T.K., Lynch, I., Hoecke, K.V., Miermans, C.J.H., Schamphelaere, K.A.C.D., Janssen, C.R., Dawson, K.A., Stuart, M.A.C., Meent, D.V.D., 2010. Effect of natural organic matter on cerium dioxide nanoparticles settling in model fresh water. Chemosphere 81, 711–715. http://dx.doi.org/10.1016/j.chemosphere.2010.07.062.

Quik, J.T.K., Velzeboer, I., Wouterse, M., Koelmans, A.A., van de Meent, D., 2014. Heteroaggregation and sedimentation rates for nanomaterials in natural waters. Water Res. 48, 269–279. http://dx.doi.org/10.1016/j.watres.2013.09.036.

Rapin, F., Klein, A., 2011. Assessment of the input from the tributaries into the Lake Geneva and into the Rhône downstream of Geneva. Rapp. Comm. Int. Prot. Eaux Léman Contre Pollut. 157–178.

Reed, K., Cormack, A., Kulkarni, A., Mayton, M., Sayle, D., Klaessig, F., Stadler, B., 2014. Exploring the properties and applications of nanoceria: is there still plenty of room at the bottom? Environ. Sci.: Nano 1, 390–405. http://dx.doi.org/10.1039/C4EN00079J.

Sani-Kast, N., Scheringer, M., Slomberg, D., Labille, J., Praetorius, A., Ollivier, P., Hungerbühler, K., 2015. Addressing the complexity of water chemistry in environmental fate modeling for engineered nanoparticles. Sci. Total Environ. 535, 150–159. http://dx.doi.org/10.1016/j.scitotenv.2014.12.025 Special Issue: EngineeEred nanoparticles in soils and waters.

Schaumann, G.E., Philippe, A., Bundschuh, M., Metreveli, G., Klitzke, S., Rakcheev, D., Grün, A., Kumahor, S.K., Kühn, M., Baumann, T., Lang, F., Manz, W., Schulz, R., Vogel, H.-J., 2015. Understanding the fate and biological effects of Ag- and TiO2-nanoparticles in the environment: the quest for advanced analytics and interdisciplinary concepts. Sci. Total Environ. 535, 3–19. http://dx.doi.org/10.1016/j.scitotenv.2014.10.035 Special Issue: Engineered nanoparticles in soils and waters.

Singh, C., Friedrichs, S., Ceccone, G., Gibson, N., Jensen, K.A., Levin, M., Infante, H.G., Carlander, D., Rasmussen, K., 2014. Cerium Dioxide, NM-211, NM-212, NM-213. Characterisation and Test Item Preparation. European Commission, Joint Research Centre, European Union http://dx.doi.org/10.2788/80203.

Smith, E.J., Davison, W., Hamilton-Taylor, J., 2002. Methods for preparing synthetic freshwaters. Water Res. 36, 1286–1296. http://dx.doi.org/10.1016/S0043-1354(01)00341-4.

Strawczynski, A., 2011. Comparative interlaboratory analyses. Rapp. Comm. Int. Prot. Eaux Léman Contre Pollut. 191–198.

Wilkinson, K.J., Balnois, E., Leppard, G.G., Buffle, J., 1999. Characteristic features of the major components of freshwater colloidal organic matter revealed by transmission electron and atomic force microscopy. Colloids Surf. Physicochem. Eng. Asp. 155, 287–310. http://dx.doi.org/10.1016/S0927-7757(98)00874-7.

Yang, K., Lin, D., Xing, B., 2009. Interactions of humic acid with nanosized inorganic oxides. Langmuir 25, 3571–3576.

Zhou, D., Abdel-Fattah, A.I., Keller, A.A., 2012. Clay particles destabilize engineered nanoparticles in aqueous environments. Environ. Sci. Technol. 46, 7520–7526. http://dx.doi.org/10.1021/es3004427.

Chapter V

Aggregation of CeO_2 NPs and alginate coated CeO_2 NPs in changing environmental conditions

Published as

Oriekhova, O., Le Coustumer, P., and Stoll, S., 2017, Impact of biopolymer coating on the colloidal stability of manufactured CeO_2 nanoparticles in contrasting water conditions, Colloids and Surfaces A, v. 533, pp. 267–274 (Paper III).

V.1 Introduction

CeO_2 manufactured nanoparticles (MNPs) released to aquatic systems will be coated by natural substances, thereby modifying their surface properties. Stability over time and potential transformations of such coatings due to changing environmental conditions such as dilution, change of water pH, ionic strength and presence of various natural compounds is a key question for the evaluation of the CeO_2 MNMs fate and ecotoxicity. One of the main aquagenic components that will control the fate and coating of MNMs in the environment is natural organic matter (NOM). NOM in aquatic systems is ubiquitous and mainly composed of humic substances and biopolymers (polysaccharides). In freshwaters, polysaccharide content can reach from 10 to 30 % of the total amount of NOM (Buffle et al., 1998). The concentration of NOM in natural waters will depend on the water source and season. For example, in Lake Geneva, Switzerland the typical concentration of dissolved carbon is approximately 1 mg C/L (Strawczynski, 2012, 2008). Alginate is a polysaccharide which is commonly used as a relevant model and surrogate for natural polysaccharides (Augst et al., 2006). Disaggregation or stabilisation due to alginate coating can occur to MNPs released in aquatic systems (Loosli et al., 2015, 2013). Surface coating is expected to dominate the MNP surface properties (Kavok et al., 2017; Lima-Tenório et al., 2016) and often makes the surface potential of MNPs more negative in aquatic systems leading to a decrease in aggregation rate. However, coating property and stability with time is influenced by external factors such as pH, light radiation, competitive adsorption processes between water compounds and different natural organic matter fractions (Auffan et al., 2014; Tella Marie et al., 2014) implying the modification of MNP properties.

There is still not clear understanding of several key questions about aging and stability of naturally coated MNPs in aquatic systems. Particularly, the effect of pH on the coating properties as well as the role of surface charge change and its implication in the mechanism of aggregation in complex environmental matrices.

In this chapter, we used alginate as a model of natural polysaccharide to form an organic coating around CeO_2 MNPs and we studied alginate adsorption on CeO_2 in changing alginate concentration. Two different electrostatic scenarios at $pH > pH_{PZC}$ and $pH < pH_{PZC}$ were considered. The stability of alginate coating in changing pH conditions and in synthetic and natural waters was also investigated. We used SEM and TEM analysis to gain an insight into the homo- and heteroaggregate structures in various

environmental and coating conditions. DLS and Doppler electrophoresis techniques were also used to measure surface charge and z-average diameter changes.

V.2 Main results

To investigate the alginate ability to modify the surface properties of pristine CeO_2 MNPs, two different surface charge scenarios were considered. First, when pH < pH_{PZC}, CeO_2 MNPs and alginate are oppositely charged, i.e. the conditions are favorable for interaction. Increase of alginate concentration is found to change CeO_2 surface charge from positive to negative values. The isoelectric point (IEP) is achieved at 0.65 ± 0.05 mg/L alginate concentration and the aggregate z-average hydrodynamic diameters increases up to 922 ± 217 nm. Above 1 mg/L alginate, CeO_2 MNPs are found stabilised with zeta potential values close to –20 mV and a decrease of the z-average diameter is observed down to 183 ± 8 nm (at 2 mg/L alginate). Second, when pH > pH_{PZC} both CeO_2 and alginate have the same surface charge (negatively charged) and thus no significant effect of alginate is observed.

The stability of alginate coating around CeO_2 MNPs was investigated in pH range from 3.0 to 10 ± 0.2. The surface charge of CeO_2/alginate complexes is found negative in the entire pH range (Fig. V.1a), however, two different regions are observed. From pH 3.0 up to 6.8 a significant decrease of the zeta potential values from –24.0 ± 0.4 mV to –45.0 ± 3.0 mV was found. This pH corresponds to the pH_{PZC} of CeO_2 MNPs. Above this pH, a zeta potential plateau is obtained with a mean value equal to –45.0 ± 1.1 mV. Decrease of the zeta potential is attributed to the progressive neutralisation of the CeO_2 positive surface charges with increase of pH until the moment when all surface charges are switched off at pH 6.8. Z-average diameters are stable below pH 6.8 with a mean value equal to 188 ± 6 nm and above pH 6.8 the hydrodynamic diameters are slightly increased to 207 ± 9 nm. The change in size of coated particles can be explained by the modification of alginate coating. The structural properties of alginate could be modified by changes of pH. Below pH 6.8 CeO_2 MNPs and alginate form compact complexes due to the strong electrostatic interactions (Fig. V.1b). At higher pH ($\geqslant$ 8) alginate adopts more extended conformations which leads to the increase of alginate coating thickness.

To investigate the impact of natural water compounds such as natural dissolved organic matter and inorganic colloids as well as ionic composition on the stability of

pristine CeO_2 MNPs and CeO_2 in the presence of alginate, filtered water from Lake Geneva was considered. Pristine CeO_2 MNPs are found to form rapidly heteroaggregates with z-average hydrodynamic diameters up to 2250 nm and negative surface charges (Fig. V.2). Heteroaggregation occurred due to the specific adsorption of divalent cations (Ca^{2+} and Mg^{2+}) as well as complexation processes with naturally present dissolved compounds. The addition of high concentration (2 mg/L) alginate in lake water is found to promote stabilisation via the coating formation around CeO_2 MNPs with mean z-average diameter value equal to 286 ± 17 nm during 120 min. At smaller alginate concentrations (0.25 and 0.5 mg/L), heteroaggregation is observed and z-average diameter increases up to 1443 ± 159 nm after 120 min.

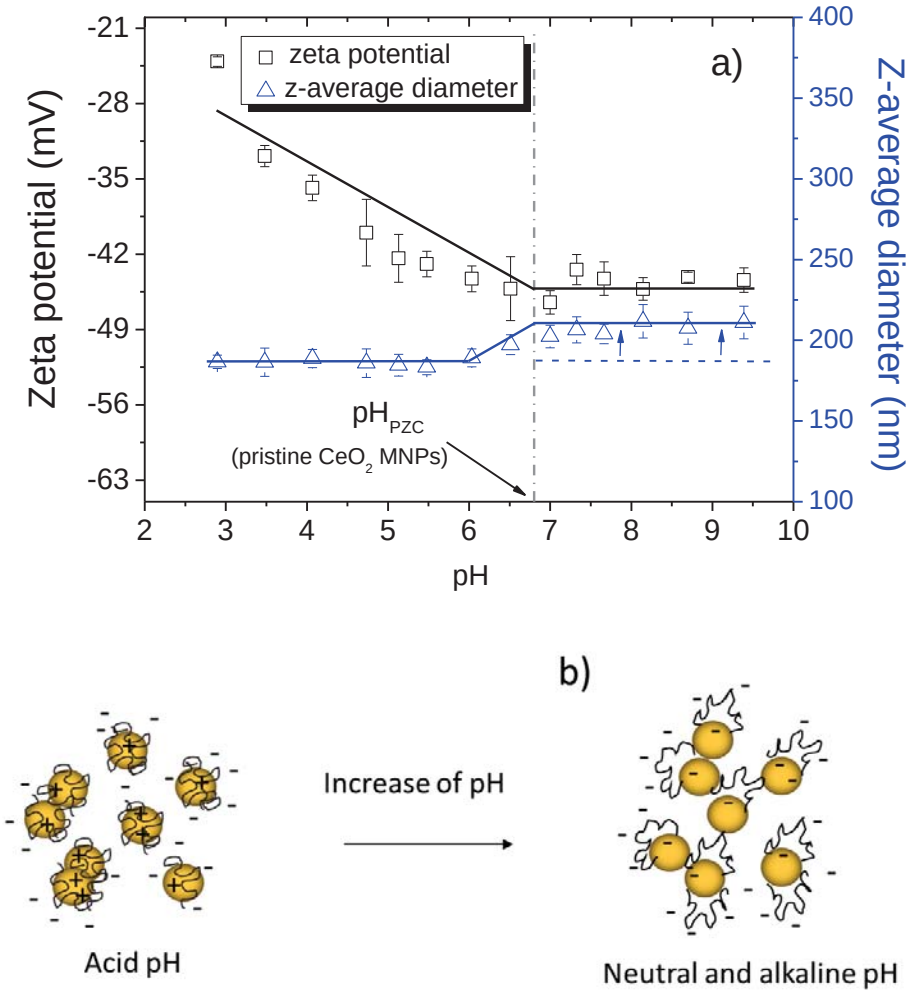

Fig. V.1. (a) Zeta potentials and z-average hydrodynamic diameters of a 50 mg/L CeO_2 MNPs coated with a 2 mg/L alginate in different pH conditions. CeO_2/Alginate complexes are negatively charged in the full pH range. (b) schematic representation of alginate conformational changes at the MNP surface. At neutral and alkaline pH alginate has more extended structure compared to its structure in acid pH.

To get insight into the morphology of the aggregates in lake water TEM analysis was performed (Fig. V.2c). In this figure we can distinguish the presence of a large fibrillar network of NOM and CeO_2 MNP aggregates.

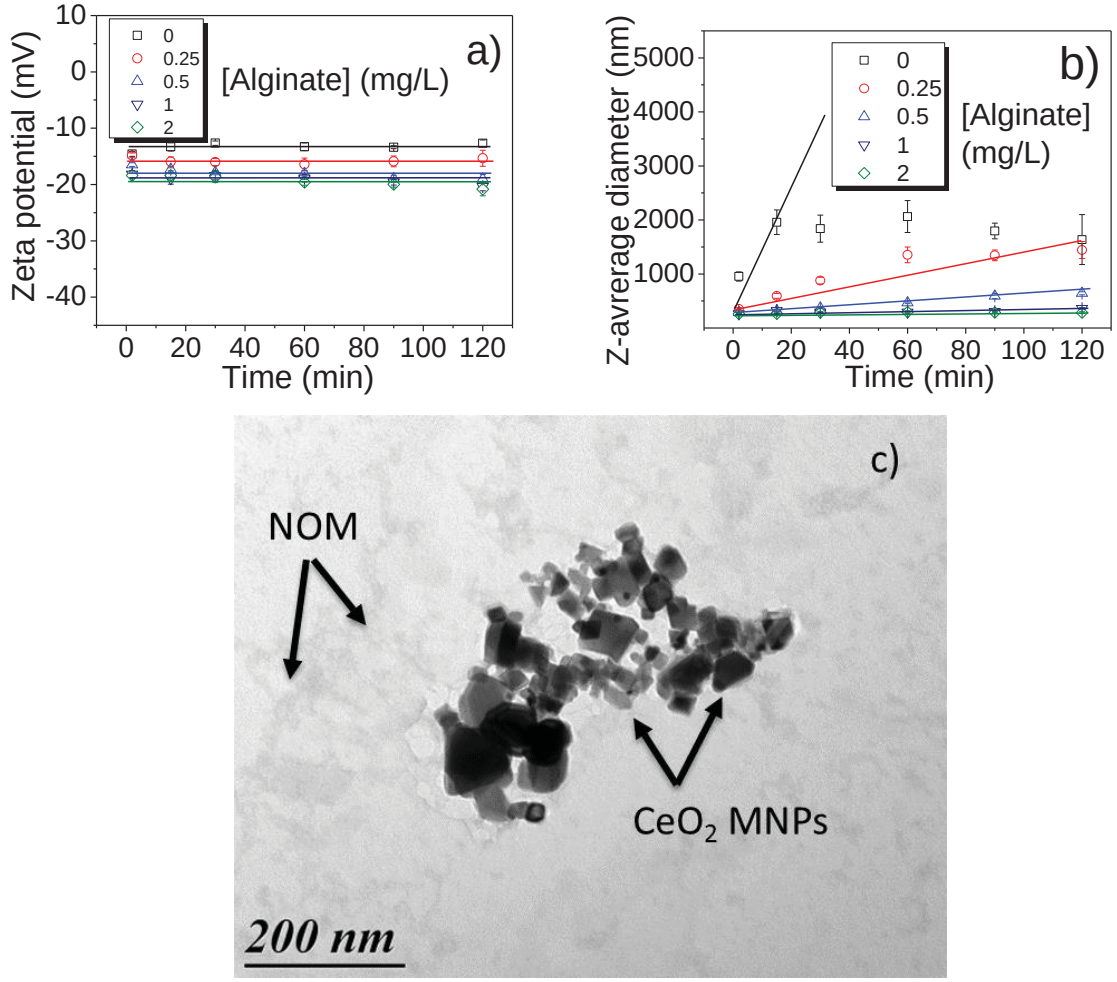

Fig. V.2. Time variation of (a) zeta potentials, (b) z-average hydrodynamic diameters as a function of alginate concentrations in Lake Geneva water. Important changes of zeta potentials are observed if comparison is made with ultrapure water towards less negative values which promote aggregation. (c) TEM micrography of CeO_2 MNPs in Lake Geneva water showing the presence of a large fibrillar network and CeO_2 MNP aggregates.

We demonstrated that concentration of alginate and pH play a crucial role in the stability of coating around CeO_2 MNPs and its environmental identity. The stabilisation of CeO_2 MNPs is achieved by the formation of coating with alginate at concentration above 1 mg/L. The heteroaggregation of CeO_2 is observed in lake water. The importance of heteroaggregation is controlled by the alginate concentration. Our results also

demonstrated that when alginate coating is formed, coating is persistent in pH changing conditions.

V.3 References

Auffan, M., Masion, A., Labille, J., Diot, M.-A., Liu, W., Olivi, L., Proux, O., Ziarelli, F., Chaurand, P., Geantet, C., Bottero, J.-Y., Rose, J., 2014. Long-term aging of a CeO2 based nanocomposite used for wood protection. Environ. Pollut. 188, 1–7. https://doi.org/10.1016/j.envpol.2014.01.016

Augst, A.D., Kong, H.J., Mooney, D.J., 2006. Alginate Hydrogels as Biomaterials. Macromol. Biosci. 6, 623–633. https://doi.org/10.1002/mabi.200600069

Buffle, J., Wilkinson, K.J., Stoll, S., Filella, M., Zhang, J., 1998. A Generalized Description of Aquatic Colloidal Interactions: The Three-colloidal Component Approach. Environ. Sci. Technol. 32, 2887–2899. https://doi.org/10.1021/es980217h

Kavok, N., Grygorova, G., Klochkov, V., Yefimova, S., 2017. The role of serum proteins in the stabilization of colloidal LnVO4:Eu3+ (Ln = La, Gd, Y) and CeO2 nanoparticles. Colloids Surf. Physicochem. Eng. Asp. 529, 594–599. https://doi.org/10.1016/j.colsurfa.2017.06.052

Lima-Tenório, M.K., Pineda, E.A.G., Ahmad, N.M., Agusti, G., Manzoor, S., Kabbaj, D., Fessi, H., Elaissari, A., 2016. Aminodextran polymer-functionalized reactive magnetic emulsions for potential theranostic applications. Colloids Surf. B Biointerfaces 145, 373–381. https://doi.org/10.1016/j.colsurfb.2016.05.020

Loosli, F., Coustumer, P.L., Stoll, S., 2013. TiO2 nanoparticles aggregation and disaggregation in presence of alginate and Suwannee River humic acids. pH and concentration effects on nanoparticle stability. Water Res. 47, 6052–6063.

Loosli, F., Le Coustumer, P., Stoll, S., 2015. Effect of electrolyte valency, alginate concentration and pH on engineered TiO2 nanoparticle stability in aqueous solution. Sci. Total Environ., Special Issue: Engineered nanoparticles in soils and waters 535, 28–34. https://doi.org/10.1016/j.scitotenv.2015.02.037

Strawczynski, A., 2012. Comparative interlaboratory analyses. Rapp Comm Int Prot Eaux Léman Contre Pollut Camp. 151–160.

Strawczynski, A., 2008. Comparative interlaboratory analyses. Rapp Comm Int Prot Eaux Léman Contre Pollut Camp. 163–175.

Tella Marie, Auffan Mélanie, Brousset Lenka, Issartel Julien, Kieffer Isabelle, Pailles Christine, Morel Elise, Santaella Catherine, Angeletti Bernard, Artells Ester, Rose Jérôme, Thiéry Alain, Bottero Jean-Yves, 2014. Transfer, Transformation, and Impacts of Ceria Nanomaterials in Aquatic Mesocosms Simulating a Pond Ecosystem. Environ. Sci. Technol. 48, 9004–9013. https://doi.org/10.1021/es501641b

Paper III

Oriekhova, O., Le Coustumer, P., and Stoll, S., 2017, Impact of biopolymer coating on the colloidal stability of manufactured CeO_2 nanoparticles in contrasting water conditions, Colloids and Surfaces A, v. 533, pp. 267–274

Colloids and Surfaces A 533 (2017) 267–274

Contents lists available at ScienceDirect

Colloids and Surfaces A

journal homepage: www.elsevier.com/locate/colsurfa

Impact of biopolymer coating on the colloidal stability of manufactured CeO_2 nanoparticles in contrasting water conditions

Olena Oriekhova[a], Philippe Le Coustumer[b,c], Serge Stoll[a,*]

[a] Department F.-A. Forel for Environmental and Aquatic Sciences, University of Geneva, Faculty of Science, Uni Carl Vogt, Group of Environmental Physical Chemistry, 66, Boulevard Carl-Vogt, CH-1211 Geneva 4, Switzerland

[b] EA 4592 Géoressources & Environnement, ENSEGID, Université Bordeaux 3, 1 allée F. Daguin, 33607 Pessac, France

[c] UFR STM, Université Bordeaux 1, B.18 Av. Des facultés 33405 Talence, France

GRAPHICAL ABSTRACT

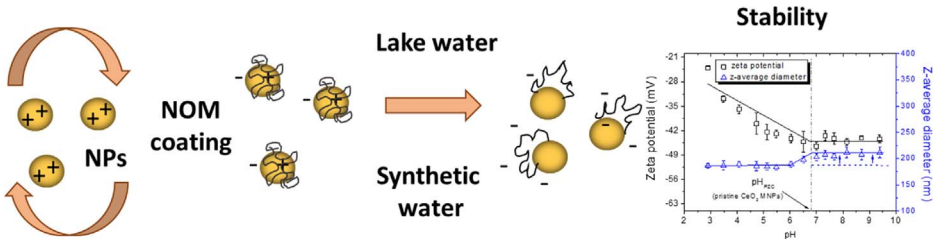

ARTICLE INFO

Keywords:
CeO_2 nanoparticle
Alginate coating
Coating stability
Heteroaggregation
Synthetic water
Lake Geneva water

ABSTRACT

The use of cerium dioxide manufactured nanoparticles (CeO_2 MNPs) at a large scale in the industry, automotive and everyday products is resulting in a continuous emission and release of CeO_2 MNPs to the aquatic environments. In such complex systems, MNPs interact with water components, including biopolymers, resulting in MNP coating which give a new environmental identity to the MNPs and greatly influence their fate, transport and biological impact. MNP surface properties, aggregation, media composition such as ionic composition and pH, strongly influence the importance of natural organic matter coating and coating stability with time. In our study, we are using alginate, a relevant surrogate of natural organic polysaccharides, to coat CeO_2 MNPs under different conditions from ultrapure water to synthetic and natural waters. First, the most favourable conditions of alginate coating are defined and then the stability of this coating in changing pH condition is investigated. Then alginate coating impact, at variable alginate concentration, is studied in synthetic and natural waters and comparison is made with ultrapure water. The possible interaction mechanisms between alginate, CeO_2, dissolved ions (in particular divalent cations) and natural inorganic compounds are discussed. Our finding demonstrates that alginate concentration, solution pH and presence of divalent cations are key parameters defining the stability and effect of alginate coating and that once formed the biopolymer coating is found irreversible with time and when changing the solution chemistry.

1. Introduction

The wide application of manufactured nanoparticles (MNPs) has increased the risk of their emission, release and environmental exposure [1–3]. Cerium dioxide (CeO_2) is one example of MNPs that are commercially used at a large scale in nano automotive products as

Abbreviations: MNPs, Manufactured nanoparticles; NOM, Natural organic matter; SEM, Scanning electron microscope; TEM, Transmission electron microscope; SI, Supporting information; IEP, Isoelectric point

* Corresponding author.
E-mail addresses: Olena.Oriekhova@unige.ch (O. Oriekhova), philippe.le-coustumer@u-bordeaux1.fr (P. Le Coustumer), Serge.Stoll@unige.ch (S. Stoll).

http://dx.doi.org/10.1016/j.colsurfa.2017.07.069
Received 11 July 2017; Accepted 23 July 2017
Available online 25 July 2017
0927-7757/

catalytic converters and diesel fuel additives to produce synthetic gas and reduce exhaust emissions, as polishing agents in chemical and mechanical polishing, planarization processes to produce transparent surfaces and as a component of compact fluorescent light tubes and interior coatings of self-cleaning ovens [4]. CeO_2 MNPs have found therefore wide applications owing to their physicochemical properties but pose a threat for the environment, for example, due to their active redox property [5–7]. Studies also demonstrate that CeO_2 MNPs have long persistence time after biological treatment in waste water treatment plants, accumulate in sludge [8,9] which results to the release of these MNPs with effluents into natural waters. After release, stability of MNPs generally depends on both nanoparticle and water properties [10,11]. One major natural water component which is expected to control the fate of MNPs is natural organic matter (NOM) [12,13]. NOM in aquatic systems is ubiquitous and mainly composed of humic substances and biopolymers (polysaccharides). In freshwaters, polysaccharide content can reach from 10 to 30% of the total amount of NOM [14] .

Alginate is a polysaccharide which is commonly used as a relevant model and surrogate of natural polysaccharides [15]. Alginate is produced by some bacteria or brown algae and can be part of the algae cell walls [16]. Alginate has been used for various purposes [17,18] including applications for the improvement of water treatment processes [19,20] and for the sorption and elimination of pollutants such as heavy metals [21,22]. Alginate can have various effects on MNPs released in aquatic systems such as disaggregation or stabilization due to alginate coating [23,24]. Surface coating is expected to dominate the MNP surface properties [25,26] and often makes the surface potential of MNPs more negative in aquatic systems leading to a decrease in aggregation rate. However, coating property and stability with time is influenced by external factors such as pH, light radiation, competitive adsorption processes between water compounds and different natural organic matter fractions [27,28] implying the modification of MNP properties.

Aggregation of pristine and citrate coated CeO_2 nanoparticles was investigated in Volvic® water and in a mesocosm [27]. After one week 81% of the cerium from pristine nanoparticles was found in the sediment. However, for coated particles the concentration of cerium in the sediments was found to increase gradually and reach a maximum after four weeks. Such behavior was attributed to the degradation of the citrate coating because of dilution effects and light radiation. The authors assumed that in mesocosm experiments both homoaggregation and heteroaggregation were occurring due to surface charge changes and presence of natural colloids. It was shown that citrate coating of cerium dioxide nanocomposite was degraded during a long term aging under artificial daylight inducing surface changes and molecular reorganization of initial nanocomposite [28] and that the coating properties could change with time and have an impact on the final MNP properties, behavior in the environment [29,30] and therefore on living organisms [5,30,31].

Despite such findings, several key questions about aging and stability of natural organic coating around MNPs in aquatic systems are still not clear and need to be elucidated. In particular, the effect of pH on the coating properties is not well understood as well as the role of surface charge change and its implication in the mechanism of aggregation in complex environmental matrix. In addition, detailed mechanistic investigations in realistic environmental conditions such as in natural waters or at least in synthetic waters are also needed.

In the work presented here, we used alginate as a model of natural polysaccharide to form an organic coating around CeO_2 MNPs and alginate adsorption on CeO_2 in changing alginate concentration condition was studied. Two different electrostatic scenarios at $pH > pH_{PZC}$ and $pH < pH_{PZC}$ to investigate the effect of particle surface charge on the coating were considered. Then after formation of CeO_2/alginate complexes the stability of alginate coating in changing pH conditions was investigated. The effect of alginate coating in synthetic and natural waters and the possible interaction mechanisms were also investigated by considering surface charge and z-average changes. SEM and TEM analysis were used to gain an insight into the homo- and heteroaggregate structures in various environmental and coating conditions.

2. Materials and methods

2.1. Methods

2.1.1. Zeta potential and size distribution analysis

Z-average hydrodynamic diameters of pristine (uncoated) CeO_2 MNPs and mixtures of CeO_2 in presence of alginate as well as MNPs in synthetic and natural waters were measured with a Malvern Zetasizer Nano ZS (Malvern Instruments Ltd, UK). The autocorrelation function accumulated at least ten runs for each samples for five parallel measurements with time delay of 5 s. The hydrodynamic diameter d_H was calculated from the transitional diffusion coefficient D using the Stokes-Einstein equation. The polydispersity index was found less than 0.6 in all our measurements. To obtain information on the surface charge and changes via the zeta potential, the electrophoretic mobility was measured using the Doppler technique with the Malvern Zetasizer Nano ZS and the Smoluchowski approximation model was applied [32].

2.1.2. SEM image analysis

A JSM-7001FA (JEOL) scanning electron microscope (SEM) was used to obtain images of pristine CeO_2 MNPs and mixtures of CeO_2 with alginate. For each samples, 10 µL of the MNPs dispersion were placed on one aluminum stub covered with a 5 × 5 mm silica wafer Agar Scientific (G3390) and wrapped with 3–5 nm of Pt/Pd coating.

2.1.3. TEM image analysis

A Hitachi A7650 Transmission electron microscope (TEM) was used for imaging the texture, size, distribution, and morphology of the CeO_2 MNPs and also to precise the agglomeration-dispersion trends between non-coated and coated MNPs in ultrapure, synthetic and lake waters. The TEM configuration allows both high contrast (low Z element can be imaged) and high resolution (better than 5 Å). Thus, a condenser 2 with a large aperture (100 µm apparent diameter), associated with a diaphragm objective (20 µm apparent diameter) under an 80 keV accelerating voltage have been used. The samples were prepared directly onto the copper grid covered by an amorphous carbon thin film with a thickness around 50 nm (Delta MICROSCOPIES, France). Direct sample deposition of a 2 μm^3 volume droplet using a dedicated syringe (Mettler-Toledo SAS, France) followed by several washing steps by ultrapure water, to minimize the formation of artefacts, especially for organic colloids or NOM associated with nanometric metallic trace elements [33].

2.1.4. pH measurement

The control of pH, by direct immersion of electrode in the solution, was done during all experiments with a Hach Lange HQ40d portable meter and one pH probe PHC101 (Hach Lange, Switzerland).

2.2. Materials

Uncoated CeO_2 MNPs as a powder (NM-212, JRC nanomaterial repository, Ispra, Italy) with a nominal particle diameter 28 ± 10 nm and a specific surface area equal to 27.2 ± 0.9 m^2/g [34] was used. The powder was weighed and diluted in ultrapure water (R > 18 MΩ cm, Millipore, Switzerland) and the pH was adjusted to 3.0 to obtain a 1 g/L CeO_2 stable stock suspension. After sonication, aliquots of the stock suspension were used to prepare diluted suspensions for further experiments. A 50 mg/L CeO_2 suspension was used in all experiments unless indicated. Such a concentration was considered to optimize the signal during the dynamic light scattering and electrophoretic measurements. A detailed protocol for suspension preparation is provided

in [35].

A 100 mg/L stock solution of alginate (A2158, Sigma Aldrich, Switzerland) was prepared in ultrapure water and used for further dilution. The titration of one 50 mg/L alginate solution was done to characterize alginate (SI3, Fig.S1). To adjust the pH sodium hydroxide and hydrochloride acid 0.01 M (NaOH and HCl, Titrisol®113, Merck, Switzerland) were used. For suspension homogenization, gentle agitation was applied during all the experiments with a magnet vortex and a rotational speed equal to 200 rpm.

To mimic the ionic composition of Lake Geneva water we developed a method to prepare synthetic fresh water solutions based on the works of Hammes et al. and Smith et al. [36,37]. The protocol and the corresponding concentrations of electrolytes are provided in the supporting information (SI1). The following electrolytes were used; $CaCl_2{\cdot}6H_2O$, $MgCl_2{\cdot}6H_2O$, $Mg(NO_3)_2{\cdot}6H_2O$, $CaSO_4{\cdot}2H_2O$, $CaCO_3$, $NaHCO_3$, $KHCO_3$, and all chemicals were reagent grade or better (Fluka, Acros Organics and Sigma-Aldrich, Switzerland).

Samples of natural water from Lake Geneva were collected in Versoix (Geneva, Switzerland). Before performing the experiments, water was filtered with a pore size equal to 0.45 µm, analyzed and stored in a dark place. The major ion composition and physicochemical analysis are provided in supporting information (SI2).

All stock solutions were stored in a dark place at 4 °C.

2.3. Protocols

To investigate the formation of alginate coating on MNPs a series of independent CeO_2 suspensions were prepared at 50 mg/L and variable concentrations of alginate at two pH conditions i.e. pH < pH_{PZC} and pH > pH_{PZC} were considered. The concentration of alginate varied in the range from 0.05 to 2 mg/L. Z-average hydrodynamic diameters were measured directly after suspension preparation during 1 h with 30 s time interval and then the measurement of zeta potential was done.

To study the coating stability around CeO_2 MNPs in changing pH conditions the titration was performed in a pH range from 3 to 10. First, the 50 mg/L CeO_2 suspension with 2 mg/L alginate at pH 3.0 ± 0.2 was prepared then the pH was increased up to 10. The measurements of hydrodynamic diameters and zeta potentials were done every 15 min after pH adjustment.

To investigate the behavior of CeO_2 MNPs in synthetic water, first we adjusted the concentration of alginate and pH value and then we added the CeO_2 MNPs. The appropriate amount of alginate was added to synthetic water to obtain concentration equal to 0.25, 0.5, 1 and 2 mg/L. The pH was adjusted to 8.0 ± 0.2. The last step was the addition of an aliquot of CeO_2 stock suspension to obtain a final concentration equal to 50 mg/L. The measurements of z-average diameters and zeta potential were started immediately after MNPs addition and every 30 min during 2 h. An identical procedure was used for the experiments with natural Lake Geneva water.

To investigate the coating properties, CeO_2 MNPs were previously coated with appropriate concentrations of alginate (0.25 and 2 mg/L), two representative conditions, and then the corresponding suspension was added to the synthetic and filtered lake water. The measurements of z-average diameter and zeta potential were done as a function of time.

3. Results and discussion

3.1. Influence of alginate concentration on the coating formation

To get an insight on the alginate ability to modify the surface properties of pristine CeO_2 MNPs two complementary experiments were conducted, based on different surface charge scenarios and by modifying the pH.

3.1.1. pH ≤ pH_{PZC}

CeO_2 MNPs in this pH region are initially positively charged (SI4, Fig. S2), contrarily to the alginate which is negatively charged in all pH range (SI3, Fig. S1). Therefore, increase of alginate concentration is found to change CeO_2 surface charge from positive to negative values due to the strong electrostatic interaction between alginate and CeO_2. Isoelectric point (IEP) is achieved when the concentration of alginate is equal to 0.65 ± 0.05 mg/L and the aggregate z-average hydrodynamic diameters increases up to 922 ± 217 nm (Fig. 1). For an alginate concentration above 1 mg/L, CeO_2 MNPs are found stabilized with zeta potential values close to −20 mV and a decrease of the z-average diameter is observed down to 183 ± 8 nm (for an alginate concentration equal to 2 mg/L).

SEM images of pristine CeO_2 MNPs and in presence of alginate (1.5 mg/L) are presented in Fig. 2. In the two cases, MNPs are found polydisperse in sizes. Some individual particles as well as aggregates are present and sizes varied from 30 nm to 200 nm. These data are in good agreement with the obtained z-average hydrodynamic diameter values. On the surface of the wafer, we also distinguish the presence of a network of alginate strings in which homoaggregates of CeO_2 are embedded.

3.1.2. pH ≥ pH_{PZC}

Zeta potentials and z-average hydrodynamic diameters of CeO_2 MNPs at pH 8, by increasing alginate concentration conditions, are presented in Fig. 3a. At this pH, both CeO_2 and alginate have the same surface charge, and are negatively charged. Therefore, no significant effect of alginate is observed. Our results indicate that in presence of electrostatic repulsions no coating is observed. Indeed, when the alginate concentration is increasing no changes in the values of zeta potential and average diameter are observed. They are stable and equal to −41.7 ± 2.2 mV and 228 ± 15 nm respectively. The TEM micrograph (Fig. 3b) also confirms that pristine CeO_2 MNPs with initial size between 10–20 nm form homoaggregates with a number of initial crystals from 10 to 100 nm and with sizes up to 200 nm.

3.2. Stability of alginate coating in changing pH conditions

To get an insight on the stability of alginate coating in changing pH conditions, a 50 mg/L CeO_2 MNP suspension with 2 mg/L alginate is prepared first at pH 3.0 ± 0.2. Then the pH is gradually increased up to 10.0 ± 0.2. In such conditions, the surface charge of CeO_2/alginate complexes is found negative in the entire pH range (Fig. 4a) but significant surface charge modifications are nevertheless observed. Increase of pH up to 6.8 leads to the decrease of the values of zeta potential from −24.0 ± 0.4 mV to −45.0 ± 3.0 mV. This pH

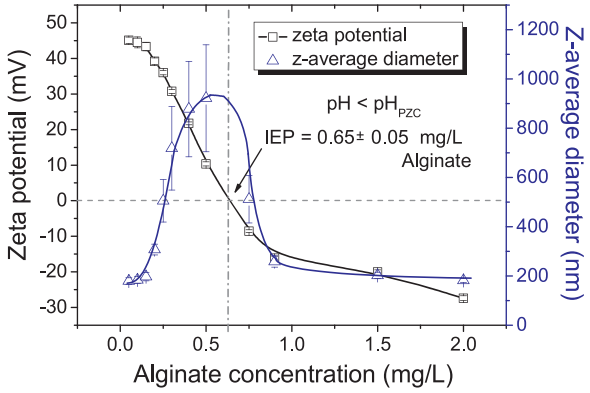

Fig. 1. Zeta potential and z-average hydrodynamic diameter of CeO_2 MNPs at different alginate concentrations at pH < pH_{PZC} (pH = 3.0 ± 0.2) in ultrapure water. The strong affinity between the positively charged CeO_2 MNPs and negatively charged alginate is mainly due to electrostatic interactions. The IEP is achieved at 0.65 ± 0.05 mg/L of alginate for a 50 mg/L CeO_2 MNP dispersion.

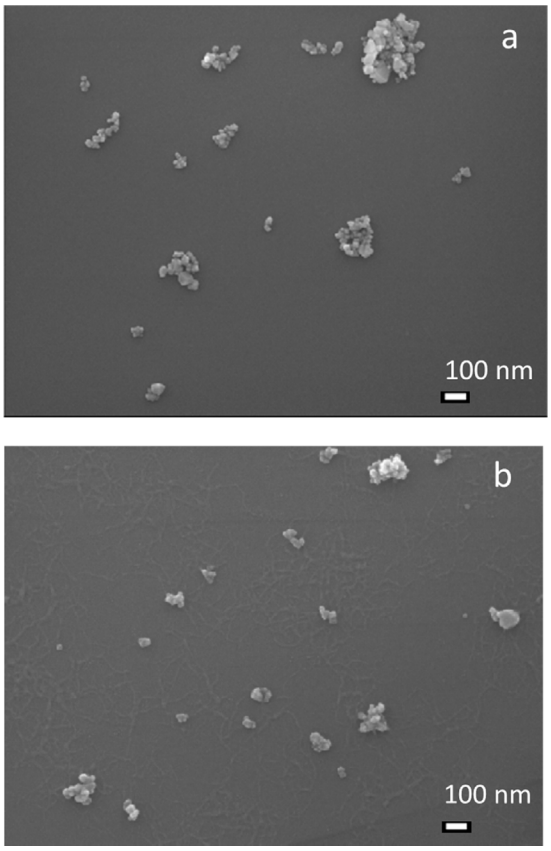

Fig. 2. SEM images of (a) pristine CeO_2 MNPs (10 mg/L) in ultrapure water at pH 3.0; (b) CeO_2 MNPs (1 mg/L) in presence of alginate (1.5 mg/L) at pH 3.0. Limited aggregation is observed in two cases due to electrostatic repulsion (a) and alginate coating (b).

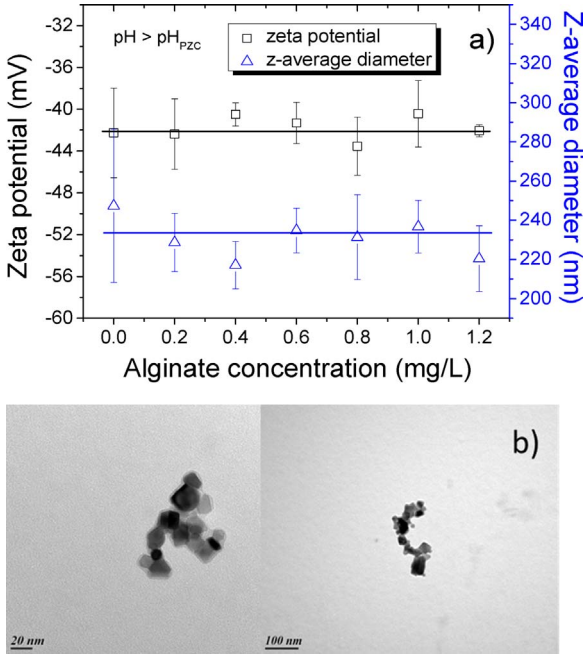

Fig. 3. Zeta potentials and z-average hydrodynamic diameters (a) CeO_2 MNPs for different alginate concentrations at pH > pH_{PZC} (pH = 8.0 ± 0.2) in ultrapure water. No significant changes are observed in presence of alginate in this electrostatic scenario (both alginate and pristine CeO_2 MNPs are negatively charged). (b) TEM micrography of pristine CeO_2 MNPs in ultrapure water (pH = 8.0 ± 0.2). Cubic crystalline form CeO_2 MNPs, pristine particles (10–20 nm) are homoaggregated.

corresponds to the pH_{PZC} of CeO_2 MNPs (SI Fig.S3). Above this pH, a zeta potential plateau is obtained with a mean value equal to −45.0 ± 1.1 mV. Decrease of the zeta potential is attributed to the CeO_2 acid base properties and therefore progressive neutralization of the MNP positive surface charges with increase of pH until the moment when all surface charges are switched off at pH 6.8.

On the other hand, z-average diameters exhibit a more complex behavior. First, diameters are stable below pH 6.8 with a mean value equal to 188 ± 6 nm. Then above pH 6.8 the hydrodynamic diameter values are slightly increased to 207 ± 9 nm. Such a variation can be attributed to the change of conformation of the alginate molecules on MNP surface. Indeed, alginate is a flexible polysaccharide with fibrillar conformation that can be easily modified with pH changes. At environmental pH alginate is most likely represented as an extended coil [14]. When positively charged MNPs are mixed with negatively charged alginate compact complexes are formed due to the strong electrostatic interactions at acid pH (Fig. 4b). With the increase of pH alginate is then expected to adopt more extended conformations even if adsorbed at the MNP surface. Such a conformational change leads to an increase of alginate coating thickness. Despite this change, coating is stable through the full pH ranges.

3.3. Stability of pristine CeO_2 MNPs in synthetic and natural waters and influence of alginate

To study the stability of CeO_2 MNPs in environmental conditions we considered two scenarios: release of pristine CeO_2 in synthetic water that mimic the ionic composition of Lake Geneva water and release of pristine CeO_2 MNPs in filtered Lake Geneva water. The first scenario addresses only the impact of ion composition whereas the second one investigates a more complex system in which additional natural water compounds such as natural dissolved organic matter and inorganic colloids with size less than 0.45 µm are present. The presence of alginate at variable concentrations is also investigated regarding the MNP stability. Based on the obtained results mechanisms responsible for MNP aggregation and stabilization are proposed.

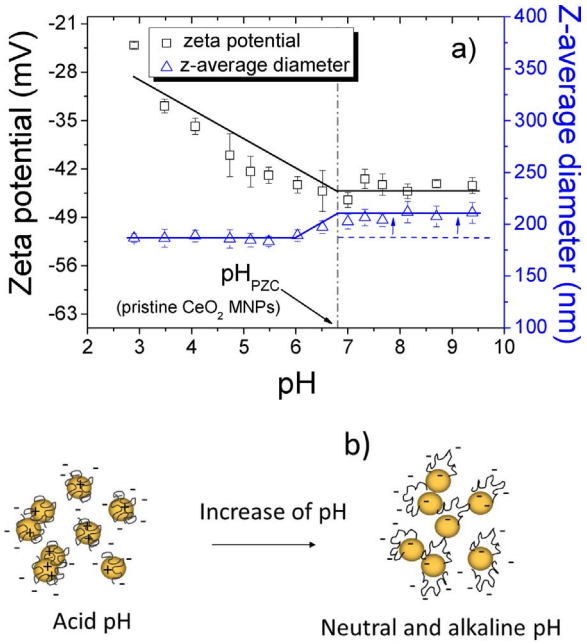

Fig. 4. (a) Zeta potentials and z-average hydrodynamic diameters of a 50 mg/L CeO_2 MNPs coated with a 2 mg/L alginate in different pH conditions. CeO_2/Alginate complexes are negatively charged in the full pH range. (b) schematic representation of alginate conformational changes at the MNP surface. At neutral and alkaline pH alginate has more extended structure compared to its structure in acid pH.

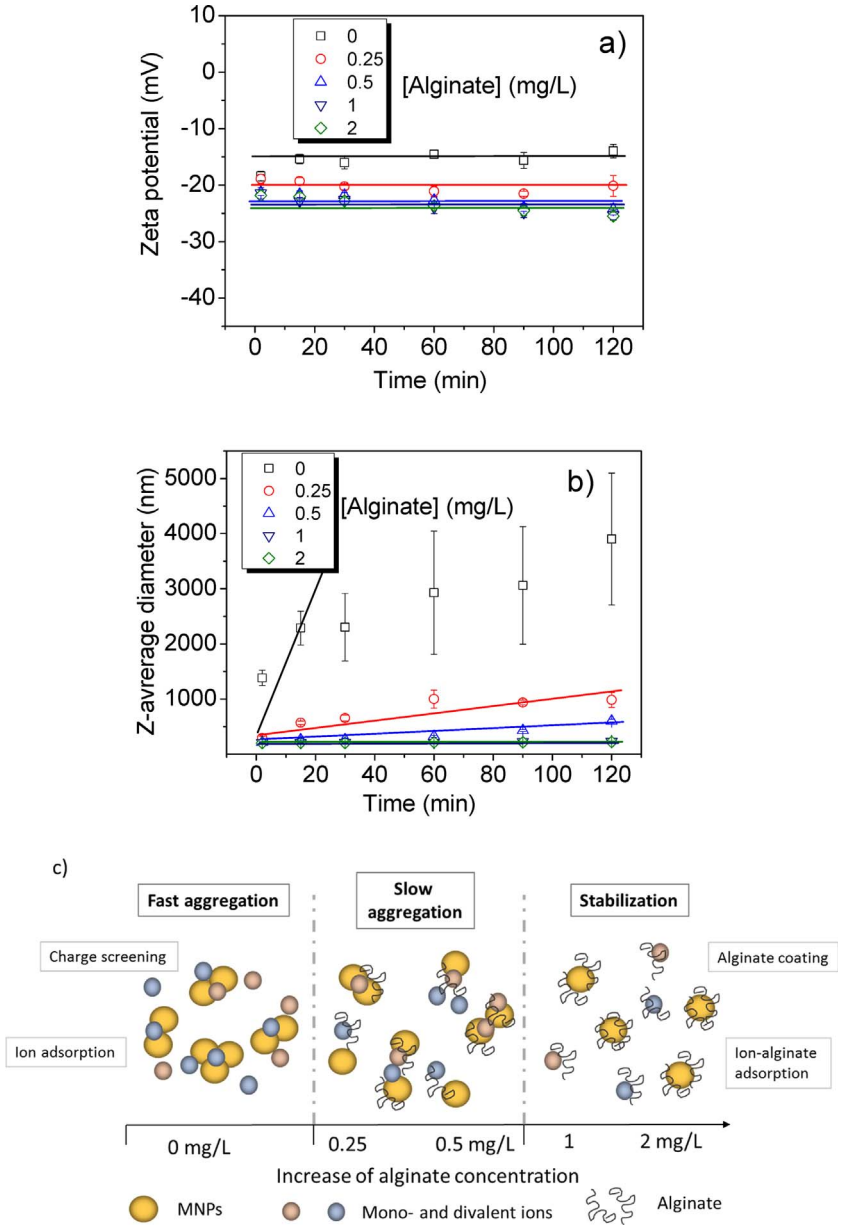

Fig. 5. Time variation of (a) zeta potentials and (b) z-average hydrodynamic diameters of CeO_2 MNPs in synthetic water at pH 8.0 ± 0.2. In comparison to ultrapure water important changes of zeta potential are observed when MNPs are introduced in synthetic water towards less negative values hence promoting aggregation. Then increasing alginate concentration has a stabilizing effect. (c) Schematic representation of aggregation and stabilization mechanisms of MNPs as a function of alginate concentration.

3.3.1. Synthetic water

Zeta potentials and z-average diameters were analyzed as a function of time. We considered a range of alginate concentration from 0 to 2 mg/L. As shown in Fig. 5a surface charge is found negative in all cases and stable with time and the mean values of zeta potential are depending on the alginate concentration. Zeta potential of pristine MNPs in synthetic water is equal to −15.6 ± 1.0 mV at pH 8.0 ± 0.2. Then the gradual increase of alginate concentration leads to the gradual zeta potential decrease (more negative). For the higher alginate concentrations, 1 and 2 mg/L, the values of zeta potential are identical and equal to −23.5 ± 0.8 mV, thus indicating a surface saturation effect.

Pristine CeO_2 MNPs, when released to synthetic water, i.e. not preliminary coated with alginate, are not stable and significant homoaggregation is observed with z-average hydrodynamic diameters up to 3500 nm (Fig. 5b) after 120 min. Such behavior is due to: i) a decrease of the surface charge due to the specific adsorption of divalent cations such as Ca^{2+} and Mg^{2+}, and ii) screening effect because of the increase of the ionic strength compared to ultrapure water (Fig. 5c) [38,39]. On the other hand, the presence of alginate in the synthetic water solutions is found to promote stabilization via the coating formation around MNPs. The impact of this coating mainly depends on the alginate concentration. At moderate alginate concentrations, 0.25 and 0.5 mg/L, we still observe homoaggregation. However, the aggregate size is smaller and the rate of aggregation is reduced if compared to the absence of alginate case. Alginate molecules are expected to interact here with ions present in solution and adsorb on MNPs via electrostatic interactions creating bridges between particles, hence resulting in the formation of aggregates. At high alginate concentration, 1 and 2 mg/L, the amount of alginate is high enough to saturate the particle surface promoting the stability of CeO_2 MNPs via steric and electrostatic repulsions as shown in Fig. 5c. Consequently, mean value of z-average diameters are found stable and equal to 220 ± 10 nm with time.

3.3.2. Natural lake Geneva water

The stability of pristine CeO_2 MNPs and CeO_2 in the presence of alginate was also studied in filtered water from Lake Geneva to understand the effect of dissolved water compounds such as naturally present organic substances and inorganic particulate matter. Pristine CeO_2 MNPs are found to form rapidly heteroaggregates with z-average hydrodynamic diameters up to 2250 nm and negative surface charges

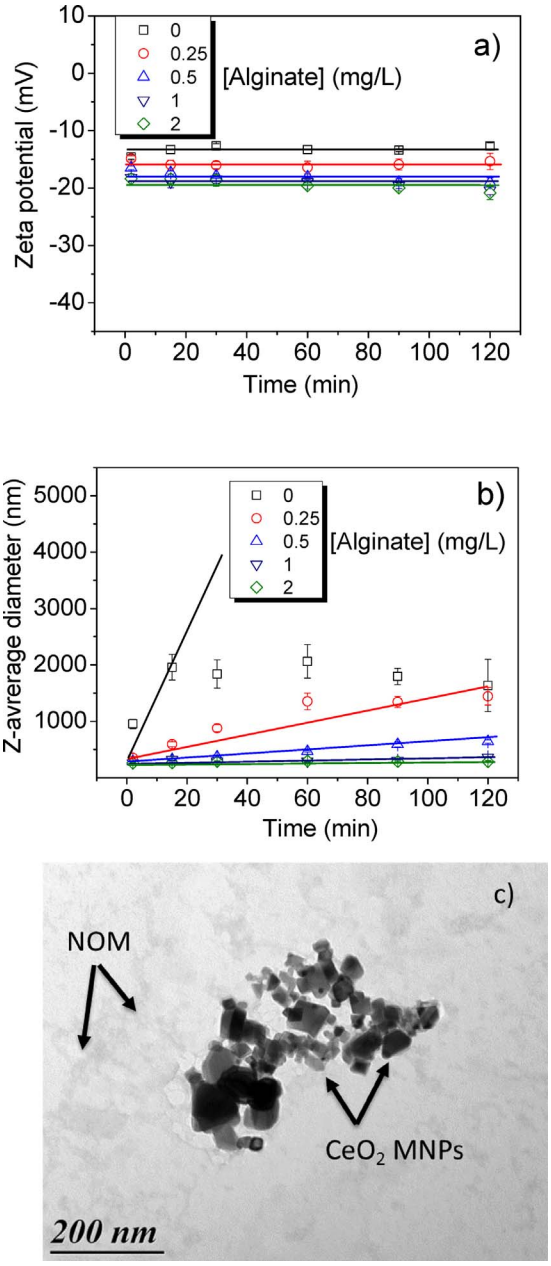

Fig. 6. Time variation of (a) zeta potentials, (b) z-average hydrodynamic diameters as a function of alginate concentrations in Lake Geneva water. Important changes of zeta potentials are observed if comparison is made with ultrapure water towards less negative values which promote aggregation. (c) TEM micrography of CeO_2 MNPs in Lake Geneva water showing the presence of a large fibrillar network and CeO_2 MNP aggregates.

(Fig. 6). Charge screening and adsorption of cations are expected to play key roles as well as complexation processes with naturally present dissolved compounds (< 0.45 μm). Despite the difficulty to evaluate the precise impact of these compounds on heteroaggregation, similar MNP behavior as in synthetic water regarding the alginate concentration is observed in lake water. Once again, high concentration of alginate (2 mg/L) leads to MNP stabilization with z-average diameters equal to 286 ± 17 nm during 120 min. It should be noted that similar stabilization effects were observed in the presence of Suwanee River humic acid (SRHA) on Ag NPs in filtered Rhine water [39], despite the nature of NOM and concentration differences (the concentration of SRHA was ten times higher compared to alginate concentration in our work).

On the other hand, at smaller alginate concentrations (0.25 and 0.5 mg/L), heteroaggregation is observed and z-average diameter

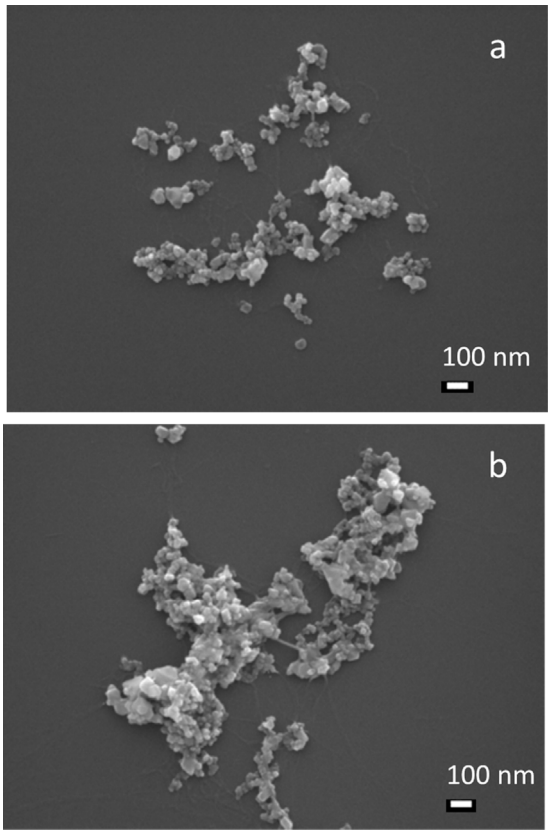

Fig. 7. SEM images of CeO_2 MNPs in (a) synthetic water and (b) filtered Lake Geneva water (pH 8.0 ± 0.2 > pH_{PZC}). [CeO_2] = 10 mg/L; [alginate] = 0.25 mg/L. Compared to synthetic water in Lake Geneva water CeO_2 MNPs are embedded in more complex environmental matrix in which heteroaggregation seems more significant.

increases up to 1443 ± 159 nm after 120 min. The zeta potential values are slightly less negative if compared to the values in synthetic water. It can be explained by the simplified composition of synthetic water which is prepared only with major ions, whereas natural water has more heterogeneous ionic composition and also contains diverse dissolved organic matter such as humic substances, polysaccharides, proteins and other biopolymers [14]. Homo- and heteroaggregates formed in synthetic and Lake Geneva waters are presented in Fig. 7 in which SEM images illustrate the heterogeneity of environmental matrix and aggregates (Fig. 7b) compared to simplified synthetic waters (Fig. 7a).

3.4. Stability of alginate pre-coated CeO_2 MNPs in synthetic and natural waters

To evaluate the impact of alginate coating formed in two different ways, we compared zeta potentials and z- average diameter variation of pristine CeO_2 MNPs (uncoated MNPs) released to synthetic water already containing alginate with CeO_2 MNPs previously coated with the same amount of alginate and then released to synthetic water (so-called pre-coated MNPs). As shown in Fig. 8 significant difference is observed between the zeta potential values indicating different surface charge equilibration processes and aggregation mechanisms. As described previously uncoated CeO_2 MNPs when released to synthetic water that contains 0.25 mg/L alginate are destabilized due to the concomitant adsorption of alginate molecules and ions which create bridges between MNPs (Fig. 8b). When pre-coated CeO_2 MNPs, already destabilized by small amount of alginate, are released to synthetic water we observe an increase of zeta potential (the value is less negative) and concomitant aggregation. Z-average diameters of pre-coated particles are initially higher compared to uncoated particles (Fig. 8b) and equal to 898 ± 122 nm and 656 ± 55 nm accordingly.

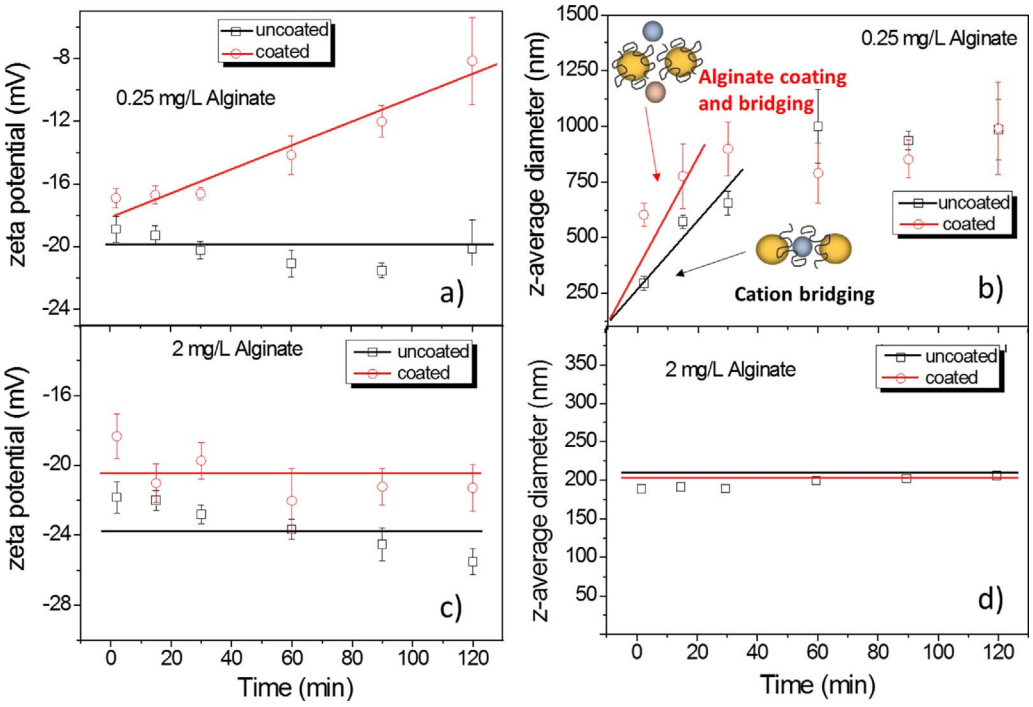

Fig. 8. (a) and (c) Time resolved variation of zeta potentials. (b) and (d) Z- average hydrodynamic diameters of pristine and coated CeO_2 MNPs with various concentration of alginate in synthetic water. pH 8.0 ± 0.2.

No aggregation is observed for the uncoated and pre-coated CeO_2 MNPs at 2 mg/L alginate despite the slight difference in zeta potentials. Z-average diameters are stable with time and are equal to 212 ± 10 nm for uncoated and 205 ± 9 nm for pre-coated CeO_2. Here again, our data indicate that CeO_2 MNP stability is largely dependent on the alginate concentration.

The stability of uncoated and pre-coated CeO_2 MNPs was also investigated in lake water (SI5, Fig.S3). We observed similar effects as in synthetic water. Pre-coated CeO_2 MNPs with 0.25 mg/L alginate have less negative values of zeta potential compared to uncoated MNPs and exhibit larger sizes for the aggregates. Overall, despite the different coating procedures the general MNPs behavior is found similar in two cases. The dominant effect attributed to the alginate concentration at low alginate concentration MNP aggregation is observed, whereas at higher alginate concentration stabilization is observed.

4. Conclusions

Our findings clearly indicate that the concentration of alginate and solution pH play a crucial role in coating properties and environmental identity of CeO_2 MNPs. Alginate concentrations above 1 mg/L are forming a stable coating around CeO_2 MNPs in ultrapure, synthetic, and natural waters, which results in CeO_2 stabilization. In synthetic waters, at low alginate concentration, the interactions between MNPs and alginate are promoted by divalent cations via specific adsorption and charge screening hence denoting the importance of water hardness. In Lake water, CeO_2 heteroaggregation is observed in all cases but its importance is altered by the alginate concentration. Our results also indicate that when alginate coating is formed, coating is persistent regarding changing pH conditions.

Acknowledgements

The authors acknowledge the financial support received from the European Commission's 7th Framework Programme project “NanoMILE” (contract no. NMP4-LA-2013-310451). We are also grateful to Agathe Martignier for her support during the SEM measurements.

Appendix A. Supplementary data

Supplementary data associated with this article can be found, in the online version, at http://dx.doi.org/10.1016/j.colsurfa.2017.07.069.

References

[1] A.B. Boxall, K. Tiede, Q. Chaudhry, Engineered nanomaterials in soils and water: how do they behave and could they pose a risk to human health? Nanomedicine 2 (2007) 919–927, http://dx.doi.org/10.2217/17435889.2.6.919.

[2] S.K. Brar, M. Verma, R.D. Tyagi, R.Y. Surampalli, Engineered nanoparticles in wastewater and wastewater sludge–evidence and impacts, Waste Manag. 30 (2010) 504–520, http://dx.doi.org/10.1016/j.wasman.2009.10.012.

[3] F. Gottschalk, T. Sun, B. Nowack, Environmental concentrations of engineered nanomaterials: review of modeling and analytical studies, Environ. Pollut. 181 (2013) 287–300, http://dx.doi.org/10.1016/j.envpol.2013.06.003.

[4] K. Reed, A. Cormack, A. Kulkarni, M. Mayton, D. Sayle, F. Klaessig, B. Stadler, Exploring the properties and applications of nanoceria: is there still plenty of room at the bottom? Environ. Sci. Nano 1 (2014) 390–405, http://dx.doi.org/10.1039/C4EN00079J.

[5] I. Rodea- Palomares, K. Boltes, F. Fernández-Piñas, F. Leganés, E. García-Calvo, J. Santiago, R. Rosal, Physicochemical characterization and ecotoxicological assessment of CeO2 nanoparticles using two aquatic microorganisms, Toxicol. Sci. 119 (2011) 135–145.

[6] J. Trujillo- Reyes, A.R. Vilchis-Nestor, S. Majumdar, J.R. Peralta-Videa, J.L. Gardea-Torresdey, Citric acid modifies surface properties of commercial CeO2 nanoparticles reducing their toxicity and cerium uptake in radish (Raphanus sativus) seedlings, J. Hazard. Mater. 263 (Part 2) (2013) 677–684, http://dx.doi.org/10.1016/j.jhazmat.2013.10.030.

[7] Y. Li, J. Niu, E. Shang, J.C. Crittenden, Influence of dissolved organic matter on photogenerated reactive oxygen species and metal-oxide nanoparticle toxicity, Water Res. 98 (2016) 9–18, http://dx.doi.org/10.1016/j.watres.2016.03.050.

[8] L.K. Limbach, R. Bereiter, E. Müller, R. Krebs, R. Gälli, W.J. Stark, Removal of oxide nanoparticles in a model wastewater treatment plant: influence of agglomeration and surfactants on clearing efficiency, Environ. Sci. Technol. 42 (2008) 5828–5833, http://dx.doi.org/10.1021/es800091f.

[9] G. Qiu, S.-Y. Neo, Y.-P. Ting, Effects of CeO2 nanoparticles on system performance and bacterial community dynamics in a sequencing batch reactor, Water Sci. Technol. 73 (2016) 95–101.

[10] A. Brunelli, A. Zabeo, E. Semenzin, D. Hristozov, A. Marcomini, Extrapolated long-term stability of titanium dioxide nanoparticles and multi-walled carbon nanotubes in artificial freshwater, J. Nanoparticle Res. 18 (2016) 113.

[11] L. Chekli, Y.X. Zhao, L.D. Tijing, S. Phuntsho, E. Donner, E. Lombi, B.Y. Gao, H.K. Shon, Aggregation behaviour of engineered nanoparticles in natural waters: characterising aggregate structure using on-line laser light scattering, J. Hazard. Mater. 284 (2015) 190–200, http://dx.doi.org/10.1016/j.jhazmat.2014.11.003.

[12] A. Philippe, G.E. Schaumann, Interactions of dissolved organic matter with natural

and engineered inorganic colloids: a review, Environ. Sci. Technol. 48 (2014) 8946–8962, http://dx.doi.org/10.1021/es502342r.
[13] M. Baalousha, Y. Nur, I. Römer, M. Tejamaya, J.R. Lead, Effect of monovalent and divalent cations, anions and fulvic acid on aggregation of citrate-coated silver nanoparticles, Sci. Total Environ. 454–455 (2013) 119–131, http://dx.doi.org/10.1016/j.scitotenv.2013.02.093.
[14] J. Buffle, K.J. Wilkinson, S. Stoll, M. Filella, J. Zhang, A generalized description of aquatic colloidal interactions: the three-colloidal component approach, Environ. Sci. Technol. 32 (1998) 2887–2899, http://dx.doi.org/10.1021/es980217h.
[15] A.D. Augst, H.J. Kong, D.J. Mooney, Alginate hydrogels as biomaterials, Macromol. Biosci. 6 (2006) 623–633, http://dx.doi.org/10.1002/mabi.200600069.
[16] W. Sabra, A.P. Zeng, Microbial production of alginates: physiology and process aspects, Alginates Biol. Appl. Springer (2009) 153–173.
[17] S.N. Pawar, K.J. Edgar, Alginate derivatization: a review of chemistry, properties and applications, Biomaterials 33 (2012) 3279–3305, http://dx.doi.org/10.1016/j.biomaterials.2012.01.007.
[18] K.Y. Lee, D.J. Mooney, Alginate: properties and biomedical applications, Prog. Polym. Sci. 37 (2012) 106–126.
[19] Z. Majidnia, A. Idris, M. Majid, R. Zin, M. Ponraj, Efficiency of barium removal from radioactive waste water using the combination of maghemite and titania nanoparticles in PVA and alginate beads, Appl. Radiat. Isot. 105 (2015) 105–113, http://dx.doi.org/10.1016/j.apradiso.2015.06.028.
[20] W. Sun, C. Zhang, W. Shi, C. Wang, X. Jiao, Heteroadsorption of 17α-ethynylestradiol by multi-walled carbon nanotubes and SiO2/Al2O3 nanoparticles: effect of surface-coated fulvic acid and alginate, Chem. Eng. J. 288 (2016) 516–524, http://dx.doi.org/10.1016/j.cej.2015.12.029.
[21] S. Bang, J.-W. Choi, K. Cho, C. Chung, H. Kang, S.W. Hong, Simultaneous reduction of copper and toxicity in semiconductor wastewater using protonated alginate beads, Chem. Eng. J. 288 (2016) 525–531, http://dx.doi.org/10.1016/j.cej.2015.12.025.
[22] P. Geetha, M.S. Latha, S.S. Pillai, B. Deepa, K. Santhosh Kumar, M. Koshy, Green synthesis and characterization of alginate nanoparticles and its role as a biosorbent for Cr(VI) ions, J. Mol. Struct. 1105 (2016) 54–60, http://dx.doi.org/10.1016/j.molstruc.2015.10.022.
[23] F. Loosli, P. Le Coustumer, S. Stoll, Effect of electrolyte valency, alginate concentration and pH on engineered TiO2 nanoparticle stability in aqueous solution, Sci. Total Environ. 535 (2015) 28–34, http://dx.doi.org/10.1016/j.scitotenv.2015.02.037.
[24] F. Loosli, P.L. Coustumer, S. Stoll, TiO2 nanoparticles aggregation and disaggregation in presence of alginate and Suwannee River humic acids. pH and concentration effects on nanoparticle stability, Water Res. 47 (2013) 6052–6063.
[25] M.K. Lima- Tenório, E.A.G. Pineda, N.M. Ahmad, G. Agusti, S. Manzoor, D. Kabbaj, H. Fessi, A. Elaissari, Aminodextran polymer-functionalized reactive magnetic emulsions for potential theranostic applications, Colloids Surf. B: Biointerfaces 145 (2016) 373–381, http://dx.doi.org/10.1016/j.colsurfb.2016.05.020.
[26] N. Kavok, G. Grygorova, V. Klochkov, S. Yefimova, The role of serum proteins in the stabilization of colloidal LnVO4:Eu3+ (Ln = La, Gd, Y) and CeO2 nanoparticles, Colloids Surf. Physicochem. Eng. Asp. 529 (2017) 594–599, http://dx.doi.org/10.1016/j.colsurfa.2017.06.052.
[27] Tella Marie, Auffan Mélanie, Brousset Lenka, Issartel Julien, Kieffer Isabelle, Pailles Christine, Morel Elise, Santaella Catherine, Angeletti Bernard, Artells Ester, Rose Jérôme, Thiéry Alain, Bottero Jean-Yves, Transfer, transformation, and impacts of ceria nanomaterials in aquatic mesocosms simulating a pond ecosystem, Environ. Sci. Technol. 48 (2014) 9004–9013, http://dx.doi.org/10.1021/es501641b.
[28] M. Auffan, A. Masion, J. Labille, M.-A. Diot, W. Liu, L. Olivi, O. Proux, F. Ziarelli, P. Chaurand, C. Geantet, J.-Y. Bottero, J. Rose, Long-term aging of a CeO2 based nanocomposite used for wood protection, Environ. Pollut. 188 (2014) 1–7, http://dx.doi.org/10.1016/j.envpol.2014.01.016.
[29] J. Jiménez- Lamana, V.I. Slaveykova, Silver nanoparticle behaviour in lake water depends on their surface coating, Sci. Total Environ. 573 (2016) 946–953, http://dx.doi.org/10.1016/j.scitotenv.2016.08.181.
[30] I. Lynch, A. Ahluwalia, D. Boraschi, H.J. Byrne, B. Fadeel, P. Gehr, A.C. Gutleb, M. Kendall, M.G. Papadopoulos, The bio-nano-interface in predicting nanoparticle fate and behaviour in living organisms: towards grouping and categorising nanomaterials and ensuring nanosafety by design, BioNanoMaterials 14 (2013) 195–216.
[31] I. Lynch, Role of the biomolecule Corona in nanoparticle fate and behavior, Nanoparticles Lung Environ. Expo. Drug Deliv. (2014) 47.
[32] J. Gregory, Particles in Water: Properties and Processes, CRC Press, 2005.
[33] M. Baalousha, M. Motelica-Heino, S. Galaup, P. Le Coustumer, Supramolecular structure of humic acids by TEM with improved sample preparation and staining, Microsc. Res. Tech. 66 (2005) 299–306.
[34] C. Singh, S. Friedrichs, G. Ceccone, N. Gibson, K.A. Jensen, M. Levin, H.G. Infante, D. Carlander, K. Rasmussen, Cerium dioxide, NM- 211, NM-212, NM-213. Characterisation and test item preparation, in: european commission JRC, Institute for Health and Consumer Protection, Sci. Tech. Res. ser. (2014) 88, http://dx.doi.org/10.2788/80203.
[35] O. Oriekhova, S. Stoll, Effects of pH and fulvic acids concentration on the stability of fulvic acids-cerium (IV) oxide nanoparticle complexes, Chemosphere 144 (2016) 131–137, http://dx.doi.org/10.1016/j.chemosphere.2015.08.057.
[36] J. Hammes, J.A. Gallego-Urrea, M. Hassellöv, Geographically distributed classification of surface water chemical parameters influencing fate and behavior of nanoparticles and colloid facilitated contaminant transport, Water Res. 47 (2013) 5350–5361.
[37] E.J. Smith, W. Davison, J. Hamilton-Taylor, Methods for preparing synthetic freshwaters, Water Res. 36 (2002) 1286–1296, http://dx.doi.org/10.1016/S0043-1354(01)00341-4.
[38] K.M. Buettner, C.I. Rinciog, S.E. Mylon, Aggregation kinetics of cerium oxide nanoparticles in monovalent and divalent electrolytes, Colloids Surf. Physicochem. Eng. Asp. 366 (2010) 74–79, http://dx.doi.org/10.1016/j.colsurfa.2010.05.024.
[39] G. Metreveli, A. Philippe, G.E. Schaumann, Disaggregation of silver nanoparticle homoaggregates in a river water matrix, Sci. Total Environ. 535 (2015) 35–44, http://dx.doi.org/10.1016/j.scitotenv.2014.11.058.

Chapter VI

Heteroaggregation of cerium dioxide nanoparticle in the presence of alginate and iron (III) oxide

Accepted in STOTEN

Oriekhova, O., and Stoll, S., 2018, Heteroaggregation of cerium dioxide nanoparticle in the presence of alginate and iron (III) oxide.

VI.1 Abstract

When manufactured nanoparticles are released to natural waters, heteroaggregation between nanoparticles and water compounds are expected to occur and play a key role in nanoparticle fate, transport and transformation in aquatic systems. In this work the heteroaggregation between CeO_2 nanoparticles and Fe_2O_3 inorganic colloids which are expected to represent the inorganic fraction from Lake Geneva water is studied. The effect of alginate and Fe_2O_3 concentration as well as ionic strength on the heteroaggregation processes is investigated by considering zeta potential and z-average diameter measurements. The kinetics of heteroaggregation of individual components as well as mixtures in increasing complexity of medium is studied. Our findings demonstrate that heteroaggregation is highly dependent on environmental conditions. In particular, the charge screening and specific adsorption of divalent cations are found to promote heteroaggregation of CeO_2 nanoparticles in synthetic and lake water. On the other hand, presence of alginate alter the heteroaggregation processes in natural water.

Keywords: CeO_2 nanoparticle, alginate coating, inorganic colloid, heteroaggregation, lake water, suspended matter

VI.2 Introduction

The progress in nanotechnology has resulted to the wide commercial production and use of manufactured nanoparticles (NPs) increasing the concern about their accumulation and fate in environmental aquatic systems. Cerium dioxide (CeO_2) NPs are used in industry and everyday products and produced on the level from hundreds to thousand tons per year (Piccinno et al. 2012). The fate of CeO_2 NPs in natural aquatic systems depends on the MNP properties such as surface charge and size but also on the water chemistry including pH, ionic composition, presence of natural organic matter (NOM) and inorganic colloids.

Natural aquatic systems are highly heterogeneous systems which contain naturally occurring colloidal particles such as natural organic matter, biological colloids, inorganic colloids etc. Because of such heterogeneity, NPs released to natural waters are interacting with different water compounds resulting in aggregation or stabilisation. It is expected that concentration of NPs released to the water body is much lower than the concentration of naturally occurring colloids (Piccinno et al. 2012; Gondikas et al. 2014; Slomberg et al. 2016) resulting to heteroaggregation between NPs and natural colloids (Wang et al. 2015; Praetorius et al. 2014; Quik et al. 2012). Moreover, Quik et al. (2012) showed that the type of aggregation (homo- or heteroaggregation) was strongly dependent on the NP concentration. When the NP concentration released to river water is relatively high (10 and 100 mg/L), homoaggregation is dominant, contrary to the relatively low concentration (1 mg/L) for which heteroaggregation with natural colloids is the main mechanism for particle elimination (Quik et al. 2012).

In order to obtain input parameters (i.e. attachment efficiencies for heteroaggregation, α_{hetero}), which are independent on the NP concentration, to use in the environmental fate models, heteroaggregation of TiO_2 NPs with natural colloids (SiO_2 particles) was performed (Praetorius et al. 2014). Authors showed that α_{hetero} is strongly dependent on solution ionic strength at pH 8 when NPs and natural colloids are both negatively charged. It was also shown that NOM (humic acid) has a stabilising effect on heteroaggregation. The experimental data could be also used to obtain the global attachment efficiency (α_{global}) which represents overall the global behaviour of the aggregating system, and, in particular, the formation of primary and secondary aggregates (Praetorius et al., 2014).

Heteroaggregation of TiO_2 NPs with a smectite clay which represent an analogue of natural colloids was evaluated to assess the main mechanisms controlling the NP aggregation in natural environment (Labille et al. 2015). It was found that the shape and dispersion state of colloids, the affinity and concentration ratio between colloids and nanoparticles are the main parameters that affect heteroaggregation. Moreover, authors showed that the presence of 1 mg/L humic acids reduce the aggregation rate.

The importance of NOM on the NP aggregation and interaction between NPs and ICs have been extensively studied separately. However, studies evaluating the impact of NOM and ICs together on NP aggregation in natural environment are still limited. In our work we concentrated mainly on the effect of two colloidal fractions, polysaccharides and inorganic colloids. The choice of these two fractions is discussed below.

Alginate is a natural polysaccharide that represents up to 30% of NOM in lake water (Buffle et al. 1998) and commonly used as a model polyelectrolyte to mimic polysaccharides from natural waters (Chen, Mylon, et Elimelech 2006). Alginate is a linear anionic polymer with a negative linear charge and carboxylic acid groups on the chain backbone (Pawar et Edgar 2012). The stabilising effect of alginate coating on iron oxide nanoparticles in biological media was shown by (Castelló et al. 2015). Alginate coated iron oxide particles were found stable up to 9 days in biological fluids. Another study indicated that the adsorption of alginate on titanium dioxide NPs induces the partial fragmentation of already formed aggregates (Loosli, Coustumer, et Stoll 2013).

Another component of natural water that is also expected to influence the fate and behaviour of NPs are inorganic colloids (ICs). The concentration of ICs in natural water is highly variable and can change from a few to hundreds mg/L (Frédérique Eyrolle et Charmasson 2004). The most common ICs are clays, aluminoscilicates and iron oxidyhydroxides (Frédérique Eyrolle et Charmasson 2004; F. Eyrolle et Charmasson 2001; Filella 2007). For example, the concentration of suspended particulate matters in river Rhône varies from 3 to 40 mg/L and is mainly represented by the presence of clay minerals, calcite, quartz, muscovite and iron oxide (sampling of Rhône water near Arles) (Slomberg et al. 2016). Another study indicates the proportions of Fe and Al observed in the colloidal phase in the river Rhône freshwaters reached 42% and 35% respectively (Frédérique Eyrolle et Charmasson 2004).

In our work we used alginate as a model of natural polysaccharides to study the heteroaggregation of CeO_2 NPs. An iron (III) oxide was chosen as an analogue of ICs as

iron oxy-hydroxides was found to be one of the main inorganic components of the Lake Geneva water column (Graham, Stoll, et Loizeau 2014). The aim of this study was to understand and establish the correlation between surface properties including surface charge, pH effect and concentration ratio with the importance of CeO_2 NP heteroaggregation in natural water. To fulfil this objective first, the heteroaggregation of a mixture composed of CeO_2 and Fe_2O_3 in absence and presence of 0.25 mg/L alginate and in increasing Fe_2O_3 concentration in ultrapure water was considered, and then filtered lake water was used. Second, the kinetics of heteroaggregation of individual components as well as mixtures of medium increasing complexity was studied. Finally, the effect of increasing alginate concentration on heteroaggregation was investigated.

VI.3 Materials and Methods

VI. 3.1 Materials

Pristine CeO_2 NPs (powder NM-212, JRC, Ispra, Italy) with nominal particle diameter 28 ± 10 nm and a specific surface area equal to 27.2 ± 0.9 m^2g^{-1} (Singh et al. 2014) were used. To prepare a 1 gL^{-1} CeO_2 stock suspension, NP powder was weighed and diluted in ultrapure water (R > 18 MΩ cm, Millipore, Switzerland) at pH 3.0 to obtain a stable suspension. Then the dilution was done and in all further experiments a 50 mgL^{-1} CeO_2 suspension was used, unless indicated. The detailed characterisation of pristine NPs is provided in supporting information of Annex 4 (Fig.VI.1 and Fig.A4.1).

Alginate (A2158, Sigma Aldrich, Switzerland) was used as a model of natural polysaccharide. A 100 mg/L stock solution was prepared in ultrapure water and used for further dilution. The detailed characterisation of alginate solution is shown in Annex 5 (A5.2).

As an analogue of inorganic colloids, iron (III) oxide (α-Fe_2O_3, 99%) (Nanoamor, Inc., USA) as a powder was used. A 1 g/L suspension was prepared and the suspension pH was set to 10. Such pH allows a better resuspension and higher stability of dispersed particle. Probe sonication was done during 15 min. Then a 100 mg/L stock suspension was prepared by dilution with ultrapure water which pH was also previously adjusted to 10. To characterise obtained particle dispersion we measured the z-average hydrodynamic diameter and zeta-potential as a function of pH. At environmentally relevant pH (pH 8.0 ± 0.2) Fe_2O_3 was found to have a negative surface charge. The detailed

particle characterisation and titration curves are provided in Fig.VI.1 and in the supporting information in Annex 4 (A4.2).

To mimic the ionic composition of Lake Geneva water, in order to test the effect of water hardness, in particular, the concentration of divalent cations such as Ca^{2+} and Mg^{2+} two electrolytes were used. Two stock solutions a 1 g/L of $CaCl_2 \cdot 6H_2O$ and $MgCl_2 \cdot 6H_2O$ (Fluka and Sigma-Aldrich, Switzerland) were prepared. They were diluted and mixed to obtain a final solution that represent synthetic water with ion concentrations equal to 45 mg/L for Ca^{2+} and 6 mg/L for Mg^{2+}.

Samples of natural water from Lake Geneva were collected in Versoix (Geneva, Switzerland). The physicochemical characterisation was performed in situ using pH (PHC101), conductivity (CDC401) and oxygen (LDO101) probes with multiparameter meter (HQ40d) (Hach Lange, Switzerland). The water ionic composition was defined by chromatographic analysis using a Dionex ICS-3000 analyzer (Dionex, Switzerland). All the parameters are provided in the supporting information in Annex 4 (A4.1). Before performing the experiments, water was filtered with a pore size equal to 0.45 μm.

All stock solutions were stored in a dark place at 4 °C.

VI.3.2 Experimental procedures and methods

Series of independent suspensions were prepared to investigate the effect of IC concentration on the heteroaggregation of CeO_2 NPs. An aliquot of CeO_2 stock suspension was added to ultrapure and lake water to obtain final concentration equal to 50 mg/L. Sodium hydroxide and hydrochloride acid 0.01 M (NaOH and HCl, Titrisol®113, Merck, Switzerland) were used to adjust the pH to 8. Variable concentrations of IC from 0 to 7.5 mg/L were added to ultrapure and lake waters before the addition of CeO_2 suspension. The measurement of z-average hydrodynamic diameter was done using a Malvern Zetasizer Nano ZS (*Malvern Instruments Ltd, UK*) directly (starting 30 sec after the mixture preparation) during 15 min with time interval 30 sec. The average value was calculated based on the last 3 min of experiments. Zeta potential was determined after the measurement of z-average diameter, i.e. 15 min after mixture was prepared. To investigate the effect of alginate, it was added to ultrapure and lake water before the addition of NPs but after IC. For the kinetics experiments the concentrations of the different compounds were equal to [CeO_2] = 50 mg/L [Fe_2O_3] = 5 mg/L, [Alginate] = 0.25 and 2 mg/L. The order of compounds addition was first water (ultrapure, synthetic, lake

waters), then IC, if needed alginate and at the end CeO_2 NPs. For the experiments with varied concentration of NPs the same procedure was used; the concentration of IC was fixed at 1 mg/L and the concentration of CeO_2 varied from 0 to 50 mg/L. The control of pH was done during all experiments with a Hach Lange HQ40d portable meter and pH probe PHC101 (Hach Lange, Switzerland).

To obtain images of CeO_2 NPs in mixture with IC and in complex matrix a JEOL JSM-7001FA scanning electron microscope (SEM) was used. For each samples, 10 µL of the NPs dispersion were placed on one aluminum stub covered with a 5×5 mm silica wafer (Agar Scientific, G3390) and wrapped with 3 – 5 nm of Pt/Pd coating. The instrument was set with following parameters: voltage 15 kV, probe current 1 nA.

The aggregation kinetics experiments were investigated by time resolved dynamic light scattering methods (DLS) using a Malvern Zetasizer Nano ZS. The hydrodynamic diameters were recorded during 15 min with 30 s time interval, starting 30 s after the mixture preparation. Average value of z-average hydrodynamic diameter and standard deviation of this value were calculated by considered two neighbor points to plot the kinetics curves. To calculate the aggregation rate (nm/min) the kinetic data of z-average hydrodynamic diameters measured over the first 5 min after mixture preparation were linearly fitted to obtain the slope. Global attachment efficiency (α_{global}) was calculated also using time resolved DLS method and represents the global behaviour of the system including homo- and heteroaggregation between pristine particles as well as NOM (Gallego-Urrea et al. 2016; Praetorius et al. 2014; Labille et al. 2015). The slope of the fitting line of the increase of z-average hydrodynamic diameters with time (first 5 min) for each particle mixture in different type of water is calculated. Attachment efficiencies are calculated by dividing these slopes for different water composition (i.e. in the reaction limited aggregation regime) by the slope of the diffusion limited aggregation regime determined under favourable conditions (i.e. critical coagulation concentration (CCC)) (Chen, Mylon, et Elimelech 2006; Gallego-Urrea et al. 2016):

$$\alpha_{global} = \frac{k}{k_{\max}}, \qquad \text{(VI.1)}$$

were k is the aggregation rate of the studied system at any specific moment (the reaction limited aggregation), k_{max} is the aggregation rate when all the collision between particles

are efficient, i.e. results in the formation of permanent contacts (diffusion limited aggregation). Such type of aggregation usually occurred when the CCC is reached.

To determine the CCC, and consequently k_{max}, the homoaggregation of pristine CeO_2 NPs in increasing NaCl concentration was performed (Annex 4, Fig. A4.8). Then the aggregation rates of different mixtures were divided by the aggregation rate at the CCC of CeO_2 NPs to obtain α_{global}, i.e. the aggregation rate of CeO_2 NPs was used as a reference for all samples in all studied conditions. The graphical representation of attachment efficiency during homoaggregation (α_{homo}) in comparison to α_{global} is also presented in Annex 4 (Fig. A4.8).

VI.4 Results and discussion

Before performing the heteroaggregation experiments between CeO_2 NPs and inorganic colloids (Fe_2O_3 ICs) in natural waters, we studied the behaviour of uncoated pristine particles as well as coated with NOM in more simplified condition (such as ultrapure water). We also characterise CeO_2 NPs, alginate and Fe_2O_3 ICs by measuring the variation of zeta potentials and z-average hydrodynamic diameters with change of pH.

VI.4.1 Characterisation of NPs and ICs

The zeta potential values as well as z-average diameters of both CeO_2 and Fe_2O_3 as a function of pH are presented in Fig.VI.1. CeO_2 NPs are positively charged below pH 6 whereas Fe_2O_3 ICs are positively charged below pH 5.0. Both are negatively charged above pH 7.0 and zeta potential is gradually decreasing with pH increase, from around +50 mV for CeO_2 and from +30 mV for Fe_2O_3 to around –45 mV and –35mV, accordingly. We defined the pH_{PZC} which is equal to 6.8 ± 0.1 for CeO_2 and 5.8 ± 0.1 for Fe_2O_3. At environmental pH 8.0 ± 0.2 both NPs and ICs are negatively charged; zeta potential of CeO_2 is equal to –37.0 ± 0.4 and of Fe_2O_3 –27.1 ± 0.6. CeO_2 NPs are stable below pH 4 and above pH 8 with mean z-average diameter equal to 173.8 ± 7.8 nm. Fe_2O_3 ICs are stable in the same pH range but with slightly smaller diameter equal to 97.7 ± 2.5. Around the PZC both NPs and ICs are aggregated with diameter approaching 1800 nm for CeO_2 and 4500 nm for Fe_2O_3. Therefore, at the PZC the size of CeO_2 homoaggregates is smaller compared to the size of Fe_2O_3 homoaggregates. Such a behaviour is due to the different shapes of the pristine particles resulting in the formation of more compact CeO_2 aggregates compared to Fe_2O_3. To gain insight into the morphology of homoaggregates and to be able to

distinguish both types of particles in a mixture, we performed SEM images of CeO_2 NPs and Fe_2O_3 ICs individually (A4.2, Fig.A4.1 and Fig.A4.2). We found that CeO_2 NPs have cubic shape whereas Fe_2O_3 ICs exhibit long needle shaped particles. We also characterise alginate which is negatively charged across the full pH range with a z-average hydrodynamic diameter that not exceed 250 nm (Fig.A4.3).

VI.4.2 CeO_2 NP heteroaggregation in presence of Fe_2O_3 ICs and alginate

Heteroaggregation of CeO_2 NPs in ultrapure water

To understand the heteroaggregation of CeO_2 NPs in presence of Fe_2O_3 ICs experiments were performed at pH 8 to approach environmental conditions. We increased the concentration of Fe_2O_3 from 0 to 7.5 mg/L and measured zeta potentials (15 min after mixture preparation) and z-average hydrodynamic diameters (every 30 s during 15 min) in absence and presence of 0.25 mg/L alginate. At this pH both CeO_2 NPs and Fe_2O_3 ICs are negatively charged and no interaction was observed because of the electrostatic repulsions (Fig.VI.2). The average value of zeta potential was found equal to –37.1 ± 1.6 mV and z-average diameter to 177 ± 9 nm. Similar results regarding heteroaggregation were obtained by considering TiO_2 NPs and SiO_2 colloids (Praetorius et al. 2014). No heteroaggregation was observed at pH 8 (at low electrolyte concentration) because of the repulsive charges between particles. In presence of alginate no significant change in the value of zeta potential (equal to –37.3 ± 1.5 mV) and z-average diameter (171 ± 8 nm) (Fig.VI.2 A and B) was observed due to the importance of repulsive interactions.

Heteroaggregation of CeO_2 NPs in lake water

To evaluate the importance of CeO_2 NP heteroaggregation in lake water we performed similar experiments as described in previous section but in filtered water from Lake Geneva. Interestingly, we observed a shift of particle zeta potential (for both cases in the presence and absence of alginate) to low values compared to ultrapure water. Zeta potential became less negative and equal to –12.0 ± 0.4 mV without alginate and –14.8 ± 0.5 mV in the presence of alginate (Fig.VI.3A). The more negative value of zeta potential in the presence of alginate is due to the additional negative charges provided by alginate (Fig. A4.3). The difference of zeta potentials observed in ultrapure water compared to lake water was attributed to the presence of positively charged ions such as Na^+, K^+, Ca^{2+} and Mg^{2+} resulting in screening effects and specific adsorption on the negative NP surface. In such conditions, heteroaggregation of CeO_2 NPs was observed. Z-average diameter was

found equal to 904 ± 148 nm without alginate and 370 ± 55 nm in the presence of 0.25 mg/L alginate (Fig.VI.3B). Alginate was found to reduce the aggregation rate process in lake water for pristine NPs due to stabilising effect (with alginate adsorption via cation bridging) (Oriekhova, Le Coustumer, et Stoll 2017). The addition and increase of Fe_2O_3 concentration resulted in the increase of heteroaggregation with and without alginate. Below 1 mg/L Fe_2O_3 the aggregate z-average diameters were found less than 1000 nm (Fig.VI.3B). Increase of Fe_2O_3 concentration resulted in larger size of the aggregates, with z-average diameters close to 3000 nm. The presence of alginate was found to have no effect above 1 mg/L Fe_2O_3, therefore, indicating dominant effect of Fe_2O_3 concentration on heteroaggregation and z-average diameter measurements in such conditions.

VI.4.3 Heteroaggregation kinetic experiments

The aim of this section was to investigate in details kinetics of heteroaggregation between CeO_2 NPs, Fe_2O_3 ICs and alginate. First, we studied the kinetics of homoaggregation of pristine CeO_2 and Fe_2O_3, then the heteroaggregation in mixtures of CeO_2 and alginate, and Fe_2O_3 and alginate. Finally, we studied the heteroaggregation of mixture CeO_2–Fe_2O_3 and of the system with including three compounds, i.e. CeO_2, Fe_2O_3 and alginate. For a more detailed understanding of the interaction mechanisms we performed experiments in ultrapure water and then in synthetic and in natural waters.

Heteroaggregation kinetics in ultrapure water

As shown in Fig.VI.4, in which z-average hydrodynamic diameters of particles in ultrapure water at pH 8.0 are presented, CeO_2 NPs and Fe_2O_3 ICs are stable at pH 8. Mean value (15 min) of z-average diameters of pristine CeO_2 NPs is equal to 192 ± 6 nm and is stable during 15 min measurement. The presence of alginate slightly reduces the value of z-average diameters which is equal to 177 ± 9 nm. Z-average diameters of Fe_2O_3 ICs and Fe_2O_3 + alginate are equal to 147 ± 6 nm and 170 ± 10 nm, respectively. By considering a mixture of CeO_2 and Fe_2O_3 without alginate z-average diameter is equal to 181 ± 8 nm. This value is found between the diameters of CeO_2 and Fe_2O_3, indicating no interaction between NPs and ICs. The presence of alginate slightly reduces z-average diameter which is equal to 161 ± 8 nm. The most important point here is to note that no heteroaggregation is observed in the mixtures between CeO_2 and Fe_2O_3 and in the mixtures CeO_2/ Fe_2O_3/Alginate in ultrapure water due to the negative surface charges of all components as indicated by the zeta potential value presented in Table VI.1.

Heteroaggregation kinetics in lake water

The time variation of z-average hydrodynamic diameters of CeO_2 NPs, Fe_2O_3 ICs, and mixtures of NPs and ICs in the presence and absence of alginate in filtered Lake Geneva water is now presented in Fig.VI.5A. Pristine CeO_2 NPs are forming aggregates in lake water (black squares) with z-average dimeter equals to 1065 ± 19 nm after 15 min. Aggregation is promoted due to the presence of divalent electrolytes, dissolved organic matter and natural colloids (Louie, Tilton, et Lowry 2013; Oriekhova et Stoll 2016). The presence of alginate reduces the aggregation rate of CeO_2 NPs from 50 ± 8 nm/min to 19 ± 4 nm/min (Fig.VI.5B). The value of the z-average diameter is also decreased and is found equal to 434 ± 10 nm. Moreover, zeta potential of CeO_2 NPs in the presence of alginate decreases compared to pristine particle and is equal to -15.0 ± 0.6 versus -12.3 ± 0.5 mV (Table VI.1) indicating NP surface coating by alginate and alginate stabilisation effect.

Table VI.1. Zeta potentials in different water samples (pH 8.0 ± 0.2)

Name of the sample	Ultrapure	Lake Geneva	Synthetic water
CeO_2	-40.3 ± 2.6	-12.3 ± 0.5	-2.0 ± 0.2
Fe_2O_3	-24.9 ± 1.6	-10.6 ± 0.4	-3.9 ± 0.3
CeO_2 + Fe_2O_3	-34.3 ± 1.4	-10.8 ± 0.4	-2.7 ± 0.3
CeO_2 + Alginate	-39.2 ± 1.4	-15.0 ± 0.6	-14.8 ± 0.4
Fe_2O_3 + Alginate	-27.5 ± 0.7	-14.4 ± 0.4	-13.4 ± 0.4
CeO_2 + Fe_2O_3 + Alginate	-36.9 ± 2.1	-13.8 ± 0.5	-9.9 ± 0.4

Pristine Fe_2O_3 ICs are also aggregated in lake water (red circles) with z-average diameter equals to 2236 ± 90 nm. The aggregation rate of Fe_2O_3 ICs is higher compared to the aggregation rate of CeO_2 NPs indicating that Fe_2O_3 aggregates growth faster compared to CeO_2 NPs. We believe it is due to the Fe_2O_3 form resulting in formation of more extended structures. In the presence of alginate, Fe_2O_3 ICs are found to have larger aggregate sizes (3051 ± 172 nm) due to the bridging effect in presence of alginate. Heteroaggregation between CeO_2 NPs and Fe_2O_3 ICs in lake water is occurring now since it was not the case in ultrapure water (Fig.VI.4). Heteroaggregation is due to the presence of natural ions (Ca^{2+}, Mg^{2+}) and organic substances which specifically adsorb on the surface of both NPs and ICs changing their surface chemistry. The presence of alginate does not have an effect on heteroaggregation in a mixture CeO_2 + Fe_2O_3 (Fig.VI.5A). In a mixture of NPs and ICs

and in natural water alginate does not have an effect on the size of heteroaggregates. In addition, the size of Fe_2O_3 aggregates is similar to the size of mixtures, probably, because of the main role of Fe_2O_3 in the process of aggregate formation and to higher contribution to the measurements.

Heteroaggregation kinetics in synthetic water

It is known that divalent cations have a significant effect on the NP stability (Liu et al. 2013; Loosli, Le Coustumer, et Stoll 2015; Chekli et al. 2015). Regarding the results obtained in previous section and in order to specifically evaluate the effect of divalent cations, synthetic water containing the same amount of Ca^{2+} and Mg^{2+} as in Lake Geneva water was prepared (more details in section 2.1). The time variation of z-average hydrodynamic diameters presented in Fig.VI.6A indicates that the same trend as in lake water is observed. Pristine CeO_2 and Fe_2O_3 are aggregated in synthetic water and the aggregation rate is slightly increased for CeO_2 and stay similar for Fe_2O_3 (62 ± 6 and 95 ± 13 nm/min, accordingly) compared to the aggregation rate in lake water 50 ± 8 and 89 ± 18 nm/min, accordingly. The presence of alginate also slightly reduces the aggregation rate for NPs but has no effect on Fe_2O_3 and on the CeO_2 + Fe_2O_3 mixture (Fig.VI.6B). However, the effect of naturally present organic matter is clearly reflected on zeta potential values (Table VI.1). Very interestingly, in synthetic water the presence of divalent electrolytes only results in lower value of zeta potential, whereas in lake water zeta potentials are more negative because of the presence of natural organic matter. Therefore, this comparative study between synthetic and natural waters highlighted the key role of divalent electrolytes in the heteroaggregation of NPs in lake water.

VI.4.4 Effect of alginate concentration on heteroaggregation in lake water

To gain an insight into the effect of alginate concentration we studied the heteroaggregation between CeO_2 NPs and Fe_2O_3 in lake water by increasing the concentration of alginate from 0.25 to 2 mg/L (Fig.VI.7). Without alginate and in the presence of 0.25 mg/L alginate, z-average diameters are found close to 2500 nm (after 15 min heteroaggregation). The presence of 2 mg/L alginate is found to significantly reduce the size of the aggregates equal to 608 ± 45 nm (after 15 min) (Fig.VI.7). The aggregation rate is also significantly reduced and is found equal to 125 ± 41 and 15 ± 2 nm/min (Fig.A4.6) in the presence of 0.25 and 2 mg/L alginate, accordingly, in good agreement with stabilisation effects related to electrostatic and steric effects (Baalousha 2009;

Oriekhova et Stoll 2016). Our findings are also supported with SEM images (Fig.VI.8). In Fig.VI.8A and B large heteroaggregates of CeO_2 and Fe_2O_3 are found and no significant difference is observed at low alginate concentrations. Whereas in Fig.VI.8C heteroaggregates are much smaller and it is possible to distinguish the presence of Fe_2O_3 connected by alginate and "individual" alginate chains on the surface of silica wafer. Therefore, in our work we showed that high alginate concentration prevent the heteroaggregation of mixtures of CeO_2 NPs and Fe_2O_3 ICs in lake water. It should be noted that the same trend was observed in synthetic water (Fig.A4.7) where the increase of alginate concentration was found to decrease the aggregation rate but less significantly compared to lake water.

The global attachment efficiency (α_{global}) which is a mixture of the attachment efficiencies of homo- and heteroaggregations (Labille et al. 2015) is given in Fig.VI.9. This figure is presenting the attachment efficiencies calculated from experimental data of pristine CeO_2 NPs and Fe_2O_3 ICs as well as their mixtures in synthetic and lake waters as a function of alginate concentration. The presence of alginate decreases the global attachment efficiency of heteroaggregates. We also observe that the attachment efficiency between pristine CeO_2 NPs is lower than between Fe_2O_3 ICs. We also shown that in mixture without alginate and at low alginate concentration the attachment efficiency is larger than 1 indicating faster formation of heteroaggregates compared to pristine CeO_2 NPs at high ionic strength (CCC), i.e. during the diffusion limited aggregation (Metreveli, Philippe, et Schaumann 2015). We believe it is because the aggregation rate of CeO_2 NPs was used as a reference for all samples.

VI.5 Conclusions

Our findings demonstrate that heteroaggregation between CeO_2 NPs and Fe_2O_3 ICs is highly dependent on environmental conditions. In ultrapure water no heteroaggregation between NPs and ICs is observed because of the presence of electrostatic repulsions. Whereas, in natural lake and synthetic waters, in the presence of multivalent ions (such as Ca^{2+} and Mg^{2+}), CeO_2 heteroaggregation is observed due to the modification of NP surface chemistry. The concentration of alginate (NOM) plays a crucial role in controlling heteroaggregation in natural waters. Without alginate and in low alginate concentration (below 0.25 mg/L) important heteroaggregation is observed, however, high alginate concentration (2 mg/L and above) prevents heteroaggregation.

VI.6 Figures

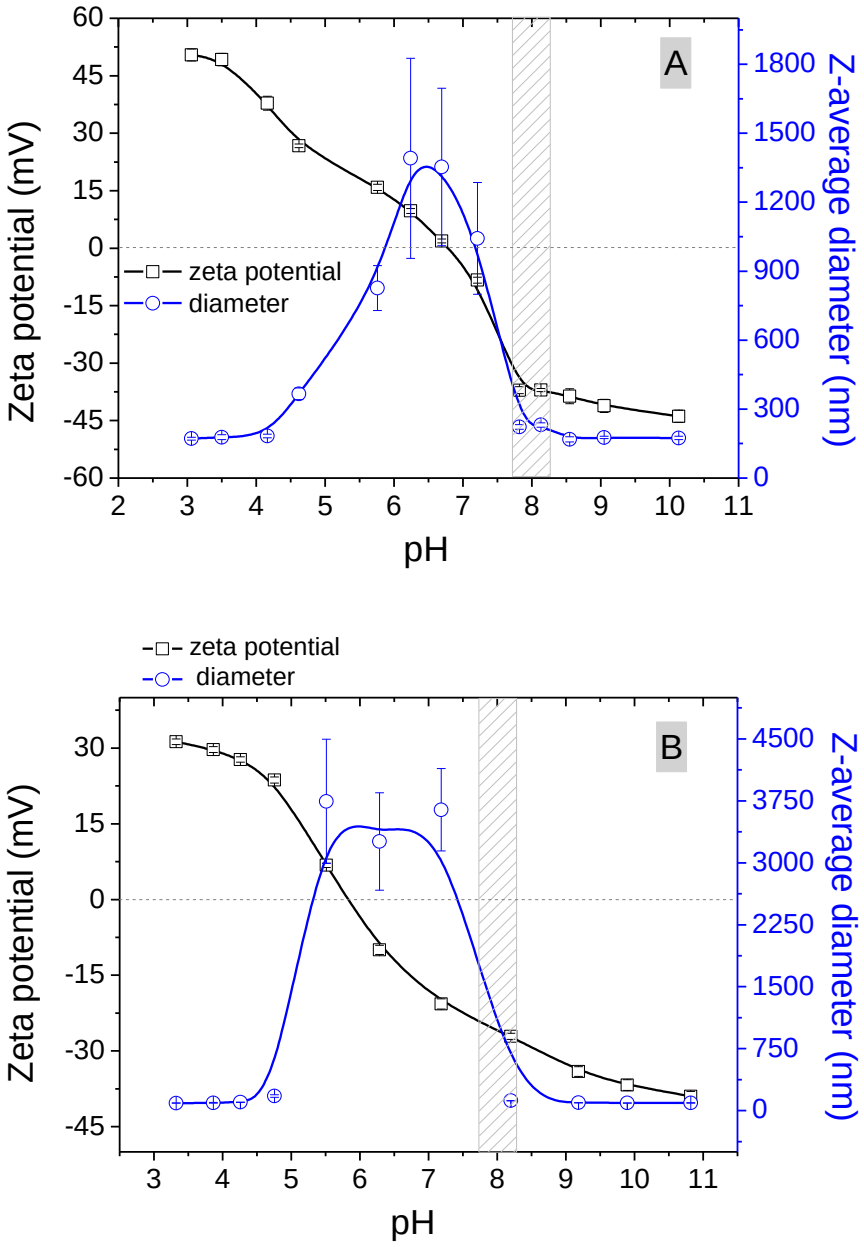

Fig.VI.1. (A) CeO_2 NP and (B) Fe_2O_3 IC zeta potential and z-average hydrodynamic diameter variation as a function of pH. Experimental conditions: [CeO_2] = 50 mg/L, [Fe_2O_3] = 10 mg/L. At environmental pH = 8.0 ± 0.2 both NPs and ICs are negatively charged.

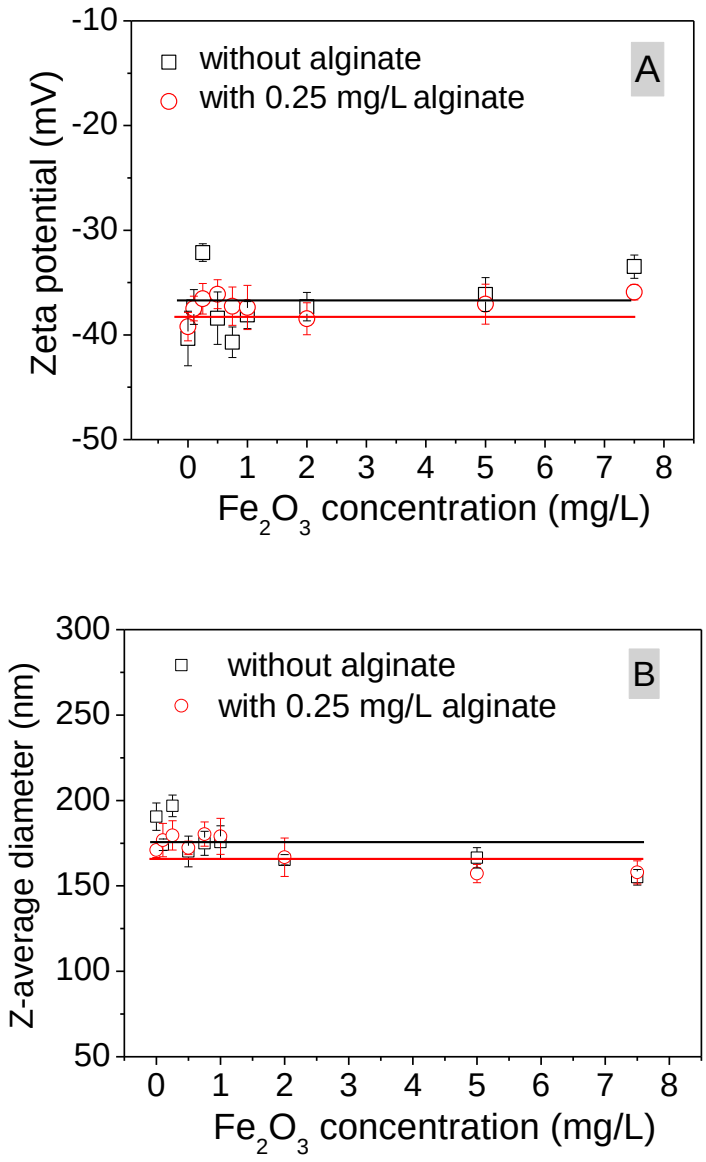

Fig.VI.2. (A) Zeta potential and (B) z-average hydrodynamic diameters of CeO_2 NPs in ultrapure water at different concentrations of inorganic colloids (Fe_2O_3) in presence and absence of alginate. Experimental conditions: pH 8.0 ± 0.2, [CeO_2] = 50 mg/L, [Alginate] = 0.25 mg/L. No heteroaggregation between NPs, ICs and alginate is observed.

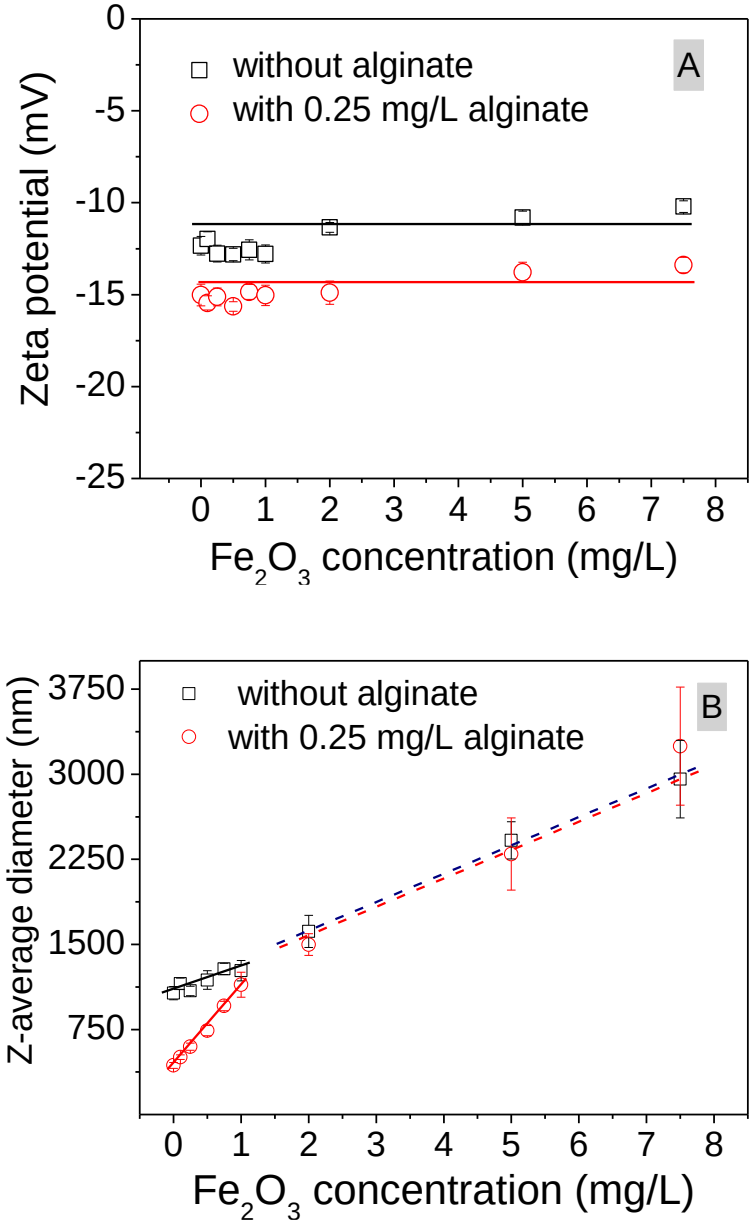

Fig.VI.3. (A) Zeta potential and (B) z-average hydrodynamic diameters of CeO_2 NPs in lake water in increasing concentration of inorganic colloids (Fe_2O_3) in presence and absence of alginate. Experimental conditions: pH 8.0 ± 0.2, [CeO_2] = 50 mg/L, [Alginate] = 0.25 mg/L. The heteroaggregation is observed with increase of IC concentration in absence and presence of alginate.

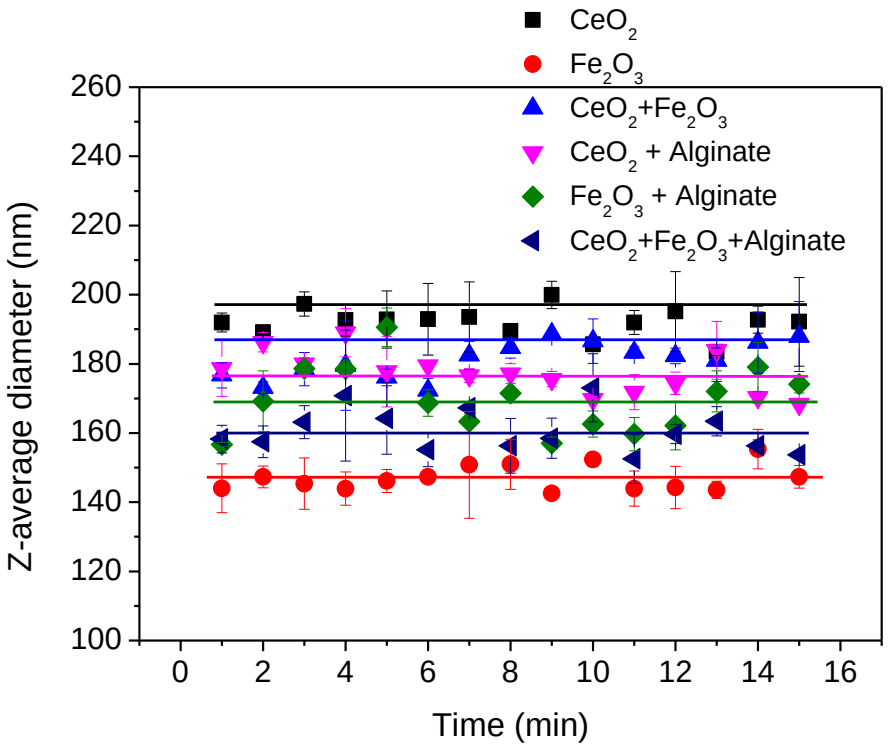

Fig.VI.4. Z-average hydrodynamic diameters of CeO_2 NPs in varied conditions: in the presence of inorganic colloids and alginate at pH > pH_{PZC} in ultrapure water. No interactions between CeO_2 NPs, Fe_2O_3 IC and alginate is observed. Experimental conditions: pH 8.0 ± 0.2, [CeO_2] = 50 mg/L [Fe_2O_3] = 5 mg/L, [Alginate] = 0.25 mg/L.

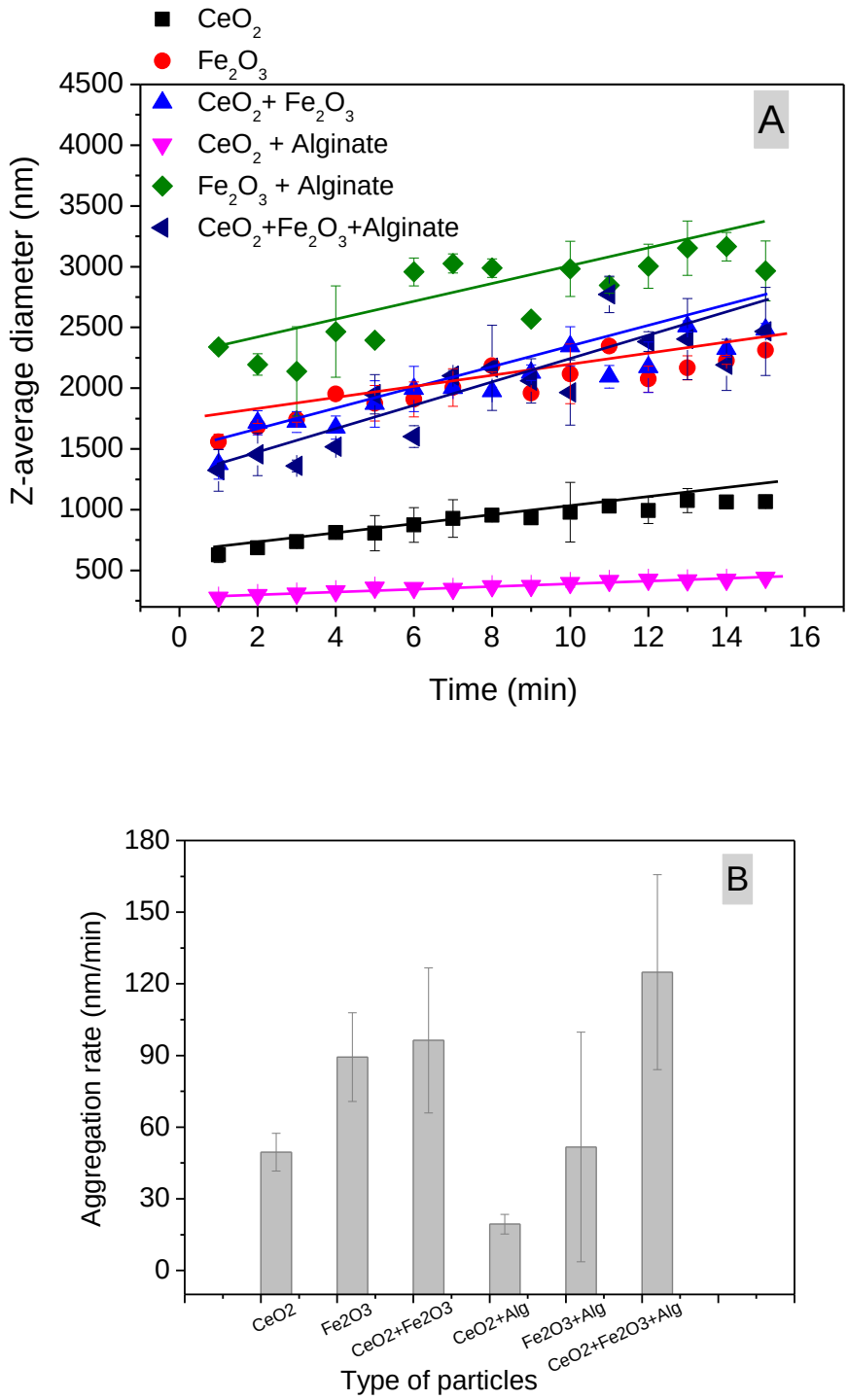

Fig.VI.5. (A) Z-average hydrodynamic diameters and (B) aggregation rate of CeO_2 NPs in Lake Geneva water: in the presence of Fe_2O_3 ICs and alginate. Experimental conditions: pH 8.0 ± 0.2, [CeO_2] = 50 mg/L [Fe_2O_3] = 5 mg/L, [Alginate] = 0.25 mg/L.

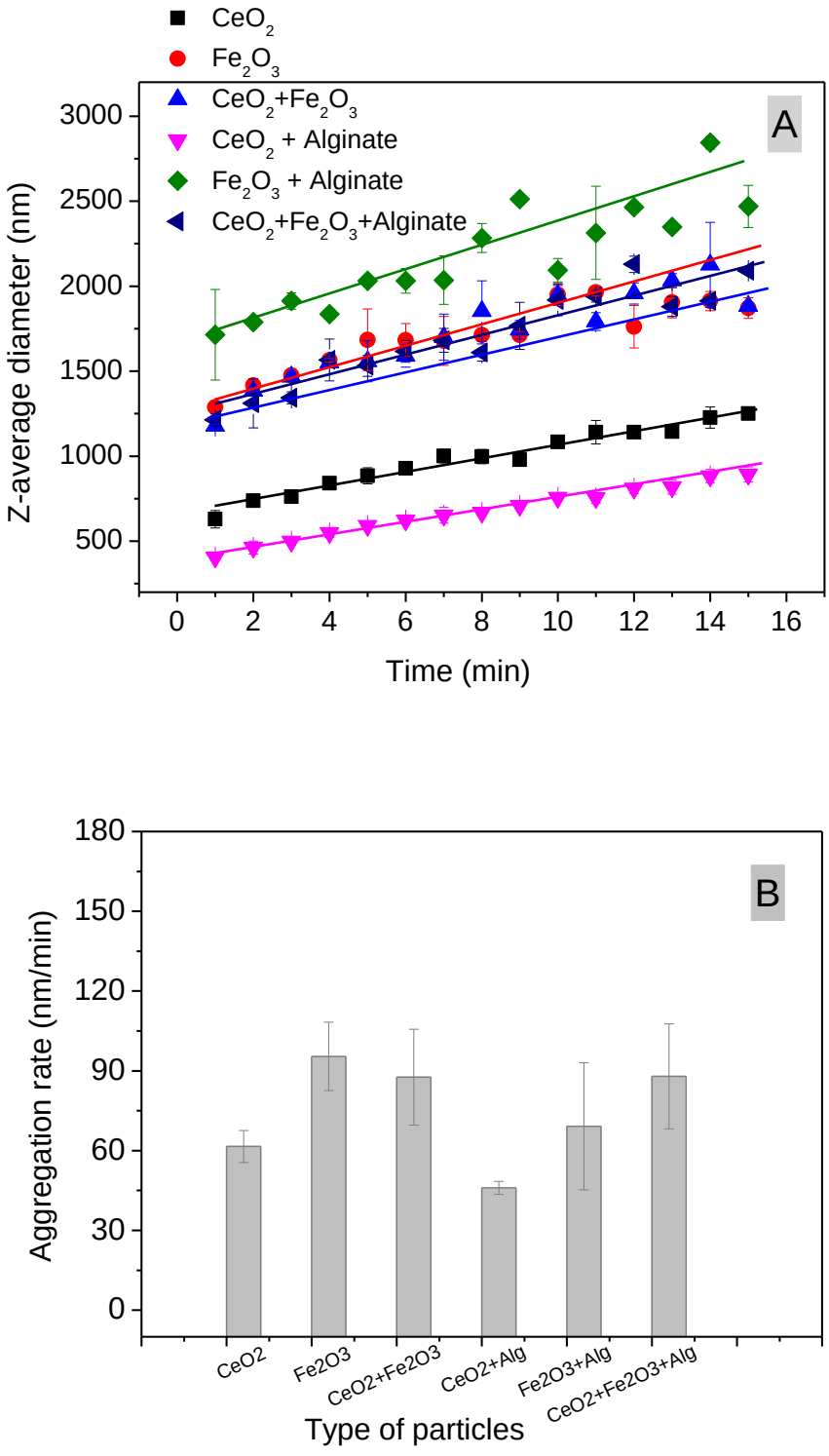

Fig.VI.6. (A) Z-average hydrodynamic diameters and (B) aggregation rate of CeO_2 NPs in synthetic water (in the presence of Ca^{2+}/Mg^{2+} ions) and in the simultaneous presence of Fe_2O_3 ICs and alginate. Experimental conditions: pH 8.0 ± 0.2, [CeO_2] = 50 mg/L [Fe_2O_3] = 5 mg/L, [Alginate] = 0.25 mg/L.

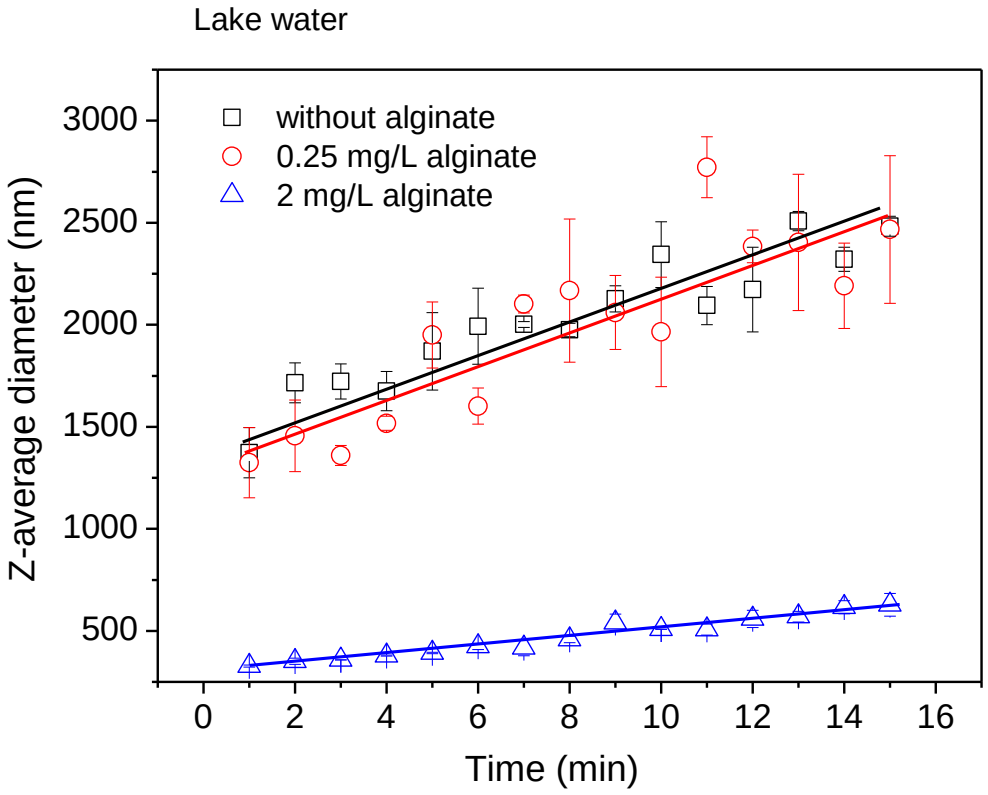

Fig.VI.7. Time variation of z-average hydrodynamic diameters of CeO_2 NPs and Fe_2O_3 ICs in Lake Geneva in varied alginate concentration. Experimental conditions: pH 8.0 ± 0.2, [CeO_2] = 50 mg/L [Fe_2O_3] = 5 mg/L, [Alginate] = 0.25 and 2 mg/L. The aggregation rate decreases with increase of alginate concentration.

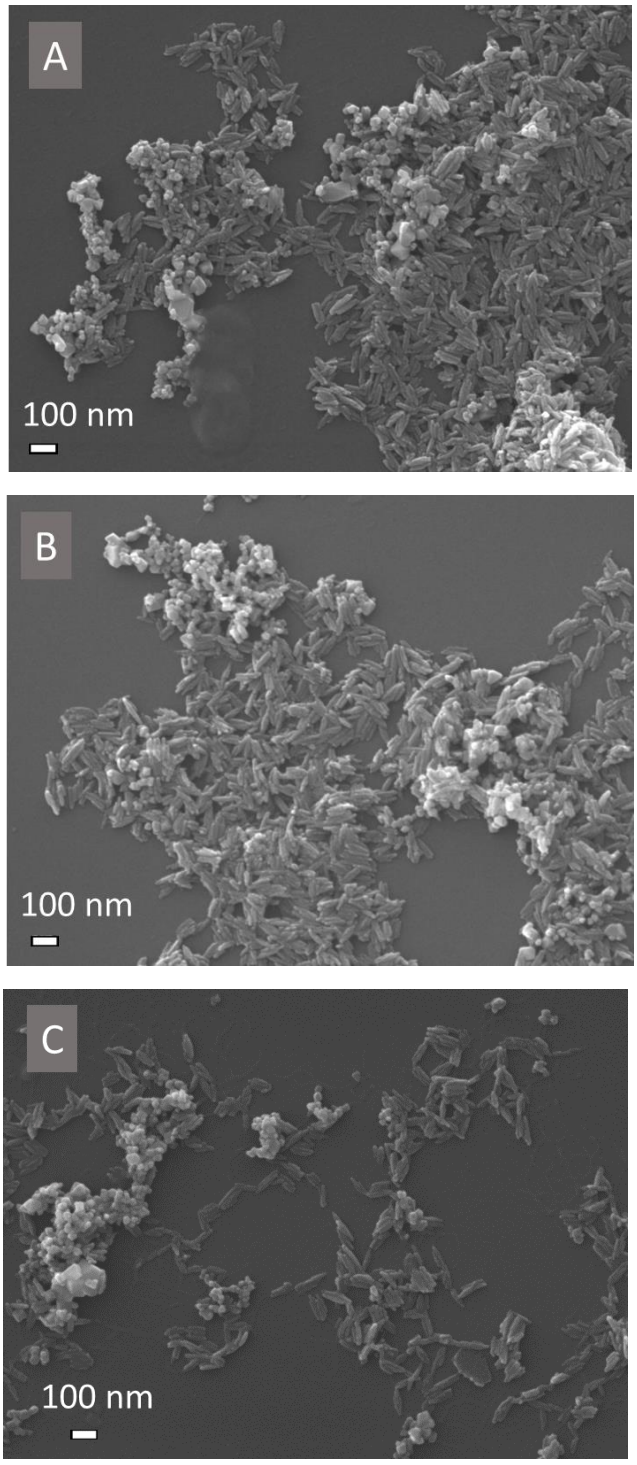

Fig.VI.8. SEM images of CeO_2 NPs and Fe_2O_3 ICs in Lake Geneva in varied alginate concentration. Experimental conditions: [CeO_2] = 10 mg/L [Fe_2O_3] = 1 mg/L (A): [Alginate] = 0 mg/L; (B) [Alginate] = 0.05 mg/L and (C) [Alginate] = 2 mg/L. With increase of alginate concentration, we observed the formation of smaller heteroaggregates corresponding to the results illustrated in Fig.VI.6.

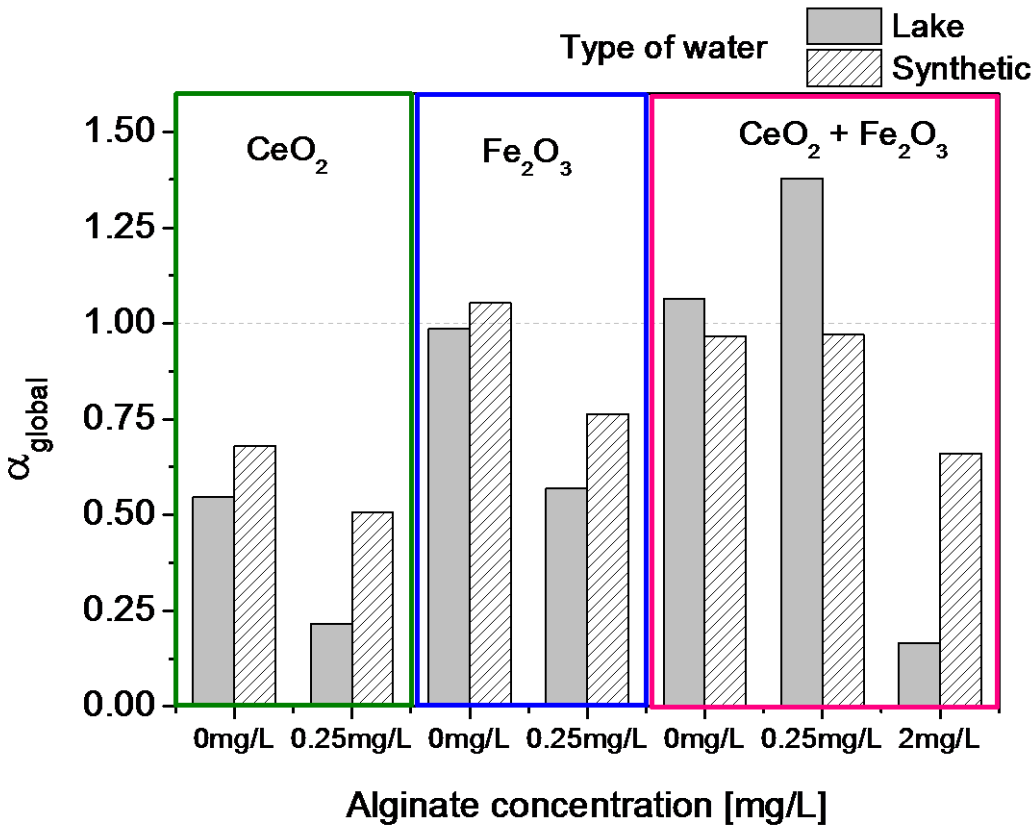

Fig.VI.9. The global attachment efficiency (α_{global}) of pristine CeO_2 NPs (green rectangle), pristine Fe_2O_3) IC (blue rectangle) and of a mixture NPs + ICs in synthetic and lake waters as a function of alginate concentration. Experimental conditions: pH 8.2 ± 0.2, [CeO_2] = 50 mg/L, [Fe_2O_3] = 5 mg/L, [Alginate] = 0; 0.25 and 2 mg/L.

VI.7 References

Baalousha, M., 2009. Aggregation and disaggregation of iron oxide nanoparticles: Influence of particle concentration, pH and natural organic matter. Sci. Total Environ. 407, 2093–2101. https://doi.org/10.1016/j.scitotenv.2008.11.022

Buffle, J., Wilkinson, K.J., Stoll, S., Filella, M., Zhang, J., 1998. A Generalized Description of Aquatic Colloidal Interactions: The Three-colloidal Component Approach. Environ. Sci. Technol. 32, 2887–2899. https://doi.org/10.1021/es980217h

Castelló, J., Gallardo, M., Busquets, M.A., Estelrich, J., 2015. Chitosan (or alginate)-coated iron oxide nanoparticles: A comparative study. Colloids Surf. Physicochem. Eng. Asp. 468, 151–158. https://doi.org/10.1016/j.colsurfa.2014.12.031

Chekli, L., Zhao, Y.X., Tijing, L.D., Phuntsho, S., Donner, E., Lombi, E., Gao, B.Y., Shon, H.K., 2015. Aggregation behaviour of engineered nanoparticles in natural waters: Characterising aggregate structure using on-line laser light scattering. J. Hazard. Mater. 284, 190–200. https://doi.org/10.1016/j.jhazmat.2014.11.003

Chen, K.L., Mylon, S.E., Elimelech, M., 2006. Aggregation kinetics of alginate-coated hematite nanoparticles in monovalent and divalent electrolytes. Environ. Sci. Technol. 40, 1516–1523.

Eyrolle, F., Charmasson, S., 2004. Importance of colloids in the transport within the dissolved phase (< 450 nm) of artificial radionuclides from the Rhône river towards the Gulf of Lions (Mediterranean Sea). J. Environ. Radioact. 72, 273–286.

Eyrolle, F., Charmasson, S., 2001. Distribution of organic carbon, selected stable elements and artificial radionuclides among dissolved, colloidal and particulate phases in the Rhône River (France): Preliminary results. J. Environ. Radioact. 55, 145–155. https://doi.org/10.1016/S0265-931X(00)00188-0

Filella, M., 2007. Colloidal properties of submicron particles in natural waters. IUPAC Ser. Anal. Phys. Chem. Environ. Syst. 10, 17.

Gallego-Urrea, J.A., Hammes, J., Cornelis, G., Hassellöv, M., 2016. Coagulation and sedimentation of gold nanoparticles and illite in model natural waters: Influence of initial particle concentration. NanoImpact 3–4, 67–74. https://doi.org/10.1016/j.impact.2016.10.004

Gondikas, A.P., Kammer, F. von der, Reed, R.B., Wagner, S., Ranville, J.F., Hofmann, T., 2014. Release of TiO2 nanoparticles from sunscreens into surface waters: a one-year survey at the old Danube recreational Lake. Environ. Sci. Technol. 48, 5415–5422.

Graham, N.D., Stoll, S., Loizeau, J.-L., 2014. Colloid characterization at the sediment-water interface of Vidy Bay, Lake Geneva. Fundam. Appl. Limnol. Für Hydrobiol. 184, 87–100.

Labille, J., Harns, C., Bottero, J.-Y., Brant, J., 2015. Heteroaggregation of Titanium Dioxide Nanoparticles with Natural Clay Colloids. Environ. Sci. Technol. 49, 6608–6616. https://doi.org/10.1021/acs.est.5b00357

Liu, J., Legros, S., Von der Kammer, F., Hofmann, T., 2013. Natural organic matter concentration and hydrochemistry influence aggregation kinetics of functionalized engineered nanoparticles. Environ. Sci. Technol. 47, 4113–4120.

Loosli, F., Coustumer, P.L., Stoll, S., 2013. TiO2 nanoparticles aggregation and disaggregation in presence of alginate and Suwannee River humic acids. pH and concentration effects on nanoparticle stability. Water Res. 47, 6052–6063.

Loosli, F., Le Coustumer, P., Stoll, S., 2015. Effect of electrolyte valency, alginate concentration and pH on engineered TiO2 nanoparticle stability in aqueous

solution. Sci. Total Environ., Special Issue: Engineered nanoparticles in soils and waters 535, 28–34. https://doi.org/10.1016/j.scitotenv.2015.02.037

Louie, S.M., Tilton, R.D., Lowry, G.V., 2013. Effects of Molecular Weight Distribution and Chemical Properties of Natural Organic Matter on Gold Nanoparticle Aggregation. Environ. Sci. Technol. 47, 4245–4254. https://doi.org/10.1021/es400137x

Metreveli, G., Philippe, A., Schaumann, G.E., 2015. Disaggregation of silver nanoparticle homoaggregates in a river water matrix. Sci. Total Environ., Special Issue: Engineered nanoparticles in soils and waters 535, 35–44. https://doi.org/10.1016/j.scitotenv.2014.11.058

Oriekhova, O., Le Coustumer, P., Stoll, S., 2017. Impact of biopolymer coating on the colloidal stability of manufactured CeO2 nanoparticles in contrasting water conditions. Colloids Surf. Physicochem. Eng. Asp. 533, 267–274. https://doi.org/10.1016/j.colsurfa.2017.07.069

Oriekhova, O., Stoll, S., 2016. Stability of uncoated and fulvic acids coated manufactured CeO2 nanoparticles in various conditions: From ultrapure to natural Lake Geneva waters. Sci. Total Environ. 562, 327–334. https://doi.org/10.1016/j.scitotenv.2016.03.184

Pawar, S.N., Edgar, K.J., 2012. Alginate derivatization: A review of chemistry, properties and applications. Biomaterials 33, 3279–3305. https://doi.org/10.1016/j.biomaterials.2012.01.007

Piccinno, F., Gottschalk, F., Seeger, S., Nowack, B., 2012. Industrial production quantities and uses of ten engineered nanomaterials in Europe and the world. J. Nanoparticle Res. 14, 1–11. https://doi.org/10.1007/s11051-012-1109-9

Praetorius, A., Labille, J., Scheringer, M., Thill, A., Hungerbühler, K., Bottero, J.-Y., 2014. Heteroaggregation of Titanium Dioxide Nanoparticles with Model Natural Colloids under Environmentally Relevant Conditions. Environ. Sci. Technol. 48, 10690–10698. https://doi.org/10.1021/es501655v

Quik, J.T.K., Stuart, M.C., Wouterse, M., Peijnenburg, W., Hendriks, A.J., van de Meent, D., 2012. Natural colloids are the dominant factor in the sedimentation of nanoparticles. Environ. Toxicol. Chem. 31, 1019–1022. https://doi.org/10.1002/etc.1783

Rice, J., 2006. Mathematical statistics and data analysis. Nelson Education.

Singh, C., Friedrichs, S., Ceccone, G., Gibson, N., Jensen, K.A., Levin, M., Infante, H.G., Carlander, D., Rasmussen, K., 2014. Cerium Dioxide, NM-211, NM-212, NM-213. Characterisation and test item preparation. European Commission, Joint Research Centre, European Union. https://doi.org/10.2788/80203

Slomberg, D.L., Ollivier, P., Radakovitch, O., Baran, N., Sani-Kast, N., Miche, H., Borschneck, D., Grauby, O., Bruchet, A., Scheringer, M., Labille, J., 2016. Characterisation of suspended particulate matter in the Rhone River: insights into analogue selection. Environ. Chem.

Wang, H., Adeleye, A.S., Huang, Y., Li, F., Keller, A.A., 2015. Heteroaggregation of nanoparticles with biocolloids and geocolloids. Adv. Colloid Interface Sci., Colloid and Polymer Interfaces in Bio-resources and Environments 226, Part A, 24–36. https://doi.org/10.1016/j.cis.2015.07.002

Chapter VII

$FeCl_3$ induced coagulation of polystyrene microspheres. Heteroaggregation of polystyrene nanoplastics

Published as

- Oriekhova, O., and Stoll, S., 2014, Investigation of $FeCl_3$ induced coagulation processes using electrophoretic measurement, nanoparticle tracking analysis and dynamic light scattering: Importance of pH and colloid surface charge, Colloids and Surfaces. A, Physicochemical and Engineering Aspects, v. 461, pp. 212-219 (Paper IV).
- Oriekhova, O., and Stoll, S., 2018, Heteroaggregation of nanoplastic particles in presence of inorganic colloids and natural organic matter, Environmental Science: Nano, v. 5, pp. 792-799(Paper V).

VII.1 Introduction

There is a growing concern about micro- and nanoplastic pollution, plastics fragments with sizes smaller than 5 mm and 5µm, accordingly, in fresh and marine water (Faure et al., 2015; Hohenblum Philipp et al., 2015; Ryan et al., 2009). In particular, micro- and nanoplastics represent a significant environmental concern since they are more easily ingested by the organisms and accumulated throughout the food chain (Wagner et al., 2014; Wright et al., 2013). Moreover, micro- and nanoplastics are not easy to detect and it poses a growing concern because of the possible release of toxic chemical additives or adsorption, accumulation and transportation of pollutants (Lee et al., 2014; Teuten et al., 2009). Polystyrene latex particles with size in the micro- and nanometre range are used as a model particle to investigate colloidal stability and behaviour of micro-/nanoparticles in complex matrix. In particular, we concentrated on two major aspects such as importance of microplastic removal and elimination in water treatment plants and importance of heteroaggregation in the transport and fate of nanoplastics in aquatic systems.

In this chapter we used two types of plastic particles. In the first study we investigated the behaviour of negatively charged micron sized polystyrene latex particles, whereas in the second study we used nanosized positively charged polystyrene latex particles. Polystyrene (PS) has been chosen since its demand in Europe, including expanded polystyrene, reaches the level of $3.4 \cdot 10^6$ tonnes per year and these polymers are used in a multiple of industrial applications (*Plastics-the Facts 2016. An analysis of European plastics production, demand and waste data*, 2016). In addition, PS plastics are difficult to recycle and are highly resistant to biodegradation (Chaukura et al., 2016; Kaplan et al., 1979).

More specifically in the first study, we investigated the destabilisation of negatively charged PS microplastics during coagulation processes with iron(III) chloride, which was used as coagulant. The aggregation kinetics of PS particles was monitored by dynamic light scattering (DLS) and electrophoretic measurements with a Malvern Zetasizer instrument at different coagulant dosages. Nanoparticle tracking analysis (NTA) was also used to obtain size distribution of pristine and coagulated particles. To obtain iron speciation at different pH, MINTEQA2 software was used. To understand and better control the coagulation processes we investigated the modification of the plastic surface

charge at different initial pH and at various dosage of $FeCl_3$. Obtained results were used to get an insight into coagulation mechanisms.

In the second study, we systematically studied the effect of natural organic matter (NOM) and inorganic colloids (IC) on the heteroaggregation of polystyrene latex nanoplastic particles. These particles were chosen as they are expected to provide, due to their positive charge, favourable conditions for interaction with negatively charged aquatic colloids. Additionally, positively charged polymeric particles were found more toxic to the living organisms (*Daphnia magna,* mice and algal species) compared to negatively charged particles (Bhattacharya et al., 2010; Harush-Frenkel et al., 2010; Nasser and Lynch, 2016). First, we characterised nanoplastics, then we investigated the effect of water components on heteroaggregation of particles and, finally, we studied the behaviour of nanoplastics when mixed with natural water from river Rhône. At the end a mechanistic interpretation of interaction processes between plastic particles and water compounds was provided.

VII.2 Main results

Characterisation of 10 mg/L PS microplastic and 50 mg/L PS nanoplastic suspensions was done in a pH range from 2 to 10. We found that microplastic particle zeta potential is negative through all pH range and vary from –10 to –70 mV. Due to the electrostatic repulsive forces, suspensions were stable with z-average diameter equal to 1030 ± 106 nm. Nanoplastic particles were positively charged at all pHs due to the presence of amidine functional groups with zeta potential changing from +48 at pH 3 to +33 mV at pH 10 and are stable with a mean z-average diameter equal to 53.1 ± 4.3 nm.

Microplastics

The behaviour of microplastic particles in an increasing concentration of coagulant, from 0.25 to 15 mg/L, was investigated at initial pH 5.5 as a function of time. We found that zeta potential did not stabilise immediately but after approximately 60 min depending on the $FeCl_3$ concentration. We also found a pH decrease with increase of coagulant dosage. The charge neutralisation occurred when the $FeCl_3$ concentration was between 1 and 2 mg/L (Fig. VII.1) which corresponds to the isoelectric point (IEP) and optimal coagulant dosage. With increase of $FeCl_3$ concentration zeta potential changed from negative (–50 mV) to positive (+40 mV) values and pH decreased from 5.5 to 3.6. Therefore, we observed three domains: below the IEP, charge neutralisation at the IEP and charge

inversion above the IEP. Such microplastic behaviour was also confirmed by the measurements of z-average hydrodynamic diameter (Fig. VII.2). Below the IEP in the presence of low concentration of coagulant (0.25 and 0.5 mg/L) no significant change in size was observed (i area). At charge neutralisation (1 and 2 mg/L $FeCl_3$), particle aggregation was observed and z-average hydrodynamic diameter was found to rapidly increase up to 2400 nm after 125 min (ii area). In the charge inversion domain (5 to 15 mg/L $FeCl_3$), z-average values of hydrodynamic diameter were found surprisingly smaller than expected and close to 300 nm (iii area).

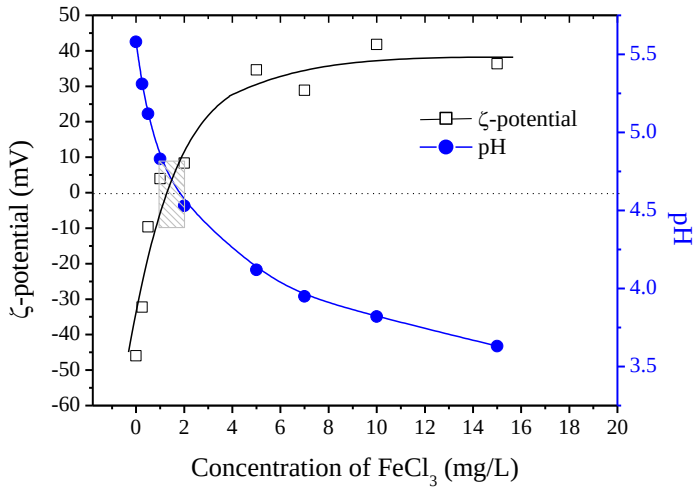

Fig. VII.1. Zeta potential and pH variation of the microplastic PS suspension as a function of coagulant concentration after stabilisation (initial pH was 5.5).

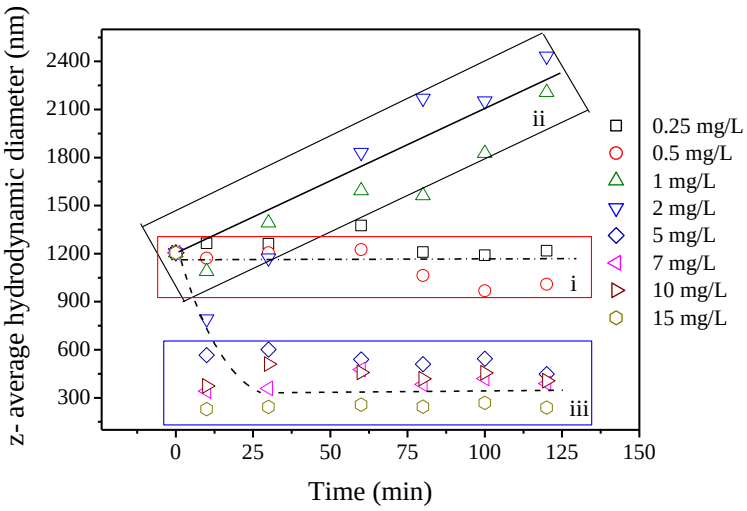

Fig. VII.2. Z-average hydrodynamic diameter variation of PS particles depending on coagulant dosage.

We attributed such a decrease in hydrodynamic diameter to the formation of iron hydroxide which was partially precipitated and dispersed in suspension independently of further pH changes. Speciation modelling as well as literature data (Larue et al., 2003; Stefánsson, 2007) confirms that in a pH range from 6 to 10, 60% of Fe(III) species in solution are considered to form insoluble iron hydroxide $Fe(OH)_3$ particles. The size distribution measured by the NTA method showed, in good agreement with DLS measurements, the presence of two independent particles with hydrodynamic diameters equal to 190 and 1000 nm (Fig. VII.3), which corresponds to the newly formed precipitated hydroxides and PS particles respectively.

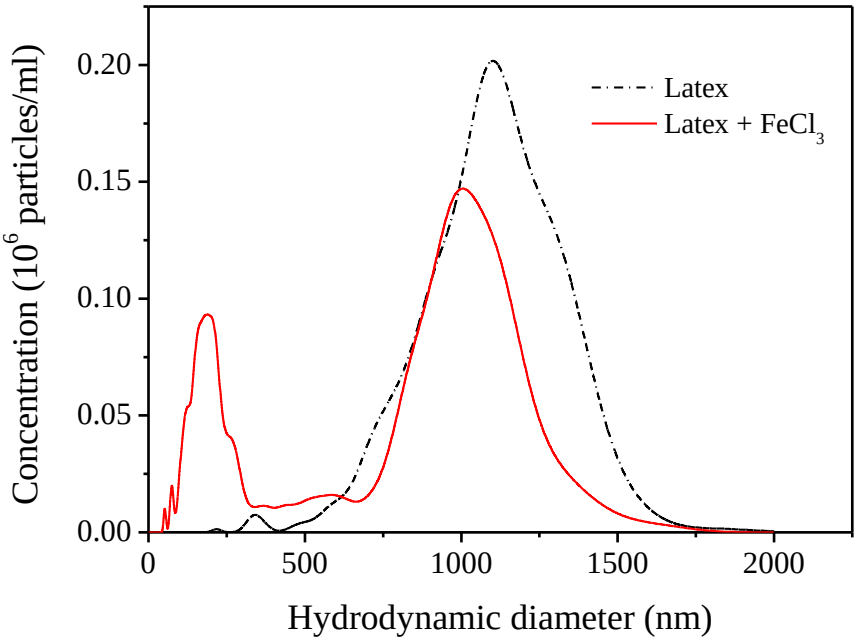

Fig. VII.3. Particle size distributions in the PS latex suspension with an excess of iron(III) chloride at pH 7 using NTA method.

Nanoplastics

Heteroaggregation experiments between PS nanoplastics and Fe_2O_3 and then between PS and mixtures of Fe_2O_3 and alginate were performed. The variation of z-average diameters with time was measured and the average value of the last 3 min measurements as well as zeta potential values were plotted in Fig. VII.4A. The zeta potential was found to change from negative to positive with the increase of nanoplastic concentration passing through the IEP at 3 mg/L for a concentration ratio PS/Fe_2O_3 equal to 3/5. Z-average diameter increased with the increase of PS concentration until it reached maximum of 1056.9 ±

46.2 nm at the IEP and then decreased with further increase of PS concentration. Such a decrease indicated that the light scattering signal was mainly due to the PS nanoplastics in suspension.

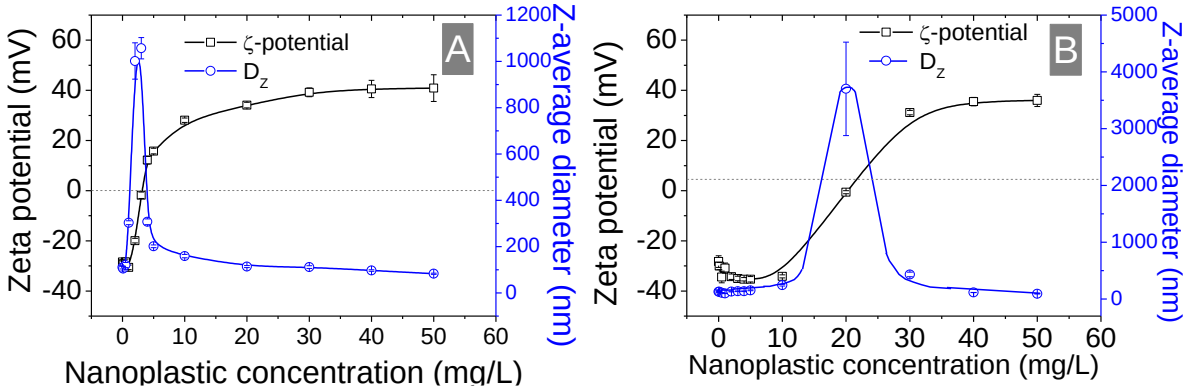

Fig. VII.4. Zeta potential and z-average diameter of a mixture of PS nanoplastics and Fe_2O_3 versus nanoplastic concentration (A) without alginate. Maximum heteroaggregation is achieved at 3 mg/L nanoplastics. (B) In the presence of alginate. Maximum heteroaggregation is achieved at 20 mg/L nanoplastics. [Fe_2O_3] = 5 mg/L, [Alginate] = 2 mg/L, pH = 8.0 ± 0.2, ultrapure water.

To investigate the effect of NOM on heteroaggregation between PS and Fe_2O_3 we used alginate. A shift of the IEP was observed in the presence of alginate. At low PS concentration, until 10 mg/L, a negative zeta potential was obtained (–33.1 ± 2.6 mV) (Fig. VII.4B). Then the IEP was achieved at 20 mg/L, indicating that more positively charged nanoplastics are needed to neutralise negative charges of both alginate and Fe_2O_3. The increase of nanoplastic concentration resulted to the charge inversion due to the excess of PS.

To investigate the effect of naturally present organic and inorganic colloids on the heteroaggregation of PS nanoplastics we used filtered water from river Rhône. When nanoplastics were mixed with Rhône water at low concentration (below 4 mg/L) we observed limited charge inversion and limited aggregation of nanoplastic particles due to the presence of dissolved electrolytes and natural organic matter (Fig. VII.5). Increase of nanoplastic concentration lead to the charge inversion and to the decrease of aggregate sizes due to the concentration effects. Maximum heteroaggregation was reached when the IEP was achieved at 5 mg/L nanoplastic concentration.

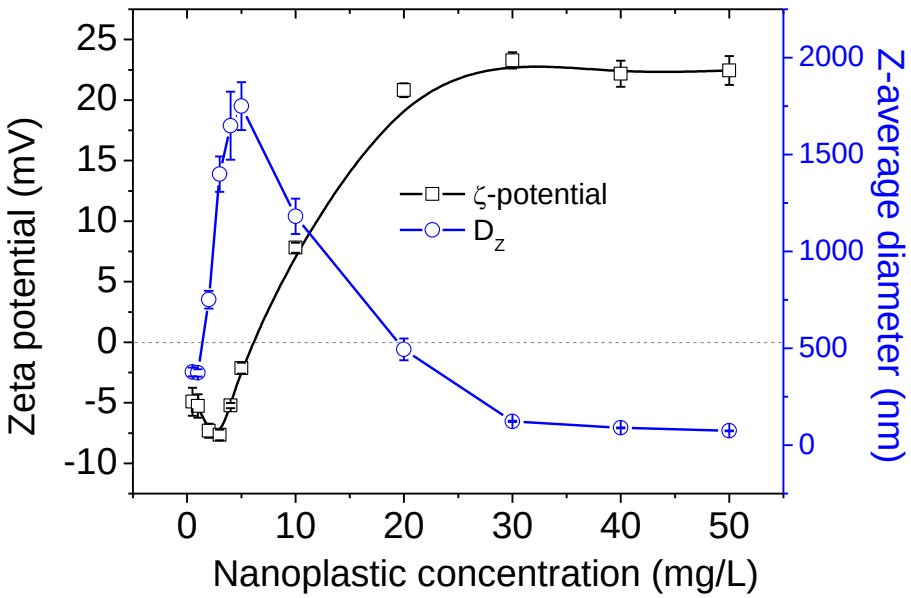

Fig. VII.5. Zeta potential and z-average hydrodynamic diameter of PS nanoplastics mixed with Rhône water versus nanoplastic concentration. pH = 8.0 ± 0.2, Rhône water filtered through 0.45 µm. The maximum heteroaggregation is achieved at 5 mg/L nanoplastics.

In the study dealing with microplastics, we demonstrated that to define the optimal coagulant dosage and to control coagulation processes the measurement of zeta potential can be used. It was shown also that the changes of PS microplastic properties, in particular the changes of surface charge, did not occur immediately, varied with time and coagulant dosage. The excess of coagulant resulted in charge inversion, which is not desirable situation, and the formation of additional nanosized iron hydroxide. The optimal condition for the microplastics destabilisation and coagulation is achieved when the dosage of coagulant was enough to neutralise the particle surface charge.

In the second study dealing with nanoplastics, we showed that heteroaggregation was induced by the presence of both Fe_2O_3 and alginate at environmental pH. It was found that the concentration ratio between Fe_2O_3, alginate and nanoplastics is an important parameter controlling the heteroaggregation rate. We have shown that the presence of alginate shifts the maximum heteroaggregation and modifies the heteroaggregation mechanism. We also showed that the aggregation rate of nanoplastics in natural water depends on nanoplastic concentration and charge neutralisation processes. We showed that the nanoplastic surface properties and variability of environmental conditions will strongly control the fate and transport of nanoplastics in natural water.

VII.3 References

Bhattacharya, P., Lin, S., Turner, J.P., Ke, P.C., 2010. Physical Adsorption of Charged Plastic Nanoparticles Affects Algal Photosynthesis. J. Phys. Chem. C 114, 16556–16561. https://doi.org/10.1021/jp1054759

Chaukura, N., Gwenzi, W., Bunhu, T., Ruziwa, D.T., Pumure, I., 2016. Potential uses and value-added products derived from waste polystyrene in developing countries: A review. Resour. Conserv. Recycl. 107, 157–165. https://doi.org/10.1016/j.resconrec.2015.10.031

Cheng, W.P., Chi, F.H., Li, C.C., Yu, R.F., 2008. A study on the removal of organic substances from low-turbidity and low-alkalinity water with metal-polysilicate coagulants. Colloids Surf. Physicochem. Eng. Asp. 312, 238–244.

Faure, F., Demars, C., Wieser, O., Kunz, M., De Alencastro, L.F., 2015. Plastic pollution in Swiss surface waters: nature and concentrations, interaction with pollutants. Environ. Chem. 12, 582–591.

Gregory, J., 2005. Particles in water: properties and processes. CRC Press.

Harush-Frenkel, O., Bivas-Benita, M., Nassar, T., Springer, C., Sherman, Y., Avital, A., Altschuler, Y., Borlak, J., Benita, S., 2010. A safety and tolerability study of differently-charged nanoparticles for local pulmonary drug delivery. Toxicol. Appl. Pharmacol. 246, 83–90. https://doi.org/10.1016/j.taap.2010.04.011

Hohenblum Philipp, Liebmann Bettina, Liedermann Marcel, 2015. Plastic and Microplastic in the Environment (No. Band 0551). Wien.

Kaplan, D.L., Hartenstein, R., Sutter, J., 1979. Biodegradation of polystyrene, poly (metnyl methacrylate), and phenol formaldehyde. Appl. Environ. Microbiol. 38, 551–553.

Larue, O., Vorobiev, E., Vu, C., Durand, B., 2003. Electrocoagulation and coagulation by iron of latex particles in aqueous suspensions. Sep. Purif. Technol. 31, 177–192.

Lee, H., Shim, W.J., Kwon, J.-H., 2014. Sorption capacity of plastic debris for hydrophobic organic chemicals. Sci. Total Environ. 470–471, 1545–1552. https://doi.org/10.1016/j.scitotenv.2013.08.023

Li, T., Zhu, Z., Wang, D., Yao, C., Tang, H., 2006. Characterization of floc size, strength and structure under various coagulation mechanisms. Powder Technol. 168, 104–110. https://doi.org/10.1016/j.powtec.2006.07.003

Lin, J.-L., Pan, J.R., Huang, C., 2013. Enhanced particle destabilization and aggregation by flash-mixing coagulation for drinking water treatment. Sep. Purif. Technol.

Morfesis, A., Jacobson, A.M., Frollini, R., Helgeson, M., Billica, J., Gertig, K.R., 2009. Role of zeta (ζ) potential in the optimization of water treatment facility operations. Ind. Eng. Chem. Res. 48, 2305–2308.

Nasser, F., Lynch, I., 2016. Secreted protein eco-corona mediates uptake and impacts of polystyrene nanoparticles on Daphnia magna. J. Proteomics, Environment and (Prote)-OMICS 137, 45–51. https://doi.org/10.1016/j.jprot.2015.09.005

Palomino, D., Hunkeler, D., Stoll, S., 2011. Comparison of two cationic polymeric flocculant architectures on the destabilization of negatively charged latex suspensions. Polymer 52, 1019–1026. https://doi.org/10.1016/j.polymer.2010.12.033

Plastics-the Facts 2016. An analysis of European plastics production, demand and waste data, 2016. . Plastics Europe.

Ryan, P.G., Moore, C.J., van Franeker, J.A., Moloney, C.L., 2009. Monitoring the abundance of plastic debris in the marine environment. Philos. Trans. R. Soc. Lond. B Biol. Sci. 364, 1999–2012.

Schumacher, H.C., Alves, M., Leite, C.A.P., Santos, J.P., Neto, É.T., Murakami, M.M., Galembeck, F., do Amaral, M., 2007. Cationic latex formation by ionic modification. J. Colloid Interface Sci. 305, 256–263.

Slomberg, D.L., Ollivier, P., Radakovitch, O., Baran, N., Sani-Kast, N., Miche, H., Borschneck, D., Grauby, O., Bruchet, A., Scheringer, M., Labille, J., 2016. Characterisation of suspended particulate matter in the Rhone River: insights into analogue selection. Environ. Chem. 13, 804–815. https://doi.org/10.1071/EN15065

Stefánsson, A., 2007. Iron (III) hydrolysis and solubility at 25 C. Environ. Sci. Technol. 41, 6117–6123.

Teuten, E.L., Saquing, J.M., Knappe, D.R., Barlaz, M.A., Jonsson, S., Björn, A., Rowland, S.J., Thompson, R.C., Galloway, T.S., Yamashita, R., 2009. Transport and release of chemicals from plastics to the environment and to wildlife. Philos. Trans. R. Soc. B Biol. Sci. 364, 2027–2045.

Wagner, M., Scherer, C., Alvarez-Muñoz, D., Brennholt, N., Bourrain, X., Buchinger, S., Fries, E., Grosbois, C., Klasmeier, J., Marti, T., Rodriguez-Mozaz, S., Urbatzka, R., Vethaak, A.D., Winther-Nielsen, M., Reifferscheid, G., 2014. Microplastics in freshwater ecosystems: what we know and what we need to know. Environ. Sci. Eur. 26, 12. https://doi.org/10.1186/s12302-014-0012-7

Wright, S.L., Thompson, R.C., Galloway, T.S., 2013. The physical impacts of microplastics on marine organisms: a review. Environ. Pollut. 178, 483–492.

Zou, J., Zhu, H., Wang, F., Sui, H., Fan, J., 2011. Preparation of a new inorganic–organic composite flocculant used in solid–liquid separation for waste drilling fluid. Chem. Eng. J. 171, 350–356.

Paper IV

Oriekhova, O., and Stoll, S., 2014, Investigation of $FeCl_3$ induced coagulation processes using electrophoretic measurement, nanoparticle tracking analysis and dynamic light scattering: Importance of pH and colloid surface charge, Colloids and Surfaces. A, Physicochemical and Engineering Aspects, v. 461, pp. 212-219.

Colloids and Surfaces A: Physicochem. Eng. Aspects 461 (2014) 212–219

Contents lists available at ScienceDirect

Colloids and Surfaces A: Physicochemical and Engineering Aspects

journal homepage: www.elsevier.com/locate/colsurfa

Investigation of $FeCl_3$ induced coagulation processes using electrophoretic measurement, nanoparticle tracking analysis and dynamic light scattering: Importance of pH and colloid surface charge

Olena Oriekhova [1], Serge Stoll *

University of Geneva, Earth and Environmental Science Section, F.-A. Forel Institute, Group of Environmental Physical Chemistry, 10 Route de Suisse, CH-1290 Versoix, Switzerland

HIGHLIGHTS

- Zeta potential of latex particles is a function of $FeCl_3$ coagulant concentration.
- Measurement of zeta potential allows controlling the latex coagulation and $FeCl_3$ dosage.
- Charge neutralization mechanism is responsible for particle aggregation at optimal dosage.
- At high $FeCl_3$ dosage, $Fe(OH)_3$ nanoparticles are concomitantly formed.
- $FeCl_3$ optimal dosage for coagulation is dependent on the initial pH suspension.

GRAPHICAL ABSTRACT

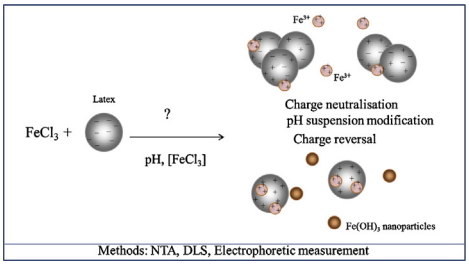

ARTICLE INFO

Article history:
Received 5 June 2014
Received in revised form 30 July 2014
Accepted 31 July 2014
Available online 9 August 2014

Keywords:
Zeta potential
Latex
Iron(III) chloride
Dynamic light scattering
Nanoparticle tracking analysis
Coagulant dosage

ABSTRACT

In water treatment processes, the optimal dosage of coagulant is highly dependent on suspended particle surface charge, size and concentration, pH and composition of water. One way to control the coagulation process can be based on the measurement of the electrophoretic mobility and determination of zeta potential.

In this study we investigated the interaction between negatively charged polystyrene latex particles and iron(III) chloride as coagulant. We combined three methods, i.e. dynamic light scattering, nanoparticle tracking analysis, and modeling to thoroughly characterize our system.

We have shown that stabilization of zeta potential occurred after 60–80 min after addition of coagulant. We demonstrated different behaviors of latex particles with $FeCl_3$ depending on the dosage of iron ions. The optimal dosage of $FeCl_3$ is equal to 1–2 mg/L for the rapid aggregation of 10 mg/L latex suspension. We found a good agreement between the aggregation rate and surface charge of the latex particles and that charge neutralization mechanism is responsible for particle aggregation. High dosage of coagulant was also found to result in formation of iron(III) hydroxide particles which diameter was about 200 nm. The initial pH is also important for latex particle coagulation. The lower initial pH of suspension is, the more rapidly the isoelectric point is achieved.

* Corresponding author. Tel.: +41 22 379 0333; fax: +41 22 379 0302.
E-mail addresses: Olena.Oriekhova@unige.ch (O. Oriekhova), Serge.Stoll@unige.ch (S. Stoll).
[1] Tel.: +41 22 379 0332.

http://dx.doi.org/10.1016/j.colsurfa.2014.07.049
0927-7757/

1. Introduction

The coagulation process is widely used in water treatment plants to remove the colloidal or suspended matter which can be both of natural and anthropogenic origin [1–7]. During this process colloidal particles form large aggregates that can be more easily and rapidly removed by flocculation or filtration. Destabilization and increase of collision efficiency between the suspended colloidal particles are achieved by adding synthetic coagulants into water [5,8]. Different types of electrolytes or polyelectrolytes are used, for example the salts of iron(III) or aluminum, and poly(dimethyl diallylammonium chloride) or polyacrylamide polymers [5,9–12]. The liquid phase needs to be rapidly separated with the highest efficiency to obtain a clear filtrate, avoid rejecting pollutants into natural aquatic systems, and maintain the maximum of pollutants in the minimum dry matter. For several reasons coagulants are not always used in a rational way for optimal coagulation condition. This optimal condition is very dependent on different factors, such as the concentration of particles, their charges and sizes, pH and solution composition which can greatly vary with time.

There are many mechanisms that can explain the coagulation process. Action of inorganic salts is based on the charge neutralization mechanism. The repulsive forces between negatively charged colloid particles disappear after the adsorption of the highly charged cations, such as Al^{3+} or Fe^{3+}, and neutralization of surface charge. The electrostatic interaction can also be screened by the cations that lead to the prevalence of attractive van der Waals forces. However, depending on the pH solution and the dosage of coagulant, hydrolysis occurs and insoluble hydroxides are formed [6,13]. It leads to the development of bigger aggregates which capture colloidal particles and then to sweep coagulation [5,14,15]. Li et al. [14] studied kaolin coagulation by aluminum sulfate (alum). They showed that the charge neutralization occurred when zeta potential of particles was close to zero and the concentration of alum was 0.1 mmol/L. The sweep coagulation took place at higher alum dose of about 1.9 mmol/L which caused precipitation of amorphous metal hydroxide. James et al. [16] studied the colloidal TiO_2-Al(III) system and demonstrated the charge reversal coagulation when zeta potential of suspension was in the range from −14 to +14 ± 4 mV at pH from 6 to 10 for different electrolyte concentrations. For larger magnitude of zeta potential the suspension was found stable. Kobayashi et al. [15] investigated the coagulation of sulfate latex beads in the presence of imogolite nano-tubes. They explained, when two mechanisms, charge neutralization and sweep coagulation are present, that coagulation is strongly charge dependent. When the surface charges of latex and imogolites have the opposite sign and the imogolites are dispersed, the coagulation happened only around the isoelectric point. When the latex particles and the imogolites have the same charge and when the imogolites are coagulated then the sweep coagulation occurred. The authors found that the efficiency of coagulation was determined by the imogolite dosage and its electrokinetic potential.

It was also found that the efficiency of coagulation process can be reduced with the increase of coagulant dosage [17] due to the reversal of particle surface charge hence resulting in a new stabilization [18–20]. Dahlsten et al. [21] studied the behavior of melamine-formaldehyde latex particles in the presence of a wide range of electrolytes (NaCl, $NaNO_3$, KNO_3, etc.). They showed that the change of zeta potential from positive (from +40 to +80 mV) to negative (about −40 mV) values was depending on the concentration of electrolytes and pH. Schumacher et al. [22] demonstrated that the anionic styrene-acrylic latex particles suspended with nonionic surfactants can stay stable in the presence of trivalent ions with high range of concentration. First the latex dispersion was stabilized with surfactant and then the iron and aluminum salt solutions were added. The particle zeta potential increased from less than −60 mV to values in excess of +40 mV in the case of Fe^{3+}. The particles did not show any aggregation behavior even at 2 mol/L counterion concentrations up to 200 days. Larue et al. [8] compared two types of coagulant dosing, chemical and electrical, as a function of pH and iron concentration to define the optimal operating conditions. They changed the concentration of iron from 10^{-3} to 6×10^{-3} mol/L and showed that the residual floc concentration decreased with the increase of iron concentration and reached a minimal value at 2×10^{-3} mol/L corresponding to optimal dosage at pH 7.5 for $FeSO_4$ and at pH 6 for $FeCl_3$ coagulant. In all cases it was found that the coagulant dosage is an important parameter that influences the coagulation process.

One of the different and possible way to control the coagulation processes is to measure the change of particle charge during the water treatment process as shown in references [23–25]. It can be done by electrophoretic measurements which allow the calculation of the zeta potentials. Zeta potential gives useful information about electrostatic interactions between particles. The electrochemical surface properties of particles control the aggregation kinetics and the interactions between particles can be described by the DLVO theory [26]. It was shown by Morfesis et al. [25] that the monitoring of zeta potential in real water treatment plants can help to maintain the optimal operating conditions. They controlled the particle stability which varied over time, and identified the maximum coagulation rate that gave a fast response to changing circumstances.

In this work we conducted electrophoretic measurements to study the behavior of negatively charged polystyrene latex particles in the presence of iron(III) chloride, which is a largely used coagulant, at different dosages. The effect of the initial pH of the suspension as well as pH changes were investigated to better understand the coagulation process and surface charge modification of latex particles in the presence of $FeCl_3$. The dynamic light scattering (DLS) method was used to determine zeta potential and z-average hydrodynamic diameter of latex particles. Employing the nanoparticle tracking analysis (NTA) we also investigated the particles distribution by size. The modeling of iron speciation was made with the MINTEQA2 software. We combined these different approaches to thoroughly characterize our system and discussed the coagulation mechanism based on detailed analysis of size distributions and electrophoretic measurements.

2. Materials and methods

2.1. Experimental methods

Zeta potential ζ and z-average hydrodynamic diameter were measured using a Malvern Zetasizer Nano ZS (Malvern Instruments Ltd, UK). Visualization and distribution of particles by size were also investigated applying nanoparticle tracking analysis (NTA) with a NanoSight LM14 instrument (NanoSight Ltd, UK).

2.1.1. DLS method

Five parallel measurements were performed for each point with time delay of 5 s. The samples temperature was 298 °K. First electrophoretic mobility U_E was measured and zeta potential was calculated using Henry equation (Eq. (1)) and Smoluchowski approximation (Eq. (2)):

$$U_E = \frac{2\varepsilon\xi}{3\eta} \cdot f(Ka), \tag{1}$$

$$U_E = \frac{\varepsilon\xi}{\eta}, \tag{2}$$

where ε corresponds to the relative permittivity ε_r (or dielectric constant) multiplied by the permittivity of free space, ε_0; η is the viscosity of the liquid; K is the Debye–Hükel

Table 1
The parameters for iron species modeling in MINTEQA2 program.

Parameter	Value
Temperature, °K	298
Concentration of $FeCl_3$, mg/L	2
pH	1–12
Ionic strength, mol/L	3.6×10^{-5} to 6.2×10^{-2} [a]

[a] pH dependent, calculated.

parameter; a is the particle radius, $f(Ka)$ equal to 3/2. We chose the Smoluchowski approximation as our system fits the parameters of Smoluchowski model [7] regarding the particle sizes and suspension ionic strength. The investigated particles have diameter equal to 0.99 μm and the concentration of electrolyte is more than 10^{-3} M of $FeCl_3$. Inserting values for permittivity and viscosity of water at 298 °K, Eq. (3) gives the relation between zeta potential and mobility:

$$\xi = 12.8U_E, \tag{3}$$

where ζ-potential is expressed in mV and electrophoretic mobility in $\mu m\, s^{-1}/V\, cm^{-1}$.

The Stokes–Einstein equation (Eq. (4)) was used to calculate hydrodynamic diameter d_H of particles from the transitional diffusion coefficient D [5,7]:

$$d_H = \frac{kT}{3\pi\eta D}, \tag{4}$$

where k is the Boltzmann's constant and T is the absolute temperature.

2.1.2. NTA method

To obtain the particle size distributions we used a NTA LM14 instrument with NTA 2.3 Analytical Software. The device analyses the particle paths under Brownian motion and determines the average distance moved by each particle in x and y direction. This value allows to obtain the diffusion coefficient and using the Stokes–Einstein equation (4) to calculate the sphere-equivalent, hydrodynamic diameter [27,28]. The results of measurements are highly dependent of the processing parameters and experimental protocol [27,29]. All measurements were repeated 3 times, i.e. 3 video were recorded for each sample. We adjusted the camera settings to visualize as many particles as possible trying to reduce the noise on the image. As our samples were polydisperse we established bigger capture time (from 90 to 160 s) to track maximum number of particles and got reliable results. The NTA LM14 instrument was adjusted and calibrated before measurement of our samples with standard polystyrene latex microspheres of 100, 200 and 400 nm. We extracted the suitable images from the video to compare different types of samples, adjusting only their brightness and contrast.

2.1.3. Modeling

To perform the modeling of iron(III) species in solution the MINTEQA2 software (developed by Allison Geoscience Consultants Inc. and HydroGeologic Inc.) was used. MINTEQA2 applies the thermodynamic and mass balance equations to solve geochemical equilibria and calculate the ion speciation/solubility. The program consists of submodels that compute the activities of cationic and anionic species and neutral ion pairs then compute the solubility of solids and minerals and in the end the mass transfer submodel calculates the mass of solid that precipitates or dissolves. [30–32].

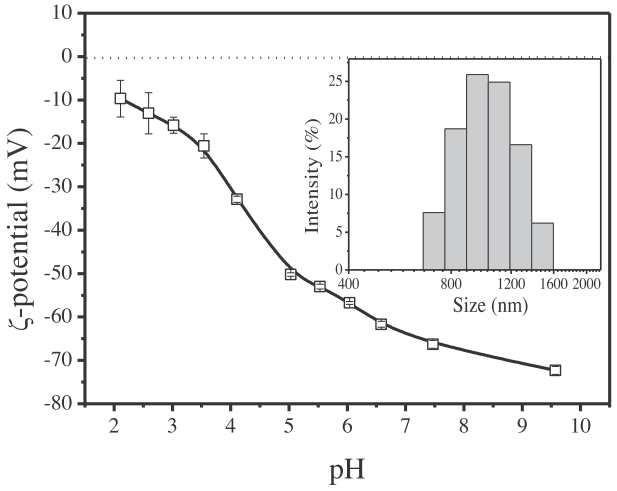

Fig. 1. Zeta potential of sulfate latex particles as a function of pH. Zeta potential is found negative in all range of adjusted pH. Size distribution (inset) of latex particles using DLS method. Z-average of hydrodynamic diameter is found equal to 1000 nm in a good agreement with TEM and NTA measurement.

To compute the activity coefficients we used the Davies equation (5), the other parameters which were used during modeling are shown in Table 1.

$$-\log f_{\pm} = 0.5 z_1 z_2 \left(\frac{\sqrt{I}}{1+\sqrt{I}} - 0.15I \right), \tag{5}$$

where $f_{\pm}$ is the mean modal activity coefficient of an electrolyte which dissociates into ions with charge z_1 and z_2; I is the ionic strength.

2.2. Materials

Latex beads (IDC Latex particles provided by Life Technologies Corporation, USA) were made of polystyrene with negatively charged sulfate functional groups on the surface. They have a diameter 0.99 μm (TEM measurement, provided by manufacturer), initial concentration 78 g/L, density at 20 °C 1.055 g/cm^3, specific surface area 5.7×10^4 cm/g and were free from surfactants.

We worked with 10 mg/L latex suspensions. A stock suspension of 1 g/L was prepared and then diluted with Milli Q water (R > 18 MΩ cm) until final concentration of 10 mg/L was achieved. pH was adjusted by adding small amount of diluted HCl and NaOH (Merck, Germany). Zeta potential of particles was found negative in all range of pH (Fig. 1). As a result, the suspension was stable due to the electrostatic repulsive forces and the z-average of hydrodynamic diameter was found also stable at about 1000 nm.

Iron(III) chloride $FeCl_3$ was used as coagulant. A stock solution of 1 g/L was prepared from iron(III) chloride hexahydrate $FeCl_3 \cdot 6H_2O$ (Merck, Germany).

After the dissolution of salt its hydrolysis occurred. Many species, such as Fe^{3+}, $Fe(OH)^{2+}$, $Fe(OH)_2{}^{+}$, $Fe(OH)_3$ and $Fe(OH)_4{}^{-}$ coexist in solution at the same time (Fig. 2). The concentration of these species depends on pH and can be described by equations of hydrolysis equilibrium (Eqs. (6)–(10)) [13,33,34]:

$$Fe^{3+} + H_2O = Fe(OH)^{2+} + H^+, \quad \log K = -2.19 \tag{6}$$

$$Fe^{3+} + 2H_2O = Fe(OH)_2{}^{+} + 2H^+, \quad \log K = -5.67 \tag{7}$$

$$Fe^{3+} + 3H_2O = Fe(OH)_3 + 3H^+, \quad \log K = -11.9 \tag{8}$$

$$Fe^{3+} + 4H_2O = Fe(OH)_4{}^{-} + 4H^+, \quad \log K = -21.6 \tag{9}$$

$$2Fe^{3+} + 2H_2O = Fe_2(OH)_2{}^{4+} + 2H^+, \quad \log K = -2.95 \tag{10}$$

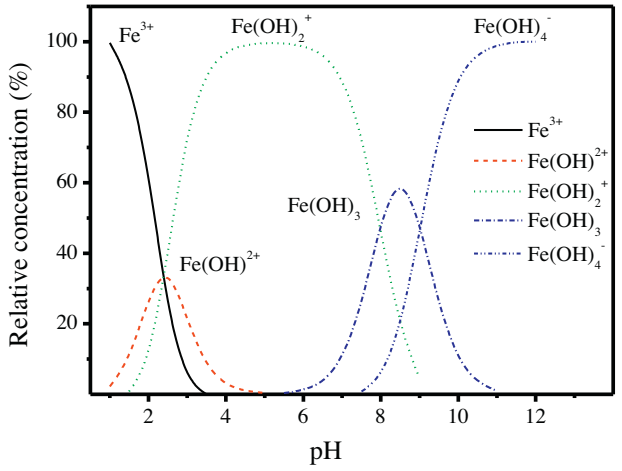

Fig. 2. Speciation of iron(III) as a function of pH for a $FeCl_3$ solution at 2 mg/L. Fe^{3+} and $Fe(OH)^{2+}$ are mainly present in solution at pH less than 3. In the pH range from 4 to 6 the highest relative concentration is obtained for $Fe(OH)_2^+$ and at pH greater than 7 $Fe(OH)_4^-$ and insoluble $Fe(OH)_3$ are present.

3. Results and discussion

The pH of initial 10 mg/L latex suspension was 5.5. It was then adjusted to 4, 7, 8 and 9, to perform the experiments at different initial pH conditions. The concentration of iron(III) chloride was then adjusted and varied for each suspension from 0.25 to 15 mg/L.

The change of latex particle zeta potential as a function of $FeCl_3$ concentration with time and with initial pH 5.5 is shown in Fig. 3. We found that addition of coagulant do not lead to immediate stabilization of the latex ζ potential. It changed from −50 to −10 mV with the presence of small amount of salt (0.25 and 0.5 mg/L), but still remained negative. The charge neutralization was found to occur when concentration of coagulant was 1–2 mg/L. The increase of $FeCl_3$ concentration from 5 to 15 mg/L was then found to result in charge inversion. Zeta potential became highly positive and stable with values comprised between +30 and +45 mV. The pH of the suspension was also found to rapidly decrease with the addition of $FeCl_3$. A pH decrease of two pH units was achieved with coagulant concentration of 15 mg/L as shown in Fig. 3b.

To get an insight into the behavior of the system after ζ potential and pH stabilization the three last values of ζ-potential and pH at 80, 100 and 120 min were considered and average values were calculated. The results are presented in Fig. 4. Continuous decrease of pH and ζ-potential increase with coagulant concentration are observed. With the increase of the iron ions concentration, pH decreases from 5.5 to 3.6. Meanwhile values of ζ-potential change from negative −50 mV to positive +40 mV, indicating an important charge reversal of latex particles. We found that the isoelectric point (IEP) was achieved when the $FeCl_3$ concentration was comprised between 1 and 2 mg/L.

In order to investigate the influence of the initial suspension pH to coagulate with $FeCl_3$ we fixed the pH of initial suspensions at 4, 5.5, 7, 8 and 9. It turned out that the behavior of the system can be divided into two regimes depending on the concentration of iron(III) chloride (Fig. 5). When the dosage of $FeCl_3$ was above 5 mg/L we did not identified significant differences between the values of zeta potential which were all found positive. On the other hand when $FeCl_3$ concentration was less than 5 mg/L we observed a difference between the values of zeta potential as a function of initial pH. Indeed the IEP was more rapidly achieved at low initial pH values regarding the $FeCl_3$ dosage. When pH was above 7, ζ-potential was within the range from −90 to −40 mV. But for acid environment, pH below 5.5, the values of ζ-potential were higher,

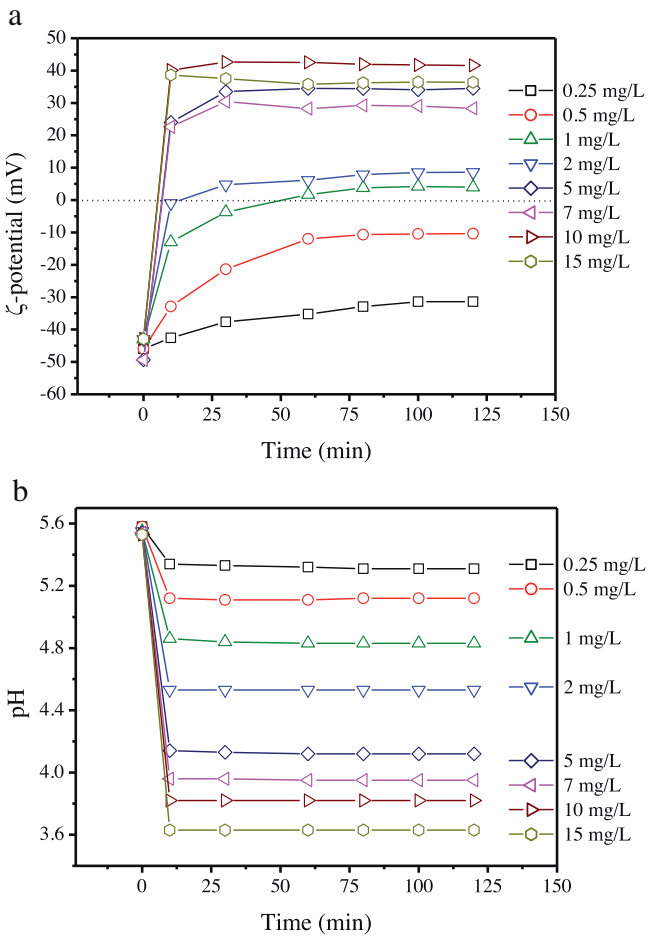

Fig. 3. Latex particle change of ζ-potential (a) and pH (b) depending on the concentration of $FeCl_3$ with time. Zeta potential stabilizes after about 80 min and pH after 10 min following the $FeCl_3$ addition. Initial pH of suspension was 5.5. It is observed that in all cases the suspension pH is decreasing with the addition of $FeCl_3$.

from −60 to −30 mV for the same $FeCl_3$ dosage. In neutral and basic environments latex particles had more negative surface charge than in acid environments. It is related with acid–basic equilibrium on the surface of latex particle. In acid environment free proton

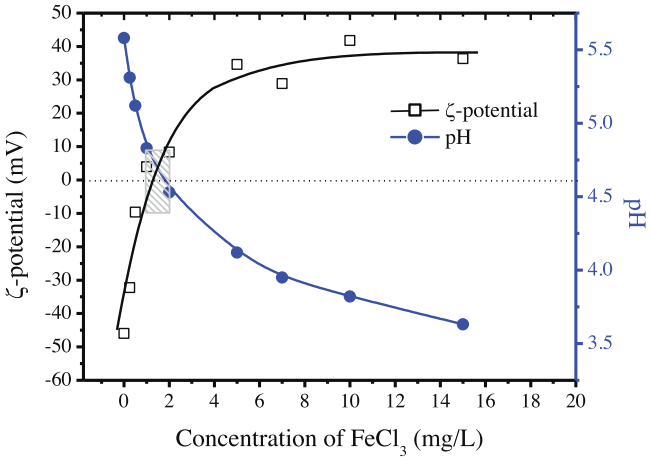

Fig. 4. Change of ζ-potential and pH of the latex suspension as a function of coagulant concentration after stabilization (initial pH was 5.5). ζ-Potential changes from negative (−50 mV) to positive (+40 mV) values and pH from 5.5 to 3.6. The neutralization of charge is achieved when the concentration of coagulant is comprised between 1 and 2 mg/L concomitantly with a decrease of the suspension pH.

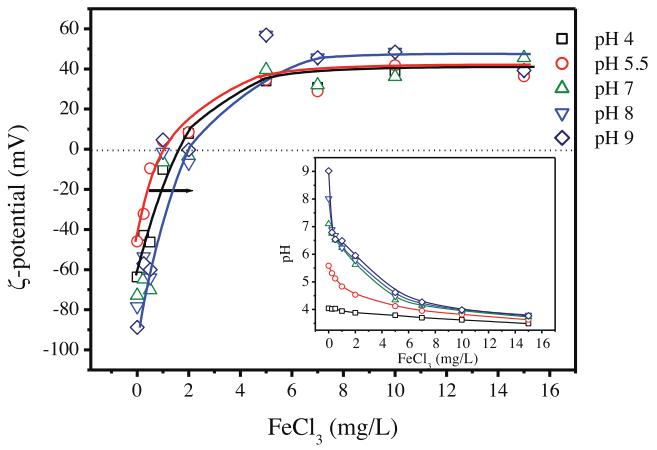

Fig. 5. Zeta potential and pH variation as a function of iron(III) chloride concentration at different initial pH. It is found that by decreasing the initial pH, surface charge neutralization is more efficient regarding the coagulant concentration. As a result less coagulant is necessary.

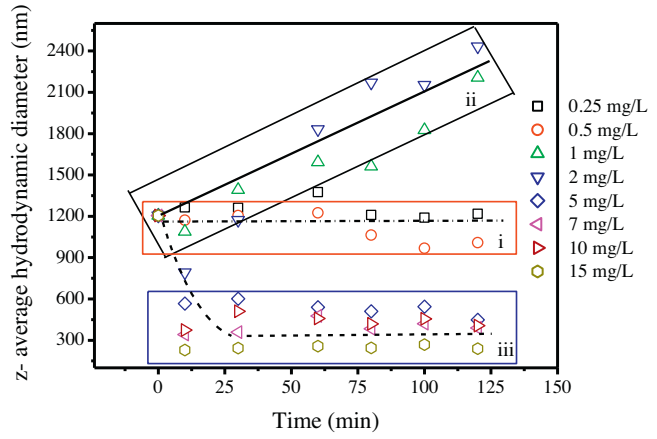

Fig. 6. Time variation of *z*-average hydrodynamic diameters of latex particles depending on coagulant dosage. There are three tendencies in particle aggregation behavior: (i) absence of aggregation below the isoelectric point (IEP); (ii) aggregation at the IEP according to the increase of the *z*-average hydrodynamic diameter and (iii) decrease of the *z*-average diameter above the IEP due to the concomitant formation of nanoparticles composed of $Fe(OH)_3$. Initial suspension pH equal to 7.

(H^+) is attached to the surface group, it reduces the surface charge. When the pH becomes higher H^+ left the latex surface and in basic environment zeta-potential becomes more negative. To achieve the IEP the optimal concentration of iron(III) chloride was within the range from 1 to 2 mg/L. Below this concentration the surface charge of particles stayed negative and above it we observed the surface charge inversion and the zeta potential became highly positive at about +40 mV. It should also be noted that at pH around 4 the concentration of positively charged ions such as $Fe(OH)_2^+$ and $Fe(OH)^{2+}$ is higher and such conditions are more efficient for surface charge neutralization.

To get insight into the coagulation process and aggregate formation that were occurring in the suspension we measured the *z*-average hydrodynamic diameters as a function of the coagulant concentration (Fig. 6) using DLS at initial pH 7. We found three tendencies in suspension behavior. When the concentration of coagulant was below the isoelectric point (0.25 and 0.5 mg/L $FeCl_3$), no significant size change was obtained – line dash and dots (red rectangle). At charge neutralization, for (1 and 2 mg/L $FeCl_3$), particle aggregation was observed and *z*-average hydrodynamic diameter was found to rapidly increase up to 2400 nm after about 100–125 min (straight line and black rectangle). In the charge inversion domain, for $FeCl_3$ concentration from 5 to 15 mg/L, *z*-average values of hydrodynamic diameter were surprisingly found smaller than expected and close to 300 nm (dash line and blue rectangle). It is known that at pH above 6 and until pH 10 about 60% of Fe(III) species in solution (Fig. 2) are considered to form insoluble iron hydroxide $Fe(OH)_3$ [8,13,35]. After the formation of $Fe(OH)_3$ it partially precipitated and stayed in suspension independently of further changes of pH, thus explaining the decrease of the mean *z*-average value of hydrodynamic diameter. This important observation was checked by considering the size distributions using DLS (Fig. 7a). We found two distinct particle size distributions in suspension with mean *z*-average diameters of about 160 nm and 1000 nm. The NTA method was also used to determine the size distribution and a similar result was found (Fig. 7b) with hydrodynamic diameters equal to 190 nm and 1000 nm respectively in agreement with the DLS measurement. As the average diameter of the latex particles was 0.99 μm we concluded that the presence of these nanosized particles corresponded to aggregates composed of precipitated hydroxides.

We extracted two images from NTA video recordings to compare latex suspensions, only, with mixtures of latex and iron(III) chloride (7 mg/L) (Fig. 8). It can be seen (Fig. 8b) that in mixed

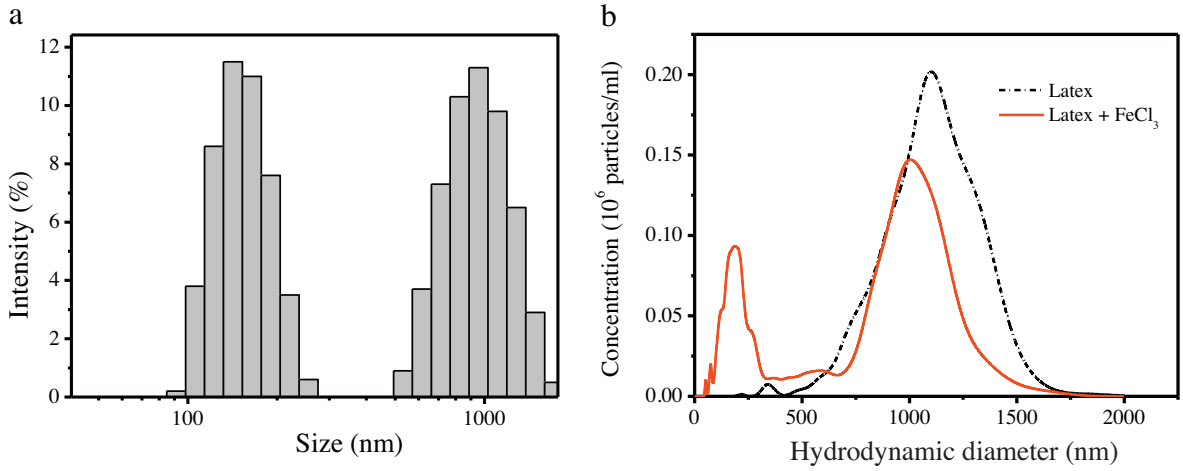

Fig. 7. Size distributions of particles in the latex suspension with an excess of iron(III) chloride at pH 7 and by using DLS (a) and NTA (b) methods. Two different particle sizes of about 190 and 1000 nm are observed concomitantly with the charge inversion of the latex particles. It should be noted that a better resolution is achieved with the tracking analysis technique.

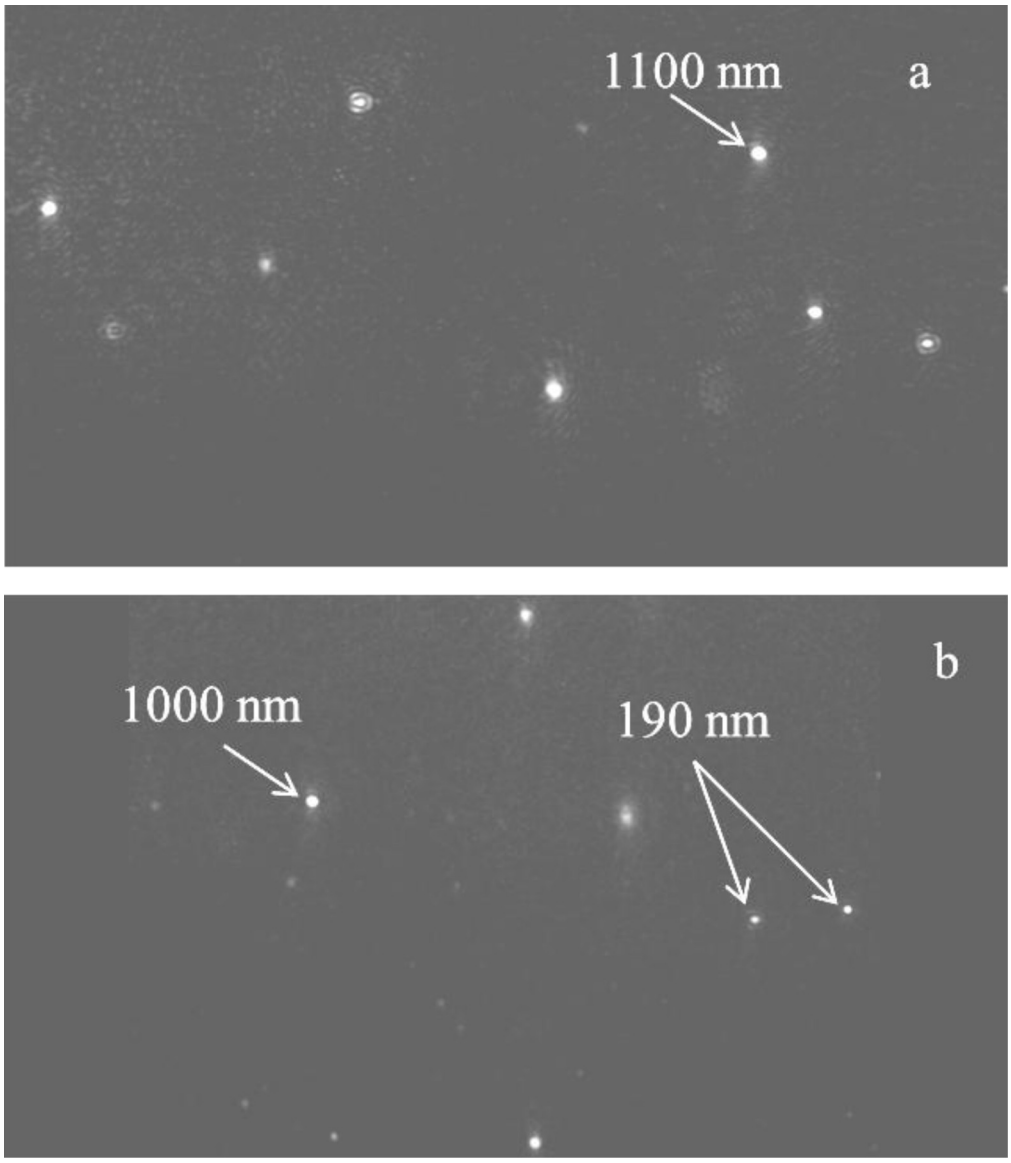

Fig. 8. Pictures from NTA videos corresponding to a suspension containing only latex particles (a) and a suspension of latex particles with $FeCl_3$ (b). We found two different species of size 190 and 1000 nm in the second suspension which indicated the formation of $Fe(OH)_3$ insoluble nanoparticles.

suspensions there were two independent species of size about 190 and 1000 nm that were attributed to iron(III) hydroxide and latex particles respectively. Here, two different methods allowed the visualization of nanosized iron(III) hydroxide formation, which is important for understanding the coagulation mechanism of latex particles in the presence of an excess of iron salt. Most importantly for water treatment processes it is shown here that the excess of iron is removed via the formation nanosized iron particles.

In order to understand the mechanism of particle interaction we measured zeta-potentials and *z*-average hydrodynamic diameters of a dispersion containing iron(III) hydroxide (Fig. 9). We found that the formed nanoparticles were positively charged with zeta-potential of +30 mV. We also measured the size distribution of particles and the *z*-average hydrodynamic diameter was found equal to 168 nm (after 30 min from the beginning of experiment). This means that the coated latex and precipitated nanoparticles have the same surface properties and surface charges and therefore not aggregate.

The mechanism of particle interaction and surface charge modification in the presence of $FeCl_3$ at different dosage and at different

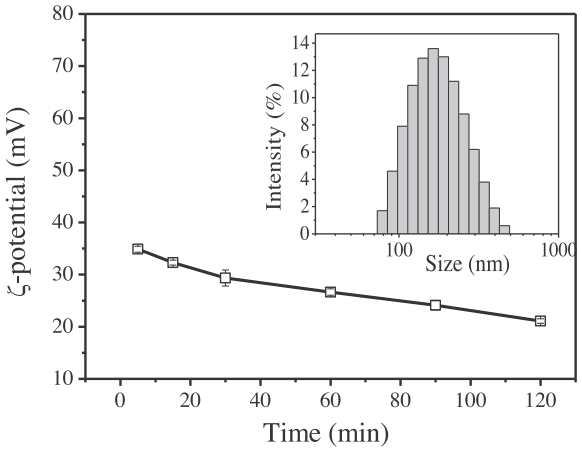

Fig. 9. Time variation of zeta-potential of iron(III) hydroxide and corresponding size distribution (inset) formed during the experiment. Zeta-potential is positive and is around +30 mV. *Z*-average hydrodynamic diameter is equal 168 nm.

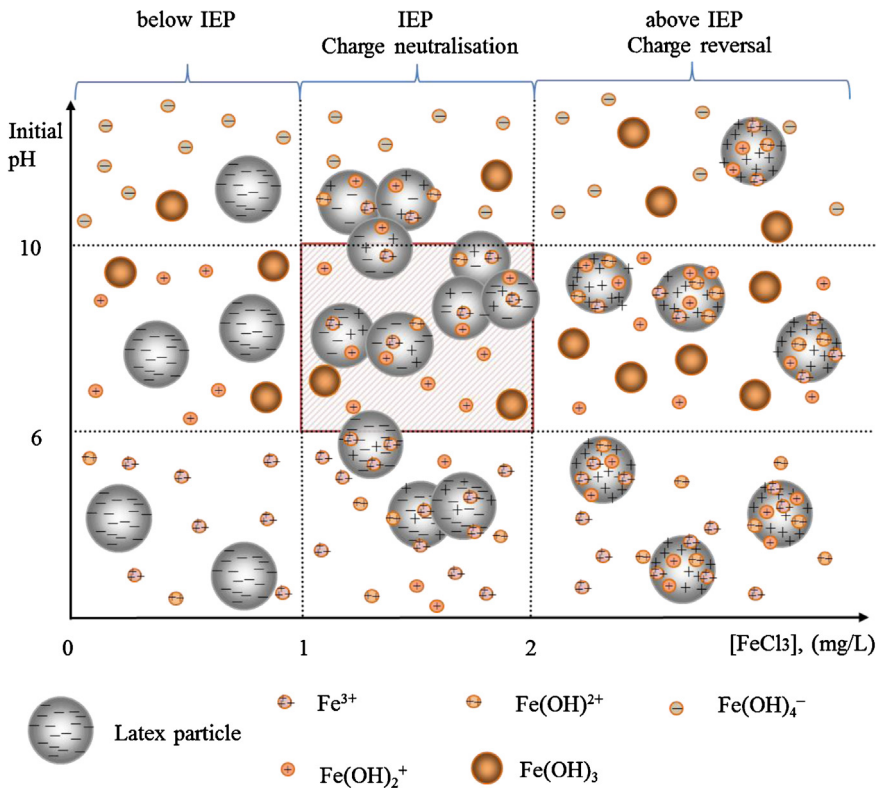

Fig. 10. Schematic representation of the behavior of the latex suspension (10 mg/L) as a function of iron(III) chloride concentration and pH. The isoelectric point is achieved when the $FeCl_3$ concentration was 1–2 mg/L. The charge neutralization mechanism is found responsible for particle aggregation. It is shown that pH is also playing an important role in the latex particle coagulation.

initial pH is schematically presented in Fig. 10. Below the IEP all latex particles are negatively charged and the suspension is stable. The addition of small amount of coagulant under the 1 mg/L does not dramatically change the latex stability. According to our model (Fig. 2) Fe^{3+}, $Fe(OH)^{2+}$ and $Fe(OH)_2^{+}$ ions are present in solution below pH 6, but, with regards to the latex concentration this quantity of positively charged ions is not high enough to change the surface charge of particles and induce aggregation. Therefore zeta potential of particles remains negative. In the range of dosage from 1 to 2 mg/L of $FeCl_3$ the coagulation of particles occurred. The iron ions are adsorbed on the latex surface and it results to charge neutralization. The addition of higher concentrations of coagulant brings more iron species in suspension, which leads to charge inversion of particles in positive sign and the repulsion forces stabilize the suspension. At the same time, above pH 6 the formation of iron hydroxide occurred that leads to its partial precipitation as nanoparticles, but this process does not influence the already stabilized latex. The best condition for coagulation process is shown in Fig. 9, when the concentration of coagulant is comprised between 1 to 2 mg/L and initial pH from 6 to 10.

4. Conclusion

The surface charge modification and aggregation process induced by $FeCl_3$ at different pH and coagulant dosage are discussed here. Based on our results it is found that zeta potential measurements can be used to control the coagulation process and to establish the optimal conditions of coagulant dosage. It is shown that adding a given dose of coagulant does not lead to immediate change in surface charge in particular when the coagulant dosage is low. We demonstrated different behaviors of latex particles depending on the dosage of iron ions. The excess of $FeCl_3$ is resulting to the formation of positively charged $Fe(OH)_3$ nanoparticles but also to charge inversion which is not a desirable situation. The initial pH is also important to consider to improve the efficiency of $FeCl_3$ as coagulant regarding the dose to use to attain the isoelectric point (IEP). The lower initial pH of suspension is, the more rapidly the IEP is achieved. In addition, there are three tendencies in particles behavior depending on concentration of iron(III) chloride: stabilization below the IEP, aggregation (at the IEP) and restabilization above the IEP. The primary mechanism that is responsible for latex coagulation is charge neutralization.

Acknowledgements

The authors are grateful to Arnaud Clavier for introduction to modeling program MINTEQA2, Fabrice Carnal for images processing and Frédéric Loosli for help with experimental design and useful suggestions.

We also acknowledge the financial support received from the Swiss National Foundation (project 200021_135240) and nanoMILE FP7 project.

References

[1] M. Meybeck, A.J. Horowitz, C. Grosbois, The geochemistry of Seine River Basin particulate matter: distribution of an integrated metal pollution index, Sci. Total Environ. 328 (2004) 219–236.
[2] H. Jiang, Z. Yan, Y. Zhao, X. Hu, H. Lian, Zincon-immobilized silica-coated magnetic Fe_3O_4 nanoparticles for solid-phase extraction and determination of trace lead in natural and drinking waters by graphite furnace atomic absorption spectrometry, Talanta 94 (2012) 251–256.
[3] C. Neal, H. Jarvie, P. Rowland, A. Lawler, D. Sleep, P. Scholefield, Titanium in UK rural, agricultural and urban/industrial rivers: geogenic and anthropogenic colloidal/sub-colloidal sources and the significance of within-river retention, Sci. Total Environ. 409 (2011) 1843–1853.
[4] P. Westerhoff, G. Song, K. Hristovski, M.A. Kiser, Occurrence and removal of titanium at full scale wastewater treatment plants: implications for TiO_2 nanomaterials, J. Environ. Monit. 13 (2011) 1195–1203.

[5] J. Gregory, Particles in Water: Properties and Processes, CRC Press, 2005.
[6] J. Duan, J. Gregory, Coagulation by hydrolysing metal salts, Adv. Colloid Interface Sci. 100 (2003) 475–502.
[7] M. Elimelech, X. Jia, J. Gregory, R. Williams, Particle Deposition & Aggregation: Measurement, Modelling and Simulation, Butterworth-Heinemann, 1998.
[8] O. Larue, E. Vorobiev, C. Vu, B. Durand, Electrocoagulation and coagulation by iron of latex particles in aqueous suspensions, Sep. Purif. Technol. 31 (2003) 177–192.
[9] J.-L. Lin, J.R. Pan, C. Huang, Enhanced particle destabilization and aggregation by flash-mixing coagulation for drinking water treatment, Sep. Purif. Technol. (2013).
[10] D. Palomino, D. Hunkeler, S. Stoll, Comparison of two cationic polymeric flocculant architectures on the destabilization of negatively charged latex suspensions, Polymer 52 (2011) 1019–1026, http://dx.doi.org/10.1016/j.polymer.2010.12.033.
[11] J. Hierrezuelo, A. Vaccaro, M. Borkovec, Stability of negatively charged latex particles in the presence of a strong cationic polyelectrolyte at elevated ionic strengths, J. Colloid Interface Sci. 347 (2010) 202–208.
[12] I. Pinheiro, P.J. Ferreira, F.A. Garcia, M.S. Reis, A.C. Pereira, C. Wandrey, et al., An experimental design methodology to evaluate the importance of different parameters on flocculation by polyelectrolytes, Powder Technol. 238 (2013) 2–13, http://dx.doi.org/10.1016/j.powtec.2012.08.004.
[13] A. Stefánsson, Iron (III) hydrolysis and solubility at 25 °C, Environ. Sci. Technol. 41 (2007) 6117–6123.
[14] T. Li, Z. Zhu, D. Wang, C. Yao, H. Tang, Characterization of floc size, strength and structure under various coagulation mechanisms, Powder Technol. 168 (2006) 104–110, http://dx.doi.org/10.1016/j.powtec.2006.07.003.
[15] M. Kobayashi, M. Nitanai, N. Satta, Y. Adachi, Coagulation and charging of latex particles in the presence of imogolite, Colloids Surf. A 435 (2013) 139–146, http://dx.doi.org/10.1016/j.colsurfa.2012.12.057.
[16] R.O. James, G.R. Wiese, T.W. Healy, Charge reversal coagulation of colloidal dispersions by hydrolysable metal ions, J. Colloid Interface Sci. 59 (1977) 379–385, http://dx.doi.org/10.1016/0021-9797(77)90023-6.
[17] J. Zou, H. Zhu, F. Wang, H. Sui, J. Fan, Preparation of a new inorganic–organic composite flocculant used in solid–liquid separation for waste drilling fluid, Chem. Eng. J. 171 (2011) 350–356.
[18] B.-Y. Gao, Q.-Y. Yue, Y. Wang, Coagulation performance of polyaluminum silicate chloride (PASiC) for water and wastewater treatment, Sep. Purif. Technol. 56 (2007) 225–230.
[19] W.P. Cheng, F.H. Chi, C.C. Li, R.F. Yu, A study on the removal of organic substances from low-turbidity and low-alkalinity water with metal-polysilicate coagulants, Colloids Surf. A 312 (2008) 238–244.
[20] R.V. Lauzon, E. Matijević, Stability of polyvinyl chloride latex. II. Coagulation by metal chelates, J. Colloid Interface Sci. 37 (1971) 296–302.
[21] P. Dahlsten, P. Próchniak, M. Kosmulski, J.B. Rosenholm, Electrokinetic behavior of melamine–formaldehyde latex particles at moderate electrolyte concentration, J. Colloid Interface Sci. 339 (2009) 409–415.
[22] H.C. Schumacher, M. Alves, C.A.P. Leite, J.P. Santos, É.T. Neto, M.M. Murakami, et al., Cationic latex formation by ionic modification, J. Colloid Interface Sci. 305 (2007) 256–263.
[23] E.L. Sharp, P. Jarvis, S.A. Parsons, B. Jefferson, The impact of zeta potential on the physical properties of ferric-NOM flocs, Environ. Sci. Technol. 40 (2006) 3934–3940.
[24] E.L. Sharp, S.A. Parsons, B. Jefferson, Seasonal variations in natural organic matter and its impact on coagulation in water treatment, Sci. Total Environ. 363 (2006) 183–194.
[25] A. Morfesis, A.M. Jacobson, R. Frollini, M. Helgeson, J. Billica, K.R. Gertig, Role of zeta (ζ) potential in the optimization of water treatment facility operations, Ind. Eng. Chem. Res. 48 (2009) 2305–2308.
[26] P. Leroy, N. Devau, A. Revil, M. Bizi, Influence of surface conductivity on the apparent zeta potential of amorphous silica nanoparticles, J. Colloid Interface Sci. 410 (2013) 81–93, http://dx.doi.org/10.1016/j.jcis.2013.08.012.
[27] P. Hole, K. Sillence, C. Hannell, C.M. Maguire, M. Roesslein, G. Suarez, et al., Interlaboratory comparison of size measurements on nanoparticles using nanoparticle tracking analysis (NTA), J. Nanopart. Res. 15 (2013) 1–12, http://dx.doi.org/10.1007/s11051-013-2101-8.
[28] B. Carr, A. Malloy, NanoParticle Tracking Analysis – The NANOSIGHT System, 2006.
[29] J.A. Gallego-Urrea, J. Tuoriniemi, T. Pallander, M. Hassellöv, Measurements of nanoparticle number concentrations and size distributions in contrasting aquatic environments using nanoparticle tracking analysis, Environ. Chem. 7 (2010) 67–81.
[30] S.R. Peterson, C.J. Hostetler, W.J. Deutsch, C.E. Cowan, Minteq User's Manual, Pacific Northwest Lab, Richland, WA, 1987, Nuclear Regulatory Commission, Washington, DC, Div. of Waste Management.
[31] A.R. Felmy, D.C. Girvin, E.A. Jenne, MINTEQ – A Computer Program for Calculating Aqueous Geochemical Equilibria: February 1984, National Technical Information Service, 1984.
[32] J.W. Ball, E.A. Jenne, D.K. Nordstrom, Additional and Revised Thermochemical Data and Computer Code for WATEQ2: A Computerized Chemical Model for Trace and Major Element Speciation and Mineral Equilibria of Natural Waters, Water Resources Division, US Geological Survey, 1980.
[33] R.M. Cornell, U. Schwertmann, The Iron Oxides: Structure, Properties, Reactions, Occurrences and Uses, John Wiley & Sons, 2003.
[34] D.W. Barnum, Hydrolysis of cations. Formation constants and standard free energies of formation of hydroxy complexes, Inorg. Chem. 22 (1983) 2297–2305, http://dx.doi.org/10.1021/ic00158a016.
[35] W. Feng, D. Nansheng, Photochemistry of hydrolytic iron (III) species and photoinduced degradation of organic compounds. A minireview, Chemosphere 41 (2000) 1137–1147.

Paper V

Oriekhova, O., and Stoll, S., 2018, Heteroaggregation of nanoplastic particles in presence of inorganic colloids and natural organic matter, Environmental Science: Nano, v. 5, pp. 792-799.

Environmental Science Nano

PAPER

Cite this: *Environ. Sci.: Nano*, 2018, 5, 792

Heteroaggregation of nanoplastic particles in the presence of inorganic colloids and natural organic matter†

Olena Oriekhova and Serge Stoll *

Received 24th November 2017,
Accepted 1st February 2018

DOI: 10.1039/c7en01119a

rsc.li/es-nano

The presence and accumulation of micro- and nanoplastics in marine and fresh waters represent a huge environmental concern. Due to the complexity of nanoplastic surface chemistry and impact of the surrounding aquatic environment, the fate of nanoplastics is still difficult to evaluate. Our study aims to explore the effect of different water components such as natural organic matter and inorganic colloids as well as water composition on the stability of polystyrene nanoplastics. Heteroaggregation experiments are performed under contrasting conditions by considering mixtures of three components: nanoplastics, Fe_2O_3 and alginate and at different concentration ratios. It is found that the charge neutralization mechanism in most cases is responsible for the formation of large heteroaggregates. A shift in the optimal heteroaggregation concentration is observed in the presence of alginate indicating competitive effects between alginate and Fe_2O_3. The formation of primary heteroaggregates is found to be a requisite before the formation of large structures. The behavior of polystyrene nanoplastics is also studied here in natural water from the Rhône river. Nanoplastic particles are found to rapidly change their surface charge from positive to negative and form small heteroaggregates at low concentration. Increasing the nanoplastic particle concentration is found to result in the formation of large heteroaggregates when the isoelectric point is achieved indicating the importance of nanoplastic surface charge neutralization.

Environmental significance

Plastic pollution of aquatic systems has emerged as one of the most important environmental issues. Most of the attention has concentrated on the behavior of microplastics in the marine environment and relatively little attention has been paid to date to nanoplastics in fresh water systems. This study aims to improve our understanding of the effect of water components such as natural organic matter, inorganic colloids and ionic composition on the stability of polystyrene nanoplastics and the formation of heteroaggregates. Heteroaggregation between nanoplastics and aquagenic compounds is investigated under various contrasting conditions to derive a detailed mechanistic description of heteroaggregation based on different scenarios and systematic measurements. The formation of large heteroaggregates is governed by complex mechanisms of surface charge modification, electrostatic interactions, divalent cation absorption, and bridging processes. In most cases, it is shown that charge neutralization at the isoelectric point is a requisite for the formation of large heteroaggregates composed of nanoplastics and that heteroaggregation is one key process controlling the environmental identity of nanoplastics.

Introduction

The huge amount of plastic items which are produced for our benefits has led to the accumulation of plastic fragments in marine and fresh water environments.[1–3] The major pathways of plastics to the environment concern wastewaters, urban runoffs and degradation of already present larger fragments into smaller micro- and nano-sized particles.[4–6] Such micro- and nanoplastics represent a significant environmental concern since they are more easily ingested by organisms and accumulated throughout the food chain.[7–9] Moreover, nanoplastics are not easy to detect and pose a growing concern because of the adsorption, accumulation and transport of toxic chemical additives (polycyclic aromatic hydrocarbons, polychlorinated biphenyls, petroleum hydrocarbons, organochlorine pesticides, *etc.*) and possible release of these pollutants.[10–12] Most of the research studies focus on the monitoring of plastic pollution in the marine environment and only a few of them address the plastic pollution in fresh water, despite the fact that the main source of microplastics in marine water is run-off from metropolitan area rivers.[13–15]

Group of Environmental Physical Chemistry, Department F.-A. Forel for Environmental and Aquatic Sciences, Institute of Environmental Science, University of Geneva, Uni Carl Vogt, 66, boulevard Carl-Vogt, CH-1211 Geneva 4, Switzerland. E-mail: Olena.Oriekhova@unige.ch, Serge.Stoll@unige.ch; Tel: +41 22 379 0332, +41 22 379 0333

† Electronic supplementary information (ESI) available. See DOI: 10.1039/c7en01119a

In Switzerland, microplastics of different types, origins and compositions were found in samples from lakes Geneva, Constance, Neuchâtel, Maggiore, Zurich and Brienz.[3]

Different sources of plastic pollution from the direct rejection of plastic litter, from the washing liquid of synthetic clothes, from thermal cutting and 3D printing, and from cosmetics have been identified.[16–20] An additional source of plastic pollution has resulted from the use of sewage sludge which contains plastic pollution as a fertilizer.[21] Rain events and infiltration will result in the transport of these compounds to groundwater and rivers.

Plastics can be grouped into two categories: primary and secondary materials.[22] Primary plastics are plastic particles specifically produced as micro- or nano-sized particles and mainly used in industry as abrasive agents or in cosmetics as facial cleaners. Meanwhile, secondary plastic is a result of fragmentation and degradation processes from larger fragments of plastic litter to micro- or nano-sized fragments.[23]

There is a lack of detailed studies based on the mechanistic approach about the transformation of nanoplastics in aquatic systems. Many factors can influence the nanoplastic behavior in water. For example, there is no systematic research addressing the effect of the presence of naturally occurring organic matter (NOM) and inorganic colloids (ICs) as well as water chemistry on the fate and transport of nanoplastics. However, it is possible to use the knowledge gained in the field of nanomaterials to assess some hypotheses on the fate of micro- and nanoplastics in the environment.[22,24] It is known, from the data for manufactured metallic nanoparticles, that the presence of natural ICs will affect the environmental identity of nanoparticles *via* heteroaggregation[25–27] and that the presence of NOM can have a stabilizing effect or even lead to the redispersion of the nanoparticle aggregates formed.[28,29] To understand the effect of water compounds on the fate of micro- and nanoplastics, more studies, which take the specificity of plastic particles into account, such as particle density, surface chemistry, the mechanism of degradation and aging,[24] are needed.

In our work, we systematically studied the effect of natural organic matter (NOM) and inorganic colloids (IC) on the heteroaggregation of polystyrene latex nanoplastic particles. The polystyrene (PS) demand in Europe, including expanded polystyrene, reaches the level of 3.4×10^6 tonnes per year and these polymers are used in packaging, building and construction, electrical and electronics industries, and paints.[30] In addition, PS plastics are difficult to recycle and are highly resistant to biodegradation.[31,32] PS beads which we will use in this study are available as dispersions and will serve as model particles to assess the behavior of PS nanoplastics in the environment. These PS particles are positively charged and expected to provide favourable conditions for interaction with negatively charged aquatic colloids. In addition, positively charged polymeric particles were found to be more toxic to living organisms (*Daphnia magna*, mice and algal species) compared to negatively charged particles.[7,33,34] On the other hand, we used alginate which is a natural polysaccharide as a surrogate for NOM. As a proxy for IC, we used iron(III) oxide (α-Fe_2O_3) which is one of the most relevant ICs in the Rhône river.[35] First, PS nanoplastic particles were thoroughly characterized across the full pH range, including environmental conditions at pH 8 for which most of the experiments were performed. Then we investigated the effect of each individual water component, separately and then in mixtures. The last part of the study is devoted to the behavior of PS nanoplastics in natural water from the Rhône river. A mechanistic interpretation of different interaction processes occurring when PS nanoplastics are released to different waters is presented to gain a better picture of the nanoplastic fate in aquatic systems.

Materials and methods

Materials

Latex polystyrene nanospheres were provided from Molecular Probes® (Life Technologies Corporation, USA) with a mean diameter equal to 20 ± 0.3 nm (TEM measurements, provided by the manufacturer), density equal to 1.055 g cm^{-3} (20 °C) and specific surface area of 2.8×10^6 cm^2 g^{-1}. Amidine groups are present on the surface of PS particles making them positively charged in a large pH domain with a surface charge density equal to 3.0 μC cm^{-2}. A 400 mg L^{-1} stock suspension at pH 3.0 was prepared by diluting the original suspension with ultrapure water ($R > 18$ MΩ cm, Millipore, Switzerland), the pH of which was previously adjusted to 3. As a proxy for inorganic colloids, iron(III) oxide (α-Fe_2O_3, 99%) as a powder (NanoAmor, Inc., USA) was used. A 1 g L^{-1} suspension was prepared in ultrapure water at pH 10, and then this suspension was sonicated for 15 min with an ultrasonic probe (CV18, Sonics Vibra cell, Blanc Labo S.A., Switzerland). A 500 mg L^{-1} stock suspension was prepared with ultrapure water having a pH also previously adjusted to 10 for further dilution. Alginate (A2158, Sigma Aldrich, Switzerland) was used as a surrogate for natural polysaccharide. The molecular weight of low viscosity alginate is equal to 50 kDa.[36] A 100 mg L^{-1} stock solution was prepared in ultrapure water and used for further dilution. To adjust the pH, diluted sodium hydroxide and hydrochloric acid (0.01 M) (NaOH and HCl, Titrisol®113, Merck, Switzerland) were used. Water from the Rhône river was collected in Geneva, Jonction district (Geneva, Switzerland) and filtered through a 0.45 μm filter (Millipore, Switzerland). The physicochemical properties of this water were measured during the sampling. The ionic composition was analyzed by ionic chromatography (Dionex ICS-3000 analyzer). All measured parameters are presented in ESI† SI1. All solutions were stored in a dark place at 4 °C.

Methods

Zeta potentials and *z*-average hydrodynamic diameters were measured using a Malvern Zetasizer Nano ZS (Malvern Instruments Ltd, UK). The kinetics of heteroaggregation was measured for each point independently every 15 sec for 15 min (accumulating in total 60 measurements). Each figure data

point represents a mean value of *z*-average diameters measured during the last 3 min (*i.e.* from 13 to 15 min including).

To characterize PS nanoplastics, a 100 mL suspension of nanoplastic particles (50 mg L^{-1}) was prepared at pH 3 and then the pH was increased by addition of 0.01 M NaOH. The time delay between each measurement was at least 15 min in order to stabilize the pH. To study the interaction between alginate and PS nanoplastics, a series of independent suspensions were prepared. A 40 mg L^{-1} nanoplastic suspension was prepared by dilution with ultrapure water (pH was previously adjusted to obtain the final suspension pH equal to 8.0 ± 0.2). Then an appropriate amount of alginate was added to obtain the final concentration of alginate which was adjusted from 0.25 to 5 mg L^{-1}.

For nanoplastics mixed with water from the Rhône river, the aggregation rate (nm min^{-1}) was determined by linear fitting and from the slope of *z*-average hydrodynamic diameters measured over the first 5 min after addition of nanoplastics to water.[37,38] The aggregation rate is an important parameter, obtained experimentally, which could be used for further development of theoretical models of nanoplastic transformations and calculation of attachment efficiencies.[4,39]

In order to observe the heteroaggregate morphology, a JSM-7001FA (JEOL) scanning electron microscope (SEM) was used to obtain SEM images. For each sample, 20 μL of the nanoplastic dispersion were placed on one aluminum stub covered with a 5 × 5 mm silica wafer (Agar Scientific G3390), dried and wrapped with 3 nm of Pt/Pd coating.

Results and discussion

To understand the behavior of PS nanoplastic particles in a complex aquatic matrix, it is important to start with a simple system and then increase step by step the system complexity. First PS particles were characterized in ultrapure water under changing pH conditions. Then, heteroaggregation experiments between PS nanoplastics and individual water components (NOM and IC) were considered. In order to investigate the effects of IC and alginate separately and in mixtures, a series of experiments were designed. Then to consider a more complex and realistic picture including the combined effect of all water components, PS particles were released to the river Rhône water.

PS nanoplastic characterization

To obtain an insight into the variation of the surface charge of nanoplastic particles, titration curves were determined across the full pH range. Zeta potential was measured from pH 3 to pH 10 in 50 mg L^{-1} nanoplastic suspension. Due to the presence of amidine functional groups, the particle surface is found to be positively charged. The zeta potential varied from +48 ± 6 mV at pH 3 to +33 ± 4 mV at pH 10 (Fig. 1A). PS nanoplastic particles are stable due to the presence of positively charged functional groups and the particle

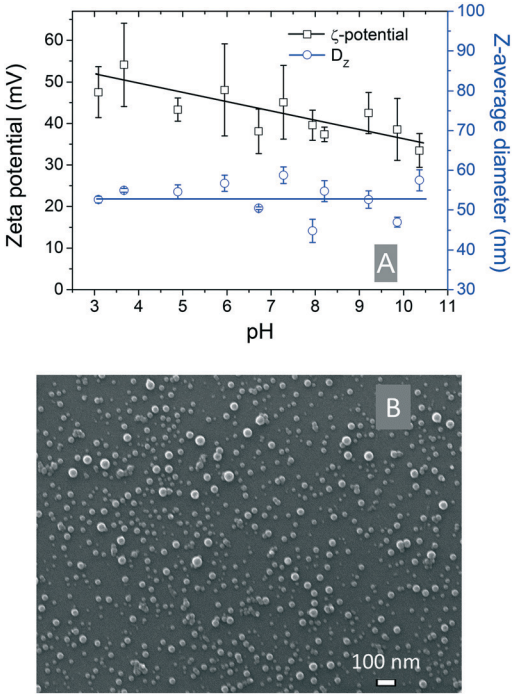

Fig. 1 (A) Zeta potential and *z*-average hydrodynamic diameter of PS nanoplastic particles at different pH values in ultrapure water. Zeta potential decreases with the increase of pH. *Z*-average hydrodynamic diameter is found to be constant with a mean value equal to 53.1 ± 4.3 nm. Experimental conditions: [PS] = 50 mg L^{-1}, initial pH 3. (B) SEM image of pristine nanoplastics in ultrapure water: [PS] = 5 mg L^{-1}, the diameter of PS particles is found to be from 25 to 63 nm.

mean *z*-average hydrodynamic diameter is equal to 53.1 ± 4.3 nm. To study the nanoplastic morphology, SEM images of 5 mg L^{-1} nanoplastics in ultrapure water were recorded. As can be seen in the SEM image presented in Fig. 1B, PS nanoplastics have a regular spherical shape and are found to be dispersed as single units. Based on SEM image analysis, 71% of the particles were found with the size varying from 20 to 30 nm, which corresponds to the data provided by the manufacturer. The *z*-average diameter measurement by DLS has a tendency to report larger particle sizes due to the ability of large particles to scatter more light as the intensity of scattered light is proportional to the sixth power of the particle diameter.[40]

Interaction between PS nanoplastics and alginate

We performed experiments at pH 8.0 ± 0.2 which is representative of fresh water conditions. A 40 mg L^{-1} nanoplastic suspension was prepared and then alginate was added to the suspension. Initially, PS nanoplastics are positively charged and stable with a zeta potential equal to +42.7 ± 9.3 mV and mean *z*-average hydrodynamic diameter equal to 65.8 ± 1.3 nm (Fig. 2A). The increase of alginate concentration is found to gradually decrease the value of zeta potential. The electrostatic interaction between positively charged nanoplastic particles and negatively charged alginate leads rapidly to charge

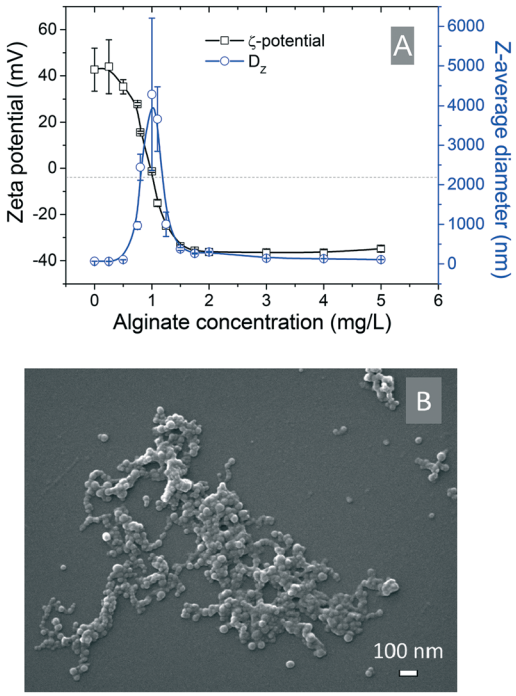

Fig. 2 (A) Zeta potential and *z*-average hydrodynamic diameter of PS nanoplastic particles at different alginate concentrations at pH = 8.0 ± 0.2 in ultrapure water. The strong affinity between the positively charged nanoplastics and negatively charged alginate is mainly due to electrostatic attractive interactions. The IEP is achieved at 1.00 ± 0.05 mg L^{-1} alginate when [PS] = 40 mg L^{-1}. (B) SEM image of nanoplastic and alginate aggregates: [PS] = 5 mg L^{-1}, [alginate] = 1 mg L^{-1}.

neutralization, the so-called isoelectric point (IEP), which occurs at 1 mg L^{-1} alginate concentration. At this stage, maximum aggregation is observed. The *z*-average diameter is found to be equal to 4245 ± 330 nm. Such a large diameter is attributed to the formation of alginate bridges[41,42] between PS particles resulting in the formation of open structures as illustrated in the SEM image in Fig. 2B. Further increase of alginate concentration leads to negative zeta potential values with a plateau at −34.9 ± 1.3 mV (5 mg L^{-1} alginate), to the decrease of the aggregate sizes and to the stabilization of nanoplastic particles. Above 2 mg L^{-1} alginate concentration, the *z*-average diameter is equal to 106.9 ± 1.6 nm (5 mg L^{-1} alginate). Stabilization is achieved herein due to the formation of alginate coating around nanoplastic particles.[28,43] The increase of particle *z*-average diameter is also attributed to the alginate coating. Alginate molecules form a layer around PS nanoplastics, with an approximate thickness of 20 nm, which increases the overall *z*-average diameter. Here, the interaction process of nanoplastic beads with alginate is also controlled by the concentration ratio between nanoplastics and alginate. At low alginate concentration, nanoplastics are expected to form primary heteroaggregates with alginate but the amount of negative charges introduced by alginate is not enough to coat the nanoplastics and has a visible effect on the aggregate size and surface charge. Then with the increase of alginate concentration, charge neutralization and bridging are responsible for the heteroaggregation of nanoplastics. At high alginate concentration, alginate covers thoroughly the surface of nanoplastics resulting in charge inversion, *i.e.* nanoplastics covered with alginate became negatively charged, and stabilization due to the electrostatic and steric repulsive forces is observed.

Heteroaggregation between PS nanoplastics and Fe_2O_3

First, a 5 mg L^{-1} suspension of Fe_2O_3 was prepared. At pH 8.0 ± 0.2, Fe_2O_3 particles are negatively charged with a zeta potential equal to −28.5 ± 0.8 mV and a *z*-average diameter of 110.2 ± 6.6 nm (Fig. 3A). The variation of *z*-average hydrodynamic diameter with time (over 15 min) upon the addition of PS nanoplastics is presented in the ESI† (Fig. S1). The *z*-average diameters (average of the last 3 min measurements) are given in Fig. 3A as well as zeta potential values. The increase of nanoplastic concentration leads to the increase of zeta potential (the values of zeta potential become less negative) until charge neutralization at the IEP. The IEP is obtained at 3 mg L^{-1} nanoplastic concentration and for a concentration ratio of PS/Fe_2O_3 equal to 3/5. Further increase of nanoplastic concentration leads to charge inversion. At 50 mg L^{-1}, the nanoplastic zeta potential is equal to +40.9 ± 5.3

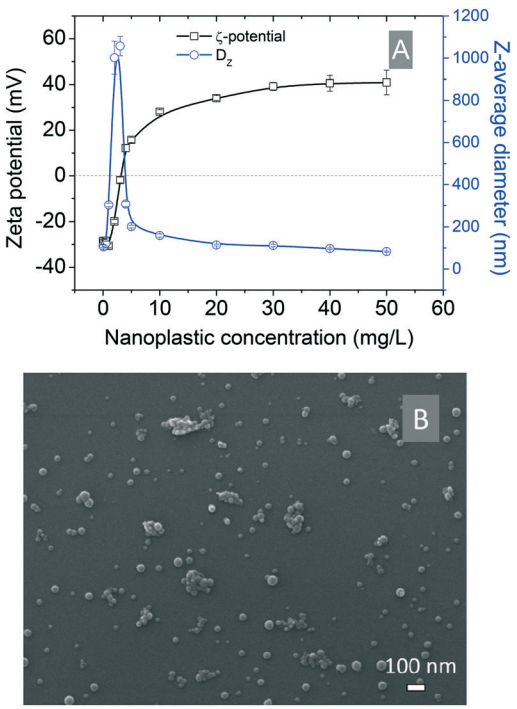

Fig. 3 (A) Zeta potential and *z*-average hydrodynamic diameter of a mixture of PS nanoplastics with inorganic colloids (Fe_2O_3) *versus* nanoplastic concentration. Experimental conditions: [Fe_2O_3] = 5 mg L^{-1}, pH = 8.0 ± 0.2, ultrapure water. Maximum heteroaggregation is achieved at 3 mg L^{-1} nanoplastic concentration at the IEP. (B) SEM image of a mixture of PS nanoplastics and Fe_2O_3: [PS] = 5 mg L^{-1}, [Fe_2O_3] = 2.5 mg L^{-1}. Nanoplastic particles are found to be adsorbed on the surface of rod-shaped Fe_2O_3 particles due to the presence of electrostatic attractive interactions.

mV due to the excess of PS particles. Heteroaggregation is already observed at 1 mg L^{-1} PS concentration as shown in Fig. S3A,† in which the size distribution during heteroaggregation is compared to the size distributions of the individual particles (Fig. S2†). The *z*-average diameter increases and reaches its maximum (1056.9 ± 46.2 nm) at the IEP corresponding to 3 mg L^{-1} nanoplastic concentration. Further increase of PS concentration leads to a fast drop in the values of the *z*-average diameter, indicating that the light scattering signal is mainly due to the PS nanoplastics. Despite the higher refractive index and bigger size of Fe_2O_3 particles, the scattering signal is still mainly due to the PS particles, because there are many more smaller PS particles.

Results indicate that PS nanoplastics adsorb on the surface of Fe_2O_3 (Fig. 3B) and heteroaggregation is observed. Maximum heteroaggregation occurs when the concentration of nanoplastics reaches the optimal value for charge neutralization between oppositely charged nanoplastics and ICs.

Effect of alginate on heteroaggregation between PS nanoplastics and Fe_2O_3

We used alginate to investigate the effect of a third component on the heteroaggregation between nanoplastics and inorganic colloids. A suspension containing Fe_2O_3 and alginate was prepared and then nanoplastics were added. Zeta potential variation and *z*-average diameters as a function of PS nanoplastic concentration are given in Fig. 4A. At low PS concentrations, from 0 to 10 mg L^{-1}, a negative zeta potential is obtained (−33.1 ± 2.6 mV). Then the IEP is achieved at 20 mg L^{-1}. Interestingly, a shift in the IEP regarding the nanoplastic concentration is observed when a comparison is made with the value obtained in the absence of alginate (3 mg L^{-1}), indicating that more positively charged nanoplastics are therefore needed to neutralize the negative charges of both alginate and Fe_2O_3. Further increase of the nanoplastic concentration was then found to result in charge inversion due to the excess of PS.

The presence of alginate is found to delay the maximum heteroaggregation due to a competitive effect between alginate and Fe_2O_3 regarding the interactions with PS particles. We assume that under such conditions, primary heteroaggregates composed of PS and alginate, PS and Fe_2O_3, PS–Fe_2O_3 and alginate are formed. By increasing the nanoplastic concentration, secondary heteroaggregates composed of primary heteroaggregates connected through alginate bridges are obtained with larger size.[26] The size of the aggregates significantly increased (3701 ± 824 nm) compared to that of heteroaggregates without alginate (1056.9 ± 46.2 nm).

PS nanoplastic heteroaggregation in Rhône river water

To obtain an insight into the effect of naturally present organic matter and inorganic colloids from river water on the heteroaggregation of PS nanoplastics, filtered Rhône water was used. When nanoplastic particles at low concentrations (below 4 mg L^{-1}) are in contact with the river water, they are found to rapidly change their surface charge from positive to negative. The zeta potential passes from +42.7 ± 9.3 to −6.1 ± 1.3 mV. Different molecular fractions (low and high weight) of naturally present organic matter and other water components, such as organic and inorganic polyions, are expected to specifically adsorb onto the nanoplastic surface causing important change of the surface charge.[44,45] The increase of nanoplastic concentration leads to the charge inversion in the same way as in ultrapure water in the presence of IC and the mixture of IC–alginate, due to the excess of nanoplastic particles (Fig. 5).

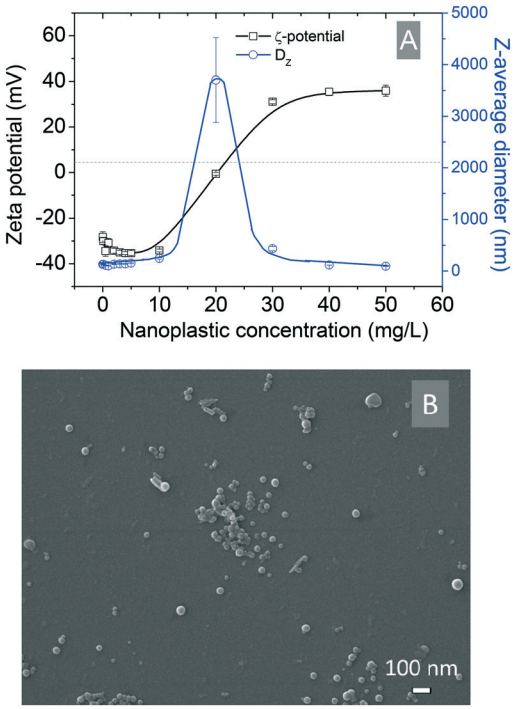

Fig. 4 (A) Zeta potential and *z*-average hydrodynamic diameter of a mixture of PS nanoplastic particles, Fe_2O_3 and alginate *versus* PS concentration. Experimental conditions: [Fe_2O_3] = 5 mg L^{-1}, [alginate] = 2 mg L^{-1}, pH = 8.0 ± 0.2, ultrapure water. Maximum heteroaggregation is achieved when [PS] = 20 mg L^{-1}. (B) SEM image of a mixture of PS nanoplastics, Fe_2O_3 and alginate: [PS] = 5 mg L^{-1}, [Fe_2O_3] = 2.5 mg L^{-1}, [alginate] = 1 mg L^{-1}.

Nanoplastic particles are slightly aggregated when they are mixed with Rhône water at low concentrations (below 1 mg L^{-1} PS) with a *z*-average diameter equal to 375.6 ± 20.8 nm. Natural polyelectrolytes are specifically adsorbed on the nanoplastic surface and modify the double-layer structure[46] resulting in changes not only in the surface charge but also in the particle size. Maximum heteroaggregation is once again achieved when the IEP is obtained (5 mg L^{-1}) with aggregate sizes equal to 1750 ± 123 nm. Zeta potential and *z*-average hydrodynamic diameter variations in Rhône water represent an intermediate situation between heteroaggregation in the presence of IC only and in the IC–alginate mixture. Further increase of nanoplastic concentration leads to the decrease of aggregate sizes due to the high PS concentration. To introduce a more quantitative approach for

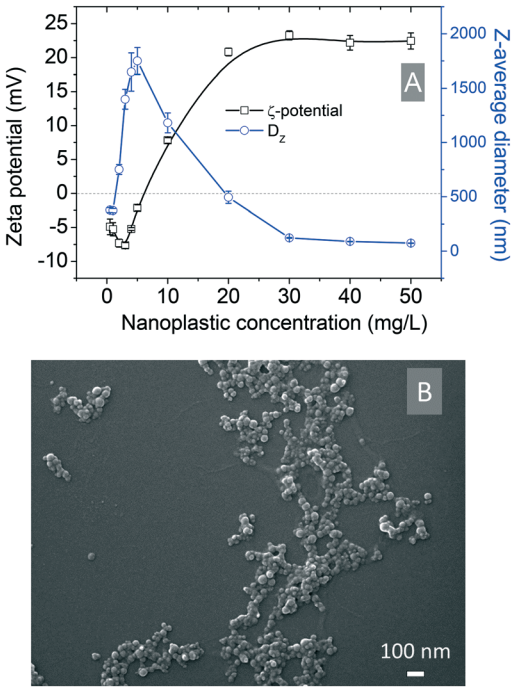

Fig. 5 (A) Zeta potential and *z*-average hydrodynamic diameter of PS nanoplastics released into Rhône water *versus* nanoplastic concentration. Experimental conditions: pH = 8.0 ± 0.2, Rhône water filtered through a 0.45 μm filter. The maximum heteroaggregation is achieved at 5 mg L^{-1} nanoplastic concentration. (B) SEM image of PS nanoplastics in Rhône water: [PS] = 1 mg L^{-1}.

interpretation of heteroaggregation data, we calculated the aggregation rate (nm min^{-1}) *versus* the increase of nanoplastic concentration (Fig. 6). The fitting parameters for linear and exponential curves in Fig. 6 are provided in the ESI† (SI4). Further increasing the PS concentration below the concentration of the maximum heteroaggregation (5 mg L^{-1}), the aggregation rate increases with the increase of nanoplastic concentration (Fig. 6), which corresponds to the aggregation

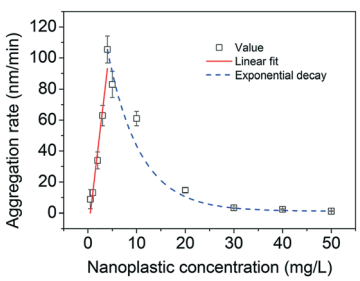

Fig. 6 Aggregation rate of PS nanoplastic particles as a function of nanoplastic concentration. The aggregation rate is determined by fitting the slope of hydrodynamic diameters measured by DLS over the first 5 min after addition of nanoplastics to Rhône water. Two distinguished parts are observed. The aggregation rate increases with the increase of particle concentration up to 4 mg L^{-1} nanoplastics (linear fit with a correlation coefficient equal to 0.954) and then exponentially decreases above this value indicating rapid restabilization of PS nanoplastics after charge neutralization of the Rhône water compounds. Linear fit and exponential decay parameters are given in the ESI† (SI4).

theory predicting the increase of collision probability with the increase of the particle concentration and is in good agreement with aggregation of metallic nanoparticles.[37,47] At higher nanoplastic concentrations, the excess of PS inhibits the heteroaggregation processes (Fig. S4†). A similar observation of the aggregation rate increase till the optimal value and then decrease was reported previously.[38,48] Indeed, the heteroaggregation rate between carbon nanotubes (CNTs) and hematite nanoparticles (HemNPs) was found to be proportional to the total concentration of CNTs and HemNPs, increasing till the optimal CNT/HemNP ratio of 0.0316 and then gradually decreasing.[38] It should be noted that in excess of PS nanoplastics the heteroaggregation still occurs according to Fig. S4A† (size distribution by intensity) in which two peaks are visible. It should be noted that if the size distribution by number (Fig. S4B†) is considered, one peak is observed indicating the outnumbering of individual nanoplastic particles over the aggregates. As a result, the mean size of the PS particles decreases indicating that more and more individual particles are stabilized by electrostatic repulsive forces.

Mechanistic description of nanoplastic interaction processes in contrasting water samples

A schematic representation of the possible mechanisms occurring when PS nanoplastics are released in different waters is shown in Fig. 7. In ultrapure water in the absence and presence of alginate, when the PS concentration is low (below 3 mg L^{-1} without alginate and at 10 mg L^{-1} in the presence of alginate), particles form primary heteroaggregates.

Increasing nanoplastic concentration leads to significant heteroaggregation *via* charge neutralisation mechanisms. In the presence of alginate, we observe a shift of maximum heteroaggregation to a higher PS concentration (20 mg L^{-1}). More positively charged nanoplastics are needed to neutralize the negative charge of both alginate and iron oxide which is consistent with our primary heteroaggregate formation. In addition, the size of the aggregates is found to be larger indicating an additional bridging mechanism between particles in the presence of alginate. Further increase of PS nanoplastic concentration leads to an excess of PS and charge inversion is observed.

In Rhône water at low nanoplastic concentrations (below 4 mg L^{-1}), we observe limited charge inversion (PS nanoplastics change their surface charge from positive to negative) as well as limited *z*-average diameters due to the presence of dissolved electrolytes and natural organic matter. Negatively charged organic matter specifically adsorbs on the positively charged nanoplastic surface, and then electrolytes, such as Ca^{2+} and Mg^{2+}, induce a bridging effect between nanoplastic particles. Maximum heteroaggregation is obtained at 5 mg L^{-1} nanoplastic concentration. At this stage of aggregation, large heteroaggregates are formed, which are composed of PS particles, multivalent ions, NOM and ICs. By increasing the PS concentration, the charge inversion is again observed.

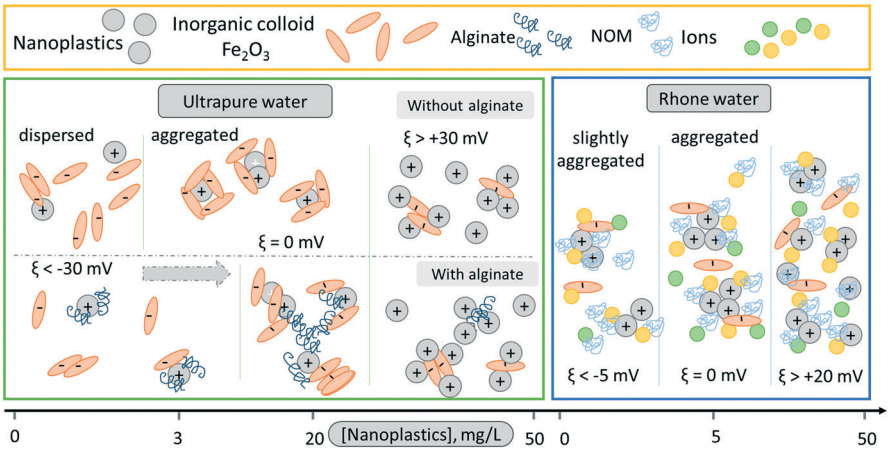

Fig. 7 Heteroaggregation mechanisms occurring when PS nanoplastics are released in different waters and in the presence of different compounds such as inorganic colloids (Fe_2O_3) and organic biomolecules (alginate). In most cases, electrostatic effects are found to play key roles and maximum heteroaggregation is observed at the heteroaggregate IEPs. The presence of alginate causes the shift of the maximum heteroaggregation to higher values of nanoplastic concentration due to neutralization of the excess of negative charges.

Conclusions

In this work, we showed the effect of contrasting water composition on the stability of positively charged polystyrene nanoplastics. Heteroaggregation at environmental pH was induced by the presence of both inorganic colloids such as Fe_2O_3 and alginate polysaccharide chains. The concentration ratio between Fe_2O_3, alginate and nanoplastics was found to be an important parameter controlling the heteroaggregation rate. Nanoplastic surface properties, more specifically the surface charge, were found to define the affinity between nanoplastics, inorganic colloids and natural organic matter. It should be noted that the presence of alginate was found to modify the heteroaggregation mechanism towards the formation of larger structures. We also showed that the aggregation rate of nanoplastics in natural water from the Rhône river is dependent on nanoplastic concentration and charge neutralization processes. Our results indicate that the nanoplastic surface properties and variability of environmental conditions will strongly control the fate and transport of nanoplastics in natural water and that heteroaggregation will play an important role in the nanoplastic environmental identity and removal from aquatic systems. It would be of great interest for future research to develop a theoretical framework taking the heteroaggregation and collision efficiencies into account which could be used for further fate modeling and risk assessment.

Conflicts of interest

There are no conflicts to declare.

Acknowledgements

The authors acknowledge support receive from the European Commission and the Swiss Secrétariat d'Etat à la Formation et à la Recherche et à l'Innovation SEFRI within the Horizon 2020 Program (NanoFASE 15.0183-2, 646002) and the University of Geneva. We are also grateful to Agathe Martignier for her support during the SEM measurements and to Alexis Pochelon for his advice with image analysis.

References

1 R. C. Thompson, Y. Olsen, R. P. Mitchell, A. Davis, S. J. Rowland, A. W. John, D. McGonigle and A. E. Russell, *Science*, 2004, **304**, 838.
2 P. G. Ryan, C. J. Moore, J. A. van Franeker and C. L. Moloney, *Philos. Trans. R. Soc., B*, 2009, **364**, 1999–2012.
3 F. Faure, C. Demars, O. Wieser, M. Kunz and L. F. De Alencastro, *Environ. Chem.*, 2015, **12**, 582–591.
4 E. Besseling, J. T. Quik, M. Sun and A. A. Koelmans, *Environ. Pollut.*, 2017, **220**, 540–548.
5 K. Mattsson, L.-A. Hansson and T. Cedervall, *Environ. Sci.: Processes Impacts*, 2015, **17**, 1712–1721.
6 A. S. Tagg, M. Sapp, J. P. Harrison and J. J. Ojeda, *Anal. Chem.*, 2015, **87**, 6032–6040.
7 F. Nasser and I. Lynch, *J. Proteomics*, 2016, **137**, 45–51.
8 M. Wagner, C. Scherer, D. Alvarez-Muñoz, N. Brennholt, X. Bourrain, S. Buchinger, E. Fries, C. Grosbois, J. Klasmeier, T. Marti, S. Rodriguez-Mozaz, R. Urbatzka, A. D. Vethaak, M. Winther-Nielsen and G. Reifferscheid, *Environ. Sci. Eur.*, 2014, **26**, 12.
9 S. L. Wright, R. C. Thompson and T. S. Galloway, *Environ. Pollut.*, 2013, **178**, 483–492.
10 H. Lee, W. J. Shim and J.-H. Kwon, *Sci. Total Environ.*, 2014, **470–471**, 1545–1552.
11 C. M. Rochman, E. Hoh, B. T. Hentschel and S. Kaye, *Environ. Sci. Technol.*, 2013, **47**, 1646–1654.
12 E. L. Teuten, J. M. Saquing, D. R. Knappe, M. A. Barlaz, S. Jonsson, A. Björn, S. J. Rowland, R. C. Thompson, T. S. Galloway and R. Yamashita, *Philos. Trans. R. Soc., B*, 2009, **364**, 2027–2045.
13 P. Hohenblum, B. Liebmann and M. Liedermann, *Plastic and Microplastic in the Environment*, Wien, 2015.

14 D. Morritt, P. V. Stefanoudis, D. Pearce, O. A. Crimmen and P. F. Clark, *Mar. Pollut. Bull.*, 2014, **78**, 196–200.

15 S. Zhao, L. Zhu, T. Wang and D. Li, *Mar. Pollut. Bull.*, 2014, **86**, 562–568.

16 M. A. Browne, P. Crump, S. J. Niven, E. Teuten, A. Tonkin, T. Galloway and R. Thompson, *Environ. Sci. Technol.*, 2011, **45**, 9175–9179.

17 L. S. Fendall and M. A. Sewell, *Mar. Pollut. Bull.*, 2009, **58**, 1225–1228.

18 H. A. Leslie, M. J. M. Van Velzen and A. D. Vethaak, *Nov. Data Set Microplastics North Sea Sediments Treat. Wastewater Effl. Mar. Biota* Amst. Inst. Environ. Stud. VU Univ. Amst.

19 H. Zhang, Y.-Y. Kuo, A. C. Gerecke and J. Wang, *Environ. Sci. Technol.*, 2012, **46**, 10990–10996.

20 B. Stephens, P. Azimi, Z. El Orch and T. Ramos, *Atmos. Environ.*, 2013, **79**, 334–339.

21 J. P. da Costa, P. S. M. Santos, A. C. Duarte and T. Rocha-Santos, *Sci. Total Environ.*, 2016, **566**, 15–26.

22 K. Syberg, F. R. Khan, H. Selck, A. Palmqvist, G. T. Banta, J. Daley, L. Sano and M. B. Duhaime, *Environ. Toxicol. Chem.*, 2015, **34**, 945–953.

23 J. Gigault, B. Pedrono, B. Maxit and A. T. Halle, *Environ. Sci.: Nano*, 2016, **3**, 346–350.

24 T. Hüffer, A. Praetorius, S. Wagner, F. von der Kammer and T. Hofmann, *Environ. Sci. Technol.*, 2017, **51**, 2499–2507.

25 J. Labille, C. Harns, J.-Y. Bottero and J. Brant, *Environ. Sci. Technol.*, 2015, **49**, 6608–6616.

26 A. Praetorius, J. Labille, M. Scheringer, A. Thill, K. Hungerbühler and J.-Y. Bottero, *Environ. Sci. Technol.*, 2014, **48**, 10690–10698.

27 J. T. K. Quik, M. C. Stuart, M. Wouterse, W. Peijnenburg, A. J. Hendriks and D. van de Meent, *Environ. Toxicol. Chem.*, 2012, **31**, 1019–1022.

28 O. Oriekhova, P. Le Coustumer and S. Stoll, *Colloids Surf., A*, 2017, **533**, 267–274.

29 F. Loosli, P. Le Coustumer and S. Stoll, *Environ. Sci.: Nano*, 2014, **1**, 154–160.

30 *Plastics-the Facts 2016*, An analysis of European plastics production, demand and waste data, Plastics Europe, 2016.

31 N. Chaukura, W. Gwenzi, T. Bunhu, D. T. Ruziwa and I. Pumure, *Resour., Conserv. Recycl.*, 2016, **107**, 157–165.

32 D. L. Kaplan, R. Hartenstein and J. Sutter, *Appl. Environ. Microbiol.*, 1979, **38**, 551–553.

33 O. Harush-Frenkel, M. Bivas-Benita, T. Nassar, C. Springer, Y. Sherman, A. Avital, Y. Altschuler, J. Borlak and S. Benita, *Toxicol. Appl. Pharmacol.*, 2010, **246**, 83–90.

34 P. Bhattacharya, S. Lin, J. P. Turner and P. C. Ke, *J. Phys. Chem. C*, 2010, **114**, 16556–16561.

35 D. L. Slomberg, P. Ollivier, O. Radakovitch, N. Baran, N. Sani-Kast, H. Miche, D. Borschneck, O. Grauby, A. Bruchet, M. Scheringer and J. Labille, *Environ. Chem.*, 2016, **13**, 804–815.

36 M. A. LeRoux, F. Guilak and L. A. Setton, *J. Biomed. Mater. Res.*, 1999, **47**, 46–53.

37 G. Metreveli, A. Philippe and G. E. Schaumann, *Sci. Total Environ.*, 2015, **535**, 35–44.

38 K. A. Huynh, J. M. McCaffery and K. L. Chen, *Environ. Sci. Technol.*, 2012, **46**, 5912–5920.

39 M. Elimelech, X. Jia, J. Gregory and R. Williams, *Particle deposition & aggregation: measurement, modelling and simulation*, Butterworth-Heinemann, 1998.

40 V. Filipe, A. Hawe and W. Jiskoot, *Pharm. Res.*, 2010, **27**, 796–810.

41 J. Buffle, K. J. Wilkinson, S. Stoll, M. Filella and J. Zhang, *Environ. Sci. Technol.*, 1998, **32**, 2887–2899.

42 R. Ferretti, S. Stoll, J. Zhang and J. Buffle, *J. Colloid Interface Sci.*, 2003, **266**, 328–338.

43 M. Baalousha, *Sci. Total Environ.*, 2009, **407**, 2093–2101.

44 S. M. Louie, E. R. Spielman-Sun, M. J. Small, R. D. Tilton and G. V. Lowry, *Environ. Sci. Technol.*, 2015, **49**, 2188–2198.

45 S. M. Louie, R. D. Tilton and G. V. Lowry, *Environ. Sci. Technol.*, 2013, **47**, 4245–4254.

46 J. Gregory, *Particles in water: properties and processes*, CRC Press, 2005.

47 A. R. Petosa, D. P. Jaisi, I. R. Quevedo, M. Elimelech and N. Tufenkji, *Environ. Sci. Technol.*, 2010, **44**, 6532–6549.

48 J. Gregory, *J. Colloid Interface Sci.*, 1973, **42**, 448–456.

Chapter VIII

Conclusions and perspectives

The wide usage of ENMs in variety industrial applications and everyday products has led to the release of those materials to the environment, in particular to the aquatic systems. The fate and behaviour of ENMs in the water body are defined by the intrinsic particle properties as well as by properties of surrounding media. Therefore, the goal of this thesis was to develop a mechanistic understanding of transformation processes of ENMs in various aquatic environments. In order to achieve this goal different types of materials and representative environmental media were used.

In Chapters III until VI, we concentrate our research on cerium dioxide (CeO_2) NPs. In Chapter III (Paper I) effect of different environmental factors such as water ionic composition, pH, presence of fulvic acid and dilution factors were investigated. CeO_2 NPs released to natural water interact with NOM and form CeO_2/NOM complexes. The outcome of the research showed that the way how those complexes are formed will influence the particle fate. Indeed, the gradual increase of FAs concentration led to the destabilisation of NPs and the formation of aggregates. However, the direct addition of FAs led to the formation of stable CeO_2/FA complexes. It was also shown that formed complexes are stable with time and not affected by variation of pH, low ionic strength and dilution.

Once the CeO_2/NOM complexes are formed it is of interest to investigate how they behave in natural water. Therefore, Chapter IV (Paper II) was dedicated to the investigation of the stability and the aggregation processes of uncoated and coated with FAs CeO_2 NPs in natural environmental conditions. The results showed the environmentally relevant concentration of FA stabilises CeO_2 NPs in ultrapure and in synthetic water. However, in natural Lake Geneva water, CeO_2 NPs were found aggregated regardless the concentration of FAs. Therefore, the presence of natural water compounds play a key role in the stabilisation of NPs in natural water. The stability of CeO_2 NPs coated with another type of NOM and stability of coating formed was investigated in Chapter V (Paper III). Alginate is a natural biopolymer which is widely used as a surrogate of natural polysaccharides. The stability of alginate coating around CeO_2 NPs was tested in changing pH, ionic strength and in natural water. Our results demonstrated that when coating is formed it is persistent with time and in changing pH. The concentration of alginate plays crucial role in CeO_2 stabilisation in ultrapure and in synthetic waters. In natural lake water heteroaggregation is observed, but is reduced by increasing the alginate concentration.

One class of components in natural water which affects the stability of nanoparticles is inorganic colloids. Heteroaggregation between CeO_2 NPs and Fe_2O_3 ICs in different environmental condition was thoroughly investigated in Chapter VI. We have found that no heteroaggregation is observed between NPs and ICs at low ionic strength due to the presence of electrostatic repulses. In synthetic and lake waters heteroaggregation is due to the modification of NP surface properties.

In Chapter VII (Paper IV and Paper V) the destabilisation of polystyrene micro- and nanoplastic particles in different conditions was investigated. The results indicate that particle surface properties, and more specifically the surface charge, define the affinity between plastics and water compounds. It was also shown that zeta potential measurements can be used to control the aggregation processes and to establish the optimal conditions to eliminate nano and micro particles from suspensions. The primary mechanism that is responsible for the particle destabilisation is charge neutralisation. It was also found that the aggregation rate of plastics in natural water is dependent on plastic concentration. Therefore, heteroaggregation will play an important role in the plastic environmental identity and removal from aquatic systems.

The research presented in this thesis showed that the stability of ENMs in environment is a complex problem and required interdisciplinary approach. In this thesis, we showed the effect of individual water compounds and their combinations on the stability of the selected ENMs and defined the mechanisms of ENM stabilisation and destabilisation. We also showed that behaviour of ENMs in synthetic water with representative composition of natural water is different from actual natural water. Reflecting the complexity of natural aquatic systems compared to artificial environmental conditions. Future researches should pay more attention to environmentally relevant experimental conditions such as low concentration of ENMs on the level of ng/L and µg/L, long-term behaviour of ENPs in natural water, where sedimentation and possible resuspension of ENPs occurred and simulated as in real environmental system. More work should be also done in the direction of the development of universal ENM stability model which takes into account heteroaggregation attachment and collision efficiencies – parameters that could be obtained during explicit experiments between different water compounds and ENMs. Regarding micro- and nanoplastic particles there is still a lot of issues to explore since this domain of research just started to develop. Some of the knowledge gained in the field of ENM stability could be transferred to the field of

nanoplastic stability in aquatic system, however, there are also differences regarding material properties, persistence in the environment and the effect on the leaving organisms. Until know most of the researches used model standard plastic particles which are easy to manipulate and understand regarding their transformation and interaction with other water components. In the future, plastic particles extracted from environment, particles which are used in products or aged particles should be used. The aging of plastic particles due to interactions with aquatic components or environmental factors and processes (UV, abrasion etc.) and the mechanisms of degradation of microplastic particles to nanoplastics are still unknown. One of the sources of micro- and nanoplastics to the environment is the municipal water treatment stations, therefore, the transformations of these particles in each step of the water treatment processes should be considered. Another direction of research is the development of the detection and identifications methods for nanoplastics in the environment. For the moment, it is laborious and manual process which introduces many artefacts. In addition, due to the transformation and aging of environmental nanoplastics such as coating with NOM successful detection, for example using Raman spectroscopy or FTIR analysis, is limited.

Annexes

Annex 1. Supporting information for the Chapter III

Annex 1.1. Effect of ionic strength

Influence of ionic strength on the CeO_2 NP aggregation.

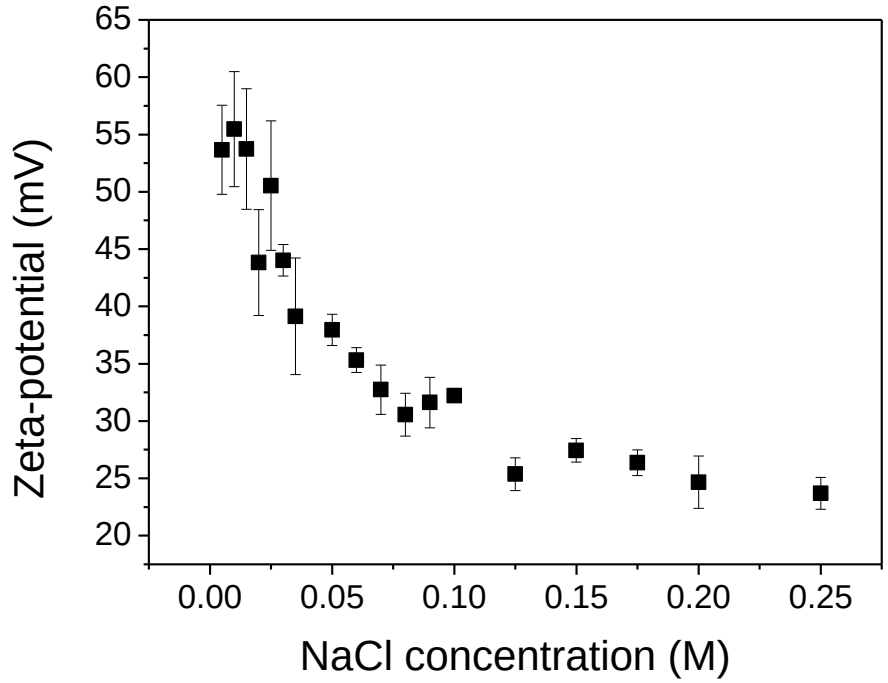

Fig. A1.1. Zeta potential of pristine CeO_2 NPs as a function of sodium chloride concentration. Zeta potential decrease with increase of ionic strength.

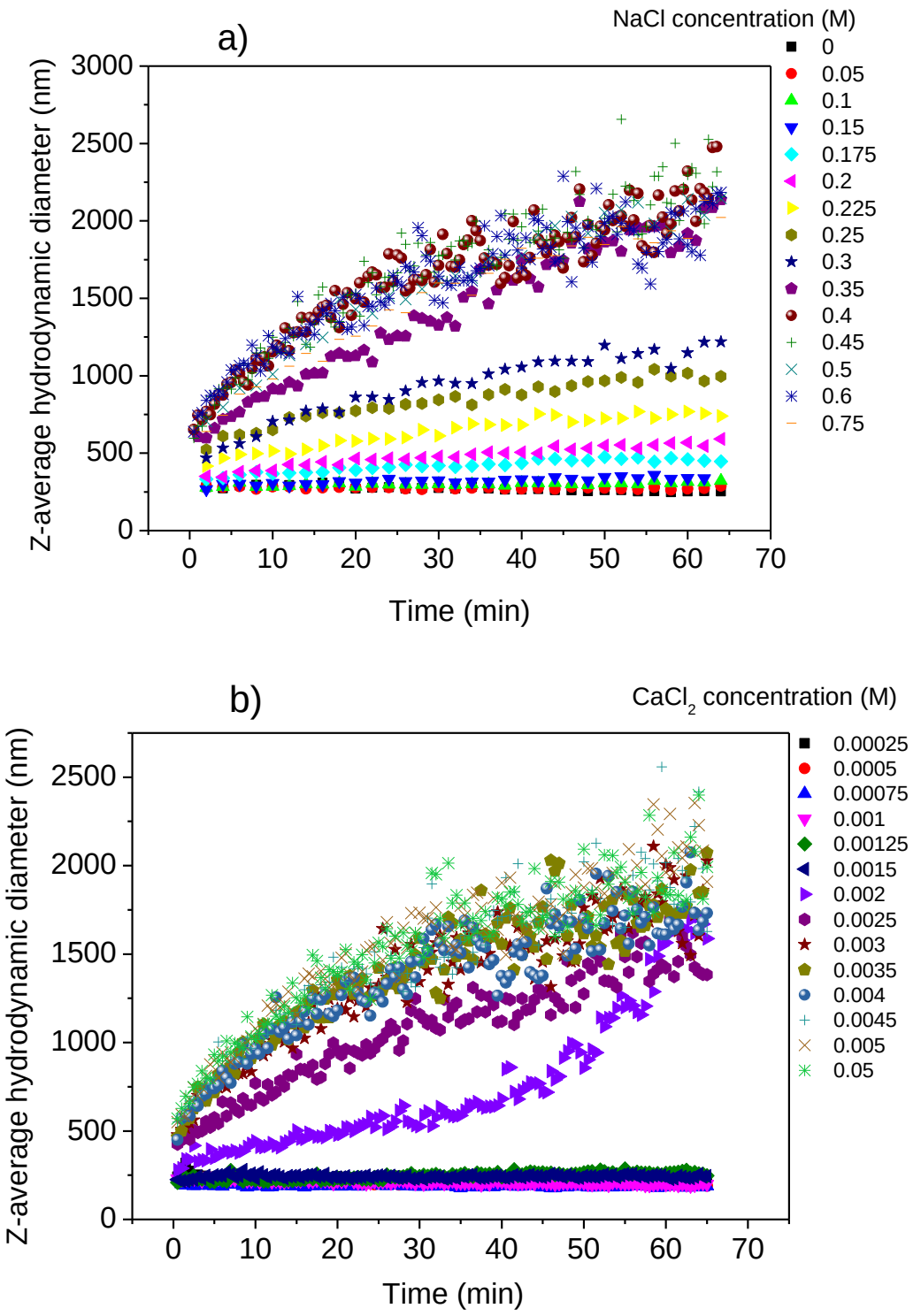

Fig. A1.2. Z-average hydrodynamic diameter variation of coated CeO_2 NPs as a function of electrolyte concentration: a) NaCl; b) $CaCl_2$. Experimental condition: [CeO_2] = 50 mg/L, [FAs] = 2 mg/L, pH = 8.0 ± 0.1.

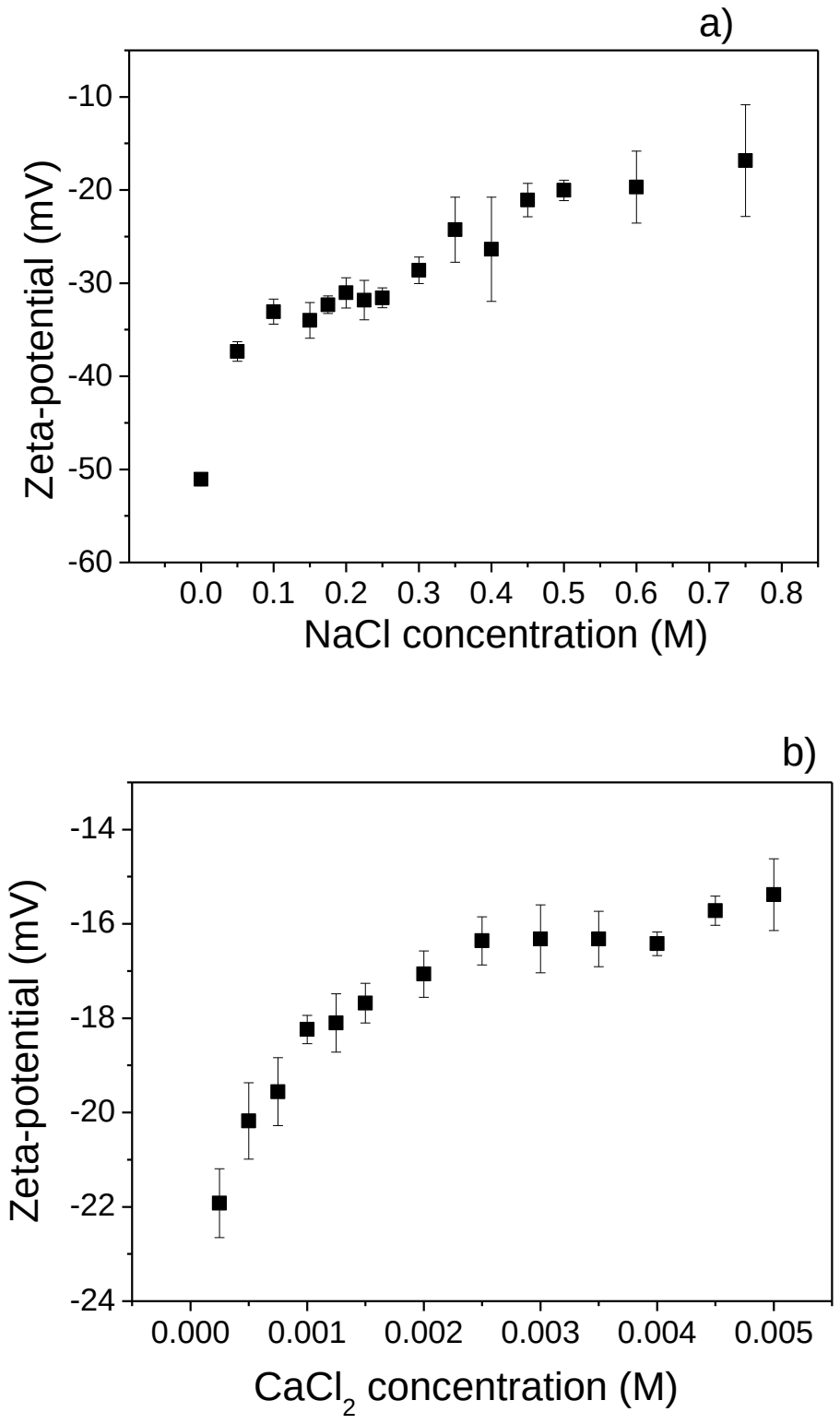

Fig. A1.3. Zeta potential of CeO_2/FAs complexes as a function of electrolyte concentration: a) NaCl; b) $CaCl_2$. Zeta potential increases with increase of ionic strength.

Calculation of ionic strength

To calculate ionic strength of NaCl and $CaCl_2$ solution next equation was used:

$$I = \frac{1}{2}\sum_{i=1}^{n} C_i z_i^2 \quad \text{(A5)}$$

where *C* is electrolyte molar concentration, M; *z* is ion valency; *n* is number of ions.

For uncoated CeO_2 NPs in NaCl solution, the CCC is equal to 0.11 ± 0.02 M, therefore according to equation (SI1) ionic strength is equal to 0.1 M.

For coated CeO_2 NPs in NaCl solution, the CCC = 0.39 ± 0.02 M, thus *I* = 0.4 M; for coated CeO_2 NPs in $CaCl_2$ solution, the CCC = 2.9 ± 0.3 mM, thus *I* = 9 mM.

For synthetic water ionic strength is taken from Table S2 and is equal to 3 mM.

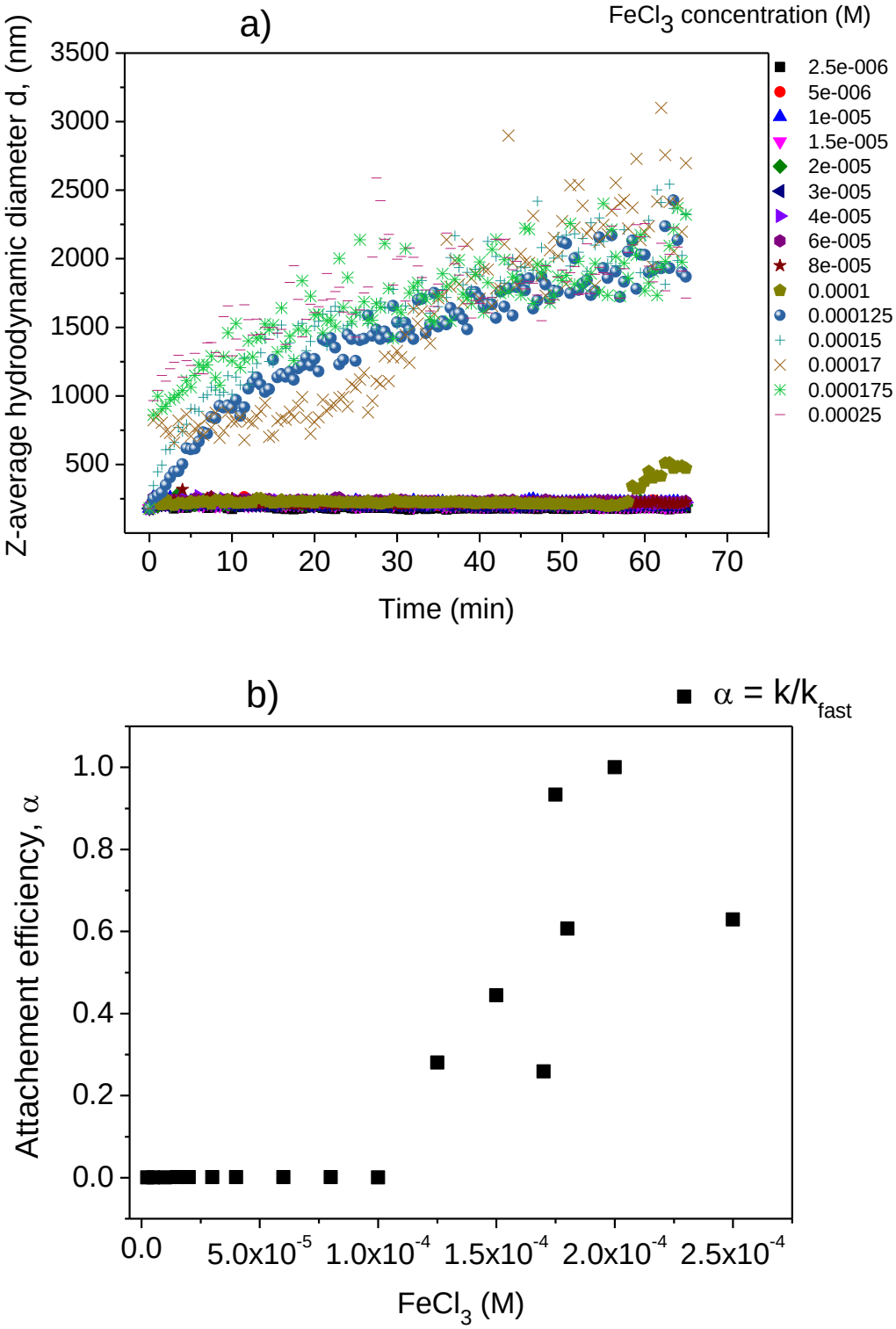

Fig. A1.4. (a) Z-average hydrodynamic diameter variation and (b) attachment efficiency of coated CeO_2 NPs as a function of iron chloride concentration. Experimental condition: [CeO_2] = 50 mg/L, [FAs] = 2 mg/L, pH = 8.0 ± 0.1.

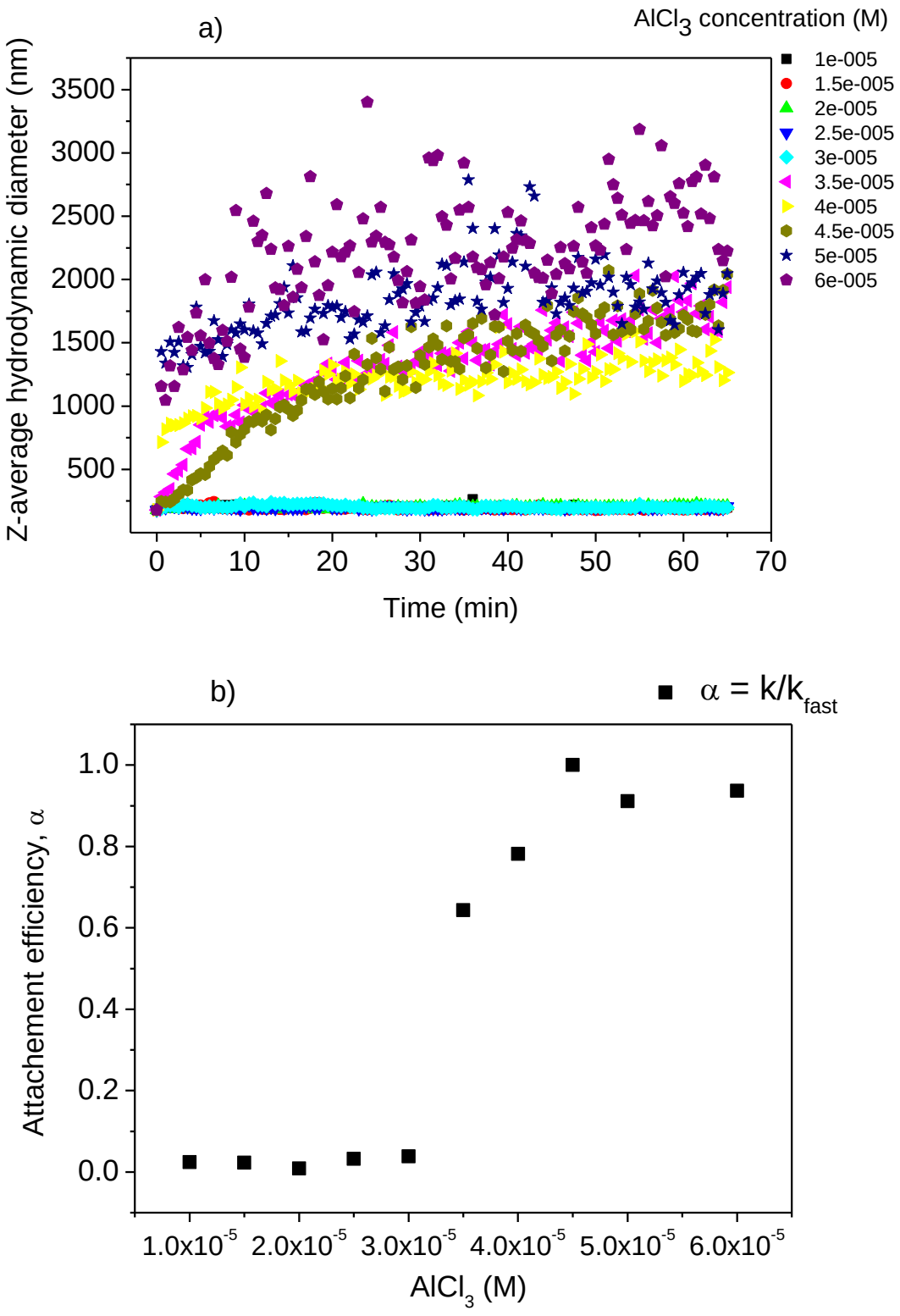

Fig. A1.5. (a) Z-average hydrodynamic diameter variation and (b) attachment efficiency of coated CeO_2 NPs as a function of aluminum chloride concentration. Experimental condition: [CeO_2] = 50 mg/L, [FAs] = 2 mg/L, pH = 8.0 ± 0.1.

Annex 1.2. Supporting information for Paper I

Introduction

The aim of this section is to provide additional information about preparation of nanoparticle suspension and supplementary materials that was not included in main text of manuscript.

The cerium(IV) oxide nanoparticles dispersion protocol

Uncoated cerium(IV) oxide (CeO_2) nanoparticles (NPs) (NM-212) was kindly provided from the JRC Nanomaterials repository, NanoMILE FP7 project.

First, we prepared the initial CeO_2 suspension with concentration 1 g L^{-1}. For further experiments initial suspension was diluted to obtain the suspension with concentration 50 mg L^{-1}. The pH was adjusted to pH 3.0 ± 0.1 to avoid the nanoparticle aggregation during the storage process.

Materials and equipment

- NP's powder;
- previously prepared deionized water at pH 3.0 ± 0.1 (deionized acid water);
- tube 50 ml and flask, which volume depends on the desired quantity of suspension;
- beaker with cooled water;
- spatula;
- pipettes;
- balance;
- ultrasonic bath (Brainson 5510, frequency 40 kHz);
- ultrasonic probe (Sonics Vibra cell, probe model CV18, Blanc Labo S.A., Switzerland).

Methods

Weigh 50 mg of CeO_2 powder in a tube of 50 ml. Wet the powder with prepared deionized acid water in order to create a thick paste. Next, fill the tube with deionized acid water until you reach 50 ml. Mix the suspension.

Put the tube with suspension in the beaker with cooled water and then place the beaker in the ultrasonic apparatus. The probe should be in the suspension, but does not reach the bottom.

Next parameters were used during the sonication process:

- ultrasonic processors – 130 Watt;
- resonance frequency of probe – 20 kHz;
- amplitude – 75 %;
- sonication time – 15 min.

Let the sample to settle down one hour, then diluted suspension can be prepared. The samples should be stored in the fridge (at about 4 °C). Before using them again, sonication should be made about 5 min in a bath sonicator.

An aliquot of initial suspension of 1 g L^{-1} was taken to prepare the diluted suspension of 50 mg L^{-1} using deionized acid or basic water depending on the desired pH

of suspension. Ionic strength was adjusted by diluted NaCl solution to obtain final concentration of NaCl 10^{-3} M. We worked with suspensions, which pHs were 3.0 ± 0.1 and 10.0 ± 0.1. Then, the sonication in the bath during 5 min should be made. Samples should be stored in the fridge and every time before carrying out the experiments we made the sample sonication in the bath (5 min).

To create this protocol we used the dispersion protocol provided by JRC and next sources of literature (Rasmussen et al., 2013; Singh et al., 2011; Taurozzi et al., 2013).

References

Rasmussen, K., Mech, A., Mast, J., De Temmerman, P.-J., Waegeneers, N., Van Steen, F., Pizzolon Jean, C., De Temmerman, L., Van Doren, E., Jensen Keld, A., 2013. Synthetic amorphous silicon dioxide (NM-200, NM-201, NM-202, NM-203, NM-204): Characterisation and physico-chemical properties. European Commission Joint Research Centre, Luxembourg: Publications Office of the European Union.

Singh, C., Friedrichs, S., Levin, M., Birkedal, R., Jensen, K.A., Pojana, G., Wohlleben, W., Schulte, S., Wiench, K., Turney, T., 2011. NM-series of representative manufactured nanomaterials: zinc oxide NM-110, NM-111, NM-112, NM-113. Characterisation and test item preparation. European Commission Joint Research Centre, Luxembourg: Publications Office of the European Union.

Taurozzi, J.S., Hackley, V.A., Wiesner, M.R., 2013. Preparation of nanoparticle dispersions from powdered material using ultrasonic disruption. National Institute of Standards and Technology.

Fulvic acids characterisation

Fulvic acids titration

The Suwannee River Fulvic acids (FAs) (Standard II, 2S101F) were purchased from International Humic Substance Society, USA. First, a 1 g L^{-1} stock solution was prepared and then diluted to 50 mg L^{-1} with addition of NaCl as background electrolyte with concentration 0.001 M. This solution at pH 3.0 ± 0.1 was titrated with diluted 0.01 M NaOH solution.

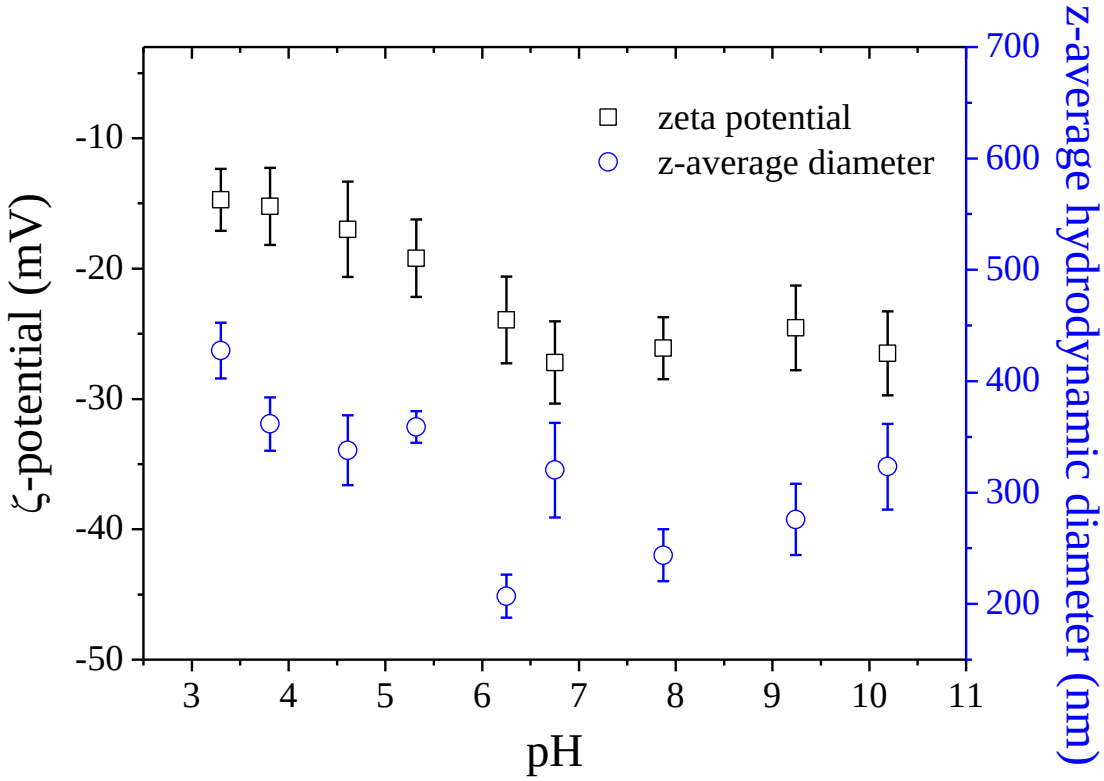

Fig. A1.6. FAs zeta potential and z-average hydrodynamic diameter variation as a function of pH. Surface charges of FAs are negative in all pH range. Z-average hydrodynamic diameter varies from 200 to 400 nm.

Size distribution of fulvic acids molecules

A 1 g L^{-1} stock solution of FAs was used to define the size distribution using NTA method. The pH was adjusted to 3.0 ± 0.1.

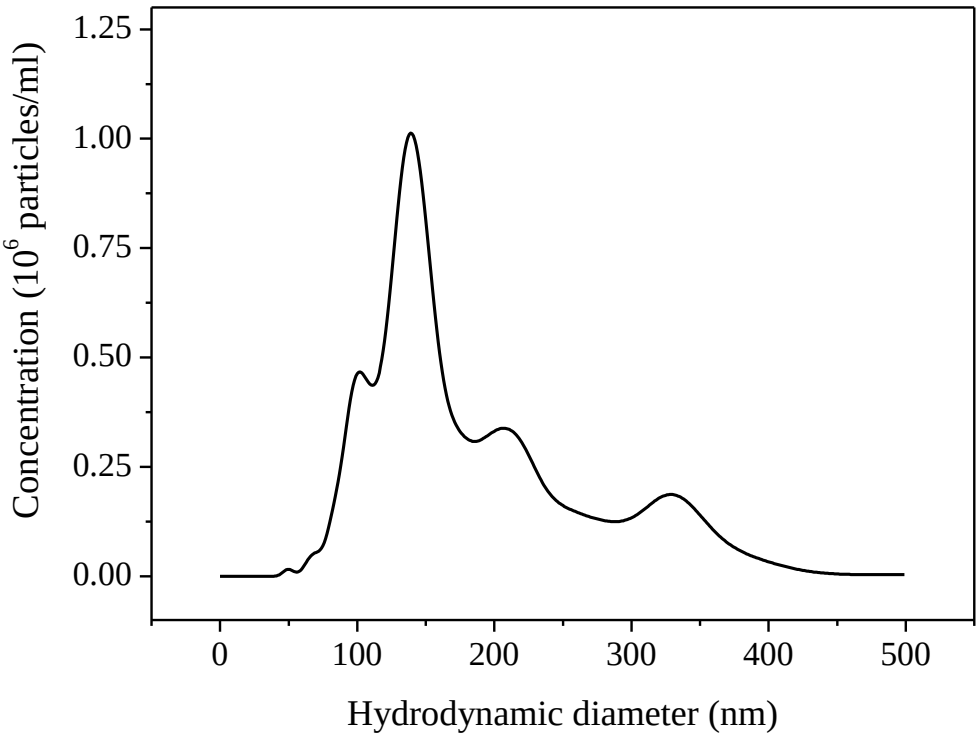

Fig. A1.7. FAs size distribution using NTA method. Average hydrodynamic diameter was found equal to 194 ± 89 nm. We observed the presence of polydispersed particles.

CeO_2 NPs characterisation

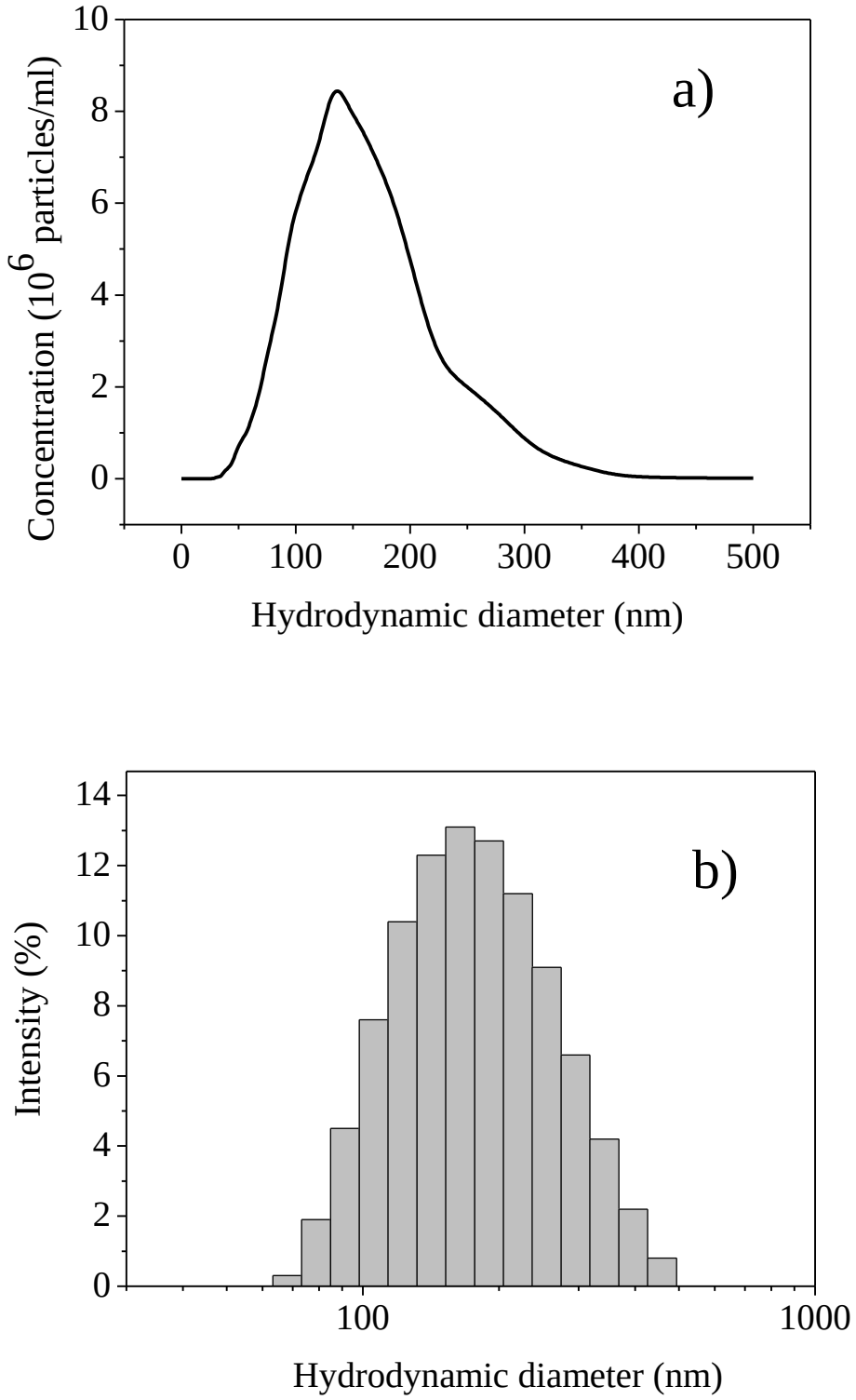

Fig. A1.8. Size distribution of CeO_2 NPs using two methods NTA (a) and DLS (b). Z-average diameter and hydrodynamic diameter were equal to 185 ± 75 nm (DLS) and 177 ± 83 nm (NTA). A good agreement was found between the two methods indicating that individual CeO_2 NPs are forming aggregates.

Annex 2. Supporting information for the Chapter IV

Supplementary data for the Paper II

A2.SI1. Preparation of synthetic Lake Geneva water.

According to (Smith et al., 2002) to synthesize natural freshwater, first, the composition of freshwater should be define then, charge balance of all ions should be established and finally the final concentration of all electrolytes calculated. We decided prepare three stock solutions with compatible combination of salts. And then we mixed the appropriate volumes of these solutions to obtain one final solution of required composition. Only $CaCO_3$ was directly added as a powder to the mixture of solutions (Hammes et al., 2013). We tried to avoid the salts with low solubility as they can precipitate from solution. In Tables A2.1 and A2.2 the ion charge balance and final salt concentration are presented.

Table A2.1
Charge balance of ions used for preparation of synthetic fresh water

Ions	mg L^{-1}	M, g mol^{-1}	n, mmole	n1, µmole	n1', µmole	µeq	adjusted
Na^+	6.42	23	0.28	279.13	279	279	250
Ca^{2+}	45.3	40	1.13	1132.5	1133	2266	1800
Mg^{2+}	6.16	24	0.26	256.67	257	514	400
K^+	1.57	39	0.040	40.26	40	40	60
				Sum	1709	3099	**2510**
Cl^-	9.13	35.5	0.26	257.18	257	257	540
$SO4^{2-}$	47.71	96	0.50	496.98	497	994	1420
NO^{3-}	0.61	62	0.0098	9.84	10	10	40
$CO3^{2-}$	46.7	60	0.78	778.33	778	1556	510
				Sum	1542	2817	**2510**

Table A2.2

Final concentration of electrolytes used for preparation of synthetic fresh water. Ionic strength of synthetic water is equal to 2.5 mM

Electrolytes	**Final required concentration, mg L^{-1}**					**In 1L**
S1	n2, μeq	Cations	Anions	Sum	M of hydrate	m, mg
$CaCl_2*6H_2O$	180	3.6	6.39	9.99	219	19.71
$MgCl_2*6H_2O$	360	4.32	12.78	17.1	203	36.54
$Mg(NO_3)_2*6H_2O$	40	0.48	2.48	2.96	256	5.12
S2						
$CaSO_4*2H_2O$	1420	28.4	56.8	85.2	172	107.75
S3						
$CaCO_3$	200	4	6	10		10
S4						
$NaHCO_3$	250	5.75	15.25	21		21
$KHCO_3$	60	2.34	3.66	6		6

The calculation of FAs concentration that should be added to synthetic water and which corresponds to the environmental value was done in following way. DOC in the Lake Geneva water varies from 0.95 to 1.15 mg L^{-1} (Table 1 (from Paper II) and Table A2.4). According to Frimmel and Abbt-Braun (1999) FAs in surface water contain from 25 to 55 % of DOC. If we consider that around 50% of DOC is present as FAs then we have to introduce 1.9 to 2.3 mg L^{-1} FAs to our solution. We chose the value equal to 2 mg L^{-1}.

A2.SI2. Characterisation of Lake Geneva water

Chromatographic analysis was performed to define the water ions composition using a Dionex ICS-3000 analyzer. The cations were run through an IonPac CS12 column and eluded with an isocratic concentration of methane sulfonic acid and water, meanwhile anions were run through an IonPac AS19 column and eluded with KOH. A certified water reference material Ontario-99 from the National Water Research Institute (Canada) was used to verify the accuracy of the measurements. All the reference material results were within the acceptance range of the certificate.

Table A2.3
Physicochemical parameters of Lake Geneva water (Mai 2015)

Parameters	**Value**
pH	8.2 ± 0.1
Conductivity, µSm cm^{-1}	298.3 ± 0.6
Oxygen, %	107 ± 0.2
Alkalinity, mg L^{-1} of $CaCO_3$	90 ± 1

Table A2.4
Major ion composition of Lake Geneva water

Name of element	**Unit**	**Value**	**SD**
Dissolved organic carbon	mg C L^{-1}	1.13	0.24
Nitrate, NO_3^{2-}	mg N L^{-1}	1.20	0.35
Sodium Na^+	mg L^{-1}	6.26	0.13
Potassium K^+	mg L^{-1}	1.63	0.13
Calcium Ca^{2+}	mg L^{-1}	44.65	1.21
Magnesium Mg^{2+}	mg L^{-1}	5.40	1.02
Sulfate SO_4^{2-}	mg L^{-1}	47.7	0.6
Phosphate PO_4^{3-}	mg P L^{-1}	0.26	0.19

Table A2.5

Elemental composition obtained during SEM imaging from EDS analysis of the CeO_2 NPs in Lake Geneva water

Element	Energy (keV)	Weight, %	Sigma	Atomic, %
Na-K	1.041	0.42	0.02	0.54
Mg-K	1.253	0.35	0.02	0.44
Si-K	1.739	87.48	0.13	93.70
S-K	2.307	0.86	0.02	0.81
Cl-K	2.621	0.88	0.02	0.74
Ca-K	3.690	3.45	0.05	2.59
Ce-L	4.837	2.75	0.10	0.59
Pt-M	2.048	3.82	0.12	0.59
Total		100.00		100.00

References

Frimmel, F.H., Abbt-Braun, G., 1999. Basic characterisation of reference NOM from Central Europe — Similarities and differences. Environ. Int., Nom-typing 25, 191–207. doi:10.1016/S0160-4120(98)00116-0

Hammes, J., Gallego-Urrea, J.A., Hassellöv, M., 2013. Geographically distributed classification of surface water chemical parameters influencing fate and behavior of nanoparticles and colloid facilitated contaminant transport. Water Res.

Smith, E.J., Davison, W., Hamilton-Taylor, J., 2002. Methods for preparing synthetic freshwaters. Water Res. 36, 1286–1296. doi:10.1016/S0043-1354(01)00341-4

Annex 3. Supporting information for the Chapter V

Supplementary data for the Paper III

Characterisation of Lake Geneva water

Table A3.1. Physicochemical parameters of Lake Geneva water (10.11.2015).

Parameters	Value
pH	8.0 ± 0.1
Conductivity, µSm/cm	270 ± 1
Oxygen, mg/L	10.8 ± 0.2
Alkalinity, mgL–1 of $CaCO_3$	90 ± 1
Temperature, °C	14.0 ± 0.2

Alginate characterisation

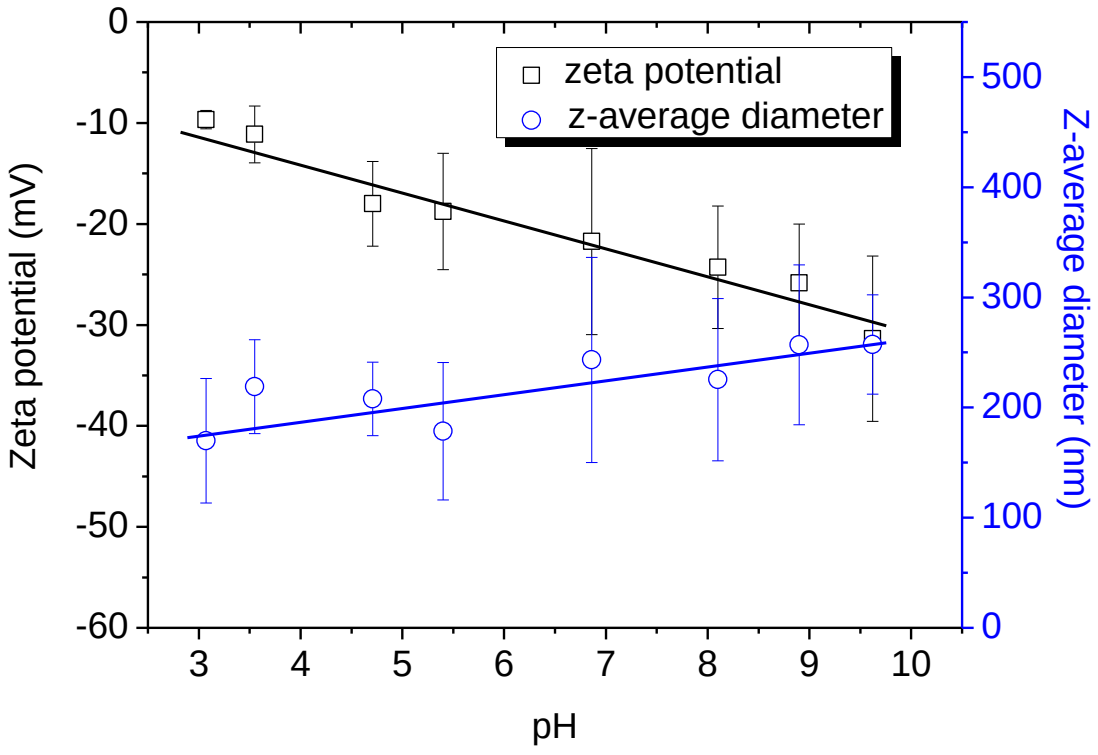

Fig. A3.1. Alginate zeta potential and z-average hydrodynamic diameter variation as a function of pH increase. Zeta potential is negative in all pH range. Z-average diameters vary from 150 to 250 nm. [Alginate] = 50 mg/L.

CeO_2 MNP characterisation

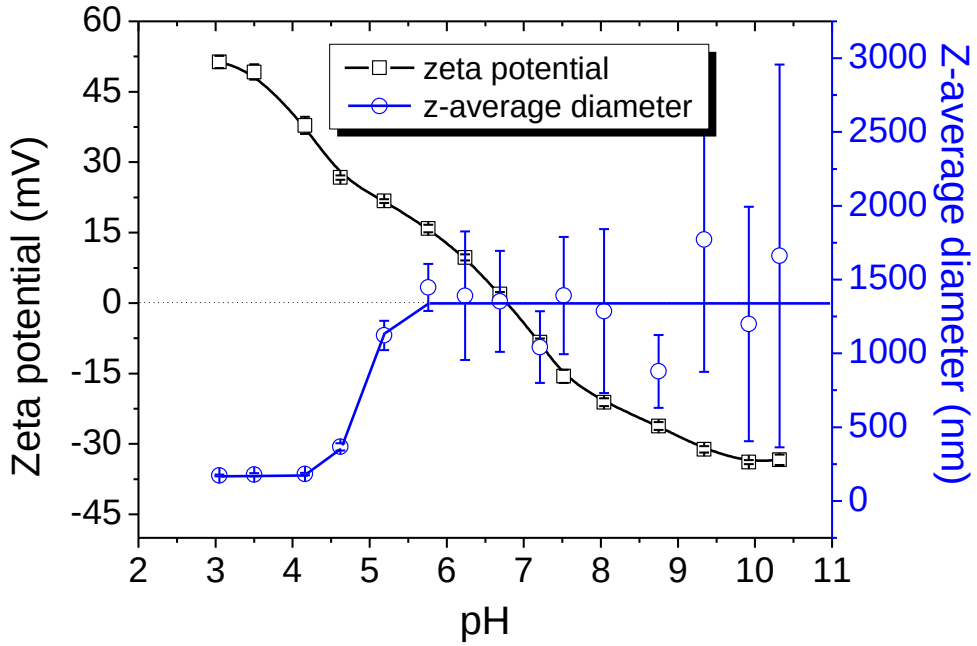

Fig. A3.2. Zeta potential and z-average hydrodynamic diameter variation of CeO_2 MNPs as a function of pH increase. In acid environment CeO_2 MNPs are positively charged whereas in alkaline environment they are negatively charged. The pH_{PZC} is found equal to 6.8 ± 0.1. Below pH 4.5 ± 0.1 nanoparticles are stable with z-average diameters less than 200 nm. [CeO_2] = 50 mg/L.

Behavior of coated and uncoated CeO_2 MNPs in filtered Lake Geneva water

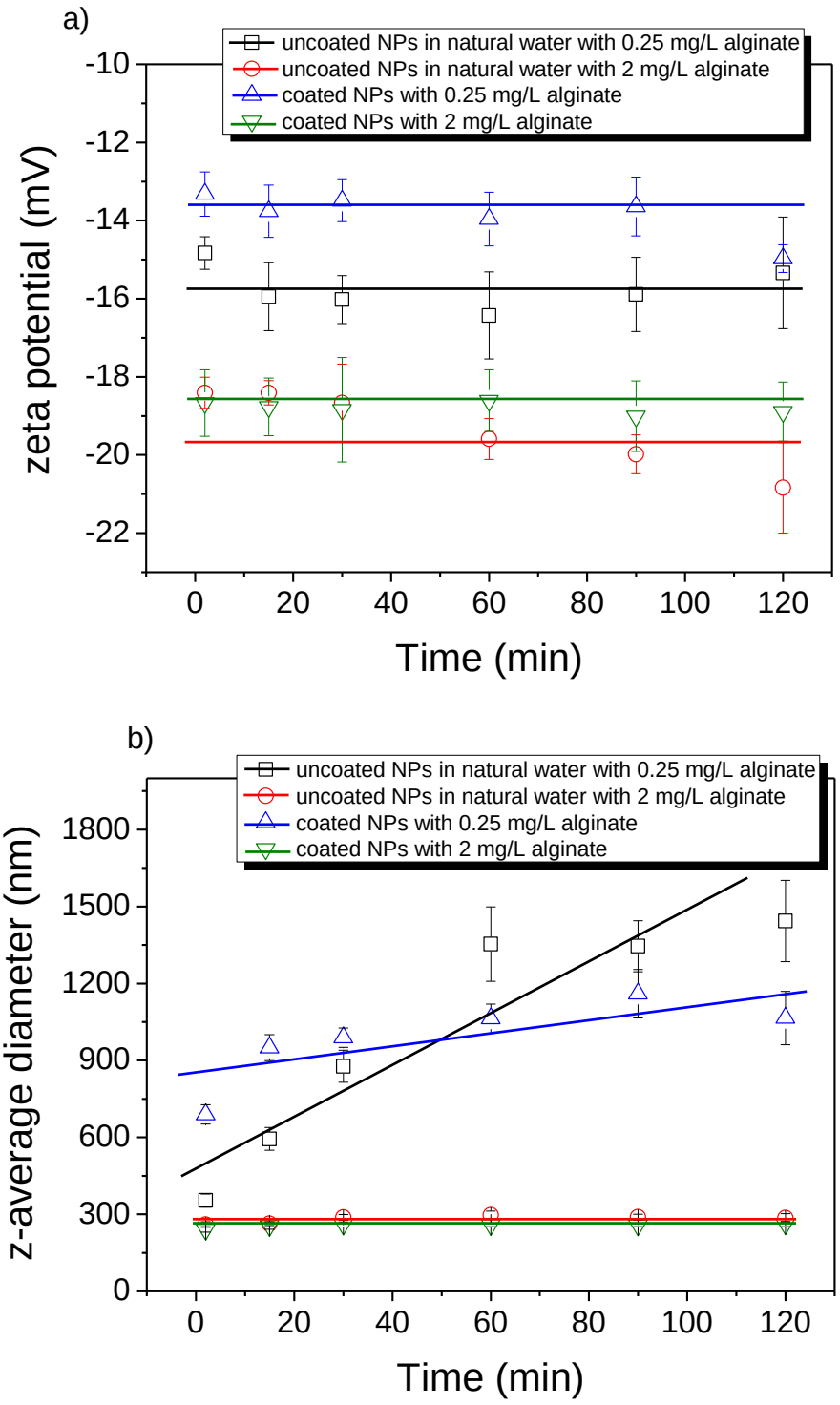

Fig. A3.3. Time variation of (a) zeta potentials and (b) z-average hydrodynamic diameters of uncoated and coated with various concentration of alginate CeO_2 MNPs in filtered water from Lake Geneva.

Annex 4. Supporting information for the Chapter VI

A4.1 Characterisation of Lake Geneva water

Chromatographic analysis was performed to define the water ions composition using a Dionex ICS-3000 analyzer. The Cations were run through an IonPac CS12 column and eluded with an isocratic concentration of methane sulfonic acid and water, meanwhile anions were run through an IonPac AS19 column and eluded with KOH. A certified water reference material Ontario-99 from the National Water Research Institute (Canada) was used to verify the accuracy of the measurements. All the reference material results were within the acceptance range of the certificate.

Table A4.1. Physicochemical parameters of Lake Geneva water (July 2016)

Parameters	**Value**
pH	8.6 ± 0.1
Conductivity, µSm/cm	285 ± 1
Oxygen, mg/L	9.8 ± 0.2
Saturation by oxygen, %	115
Redox potential, mV	192 ± 3
Alkalinity, mgL–1 of $CaCO_3$	90 ± 1
Temperature, °C	22.2 ± 0.2

Table A4.2. Major ion composition of Lake Geneva water

Name of element	**Unit**	**Value**	**SD**
Dissolved organic carbon	mg CL^{-1}	1.13	0.24
Nitrate, NO_3^{2-}	mg NL^{-1}	1.20	0.35
Sodium Na^+	mgL^{-1}	6.26	0.13
Potassium K^+	mgL^{-1}	1.63	0.13
Calcium Ca^{2+}	mgL^{-1}	44.65	1.21
Magnesium Mg^{2+}	mgL^{-1}	5.40	1.02
Sulfate SO_4^{2-}	mgL^{-1}	47.7	0.6
Phosphate PO_4^{3-}	mg PL^{-1}	0.26	0.19

A4.2 Characterisation of NPs, ICs and NOM

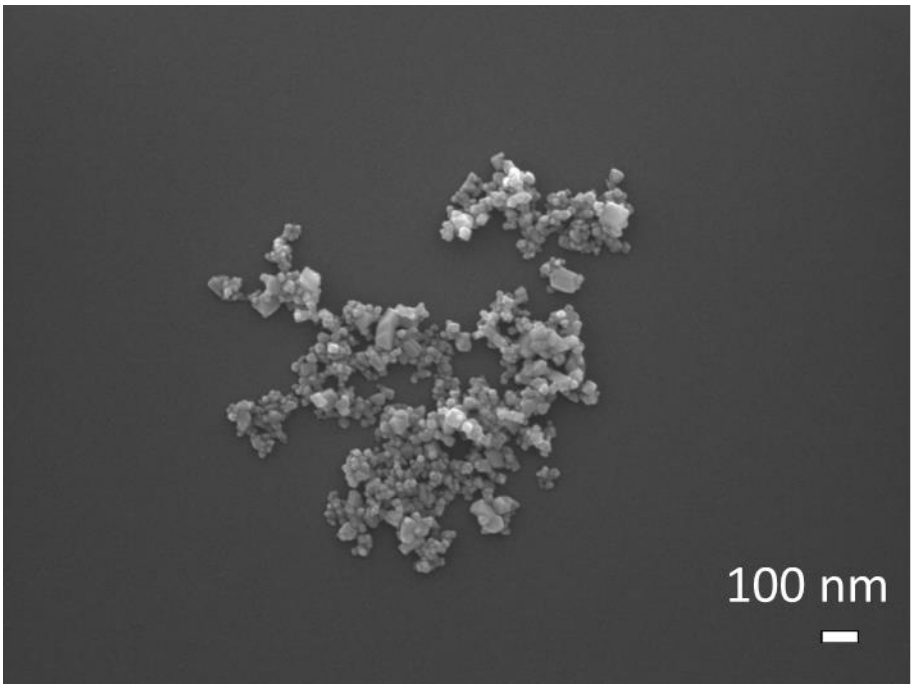

Fig. A4.1. SEM image of pristine CeO_2 NPs in ultrapure water. [CeO_2] = 10 mg/L.

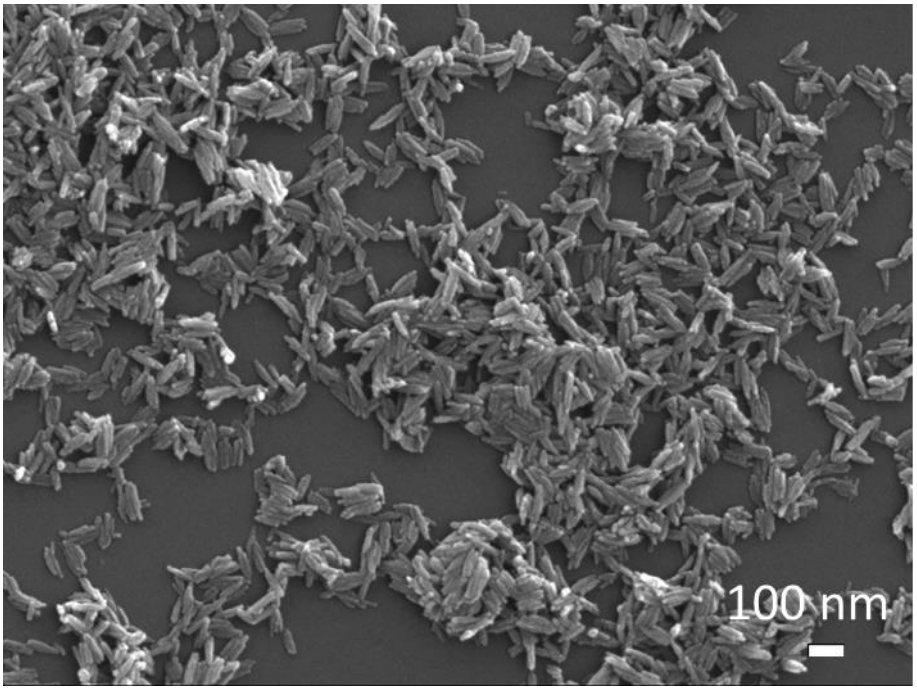

Fig. A4.2. SEM image of pristine Fe_2O_3 ICs in ultrapure water. [Fe_2O_3] = 10 mg/L.

Table A4.3. Characterisation analysis of Fe_2O_3 provided by manufacturer

Parameters	**Value**
Appearance	Red powder
pH value	6.7
Crystal	α
Original particle size, nm	30-50nm
Surface area, m^2/g	28
Purity, %	99.2

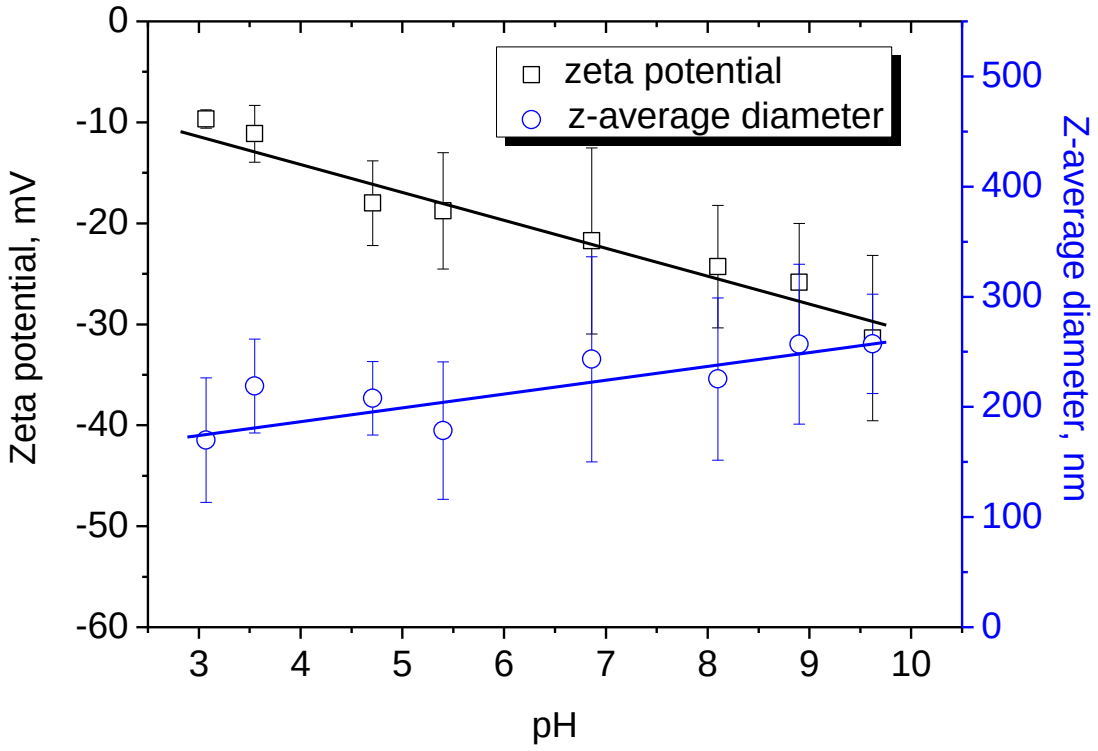

Fig. A4.3. Alginate zeta potential and z-average hydrodynamic diameter variation as a function of pH increase. Zeta potential is negative in all pH range. Z-average diameters vary from 150 to 250 nm. [Alginate] = 50 mg/L.

A4.3 Aggregation kinetics experiments

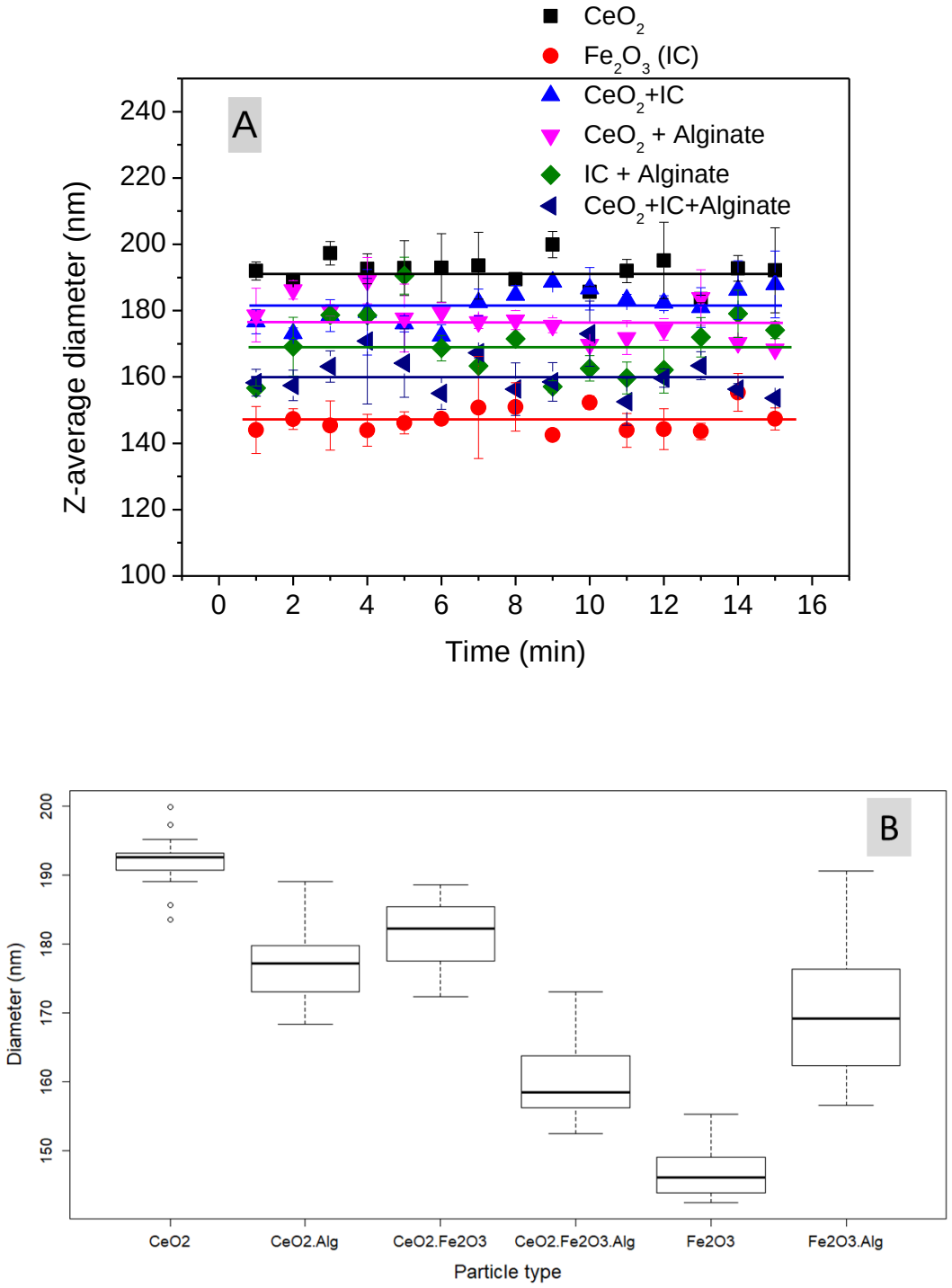

Fig. A4.4. (A) Z-average hydrodynamic diameters of CeO_2 NPs in varied conditions: in the presence of inorganic colloids and alginate at pH > pH_{PZC} in ultrapure water. (B) The boxplot of particle diameters versus type of particles. No interactions between NPs, IC and alginate is observed. Experimental conditions: pH 8.0 ± 0.2, [CeO_2] = 50 mg/L [Fe_2O_3] = 5 mg/L, [Alginate] = 0.25 mg/L.

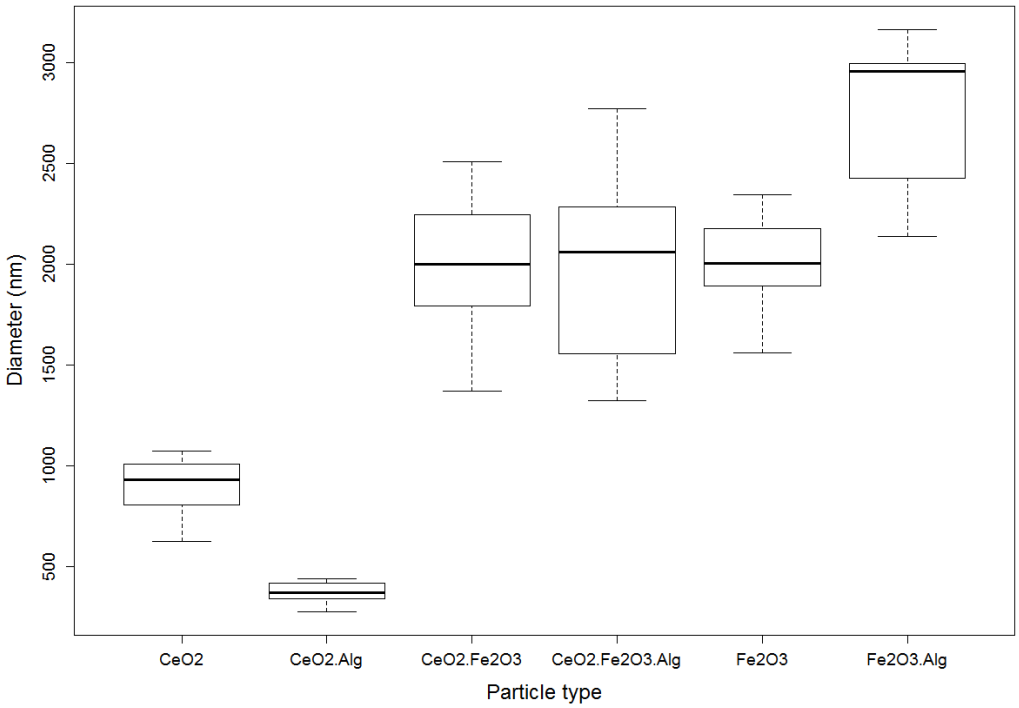

Fig. A4.5. The boxplot of particle z-average hydrodynamic diameters versus type of particles in Lake Geneva water. Experimental conditions: pH 8.0 ± 0.2, [CeO_2] = 50 mg/L [Fe_2O_3] = 5 mg/L, [Alginate] = 0.25 mg/L.

A4.4 Effect of alginate concentration on heteroaggregation

Table A4.4. Zeta potential of the mixture CeO_2 NPs + Fe_2O_3 ICs in varied alginate concentration in different water samples (pH 8.0 ± 0.2)

Alginate concentration, mg/L	Type of water		
	Ultrapure	Lake Geneva	Synthetic (Ca^{2+}/Mg^{2+})
0	-34.3 ± 1.4	-10.8 ± 0.4	-2.7 ± 0.3
0.25	-36.9 ± 2.1	-13.8 ± 0.5	-9.9 ± 0.4
2	–	-19.6 ± 0.3	-21.1 ± 0.5

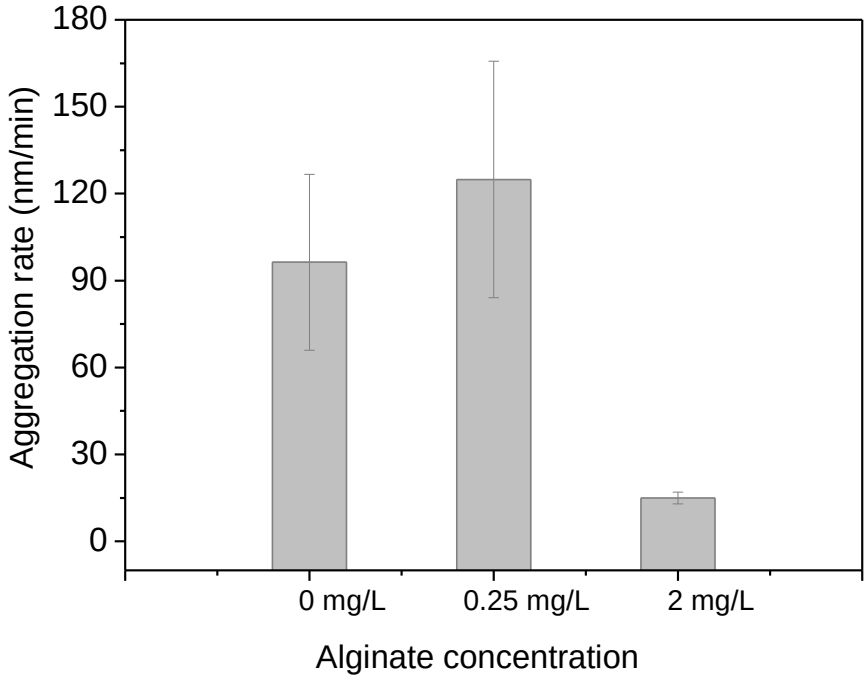

Fig.A4.6. Aggregation rate of the mixture CeO_2 + Fe_2O_3 in increasing alginate concentration in Lake Geneva water. Experimental conditions: [CeO_2] = 50 mg/L [Fe_2O_3] = 5 mg/L, [Alginate] = 0, 0.25 and 2 mg/L.

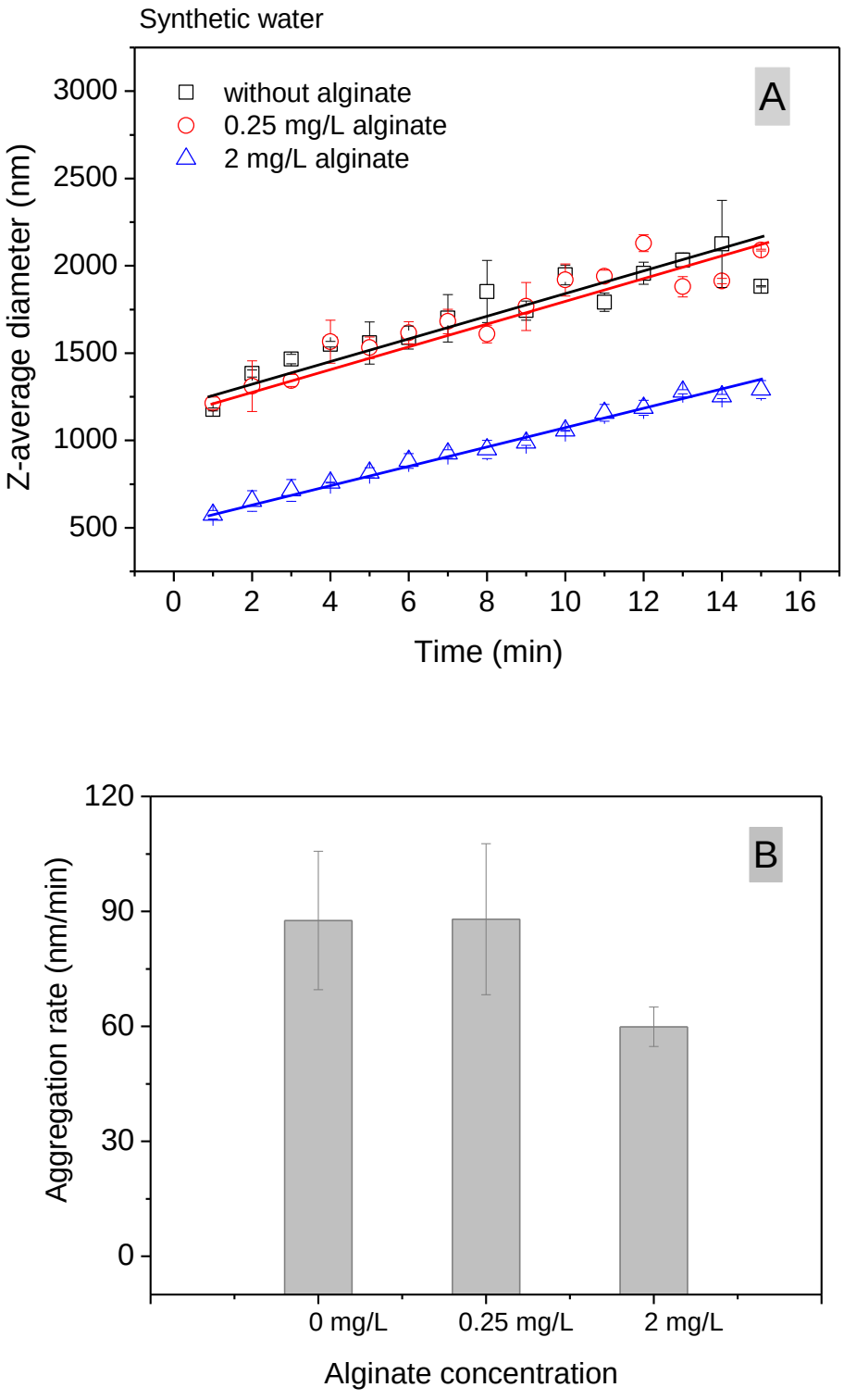

Fig. A4.7. (A) Time variation of z-average hydrodynamic diameters and (B) aggregation rate of the mixture of CeO_2 + Fe_2O_3 in synthetic water which mimic the ionic composition (Ca^{2+}/Mg^{2+}) of lake water in increasing alginate concentration. Experimental conditions: pH 8.0 ± 0.2, [CeO_2] = 50 mg/L [Fe_2O_3] = 5 mg/L, [Alginate] = 0, 0.25 and 2 mg/L. The aggregation rate decreases for the alginate concentration equals to 2 mg/L.

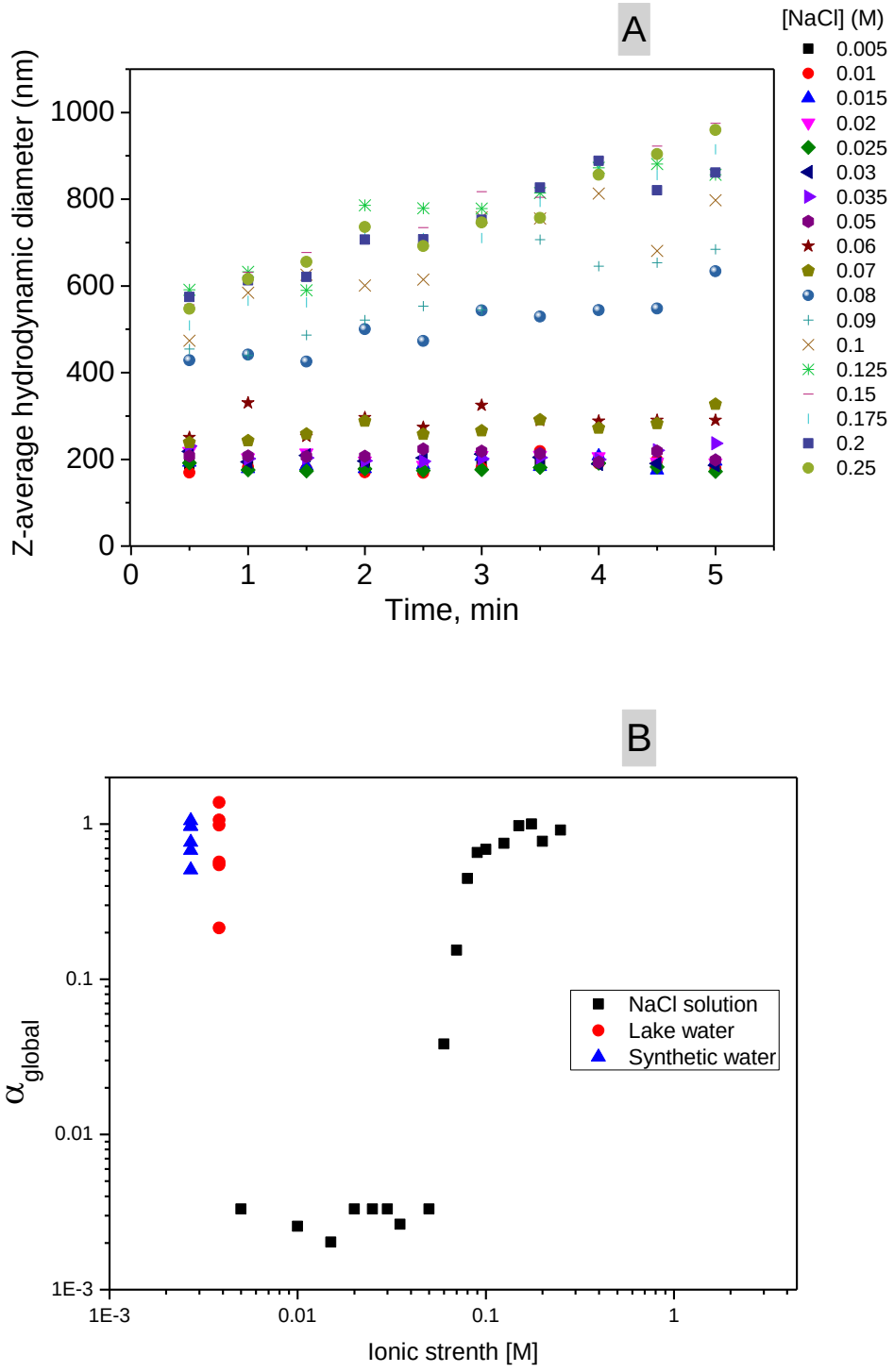

Fig. A4.8. (A) Z-average hydrodynamic diameter variation during 5 min of uncoated CeO_2 NPs as a function of salt concentration. Kinetics of aggregation is enhanced by increasing the ionic strength of the CeO_2 dispersion. (B) The attachment efficiency during homoaggregation (α_{homo}) in NaCl solution in comparison to α_{global} in synthetic and lake waters. Z-average hydrodynamic diameters increase with time and with increase of NaCl concentrations.

References

Chen, Kai Loon, Steven E. Mylon, et Menachem Elimelech. 2006. « Aggregation kinetics of alginate-coated hematite nanoparticles in monovalent and divalent electrolytes ». *Environmental Science & Technology* 40 (5): 1516‑23.

Metreveli, George, Allan Philippe, et Gabriele E. Schaumann. 2015. « Disaggregation of silver nanoparticle homoaggregates in a river water matrix ». *Science of The Total Environment*, Special Issue: Engineered nanoparticles in soils and waters, 535 (décembre): 35‑44. doi:10.1016/j.scitotenv.2014.11.058.

Annex 5. Supporting information for the ChapterVII

Electronic supplementary information for the PaperV

A5.SI1. Characterisation of water from river Rhône

Chromatographic analysis was performed to define the water ion composition using a Dionex ICS-3000 analyzer. Samples were run through an IoMNPac CS12 column to elude the cations with an isocratic concentration of methane sulfonic acid and water, meanwhile to elude the anions with KOH, the same samples were run through an IoMNPac AS19 column. A certified water reference material Ontario-99 from the National Water Research Institute (Canada) was used to verify the accuracy of the measurements. All the reference material results were within the acceptance range of the certificate.

Table A5.1 Physicochemical parameters of water from river Rhône (08.05.2017)

Parameters	**Value**
pH	7.9 ± 0.1
Conductivity, µSm/cm	302 ± 1
Oxygen, mg/L	10.4 ± 0.2
Alkalinity, mg/L of $CaCO_3$	88 ± 1
Temperature, °C	9.4 ± 0.2
Dissolved organic carbon, mg C/L	0.72 ± 0.1

Table A5.2 Major ion composition of water from river Rhône obtain using ionic chromatography

Name of element	**Unit**	**Value**	**SD**
Sodium Na^+	mg/L	6.73	0.13
Potassium K^+	mg/L	1.6	0.05
Magnesium Mg^{2+}	mg/L	5.68	0.39
Calcium Ca^{2+}	mg/L	42.33	0.32
Fluoride, F^-	mg/L	0.077	0.001
Chloride, Cl^-	mg/L	9.83	0.01
Bromide, Br^-	mg/L	0.0323	0.0003
Sulfate SO_4^{2-}	mg/L	44.71	0.06
Nitrate, NO_3^{2-}	mg/L	2.23	0.05

A5.SI2. Kinetic of aggregation between PS nanoplastics and Fe_2O_3 in ultrapure water

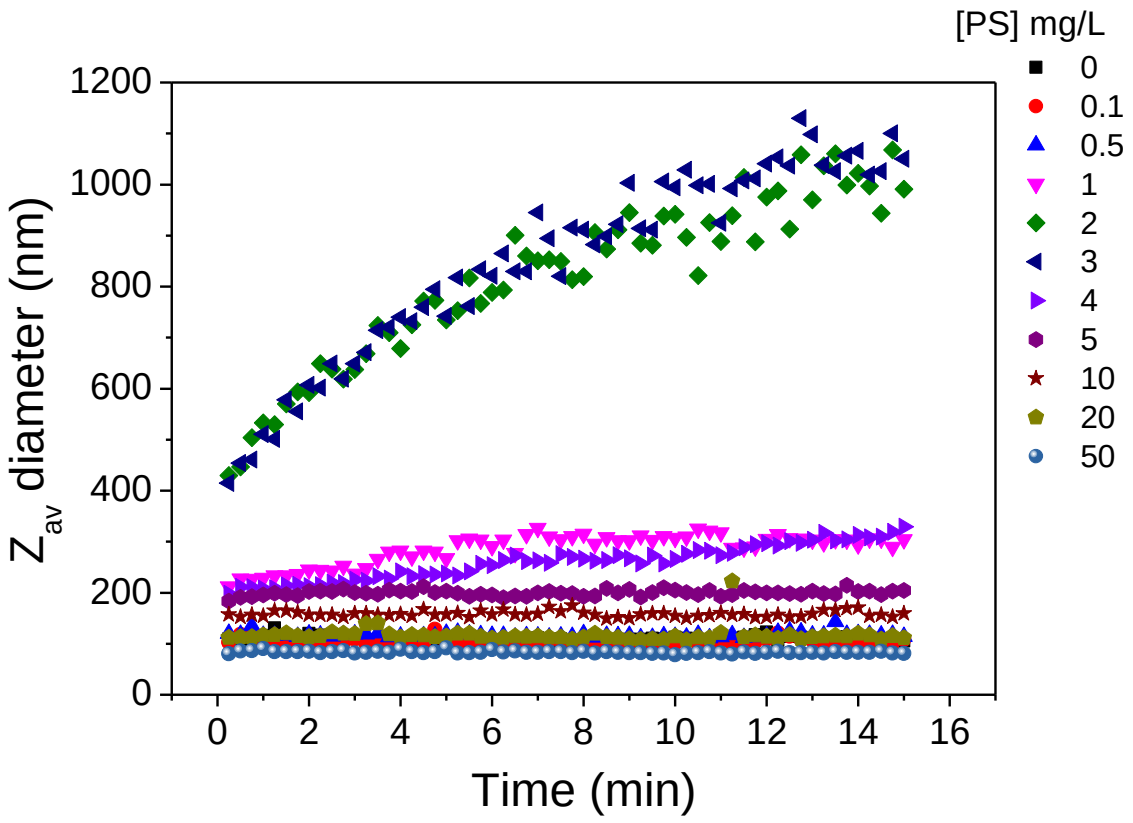

Fig. A5.1. Variation of z-average hydrodynamic diameter of PS nanoplastics with time at increasing nanoplastic concentration. Experimental conditions: [Fe_2O_3] = 5 mg/L, pH = 8.0 ± 0.2, ultrapure water.

A5.SI3. Size distribution (DLS) of PS nanoplastic particles and Fe_2O_3 particles

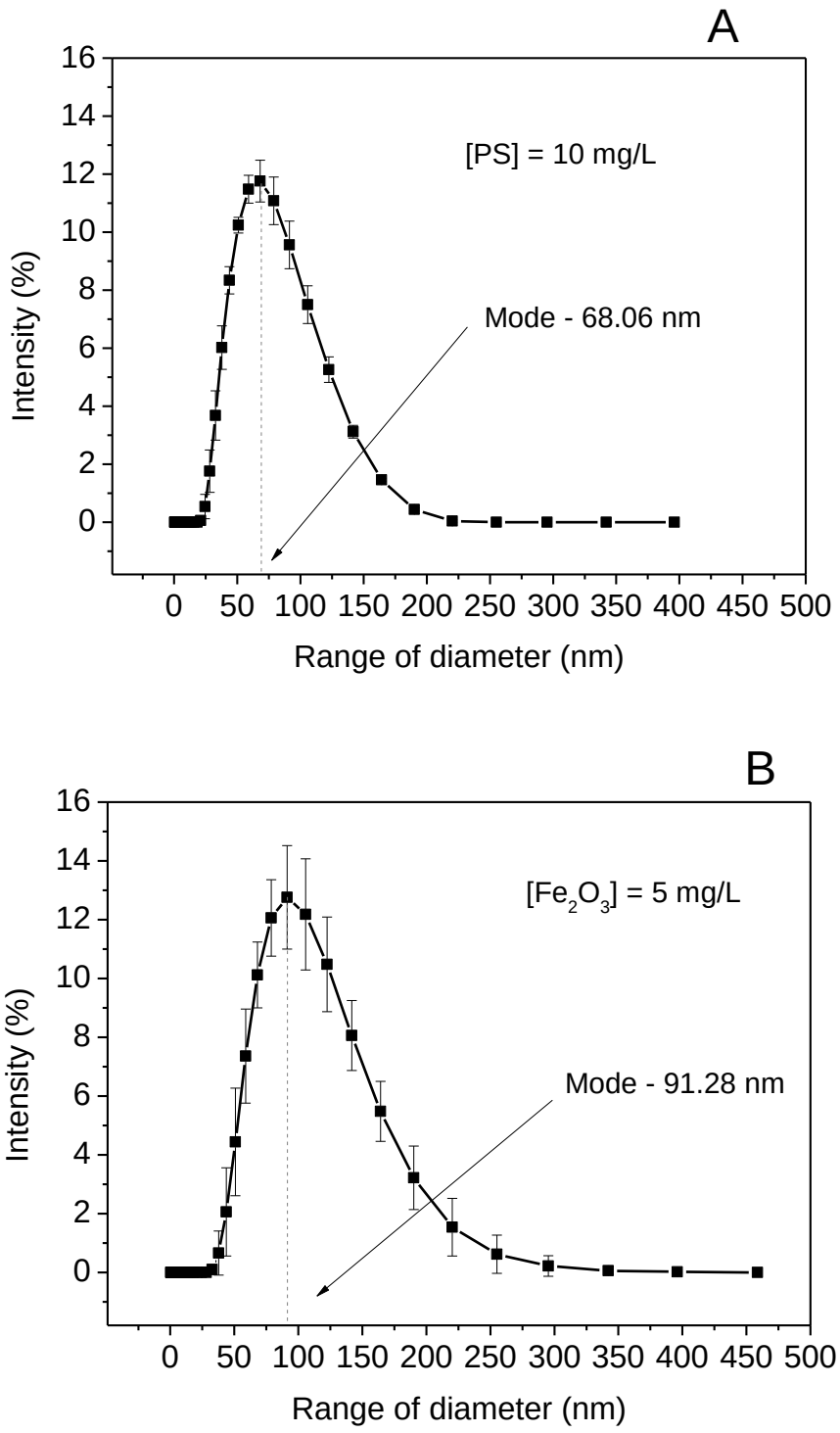

Fig. A5.2. Size distribution of PS nanoplastics (A) and Fe_2O_3 IC (B) particles individually dispersed in ultrapure water at pH 8.0 ± 0.2. Experimental conditions: [PS] = 10 mg/L, [Fe_2O_3] = 5 mg/L. The mode of the range of particle diameter is equal to 68.06 nm for PS and 91.28 nm for Fe_2O_3.

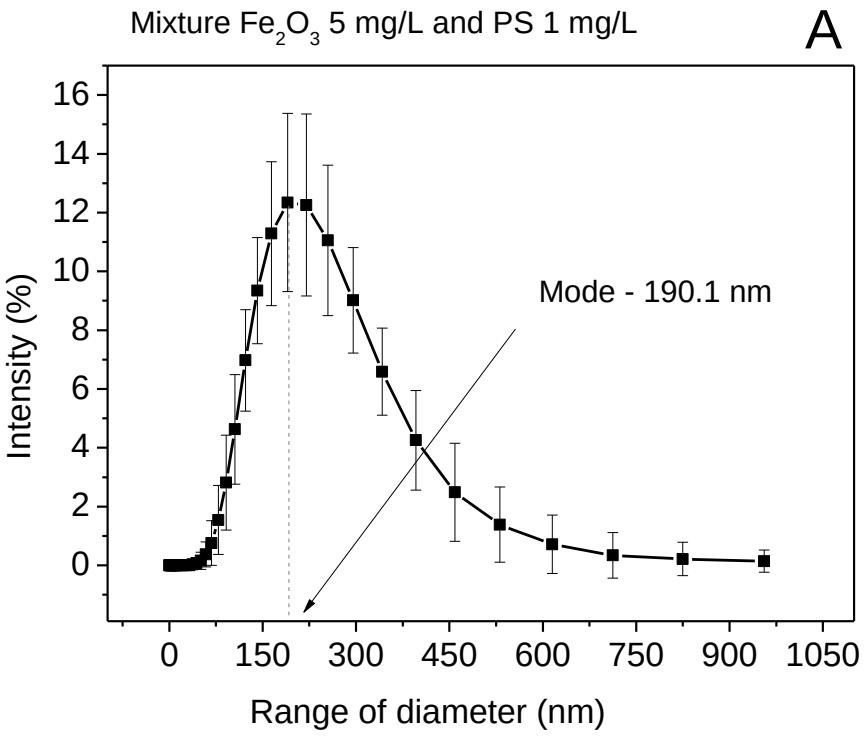
Mixture Fe_2O_3 5 mg/L and PS 1 mg/L
A
Intensity (%)
Range of diameter (nm)
Mode - 190.1 nm
0
2
4
6
8
10
12
14
16
0
150
300
450
600
750
900
1050

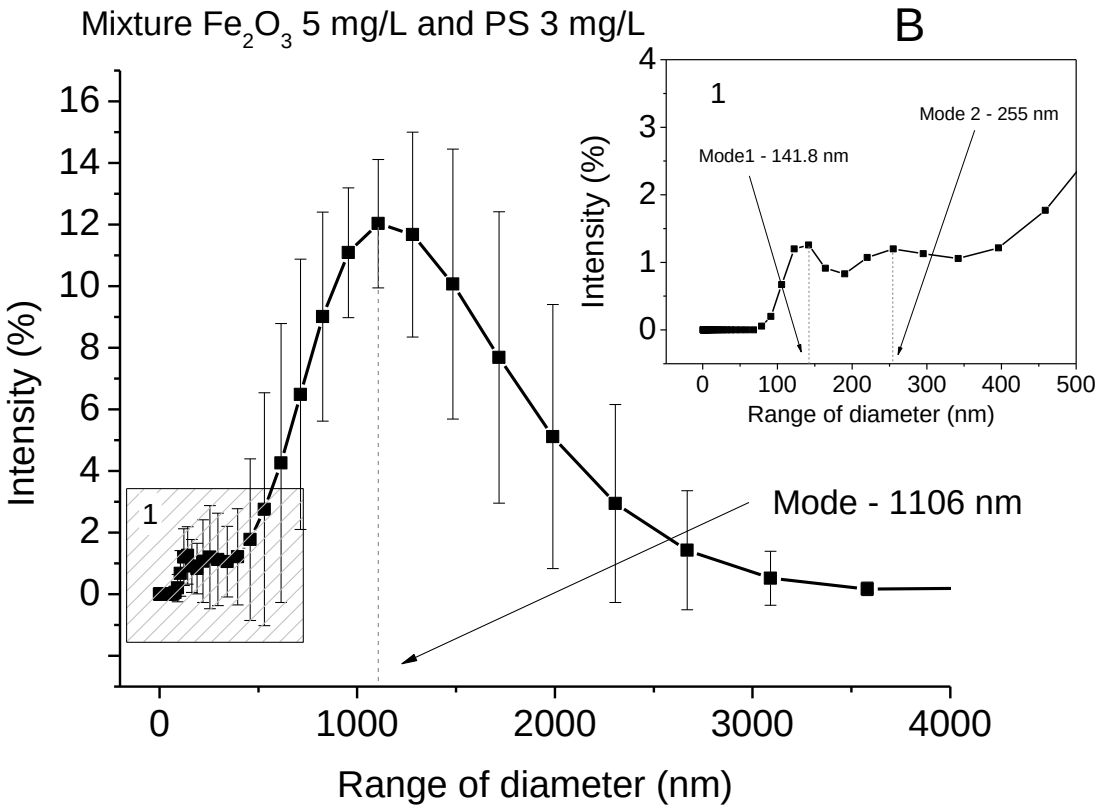
Mixture Fe_2O_3 5 mg/L and PS 3 mg/L
B
Intensity (%)
Range of diameter (nm)
Mode - 1106 nm
1
0
2
4
6
8
10
12
14
16
0
1000
2000
3000
4000
Intensity (%)
Range of diameter (nm)
Mode1 - 141.8 nm
Mode 2 - 255 nm
0
1
2
3
4
0
100
200
300
400
500

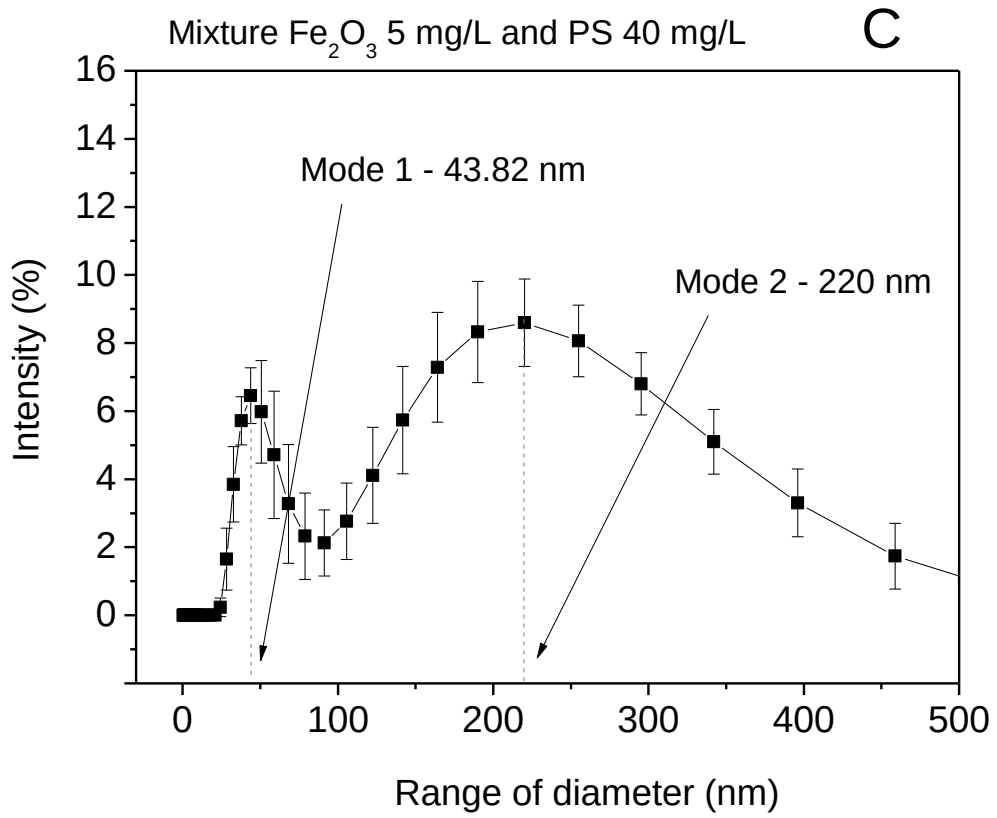

Fig. A5.3. Size distribution of a mixture of PS nanoplastics and Fe_2O_3 particles in ultrapure water at increasing nanoplastic concentration at pH 8.0 ± 0.2. Experimental conditions: [Fe_2O_3] = 5 mg/L in all samples, (A) [PS] = 1 mg/L, corresponding to the beginning of heteroaggregation, the mode of the range of particle diameter is equal to 190.1 nm.; (B) [PS] = 3 mg/L, corresponding to the peak of heteroaggregation, there are three peaks with the modes equal to 141.8 nm, 255 nm and 1106 nm; (C) [PS] = 40 mg/L, corresponding to the excess of the nanoplastic particles and limited heteroaggregation with two peaks with mode equal to 43.82 nm and 220 nm.

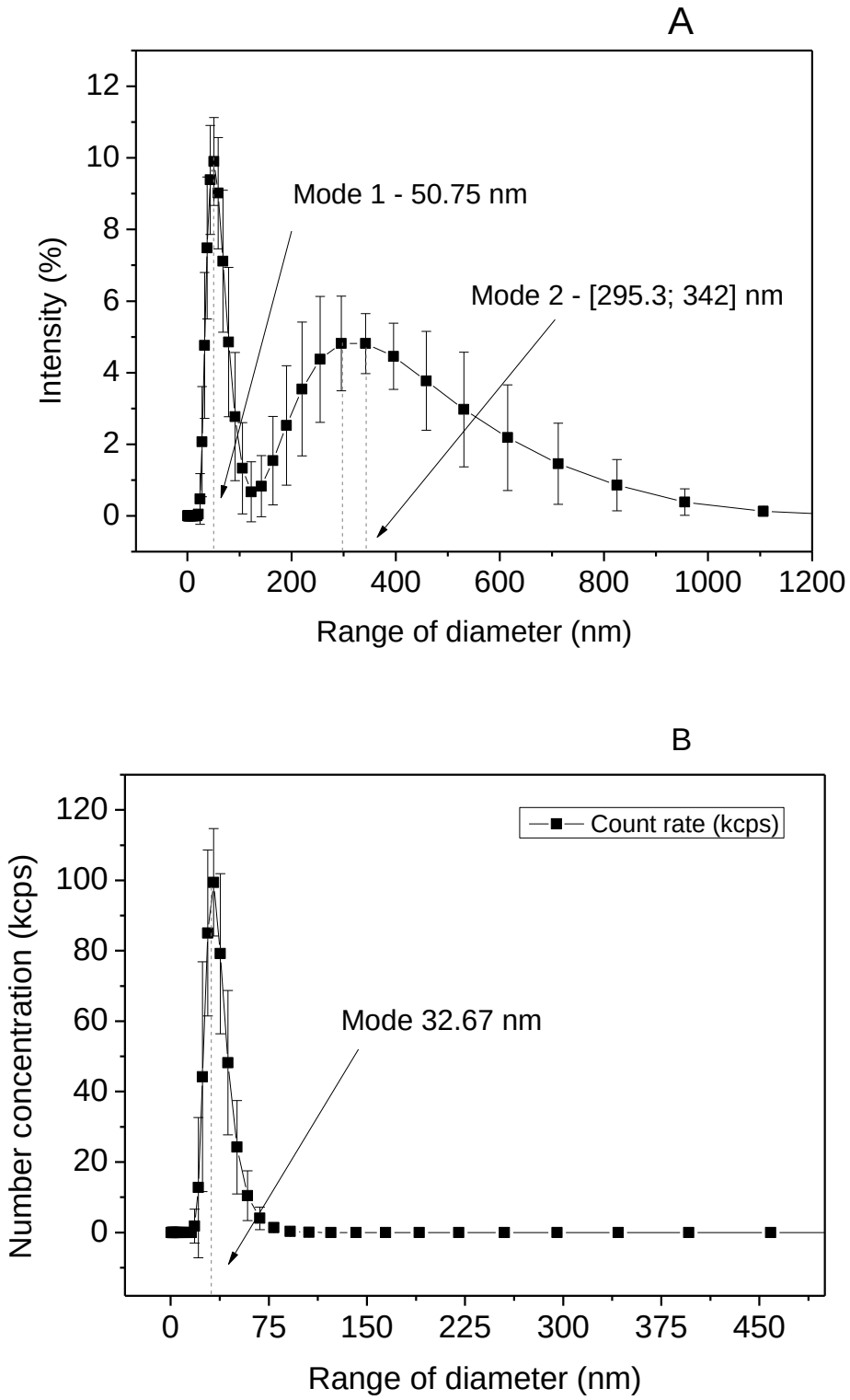

Fig. A5.4. Size distribution of PS nanoplastics in Rhône water in excess of nanoplastics. Experimental conditions: [PS] = 40 mg/L. (A) Intensity weighted distribution (%) with two peaks equal to 50.75 nm and [295.3; 342] nm corresponding to the individual PS particles and heteroaggregates; (B) Number weighted distribution (kcps) with one peak representing nanoplastics with mode equals 32.67 nm.

A5.SI4. Aggregation kinetic of PS nanoplastics in river Rhône water

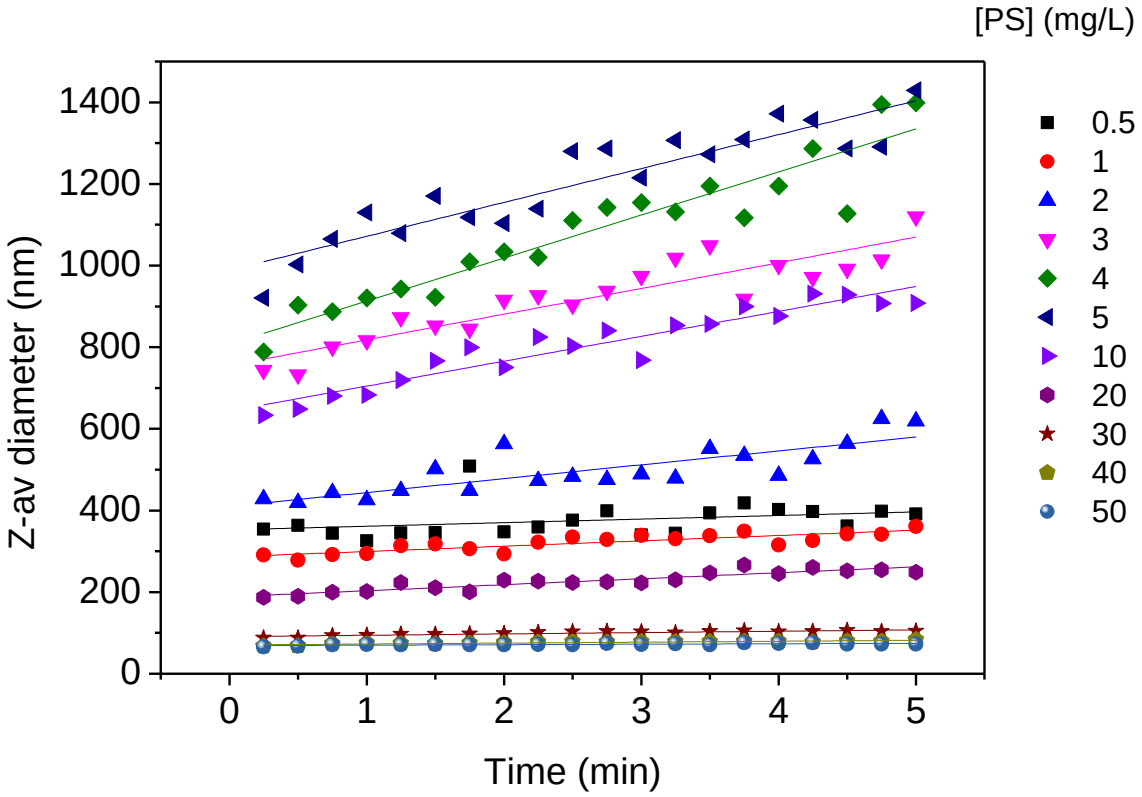

Fig. A5.5. Variation of z-average hydrodynamic diameter of PS nanoplastics with time at increasing nanoplastic concentration in Rhône water. The straight lines indicate linear fit in order to obtain the aggregation rate. Experimental conditions: Rhône water, pH = 8.0 ± 0.2.

Table A5.3 Parameters for models from Fig.6

Linear model

Equation	y = a + b*x		
Weight	Instrumental		
Residual Sum of Squares	5.53734		
Pearson's r	--		
Adj. R-Square	0.95451		
		Value	Standard Error
P	Intercept	-13.16495	4.26159
P	Slope	26.56889	2.88304

Exponential decay model

Model	ExpDec1		
Equation	y = A1*exp(-x/t1) + y0		
Reduced Chi-Sqr	7.70862		
Adj. R-Square	0.90523		
		Value	Standard Error
P	y0	1.0626	0.61771
P	A1	190.60341	42.23136
P	t1	6.6445	0.95902